Functional connectivity applications in drug-resistant epilepsy: Extending to higher frequencies

Christos Stergiadis

PhD

University of York

Physics, Engineering and Technology

October 2025

Abstract

For patients with drug-resistant epilepsy (DRE), resective surgery is the most effective treatment to achieve seizure relief. Since no single diagnostic test can delineate the epileptogenic zone (EZ), most clinical teams rely on the seizure onset zone (SOZ) identified with intracranial electroencephalography (iEEG). However, SOZ localisation requires prolonged recordings, carries risks, and does not always predict surgical success. This underscores the need for reliable interictal biomarkers to improve presurgical evaluation.

Epilepsy is progressively acknowledged as a network disease, and functional connectivity (FC) studies have highlighted the role of network hubs as potential surgical targets. Yet most studies have focused on conventional frequency bands, leaving higher frequencies (>80 Hz) underexplored, even though high-frequency oscillations (HFOs) are promising epileptogenicity markers. In this thesis, I extend interictal FC investigations at higher frequencies and assess their value in quantifying the epileptogenicity of different brain regions, identifying the EZ, and predicting surgical outcome in patients with DRE.

I analyzed iEEG from 18 patients, computing FC in data segments with and without HFOs, using both directed and undirected techniques. Graph-theoretical metrics were compared inside and outside the surgical resection across patients, revealing reduced outward strength and clustering within epileptogenic areas, in all frequencies above beta. Moreover, machine learning models trained on local network properties localised epileptogenic tissue with up to 80% accuracy, while resection of “sink” nodes (outward strength < threshold) predicted outcome with up to 83% accuracy. In addition, I evaluated the temporal variability of FC in patients with multiple-night recordings, and showed that network measures remained stable across four different nights, at multiple levels of analysis.

Collectively, these findings suggest that high-frequency interictal FC could be a robust and clinically valuable means of tracing epileptogenicity, and together with existing literature can lay the groundwork for the transition of FC-based biomarkers from research items to presurgical evaluation tools.

Contents

List of Figures

List of Tables

Acknowledgments

I would like to express my deepest gratitude to my supervisor, Professor David Halliday, for his unwavering support throughout my PhD journey. His mentorship has extended beyond academic guidance, providing me with invaluable opportunities for personal and professional growth. I am truly fortunate to have worked alongside him, and I wish him a well-deserved retirement after a remarkable career.

I will also remain continually grateful to my family and friends, whose love and encouragement have sustained me through every challenge of this chapter of my life. Finally, to my partner, Marianna, thank you for your endless support, understanding, and faith in me, which have been my greatest source of strength.

Declaration

I declare that this thesis is a presentation of original work and I am the sole author. This work has not previously been presented for a degree or other qualification at this University or elsewhere. All sources are acknowledged as references.

In addition, this thesis contains research presented in academic journals.

- Chapter 3 is based on the following publication:
  C. Stergiadis, D. M. Halliday, D. Kazis, and M. A. Klados, “Functional connectivity of interictal iEEG and the connectivity of high-frequency components in epilepsy,” Brain Organoid Syst. Neurosci. J., vol. 1, pp. 3–12, Dec. 2023, doi: 10.1016/j.bosn.2023.11.001.

- The key results from Chapter 5 are being prepared for the following publication:
  C. Stergiadis, D. M. Halliday, D. Kazis, and M. A. Klados, “High-frequency directed networks identify epileptogenic tissue and predict surgical outcome in patients with drug-resistant epilepsy”, Epilepsia

- The key results from Chapter 6 are being prepared for the following publication:
  C. Stergiadis, M.A. Klados, and D. M. Halliday, “Functional connectivity at higher frequencies remains stable across different days of iEEG monitoring in drug-resistant epilepsy patients”, Seizure - European Journal of Epilepsy

Chapter 1

Introduction to the Thesis

1.1 Clinical motivation

Epilepsy is a chronic neurological disease characterised by recurrent unprovoked seizures [1]. According to the World Health Organization (WHO), it affects approximately 50 million people worldwide, and with a prevalence between 4 and 10 per 1.000 people, it is one of the most common and well-studied neurological conditions [2]. The 2019 WHO global report on epilepsy predicts a further increase in epilepsy cases due to the rising life expectancy and the increasing proportion of people surviving insults that often lead to the disease, like birth trauma, traumatic brain injury (TBI), infections of the brain, and strokes [3]. Children are at substantially higher risk for epilepsy than young and middle-aged adults, with the incidence increasing again in people above 60 years of age [4]. Most epilepsy cases start in childhood, consistent with the developing brain's increased propensity for seizures [5], with 26% of the patients having their first seizure before the age of one [6]. Its incidence is higher (~80%) in low- and middle-income countries (Fig.1), something that can be explained by the greater exposure to perinatal risk factors, higher rates of central nervous system (CNS) infections, and TBIs associated with these nations [7].

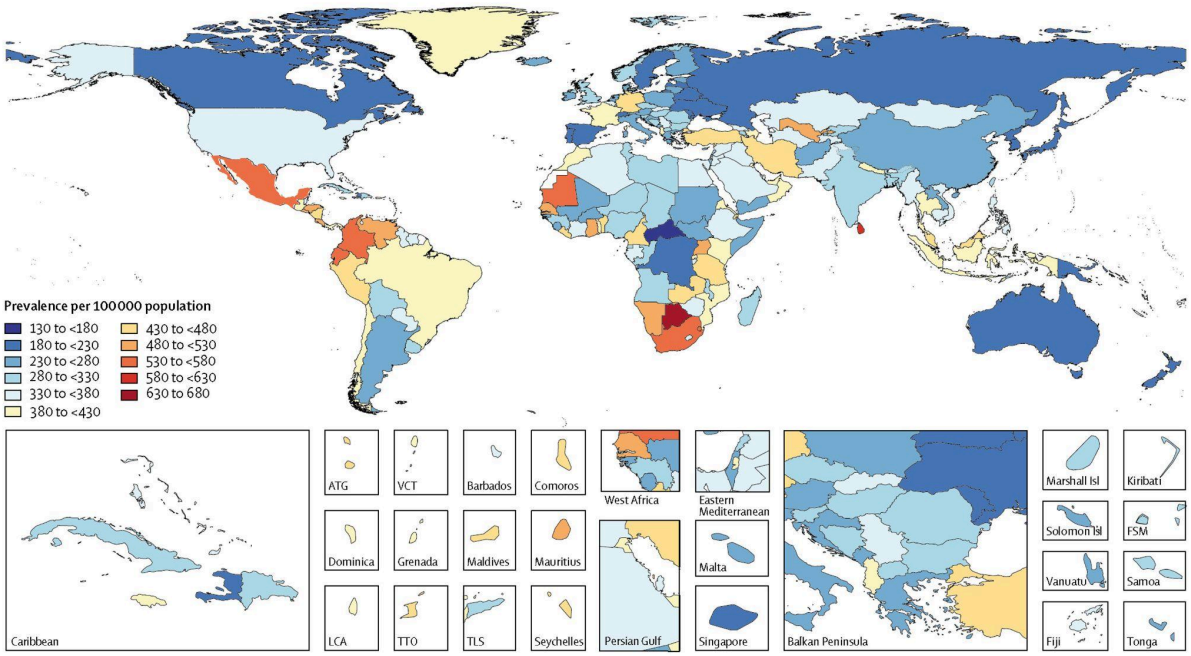

Figure 1: Age-standardised prevalence per 100.000 of idiopathic epilepsy for both sexes (2016). With permission from Global Burden of Disease 2016 Epilepsy Collaborators [8]

Regardless of demographic and aetiological factors, the burden of epilepsy is high, as it carries neurological, cognitive, psychological, and social consequences. Patients face a significantly increased risk of premature mortality (up to three times that of the general population), which is either directly attributable to epilepsy, like sudden unexpected death in epilepsy (SUDEP) and prolonged status-epilepticus, or indirect causes like seizure-induced injuries, and suicide [3]. In addition, 1 out of 3 people with epilepsy will develop psychiatric comorbidities, with depression (23%) and anxiety (20%) being the most prevalent in adults [9].

Nevertheless, epilepsy is a treatable condition, and around 70% of patients can become seizure-free and have a normal life following an accurate diagnosis and a systematic pharmacological treatment with commonly available antiseizure medications (ASMs) [8]. However, it is estimated that around 30% of the patients suffer from Drug-Resistant Epilepsy (DRE), as they present poor post-pharmacological control and continue having symptoms [10], [11]. The exact aetiology behind DRE is still unknown, however, what is now established is that the most effective way for these patients to achieve seizure relief is through surgical intervention [12].

Epilepsy surgery is defined as the resection (or laser ablation) of the brain tissue responsible for the generation of habitual seizures to render the patient seizure-free [12]. The ultimate goal of epilepsy surgery is the removal of the Epileptogenic Zone (EZ), which is a theoretical construct, defined as the cortical region that is indispensable for the generation of epileptic seizures and at the same time the minimal amount of tissue to be removed in order to achieve seizure freedom [13], [14]. The success of the surgery largely depends on the accurate delineation of the EZ during the presurgical evaluation of the patient, which is a rigorous procedure. Despite the large number of available imaging and electrophysiological modalities, like electroencephalography (EEG), magnetoencephalography (MEG), magnetic resonance imaging (MRI), functional MRI (fMRI), etc., there is still no single gold standard diagnostic biomarker of the EZ [15]. In the absence of a lesion (screened through MRI), which would provide some initial guidance, the most established biomarker is the seizure onset zone (SOZ) [15], the area where clinical seizures originate. In clinical practice, though, removing the SOZ has been regularly proven insufficient to achieve lasting seizure freedom, as the EZ usually extends beyond its margins [16]. Epileptologists also pay great attention to interictal events (events that occur at times between the seizures), like interictal epileptiform discharges (also known as interictal spikes), which have been extensively studied and widely recognised as an important biomarker of epileptic activity [17]. However, spikes lack specificity, as the cortical areas they occur in can oftentimes be larger than the actual EZ and thus can overlap with healthy surrounding tissue [18].

For the past 20 years, High-frequency oscillations (HFOs), which are short-time oscillatory field potentials with frequencies typically ranging from 80 to 500 Hz, have been regarded as a promising biomarker of epileptogenicity [19], [20]. Notably, some studies have already proposed that HFOs are better and more accurate epilepsy biomarkers compared to spikes [21], [22], [23], since they are believed to be more closely related to the epileptogenic process. However, their clinical utility remains extremely limited, mainly because the most reliable technique for detecting them on the EEG, intracranial EEG (iEEG), and MEG signals is through visual inspection of the data [24]. This procedure is very time-consuming and subjective [25]. Together with the lack of expertise and necessary equipment in many epilepsy

centres, and also due to the existence of physiological HFOs, their interpretation during the presurgical evaluation is greatly compromised [19], [26]. As such, there is an increasing need for new tools and approaches that could leverage the biomarker value of HFOs for the localisation of the EZ, while, at the same time, being more objective, accurate, and time efficient.

1.2 Research Interests and Objectives

Except for the structural dependencies, the realisation that a number of distinct and distant brain regions can be involved in the generation of seizures and interictal events implies the existence of functional connections and network-level organisation in the epileptic brain. In this sense, the idea that focal epilepsies are not in fact so focal, and may be related to networks of varying scales, has been gradually accepted in epilepsy research [27], [28], [29]. Indeed, nowadays it is established that epilepsy is a disease of disrupted brain networks [30], [31].

Functional connectivity (FC) techniques combined with mathematical concepts, like graph theory analysis, are valuable tools for quantifying these networks [32], [33], [34]. Existing literature associates the epileptogenic areas with increased FC during the interictal period and the resection of hub cortical regions with favourable patient outcomes [35], [36], [37], [38]. However, the majority of published works have studied the connectivity of the brain at the conventional frequency range, from delta (0.5 Hz) to low gamma (60 Hz) [33], [39]. Since high-frequency activity (HFA) and HFOs have been closely associated with the epileptogenic tissue, it would be of interest to extend FC investigations to higher frequencies (> low gamma). Moreover, prior studies emphasise the influence that interictal spikes can have on FC computations [34], [40], [41], [42], [43]. Still, the impact that HFO events have on FC and the associated networks remains largely unexplored. To enhance our understanding of the brain's functional integration during the interictal period, it would be essential to investigate how FC patterns and network organisation across different frequencies are modulated by the presence or absence of HFOs.

The fact that functional connectivity tools lack clinical transition [44], despite their potential advantages, highlights the need for focused research on the connectivity features that define the epileptogenic process, and characterize the EZ in particular. Thus, as addressed in Chapter 5, the aim is to “Study the characteristics and biomarker value of functional connectivity tools in the epileptic brain” by answering the questions:

RQ1: *Does FC differ significantly when computed in data segments with and without HFOs?*

RQ2: *Can specific functional connectivity measures differentiate epileptogenic from non-epileptogenic tissue in DRE patients?*

Additionally, the growing adoption of artificial intelligence (AI) and machine learning (ML) tools in healthcare, particularly in diagnosis, has enabled advancements in the automated identification of pathological regions in patients with epilepsy [45], [46], [47]. Thus, as addressed also in Chapter 5, the objectives are to: “Assess the capabilities of machine learning models trained on functional connectivity properties in identifying epileptogenic tissue”, and “Test whether resection of specific channel groups, determined by their connectivity profiles, can serve as a predictor of surgical outcome in epilepsy patients”. To do that, I seek to address the following questions:

RQ3: *Can machine learning algorithms, trained on different functional connectivity measures, predict channels that belong to the EZ?*

RQ4: *Does resection of hub/sink nodes (channels) in the generated networks predict the surgical outcomes of DRE patients?*

Finally, it is widely accepted that the robustness of newly proposed biomarkers across different methodological conditions is crucial for their transition from research to clinical practice. In that sense, stability of functional connectivity tools across different recording days would strengthen the argument for their usefulness during presurgical evaluation procedures. In addition, it has been recognised that in many pathologies, impaired tissue is generally associated with increased stability (lower entropy, stable connectivity, etc.), whereas healthy tissue is significantly more

unpredictable, mainly due to its multifunctional role in the healthy brain [48], [49], [50]. This concept can be extended in the context of epilepsy and be used for FC stability-based localisation of epileptogenic tissue. Thus, as addressed in Chapter 5, the objective is to "Investigate the stability of FC measures across different recording days and assess its biomarker value for discriminating epileptogenic from non epileptogenic tissue" by answering the questions:

RQ5: *Are functional connectivity patterns stable across four different days of recording?*

RQ6: *Does the stability of FC across separate days differ between epileptogenic and non-epileptogenic tissue?*

By providing answers to the above questions, this study aims to acquire a better understanding of the functional organisation of the epileptic brain, while at the same time providing useful directions for the tools that could contribute to the refinement of the presurgical evaluation process through objective, time-effective, and reliable approaches.

1.3 Structure of the thesis

Chapter 2 provides a background on epilepsy, describes the procedures of epilepsy surgery, and introduces the concept of epilepsy as a network disease. Chapter 3 reviews the current literature on interictal iEEG functional connectivity in the epileptic brain. Chapter 4 details the dataset and describes the methodological approach followed to generate the networks that serve as the basis for the different investigations that I focus on during later chapters. Chapter 5 investigates the network properties of epileptogenic and non-epileptogenic brain tissue, explores the potential of ML models in identifying the EZ, and tests the clinical value of resecting areas with specific network characteristics for predicting surgical outcome. Chapter 6 assesses the stability of functional connectivity patterns across different days of iEEG monitoring and evaluates its value as a biomarker for localising epileptogenic tissue. Finally, Chapter 7 concludes the thesis by discussing the practical applications and clinical translation of FC tools for the management of drug-resistant epilepsy.

Chapter 2

The Epileptic Brain

2.1 Epilepsy: Neurophysiology, clinical presentation and treatment options

This section describes the basic neurophysiological mechanisms of epilepsy, its clinical presentation in terms of the most common symptoms, and the treatment options for drug-resistant patients.

2.1.1 Neurophysiology of epilepsy

The human brain relies on electrical signals to facilitate communication between neurons and regulate its complex functions [51]. At the cellular level, this is achieved through the generation of action potentials and their propagation across neurons through electrochemical reactions based on excitatory neurotransmitters (mostly glutamate) [51], [52]. At the same time, inhibitory neurotransmitters, like gamma-amino-butyric acid (GABA), ensure sufficient inhibition to maintain controlled neural activity, shape the main brain rhythms, and protect against neurotoxicity [53].

In the healthy brain, a delicate balance between excitatory and inhibitory neurotransmission ensures stable and controlled neuronal firing (Figure 2A). However, in epilepsy, this balance is disrupted, leading to abnormal and excessive neural discharges. When hyperexcitability (a state where neurons are more likely to fire) occurs in a synchronised neuronal population, an epileptic seizure is generated [54]. Although the precise mechanisms of seizure initiation (ictogenesis) remain elusive, mainly because epilepsy may have many etiologies [55], it is widely accepted that conditions like TBI, tumours, stroke, infections, cerebral palsy, intrapartum hypoxia, and genetic or neurodegenerative disorders can lead to

long-term changes in neuronal circuitry (a process known as epileptogenesis [56], [57]), which eventually leads to epilepsy (Figure 2B). Mechanistically, the disruption of the excitation-inhibition balance can stem from disturbances in extracellular ion homeostasis, altered energy metabolism, dysfunction of neurotransmitter receptors, or altered transmitter uptake [52].

After a seizure is initiated, it can propagate in both adjacent regions (via local cortical connections) and distant areas (via long association pathways) [52]. In normal conditions, this propagation of activity could be prevented by the activation of inhibitory neurons. However, in epilepsy, excessive neural firing leads to failed inhibition and recruitment of neighbouring areas. Several pathophysiological processes contribute to seizure propagation, including:

I. Elevated extracellular K^+ levels, which reduce hyperpolarising outward K^+ currents and promote depolarisation of nearby neurons [52]
II. Increased Ca^{2+} accumulation in presynaptic terminals, enhancing neurotransmitter release [52]
III. Sustained activation of N-methyl-D-aspartate (NMDA) receptors (promoting further Ca^{2+} entry and reinforcing excitatory transmission) [52]

Seizure activity eventually ceases through mechanisms that are not fully understood but may involve depletion of neurotransmitters, activation of inhibitory circuits, changes in extracellular ion concentrations, and metabolic exhaustion of neurons [58], [59].

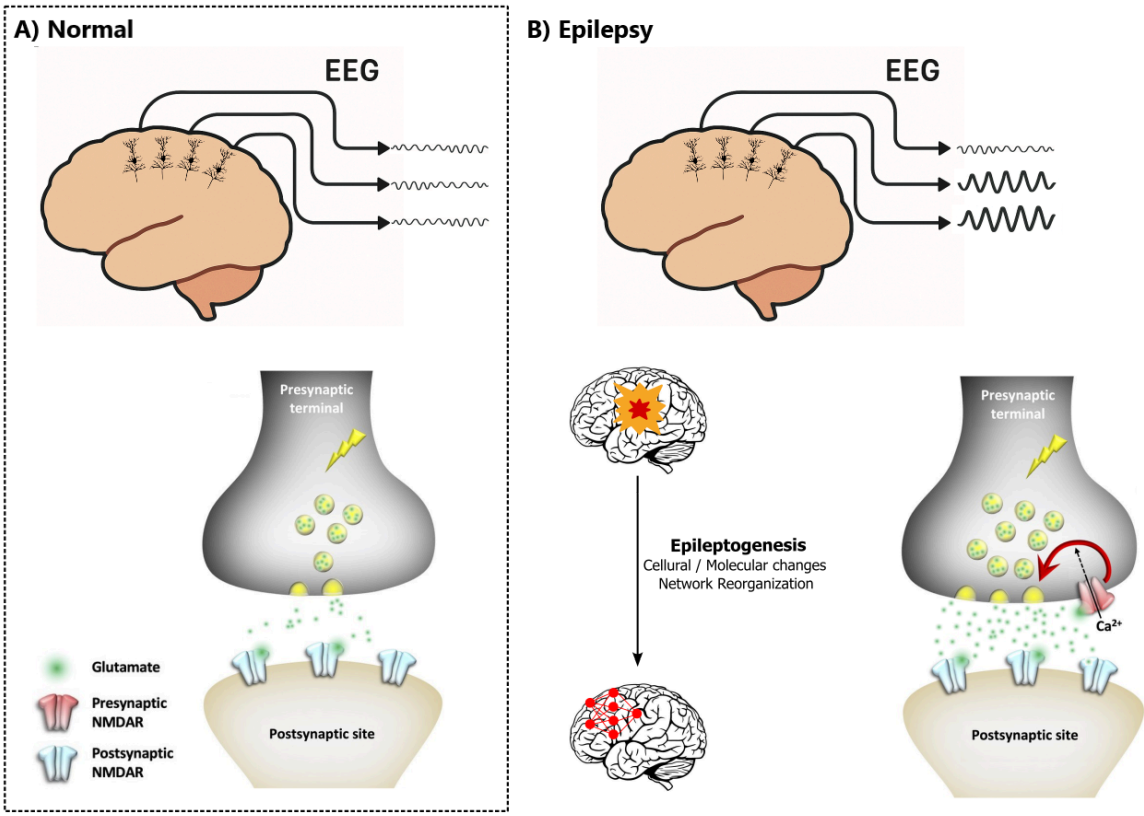

Figure 2: Electroencephalographic (EEG) pattern and neurotransmission in A) normal/healthy conditions, and B) pathological/epilepsy conditions. Molecular, cellular, and network changes occurring after an acquired brain insult reorganise the (local) connectivity of the brain, which is characterised by unstable brain states that eventually lead to seizure generation. NMDAR: N-methyl-D-aspartate receptors

2.1.2 Clinical presentation

Epilepsy is fundamentally characterised by its hallmark feature, the epileptic seizure. Seizures (from the Latin sacire- “to take possession of”) have varying presentations from unusual sensations, loss of awareness, involuntary twitching or stiffness in the body, to more severe cases with loss of consciousness and uncontrollable shaking [60]. According to the 2025 report of the International League Against Epilepsy (ILAE), seizures are classified as focal, generalised, unknown or unclassified [61]. Focal and generalised seizures are distinguished by the brain regions involved at the time of their presentation.

1) Focal seizures, which account for 61% of epilepsy cases [62], originate from a specific area in one hemisphere of the brain and spread to other regions, causing mild to severe symptoms depending on the extent of brain tissue that becomes involved. Temporal lobe epilepsy (TLE) is the most common type and accounts for approximately 60% of patients with focal epilepsy [63]. The epileptic foci can be located either in medial structures (80% of cases), such as the hippocampus or surrounding areas, or in lateral temporal areas (20% of cases) [64]. When the seizure focus is located outside the temporal lobe, the epilepsy is called extratemporal. The most frequent lobe involved in extratemporal epilepsy is the frontal lobe, which accounts for 20%-40% of the focal epilepsy cases [65]. Occipital lobe epilepsies are less common than frontal lobe, while even more rare are seizures originating from the parietal lobe. The main symptoms associated with focal seizures are summarised in Table 1.

Table 1: Clinical manifestations of focal seizures by lobe of origin

Lobe of origin	Key clinical features
Temporal lobe (~60% of focal epilepsies)	Focal aware (auras/simple partial) Fear, limb jerks, rising epigastric sensation, unpleasant smell; consciousness preserved [66] Focal impaired awareness (complex partial) Orofacial/hand automatisms, motionless stare, dystonic upper limb posturing [66] Aphasia when the dominant hemisphere is involved [67]
Frontal lobe (~20-40% of focal epilepsies)	Unilateral tonic posturing, vocalisation (screaming, laughter), speech arrest (Broca's area), repetitive complex motor movements (e.g., bicycle pedalling, pelvic thrusting) [65]
Occipital lobe (Less common than frontal lobe)	Visual auras: hallucinations, transient blindness, blinking, contralateral nystagmus [65]
Parietal lobe (Rare compared to other lobes)	Sensory phenomena: heat, numbness, electrical sensations, weakness, confusion [65]

2) Generalised onset seizures originate from both hemispheres of the brain almost simultaneously and are associated with more severe symptoms. Impairments in these cases manifest bilaterally [68]. The different types of generalised onset seizures alongside their associated symptomatology are presented in Table 2.

Table 2: Clinical manifestations of generalised seizures by seizure type

Type of seizure	Key clinical features
Absence	Brief staring episodes; more common in children than adults [69]
Myoclonic	Shock-like jerks of the body, mainly arms, head, and neck; brief duration of a few seconds [70]
Tonic	Sudden muscle stiffness, often leading to falls or injuries [70]
Atonic	Loss of muscle tone causing collapse [70]
Tonic-clonic (Grand Mal)	Two phases: (1) tonic phase with muscle stiffening and loss of consciousness, followed by (2) clonic phase with rapid, rhythmic jerks of limbs, lasting a few minutes [70] Extensive salivation and foaming in the mouth [71]

Given the heterogeneity of seizure types, individualised treatment approaches are essential to optimise therapeutic outcomes in epilepsy.

2.1.3 Pharmacological treatment

Pharmacological treatment remains the primary approach in the management of epilepsy, successfully preventing or reducing seizures in ~70% of diagnosed epileptic patients [72], [73]. Nowadays, more than 30 Food and Drug Administration (FDA)-approved ASMs are publicly available [74], [75]. This variety requires careful selection of the proposed therapy plan (when to initiate treatment and which ASM to use) based on a highly individualised risk-benefit analysis [76]. Important factors that guide ASM selection are the patient's epilepsy type, age, sex, comorbidities, and concurrent medications [77]. Almost all ASMs are effective against focal seizures, while for generalised seizures, a more limited variety of drugs with specialised

mechanisms of action are available [76]. Nevertheless, all of the medicines currently used act prophylactically, in a symptomatic manner, meaning that they target to suppress and restrict seizures rather than having an impact on the disease process [78]. The treatment plan for epileptic patients starts with a monotherapy intervention. If the chosen ASM fails to control seizures, then the dosage is gradually increased, or another monotherapy is selected, or sometimes a combination of two ASMs with different modes of action is chosen [76]. Figure 3 graphically illustrates the main antiseizure targets and drugs related to epilepsy treatment.

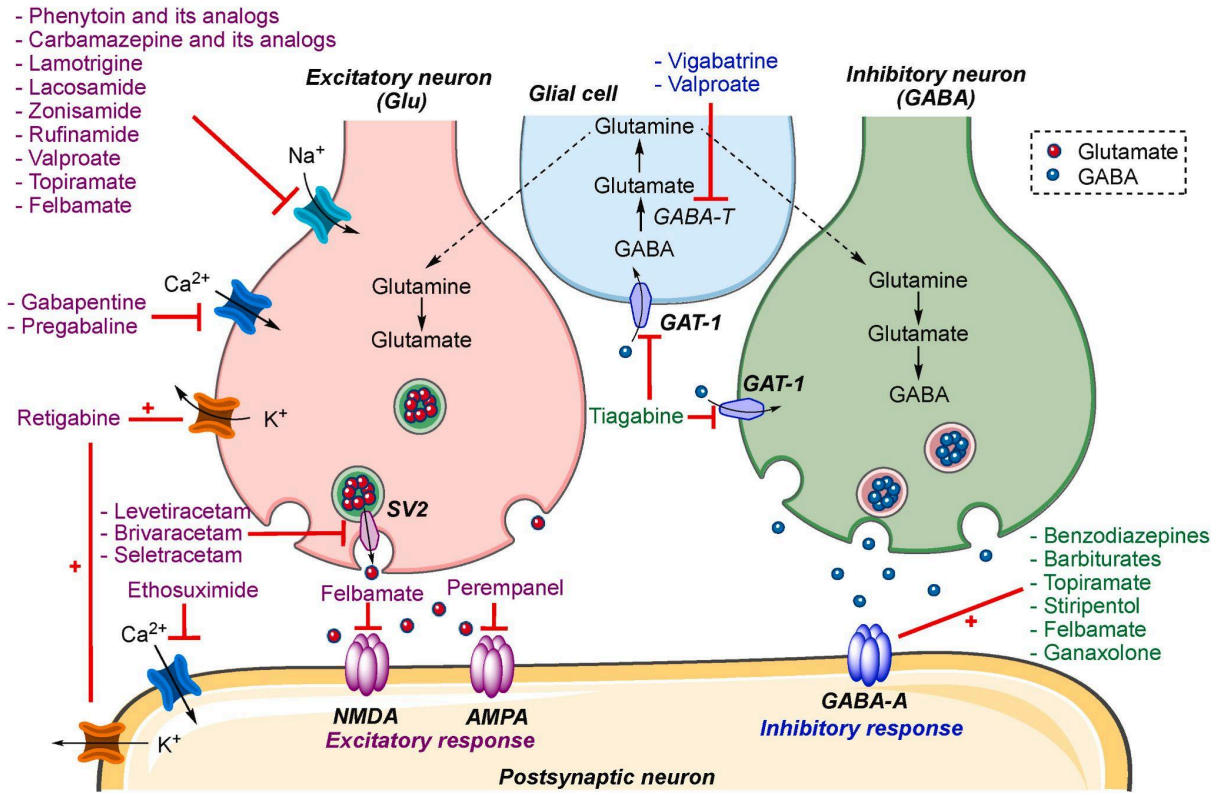

Figure 3: Graphical illustration of the excitatory (glutamate) and inhibitory (GABA) neurotransmission mechanisms, together with the main antiseizure drugs, grouped by their target. Adapted from [79].

2.1.4 Drug-resistant epilepsy

Even though the majority of epilepsy patients can live seizure-free through systematic pharmacological treatment, it is estimated that around 30% of the patients suffer from drug-resistant epilepsy, as they present poor post-pharmacological control and continue having symptoms [80]. The definition of

DRE is debatable; however, it is generally accepted that at least two suitable and tolerated ASM routines, whether as monotherapies or jointly applied, should first be attempted in order for this term to be applied [10]. An aspect that complicates the diagnosis of DRE is the high interindividual variation of epilepsy presentations, both in terms of the frequency of the habitual seizures, while also in the severity of the events in each patient [81]. These difficulties deem the establishment of a universal diagnostic protocol for DRE almost impossible. However, the International League Against Epilepsy has recently made efforts to alleviate the ambiguity around the diagnosis of DRE by proposing specific standardised requirements [81]. Several predictors are used to identify the patients at risk of developing DRE, with none, however, being conclusive enough to be considered the gold standard. “Intrinsic” factors such as idiopathic syndromes and causative neuropathology can play an important role when assessing a patient for prospective DRE [82]. Moreover, the response of the patient to the first provided ASM, family history, and a high number of seizures at the time of diagnosis are also profound predictors for the development of DRE [83]. The pathological reasons behind this condition have not yet been completely understood. However, there are several hypotheses behind pharmacoresistance in epilepsy. The “transporter” theory postulates that the overexpression of efflux transporters present in the blood-brain barrier can reduce the penetration of anti-seizure medications into the brain, limiting their effectiveness [84], [85]. Moreover, the “network hypothesis” supports that neuron degeneration and synaptic network remodelling due to seizures can contribute to the generation of an altered neural network, which prevents ASMs from reaching their target, eventually leading to DRE [86].

Despite the uncertainty around the pathogenesis of DRE, one thing is for sure: epilepsy patients with recurrent seizures should be referred to a full-service epilepsy centre as soon as possible. This is because DRE patients are at very high risk of adverse consequences, ranging from behavioural, interpersonal, and social inabilities to increased risk for injuries and premature mortality due to either seizure-related accidents or due to sudden unexpected death in epilepsy [87], [88]. However, less than 1% of patients with DRE are evaluated at an epilepsy centre [87], and those who do have an average of over 20 years after the epilepsy onset. It is important to note that epilepsy centres do more than surgery, as very often patients

who appear to be resistant to pharmacological treatments are actually not, or they do not have epilepsy at all, while for a large portion of actual DRE patients tailored therapy plans addressing the psychological and social effects of epilepsy can significantly improve their everyday life [87]. In any case, a considerable number of patients who are screened in an epilepsy centre are surgical candidates (10% to 50%) [89]. In such cases, a multidisciplinary team of experts evaluates that epilepsy surgery (ES) represents the most promising treatment to achieve seizure freedom.

2.2 Epilepsy surgery

The basic idea behind epilepsy surgery is the complete resection or disconnection of the epileptogenic zone, which is defined as the cortical region where habitual seizures originate and at the same time, the minimal amount of tissue to be resected in order to achieve seizure relief [13], [14]. The only way to determine whether epilepsy surgery was successful is to look at the patient's postoperative results: if the EZ was accurately diagnosed and removed without harming the functionally important eloquent cortex, the patient will be seizure-free with few to no functional losses. Therefore, a thorough presurgical evaluation to clearly delineate the EZ and the essential areas to be spared is crucial for the outcome of the surgery [89]. However, this is a challenging procedure, especially in cases with no specific histopathological causes (like hippocampal sclerosis, tumours, etc.), and due to the fact that no diagnostic technique is so far able to clearly define this zone [90]. In common clinical practice, each presurgical evaluation begins with a combination of a high-resolution MRI, video EEG, and neuropsychological testing [12], [89]. This early investigation can sometimes provide enough supporting evidence about the extent of the EZ and the eloquent cortex and lead directly to surgery. If this is not the case, then additional and more advanced neuroimaging methods are applied in this 1st stage evaluation. One direction is to focus on the ictal period, which is defined as the time when a seizure occurs, by using single-photon emission computed tomography (SPECT) and high-density EEG (HD-EEG) to locate the seizure onset zone. On the other hand, interictal neuroimaging through HD-EEG and MEG can also provide complementary information, such as the irritative zone, the cortical area which generates interictal electrographic spikes [91]. If the localisation of the EZ becomes feasible with a combination of the aforementioned techniques, then the functionally

eloquent cortex should be clarified to avoid language deficiencies, memory decline, and motor or visual deficits, most commonly through fMRI [12].

However, in approximately 20% of DRE patients, the delineation of the EZ can not be sufficiently accurate based solely on these non-invasive techniques, or the functionally important cortical areas are in very close proximity to the proposed resection site [92]. In such cases, the clinical team moves to “Stage 2”, where invasive neuroimaging methodologies are employed [12]. Intracranial EEG is the dominant modality in this stage. It can be applied by using subdural strip and grid electrodes after open craniotomy, known as electrocorticography (ECOG), depth electrodes, known as stereoenchephalography (SEEG), or a combination of the two. While grids and strips of subdural electrodes provide a large coverage over the bare surface of the cerebral cortex, they are often implanted in one hemisphere and do not reach deeper brain structures (e.g., hippocampus or insula) [93]. By comparison, there are cases where only depth electrodes are placed stereotactically, through a twist drill hole or burr hole under general anaesthesia. SEEG monitoring has become increasingly appealing to many epilepsy centres compared to ECoG, due to its less invasive nature, increased comfort for the patients [89], favourable morbidity profile [94], [95], and the fact that it enables bilateral monitoring of superficial and deep cortical structures [93].

Irrespective of the electrode type, iEEG implantation is guided by clinical decisions made on the basis of non-invasive parameters, with the scope to increase the accuracy in the localisation of epileptogenic tissue. A detailed schematic representation of the presurgical evaluation pipeline, from initial clinical assessment to the decision to proceed or not with surgery, is presented in Figure 4.

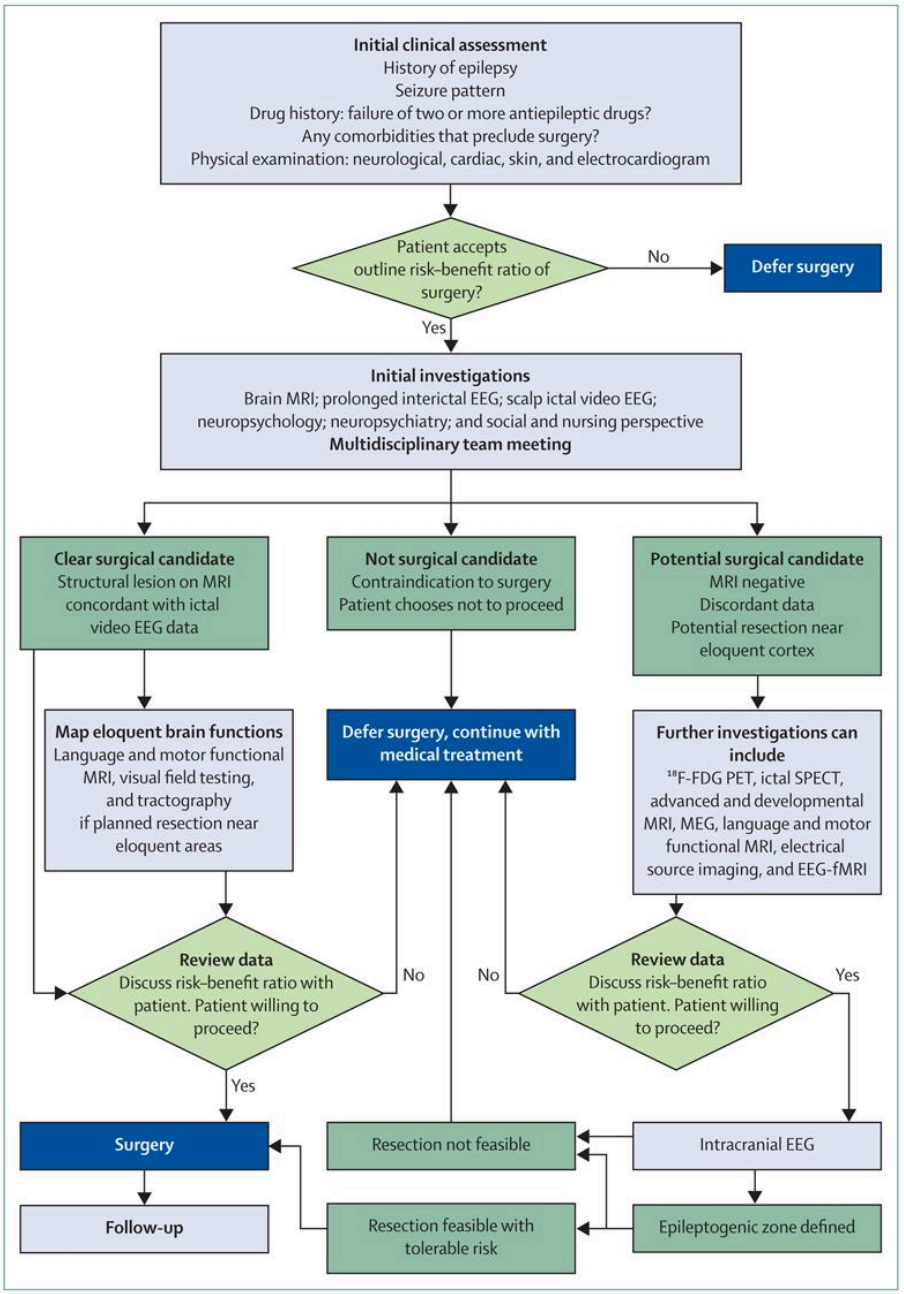

Figure 4: Graphical representation of the presurgical evaluation steps followed in standard clinical practice in epilepsy centres. Adapted from [96].

Nevertheless, despite the large number of available imaging modalities (either invasive or non-invasive), the clinical community cannot yet rely on a single diagnostic biomarker for the localisation of the EZ. A big part of this issue stems from the heterogeneity of epilepsy itself, with different underlying pathologies (hippocampal sclerosis, tumours, TBI, etc.) altering brain networks differently.

2.2.1 Current biomarkers of the epileptogenic zone

Through Stage 1 and Stage 2 neuroimaging, the clinical team proceeds to the localisation of the EZ by combining information from different biomarkers. The presence of a structural lesion, seen through MRI, helps significantly as it restricts the area of focus in the close neighbourhood of the lesion [97] (Figure 5). Assuming anatomy is structurally intact, the most established biomarker becomes the SOZ (the brain area where seizures initiate) [15], especially when defined by iEEG [18]. The SOZ is the go-to biomarker for many centres, as it provides a direct connection to the epileptogenic process, it can be directly defined through EEG and iEEG, and resection of SOZ sites has been historically associated with good surgical outcomes. Some recent studies however, question the requirement for its complete resection [98], [99]. Nevertheless, since it is an ictal biomarker and seizure generation is unpredictable, SOZ monitoring requires prolonged recordings, usually for several nights, at the expense of patient comfort, safety, and financial resources [92]. In addition, given the limited spatial sampling of iEEG, the precise borders of the true SOZ and how much it overlaps with the EZ are still uncertain [100], as the recorded seizures might be the result of propagation from neighbouring, unrecorded tissue. In that fashion, biomarkers that could estimate the EZ via interictal data, with no need for seizures to occur, would largely benefit presurgical planning. However, a definitive interictal marker for the EZ has yet to be established [101].

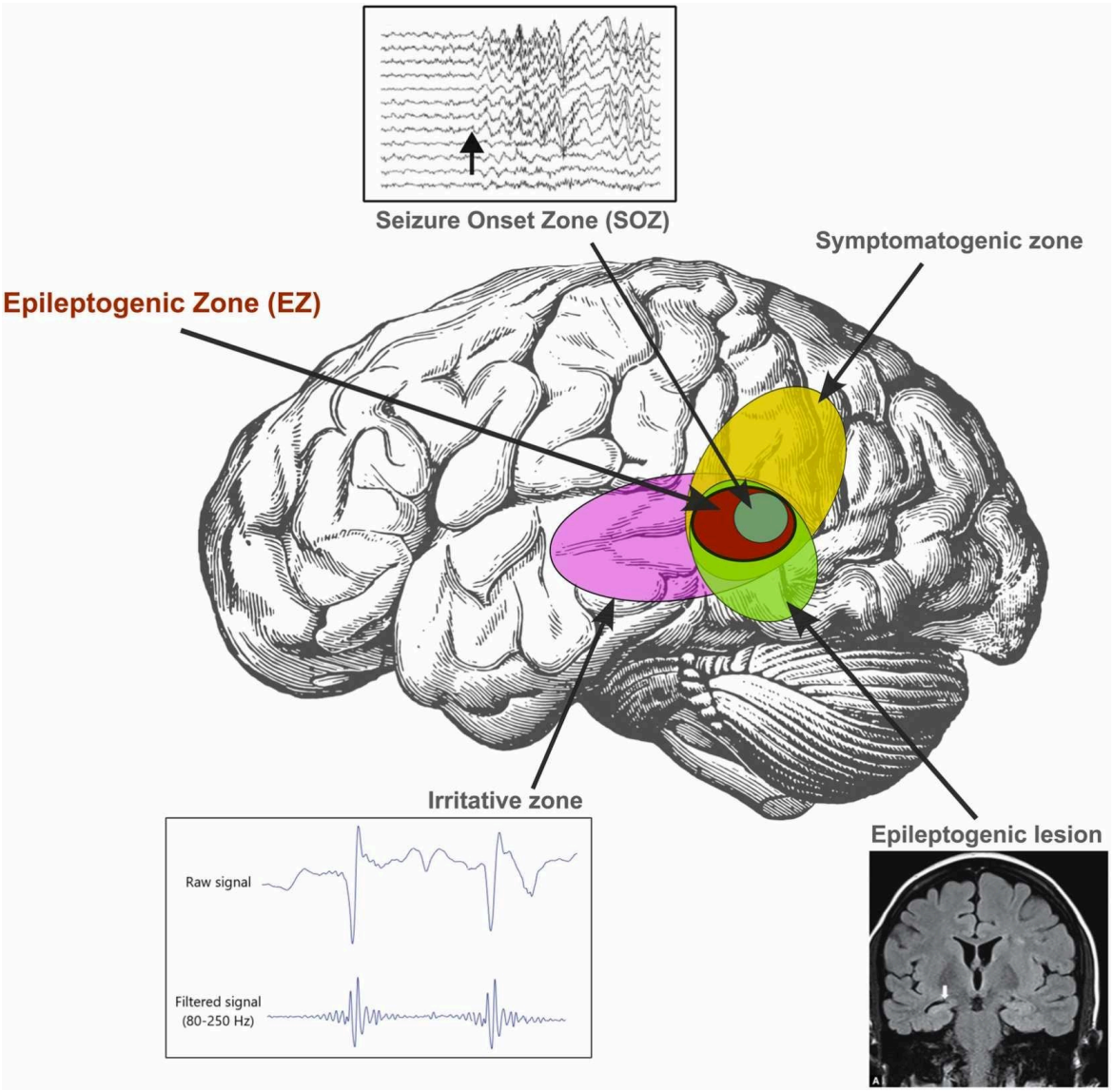

Figure 5: Different cortical zones defined through both invasive and non-invasive neuroimaging during the presurgical evaluation stage. The location and relative size of each zone vary across different clinical cases. Adapted from [33].

A traditional interictal biomarker is the Irritative Zone (IZ), the area where interictal spikes are observed. Spikes have been extensively studied and widely recognised as an important biomarker of epileptogenic activity [17], [102], [103]. As relatively large and prominent events, spikes are easy to detect in iEEG [104], while they can also be seen in non-invasive modalities like scalp EEG and MEG [105]. They are propagating events, and they can be present over large cortical areas [23], [106], while sites of spike onset correlate with the SOZ [107], [108] and resection of such sites is associated with good patient outcome post-operatively [18], [109]. However, they suffer from low specificity to the EZ, as the cortical area that they designate can

oftentimes be larger than the actual EZ and thus can overlap with surrounding tissue that needs to be preserved [18].

Another promising interictal biomarker is the HFO zone, the area where high-frequency oscillations are observed. Today, there are studies suggesting that HFOs are better and more accurate epilepsy biomarkers compared to spikes, as they are believed to be more closely related to the epileptogenic process [21], [22], [23]. However, these views have been challenged by the only clinical trial on HFO-guided tailoring of epilepsy surgery, which could not prove non-inferiority of HFOs to spike-guided surgical interventions [110]. In any case, the interest in the study and clinical value of HFOs has increased recently, with epilepsy specialists showcasing their potential in specialised international conferences and workshops, like the International Workshops on High Frequency Oscillations in Epilepsy (2012, 2016, 2024). A more detailed discussion on HFOs can be found in secion 2.2.2.

Recent studies have also consistently reported that spike ripples (co-occurrence of spikes and HFOs) localise the EZ more accurately than individual events alone [111], [112]. This complex interictal biomarker demonstrates greater spatial specificity compared to interictal spikes and is more reliably pathological than isolated ripples (which may also reflect physiological activity).

Table 3 provides a summary of the basic characteristics of the aforementioned EZ biomarkers.

Table 3: Comparison of existing biomarkers of the epileptogenic zone

Biomarker	Recording modality	Epileptic state	Sensitivity / specificity to the EZ	Practical burden	Typical pitfalls
Metabolic / Structural markers	MRI (lesions), PET, SPECT, fMRI	Interictal / baseline	High specificity when lesion present; Variable sensitivity	-Widely available; -Non-invasive	-Lesion–EZ mismatch; -Non-lesional cases; -Metabolic changes not always epileptogenic
Seizure Onset Zone (SOZ)	iEEG, scalp EEG	Ictal	High sensitivity; Moderate specificity (may include propagation)	-Requires prolonged inpatient recordings; -Invasive	-Limited spatial sampling -Seizure unpredictability -Discomfort/cost
Irritative Zone (Spikes)	Scalp EEG, MEG, iEEG	Interictal	Moderate sensitivity; Low specificity (large areas)	-Easier to detect; -Widely available	-Overestimates EZ, overlaps with healthy cortex -Propagation effects
HFO Zone (HFOs)	iEEG (also scalp/HD-EEG emerging)	Interictal (mainly NREM sleep)	Higher specificity than spikes; Sensitivity variable	-Requires high-bandwidth recording and expert review	-Physiological HFOs (mostly hippocampal) -Labour-intensive visual detection, lack of standardisation
Spike–Ripples	iEEG (ideally bandwidth >1 kHz)	Interictal	Higher specificity than spikes or HFOs alone; Promising sensitivity	-Similar technical demands as HFOs; -Emerging automated tools	-Limited validation

2.2.2 High-frequency oscillations in epilepsy

Almost 25 years ago, high-frequency oscillations were recorded from the human epileptic brain [113]. HFOs are short-time local oscillatory field potentials, with frequencies ranging from 80 Hz to 500 Hz [20], [114], typically divided into ripples (80–250 Hz) (Figure 6A) and fast ripples (250–500 Hz) (Figure 6B). Although this frequency-based classification is widely used, it is not universal, as different groups adopt slightly different cutoffs (i.e ripples up to ~200Hz, fast ripples beyond 500 Hz, etc.), with this variability complicating cross-study comparisons and contributing to the limited generalizability of HFO findings. HFOs are most commonly recorded during non-rapid eye movement (NREM) sleep, as muscle artifacts are less frequent at this time [115]. The most established definitions want these events to have at least

four oscillations clearly standing from the background [116], [117], [118], with some research groups, however, choosing slightly different definitions (i.e a criterion of at least 3 oscillations), further preventing the establishment of a consensus [115]. As of now, the neuronal and circuit substrates of HFOs remain elusive [119]. One prominent theory suggests that pathological HFOs are generated by synchronised action potential firing of principal cells, within small, discretely located neuronal clusters [120], [121]. Due to physiological restrictions, the firing rate of these cells is limited, so even single epileptic neurons cannot fire with frequencies >300 Hz [121]. Subsequently, the fast ripples that are observed are considered “emergent” HFOs as they represent the net frequency of neuronal populations oscillating at lower frequencies [121]. This out-of-phase firing between the different neuronal clusters could be due to cell loss, which would lead to a decreased synchronisation of ephaptic interactions. Another generative mechanism of HFOs highlights the importance of interneurons, as previous studies in the human epileptic hippocampus have demonstrated that interneurons begin to discharge early in the presentation of a ripple, much earlier than the firing of pyramidal cells [122]. GABAergic interneurons in particular have been found to have an active role in the generation of HFOs, as increased GABA synaptic activity is related to the interictal fast ripples in the epileptogenic zone [119]. This increased activity could aid in the disposal of excessive excitability of cortical pyramidal neurons in the EZ, or advance the neuronal network synchrony [119].

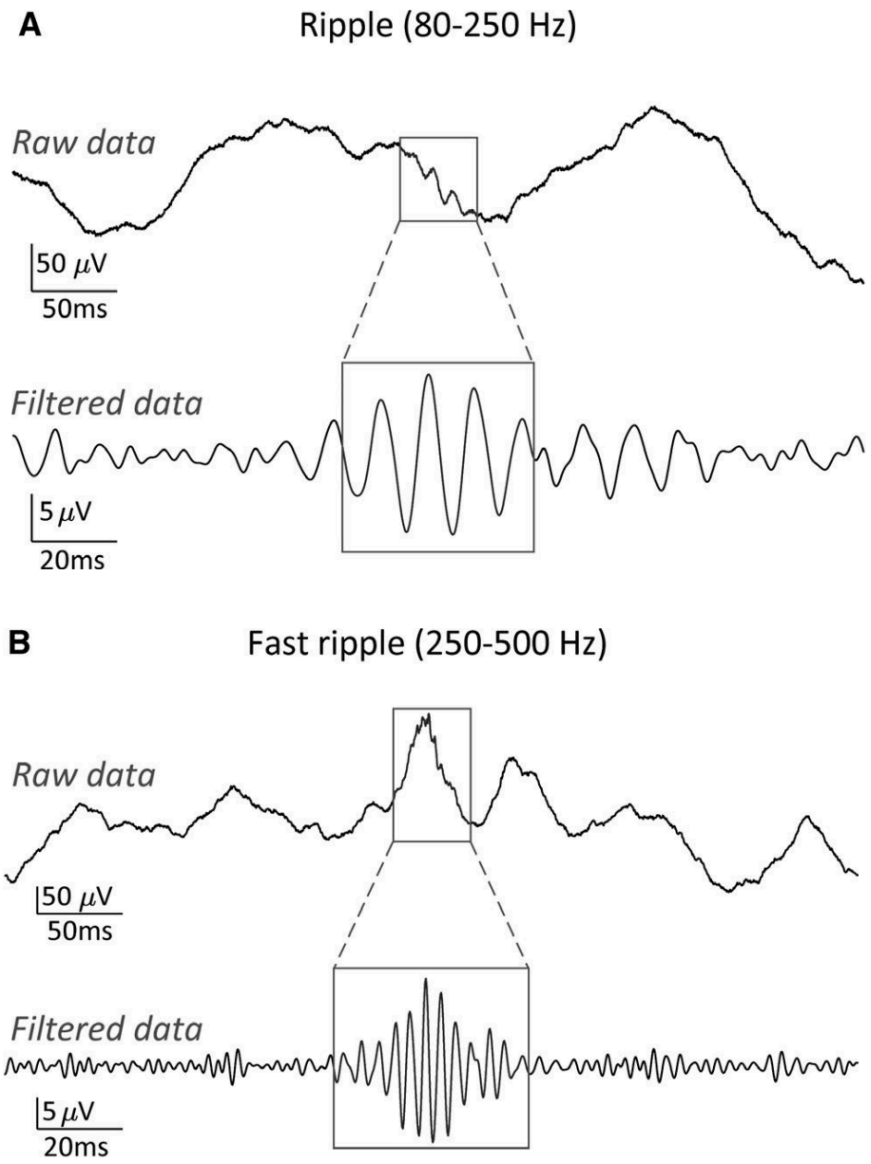

Figure 6: High-frequency oscillation (HFO) examples. The events are difficult to detect in the raw (broadband) signal but become much more distinct from the background once a band-specific filter is used. Adapted from [115].

No matter what the underlying cellular mechanisms are, HFOs are now well-described electrophysiologic events, closely linked to the epileptogenic tissue. Their low amplitude (usually measured in μV) and short duration (tens to hundreds of milliseconds) make them much easier to observe in intracranial recordings, where artifacts and resistance from the scalp are eliminated. However, due to recent advancements in brain recording technologies, there are now more than 60 studies analysing HFOs captured through scalp EEG recordings [116].

HFO limitations

Research in this area has demonstrated that the pre-surgical diagnosis and the surgical outcome of patients with DRE may be improved by removing the tissue that generates HFOs [123], [124], [125], [126], [127]. Despite the encouraging results, there is still strong debate on whether HFOs are suitable for the identification and monitoring of epilepsy in clinical settings [128], [129]. From an operational perspective, this could be attributed to the lack of expertise and available equipment required (i.e, amplifiers, analysis tools, etc.) for the recording and interpretation of HFOs in many epilepsy centres. Moreover, HFOs are also generated under normal physiological conditions [130], especially in the hippocampus [131]. Physiological HFOs have an established role in memory consolidation [132], motor, and language processes [133]. They have also been observed in the amygdala and areas of the neocortex with iEEG [134], while a recent work on non-invasive investigations of the neocortex (HD-EEG + source imaging) has shown high rates of physiological HFOs at the sensorymotor cortex, followed by parietal, temporal and frontal regions [135]. Physiological HFOs have shorter duration [135], [136], lower amplitude [136], [137], and higher frequencies compared to pathological ripples [134], [137]. They also have less variable amplitudes and duration [135], [138], and their inter-electrode latency is longer [112]. The current ambiguity on how to distinguish physiological from pathological HFOs compromises their utility [134], [137], [139]. In addition, one of the major drawbacks that prohibits HFOs from entering clinical practice is that the most reliable technique for detecting them is visual inspection of the data [140]. This is a very time-consuming procedure, which should be performed by trained specialists with experience in the detection of these very specific oscillations. A striking example is that for just 10 minutes of a 10-channel iEEG recording, a clinician needs almost 10 hours to accurately detect the HFOs [141]. In addition, visual detection is subject-dependent and prone to errors due to the human factor [142]. For these reasons, the development of automatic HFO detectors has drawn a lot of attention during the past ten years, and since there is not an established gold-standard algorithm yet, it remains a focus of ongoing research [143], [144].

Automatic HFO detectors

A substantial number of HFO detectors have already been published, with no recommendations, however, on when an algorithm should be used over another, and which are the best parameters for its implementation [115]. Most automatic detectors have a specific sequence of steps in order to optimally detect the HFO events and omit false positive detections. More specifically, the first step is usually the initial event detection, meaning a first separation of HFO events from background activity. For this purpose, the vast majority of detectors rely on energy-based metrics, such as the root-mean-square (RMS) amplitude [134], [145], power [146], [147], and line length [148], or use other techniques such as a median filter [149] and the amplitude of local peaks [150]. After calculating the energy, events that exceed a pre-determined threshold for a minimum duration are identified as potential HFOs.

The second step of the automatic detection procedure is the rejection of false positive events, which are mainly related to high-frequency activity produced due to the filtering of a sharp transient in the iEEG [144]. Discarding false positives could be done by evaluating the event's characteristics, like testing whether their duration exceeds a certain threshold, or checking the existence of fast direct current (DC) drifts and artifacts in the common average, indicating that the event is too spatially widespread to be an HFO [115]. Other, more refined approaches, leverage the unique representation of HFOs in the time-frequency domain, which appear as "islands" of increased power at high frequencies (Figure 7), to automatically discard the false positive detections [151], [152], [153]. Irrespective of their different approaches, the use of automatic HFO detectors is compromised by the need for optimal parameter finetuning, which is patient- [129] or even electrode-specific [150], and performance validation, which again involves human intervention and visual analysis [115].

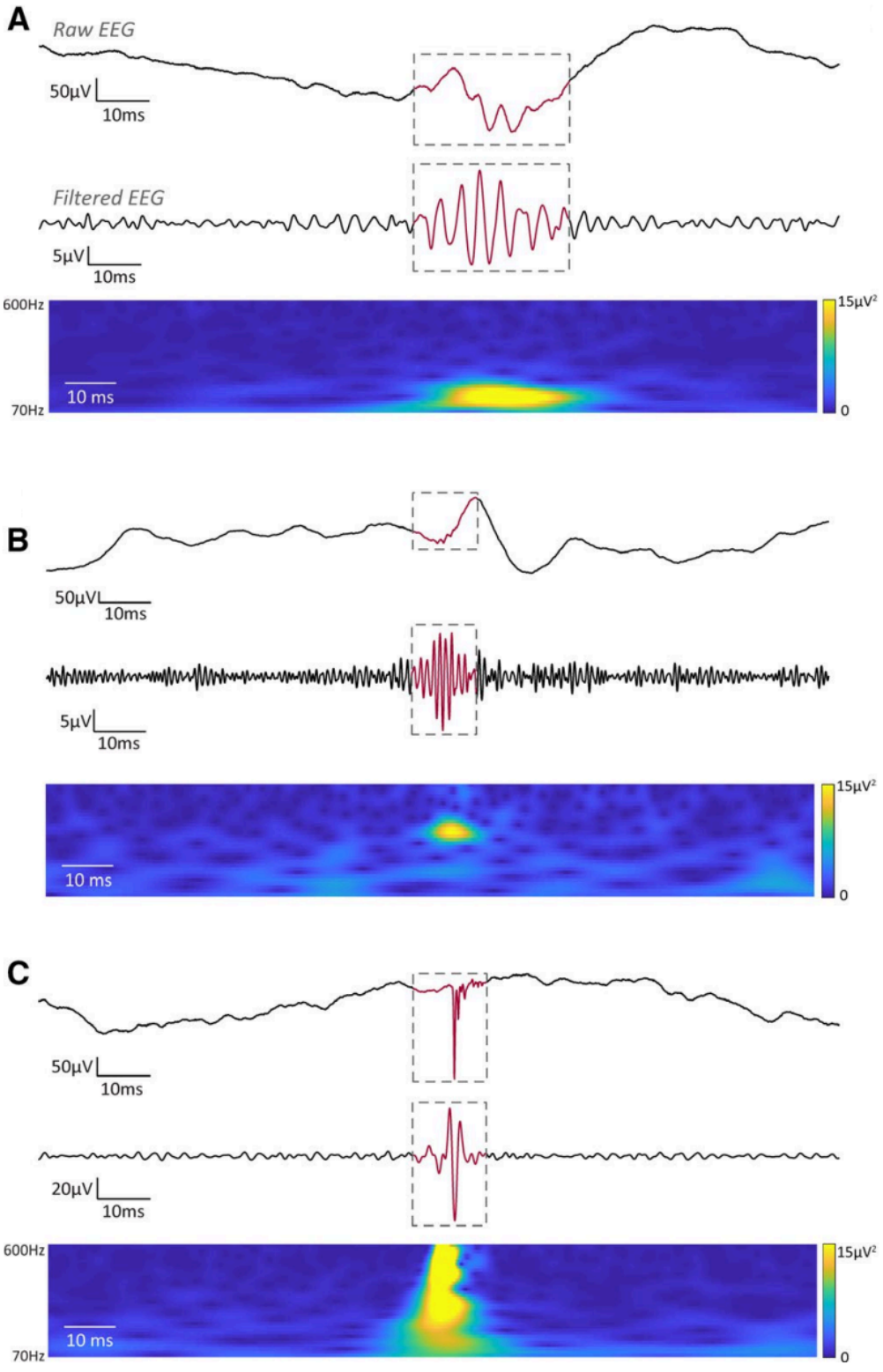

Figure 7: Representative examples of time-frequency decompositions of a) a ripple (80-250 Hz), b) a fast ripple (250-500 Hz), and c) an artifact consisting of a narrow, high-amplitude spike. Adapted from [115].

The overall difficulty in accurately detecting and interpreting pathological HFOs in common practice, together with their documented value as a marker of epileptogenicity, has spurred new research into more efficient ways of harnessing their biomarker potential. It is true that up until now, HFOs are primarily assessed in terms of their rate (events per minute) to quantify the epileptogenicity of a region [110], [154], [155], while some other characteristics, such as their amplitude [156], [157] and duration [158] have also been found to differentiate between healthy (physiological HFOs) and epileptic tissue (pathological HFOs). Even though the literature is heavily dominated by discrete detection of HFOs, other techniques have also been proposed, mainly regarding the computation of specific measures in the entire length of the iEEG signal at high frequencies. These methods have some methodological and practical advantages, as they are not constrained by the lack of a universal agreement on the exact definition of HFOs (frequency margins, number of oscillations, etc.), which very frequently vary across the different research teams and epilepsy centres, while they also include a smaller number of interdependent parameters that need to be optimised [115]. Computing specific metrics in the whole extent of the signal could also be more efficient, requiring less computational time compared to HFO events detection and interpretation. For example, the skew of the distribution of power values was found to be higher in the SOZ compared to non-SOZ areas in different frequency bands (5-80Hz, ripples, and fast-ripples) [159]. Significant interest has also emerged in techniques that quantify the cross-frequency coupling between high-frequency amplitude and low-frequency phase, most commonly through the modulation index (MI). An early study found that the coupling between amplitude in the frequency range of 80-150 Hz with low-frequency phase (1-25Hz) was significantly elevated in the “ictal core” compared to peripheral regions [160], with the same results being also reported later for the SOZ [161], [162]. However, the literature on these types of techniques is sparse and unstructured.

On the other hand, during the last decade, significant emphasis has been given to the analysis and interpretation of functional connectivity measurements, computed in EEG, iEEG and MEG signals, as epilepsy has been progressively acknowledged as a disease of disrupted brain networks [33], [34].

2.3 Epilepsy as a network disease

The fact that the brain is a complex network is heavily supported by the huge number of neuroanatomic and neurophysiologic evidence, ranging from microscale to macroscale studies [163]. In this sense, the idea that focal epilepsies are not in fact so focal, and may be related to networks of varying scales, has been gradually accepted in epilepsy research [27], [28], [29]. Indeed, in very early SEEG studies, Bancaud and Talairach observed that in some lesional epilepsy patients, the electrical discharges arising from the cerebral lesion did not respect anatomic boundaries [164]. Moreover, they also reported that seizures could be observed to arise from structures quite distant from the lesion and sometimes even different from the region where interictal spikes were most frequently observed. These observations showed the way for the generation of the concept of epileptogenic networks. The SEEG recordings played a very important role in this, as they provided simultaneous recordings from both cortical and subcortical structures, which were seen to be concurrently involved in seizure generation and propagation [163].

As epileptogenic networks, we nowadays define the brain regions that are involved in the generation and propagation of epileptic activity. They are a key concept for interpreting the epileptic process, which is extremely important in the context of epilepsy surgery [163]. Of course, in some cases, the EZ is defined by a relatively restricted region of the brain, in which the seizure generator corresponds to a unique dysfunctional area, like, for example, in some cases described by Rosenow and Luders [14]. However, there are many examples where the seizure onset is characterised by simultaneous activation of distinct and distant brain regions [29], [165]. The spatial organisation in such cases cannot be adequately described by the theory of the single focus, while epileptogenic networks provide a more comprehensive approach [163]. Figure 8 depicts the concept of the epileptogenic network alongside some of the most commonly known presurgical evaluation cortical zones.

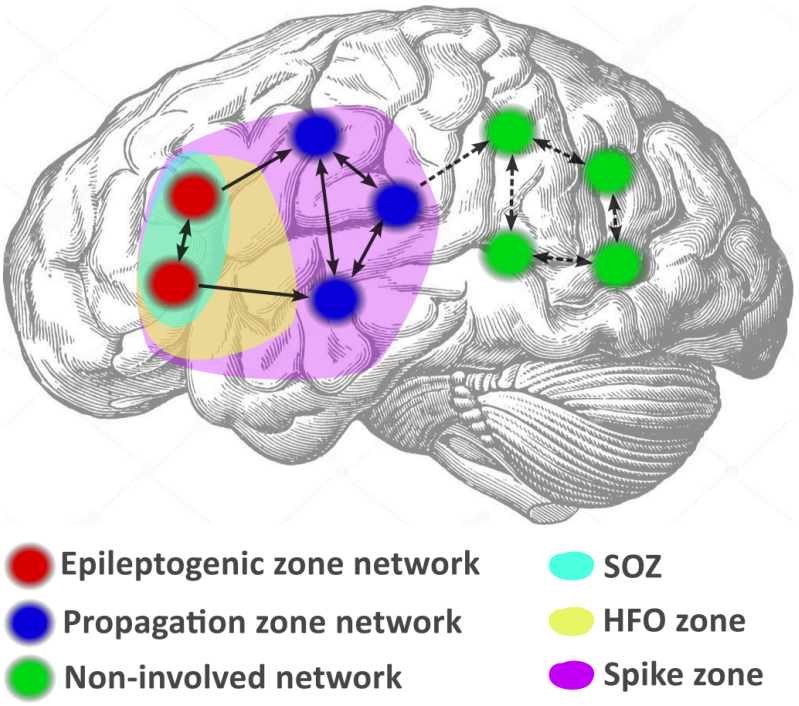

Figure 8: Schematic representation of the epileptogenic network together with some of the commonly known presurgical evaluation cortical zones. The epileptogenic network consists of the primary generators of epileptogenic activity (epileptogenic zone network), areas that this activity propagates to (propagation zone network), and areas that are not involved in epileptogenicity. SOZ: seizure onset zone, HFO: high-frequency oscillations

Interestingly, the actual neuropathologic mechanisms behind the generation and propagation of epileptic activity are not fully understood. The propagation of seizures is a complex construct that does not follow the classical propagation pattern of nerve flux [163]. Long delays are commonly observed between one area to another, something that may be attributed to biological changes in the involved regions [166], [167]. Structural connectivity also plays an important role in determining which anatomic sites are involved in each patient, as both cortical and subcortical structures are involved [168]. As a result, the propagation process is regulated by both local anatomic as well as connectivity properties and mechanisms, rather than passive conduction [163].

A thorough understanding of the network patterns underlying the epileptogenic process is essential for moving the promising field of network-based epilepsy biomarkers forward. This research path has skyrocketed in the recent epilepsy literature, especially through functional connectivity studies, which provide

quantifiable evidence of the underlying networks [33], [34]. In the following chapter, I define FC, discuss in depth the existing literature on interictal FC investigations of the epileptic brain, and identify the specific research gaps that I aim to address in the subsequent chapters.

Chapter 3

Functional Connectivity in the Epileptic Brain: Insights from Interictal iEEG studies

It has long been known that epileptic phenomena are associated with changes in brain synchrony [163]. Numerous studies have demonstrated that seizures (preictal, ictal, and postictal states) are associated with abnormal synchronisation of different (and often distant) brain structures, as indicated by connectivity studies [169], [170], [171], [172], [173]. A frequently reported pattern concerns increased synchronisation during the immediate preictal period followed by a subsequent decrease at seizure onset (ictal), and a re-increase after seizure termination (postictal) [170], [171]. This synchronisation/desynchronisation characteristic of the epileptogenic tissue has also been supported by graph theory works, which reported direct association between the seizure onset zone and nodes with increased total and outward strength during preictal [174] and ictal periods [175]. Cerebral connectivity, however, is also notably altered during the interictal period [34]. In this chapter, I provide an overview of interictal iEEG functional connectivity in the the epileptic brain, with a focus on its reported relevance and added value for epilepsy surgery.

3.1 Functional connectivity in the brain

Functional connectivity (FC) describes the statistical link between activities recorded from distinct brain structures, indicating how closely the underlying neuronal populations operate in sync [34]. The first attempts of FC analysis in EEG signals were made in the 1950s [176], and on ictal recordings in the 1980s [177]. Since then, the methods have developed following the rise of computers and digital

EEG systems [34], leading nowadays to an abundance of FC techniques. Nevertheless, according to studies that evaluated these methods in simulated signals, none of them is universal and their performance is strongly dependent on the type of model and dataset used [178], [179]. The different FC techniques can be distinguished based on some of their characteristics. A first distinction can be made according to methods being model-based or model-free. Model-based FC assumes linearity for the interactions between the studied signals, and includes techniques like simple correlation (Pearson), coherence and Granger causality [180]. On the other hand, model-free techniques, such as nonlinear correlation (h^2), mutual information, and transfer entropy, make fewer assumptions about the underlying process and are sensitive to both linear and nonlinear interactions [34]. A second differentiation has to do with whether FC is computed from the time (e.g., correlation, cross correlation, mutual information, and transfer entropy) or frequency domain representation of the signals (e.g., coherence, phase locking value, and phase slope index). For the latter, a Fourier or a wavelet transform usually decomposes the signals, and the interdependence between them is computed based on these frequency-resolved coefficients. Another distinction has to do with the ability of the FC method in revealing the directionality of the flow of information. Several methods can assess directionality (e.g., cross correlation, Granger causality, transfer entropy), while others cannot estimate this feature (e.g., simple correlation, mutual information, coherence, phase locking value). Directed connectivity techniques can range from the estimation of propagation delays using correlation measures (r or h^2), to stronger statements, like causality relationships between time series, such as the ones studied with Granger causality and transfer entropy [34].

Irrespective of the connectivity technique, when working with FC in electrophysiological data, and especially in intracranial EEG, there are important methodological aspects that need to be taken into account. Some of the parameters that may influence the results of iEEG FC analyses include: algorithms and parameters used [178], [179], montage and reference used [181], [182], distance between recorded channels [36], [183] (Figure 9A), duration of the period analyzed [184], frequency band under study [34] (Figure 9B), effect of the partial spatial sampling [185], power spectrum of the signals [186], and presence of interictal

epileptiform discharges (IEDs) [40] (Figure 9C). These should be kept in mind during the interpretation of the findings.

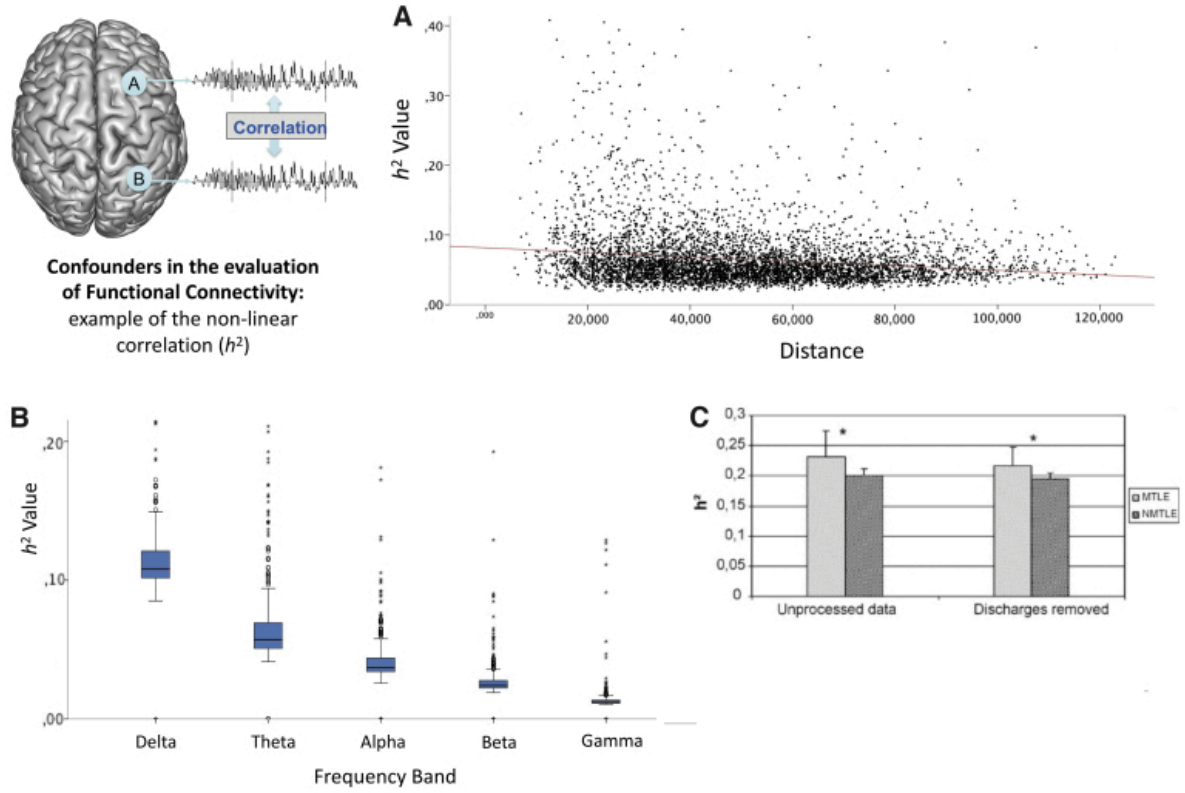

Figure 9: Confounders that may influence the functional connectivity estimates, through the example of the nonlinear correlation coefficient (h^2), adapted from [34]: A) Functional connectivity decreases as the inter-electrode distance increases. B) At higher frequencies, the connectivity values tend to be lower. C) The presence of IEDs in the data leads to slightly elevated FC compared to data segments with no IEDs, without, however, altering the level of difference between areas.

3.2 Functional connectivity during the interictal period

As mentioned above, studying the epileptic brain during the interictal period has gained the attention of the research community, mainly due to its inherent advantages over ictal recordings. Below, I review the current literature on interictal iEEG FC and its applications in identifying epileptogenic tissue and predicting surgical outcome in DRE patients. My discussion here extends insights from a review paper we recently published in the Brain Organoids and System Neuroscience Journal [33].

3.2.1 Existing literature on the links between interictal iEEG FC and epileptogenicity

Several studies have investigated interictal iEEG functional connectivity to explore if and how it is linked with the epileptogenicity of different brain structures. Different ways for grouping these works have been previously suggested. A recent review paper reported studies based on ECoG recordings separately from those that used SEEG [34], following the notion that the assessment of FC and brain networks is not superimposable when using different iEEG modalities [187]. In our own review paper, we made a distinction between studies that report interictal brain synchronicity after assessing the FC measures themselves, and those that compute and interpret graph theory properties (local or global) [33]. In the discussion that follows, I use no specific distinction criteria, since my work here is exploratory in nature, and it would be impractical to assign a study to a group while simultaneously assessing for all different features of interest (i.e. FC measures, graph properties, frequencies, etc.). I rather use a chronological order for reporting previous works to examine the evolution of interictal FC applications in epilepsy through the years.

One of the earliest attempts of interictal iEEG FC analysis was made by Towle et al. in 1998, who found local regions of high FC (coherence) over the diseased temporal lobe in 6/7 TLE patients, using ECoG recordings [188]. These early results were reinforced a year later by Arnold et al., who reported that the seizure-generating area of the brain exhibited higher FC than other regions, using a nonlinear interdependence measure [189]. In one of the first purely SEEG FC studies, Morman et al. (2000) computed the mean phase coherence (MPC) on bilateral SEEG recordings of 17 TLE patients, demonstrating increased synchronisation on the side of the epileptogenic focus compared to its contralateral non-focal analogue [190]. MPC was also used by Schevon et al. (2007), in an EGoG study, showing that local hypersynchrony regions (brain areas having markedly higher levels of synchrony compared to surrounding regions) had a significant association with the clinically determined EZ, however, not overlapping precisely but rather being adjacent to it [191]. Hypersynchronous structures were also found to overlap with the SOZ, in a combined ECoG-SEEG study of 6 neocortical epilepsy patients two years later (2009) [192]. In a larger work, Ortega et al. (2008), extended

the range of connectivity techniques (linear correlation, mutual information, and phase synchronisation) and frequencies (up to 400 Hz), also revealing clusters of local hypersynchrony in the temporal neocortex of 29 TLE patients [193].

Subcortical structures have also been found to be highly connected when belonging to the EZ. In a comparison study, Bettus et al. (2008) used SEEG to compare the FC in mesial temporal structures (hippocampus, entorhinal cortex, and amygdala) of 21 patients with Mesial Temporal Lobe epilepsy (MTLE) to a group of 14 non-MTLE patients, revealing significantly increased connectivity for the MTLE group [42]. Interestingly, these differences persisted even when spikes were removed. In the same line of comparison studies, a work by Warren et al. (2010) was the only one which compared data from epilepsy patients with patients without epilepsy (implanted for refractory facial pain), using ECoG recordings [194]. By computing linear correlation and MPC, they found that between connectivity (SOZ-non SOZ) was significantly lower than 1) within connectivities (SOZ-SOZ and non SOZ-non SOZ) and 2) the FC in controls [194]. A later work by Bettus et al. (2011) showed higher FC within the EZ (area primarily involved in seizures + having spikes) and the irritative zone (area secondarily involved in seizures + having spikes) than within the non-involved zones (NIZ) (areas with no spikes) [195]. These results were replicated later in a larger dataset (59 patients) by Lagarde et al. (2018), who used h^2 and showed that within-zone FC followed a hierarchy: within FC in EZ > within FC in propagation zone (PZ) > within FC in NIZ, with the EZ preferentially linked with the PZ rather than the NIZ [183].

Links between iEEG FC and epileptogenicity (Graph theory evidence)

The rise of graph theory tools for the analysis of brain networks has been a stepping stone for advancing FC-based investigations of the EZ. By considering iEEG electrodes as nodes and the connectivity values between them as edges, graph theory measures allow for a comprehensive grasp of the local topology of the network. In this line, Wilke et al. (2011) calculated betweenness centrality (BC) using directed transfer function (DTF) in a cohort of 25 patients [196], demonstrating that regions exhibiting high values of BC interictally are in close proximity to the SOZ,

especially in the gamma band. Varotto et al. (2012) also reported increased BC in the gamma band at contacts located inside the lesion of focal cortical displasia (FCD) II patients compared to outside [170]. This work also showed a significant increase in outgoing connections (out-density) inside compared to outside the lesion. Other local graph measures have also been associated with the EZ. The clustering coefficient and the characteristic path length, computed using synchronisation likelihood, were found to be significantly increased in the temporal lobe of MTLE patients compared to non-MTLE [40]. The same year, van Diessen et al. (2013) reported decreased nodal strength and eigenvector centrality (EC) in channels linked with the EZ (defined by HFOs and the SOZ), compared to the NIZ channels [197].

A series of works, all from the same research group, focused on the investigation of alpha band FC using graph theory in resting state SEEG data (awake, eyes closed or eyes-open). First, Goodale et al. (2020) used imaginary coherence to calculate the FC in 15 patients at rest (eyes closed) and found higher clustering coefficient, nodal BC, and edge BC in the clinically defined EZ compared to non-EZ areas [36]. Later the same year, Narasimhan and colleagues explored additional FC methods (imaginary coherence, mutual information, partial directed coherence, and directed transfer entropy) and extended the previous cohort to 25 patients [198]. This work found significantly increased strength and inward strength in ictogenic regions (clear seizure onset) compared to iritative and uninvolved areas, with their results also demonstrating a trend (non-significant, $p > 0.05$) for decreased outward strength in ictogenic areas. A later work from the same group (2022) confirmed the increase of alpha inward strength in the EZ compared to non-EZ tissue [199], something that was also observed in broadband (1-250 Hz) by another team, later the same year [41].

Taking into consideration that using either the clinically defined EZ or the SOZ for defining the epileptogenic areas of patients comes with inherent limitations, such as the misjudgement of the EZ or the potential incomplete coverage of the true SOZ, led some researchers on the use of an operational definition of the EZ, namely the Resection Zone (RZ). Despite this definition is pragmatic and close to the clinical practice of epilepsy surgery, it also has several disadvantages:

I. Patients who do not continue with the surgery are excluded (up to 50% of SEEG-explored patients) [34]
II. Non epileptic regions can oftentimes be included in the resection (e.g., anterior temporal lateral neocortex in standard anterior temporal lobectomy, or lateral structures on the surgical access to mesial EZ) [34]
III. Epileptic tissue could be exluded due to its proximity to the eloquent cortex [34]

Following this direction, Park and Madsen (2018) showed that interictal FC (nodal outward strength) predicted better than chance the EZ (defined by the Ictally Active Electrodes) and the RZ [200]. Shah et al. (2019) also investigated the connectivity properties of resected and non-resected tissue [38]. By computing linear correlation on iEEG data of 27 patients, they found a gradual decrease of FC (nodal strength): within-RZ > RZ-non RZ > within-non RZ in all bands. A recent work by Rijal et. al. (2023) explored FC both between resected vs. non-resected electrodes and also between clinically defined SOZ vs. non-SOZ channels [37]. By studying 31 patients using amplitude envelope correlation (AEC), orthogonalized AEC (oAEC), and phase locking value (PLV), they found increased nodal strength inside resection compared to outside resection only in good outcome patients. The same pattern was also reported for the SOZ, however, in fewer frequencies. An interesting finding of this work was that, in the presence of spikes, nodal strength was elevated compared to iEEG data without spikes. A similar work from the same group has also assessed oAEC and PLV in data with and without spikes in 37 patients [31]. They found increased nodal strength inside resection in good outcome patients for data with IEDs and without IEDs. They also found increased centralities (mainly betweenness and closeness) inside resection compared to outside in good outcome patients.

The studies discussed above, which are summarised in Table 4, consistently highlight the correlation between local clusters of increased FC with epileptogenic tissue.

Table 4: Summary of studies on interictal functional connectivity using intracranial EEG. Studies are presented in chronological order.

Authors	Patient population	FC method	Frequency range	Findings
Towle et al. (1998)	25 patients (12 TLE)	coherence	δ to high β (1-32 Hz)	Localised regions of high coherence inside/near the EZ
Arnold et al. (1999)	2 patients (1 MTLE, 1 neocortical)	"nonlinear interdependence"	broadband (0.5-40 Hz)	Increased FC (interdependence) in the EZ
Morman et al. (2000)	17 patients with TLE	mean phase coherence	broadband (0.5-85 Hz)	Increased synchronisation in the cortical side of the EZ
Schevon et al. (2007)	9 neocortical patients	mean phase coherence	broadband (0.1-54 Hz or 0.5-65 Hz)	Area of local hypersynchrony overlapping with the EZ (not completely, rather being adjacent)
Ortega et al. (2008)	29 patients with TLE	linear correlation, mutual information, and phase synchronization	broadband (0.5-400 Hz)	Clusters of local hypersynchrony in the temporal neocortex
Bettus et al. (2008)	35 patients (21 MTLE, 14 non-MTLE)	Nonlinear correlation (h^2)	δ to high γ (0.5-97 Hz)	For θ, α, β and γ bands: Increased FC (h^2) in mesiotemporal structures when they belong to the EZ
Dauwels et al. (2009)	6 neocortical patients	cross-correlation, directed transfer function, phase synchrony, magnitude coherence	broadband (4-30 Hz)	Overlap between areas of local hypersynchrony and the SOZ
Warren et al. (2010)	4 epilepsy vs. 2 chronic pain patients	linear cross-correlation, mean phase coherence	δ to HFOs (0.5 - 500 Hz)	For all bands except HFOs: between FC (SOZ-non SOZ)< within FC (SOZ-SOZ or nonSOZ-nonSOZ)< between FC in healthy (no epilepsy)
Bettus et al. (2011)	5 patients with TLE	nonlinear correlation (h^2)	δ to γ bands (0.5-80 Hz) + broadband	For β band: Higher FC within the EZ and the irritative zone (area secondarily involved in seizures) than within the NIZ

Wilke et al. (2011)	25 neocortical patients	directed transfer function	θ to γ bands (3-50 Hz)	For γ band: Close proximity between active areas (regions exhibiting high amounts of BC interictally) and the SOZ
Varotto et al. (2012)	10 neocortical patients (FCD II)	partial directed coherence	δ to γ bands (1-80 Hz)	For γ band: Increased BC at contacts located inside the lesion of FCD II patients compared to outside
Bartolomei et al. (2013)	19 patients (11 MTLE, 8 non-MTLE)	synchronization likelihood	δ to γ bands (0.5-90 Hz) + broadband	For all but γ bands: Increased clustering coefficient and characteristic path length in mesiotemproral structures when they belong to the EZ
van Diessen et al. (2013)	12 patients	phase lag index	δ to γ bands (0.5-50 Hz) + broadband	Decrease in strength and EC at the theta band, in channels linked with the EZ, compared to the NIZ channels
Lagarde et al. (2018)	59 patients (20 TLE)	nonlinear correlation (h^2)	δ to γ bands (0.5-80 Hz) + broadband	For broadband: Gradual decrease of FC: EZ > PZ > NIZ They also showed that EZ is preferentially linked with the PZ than the NIZ
Park and Madsen (2018)	25 patients (10 TLE)	granger causality	broadband (~0.5-100 Hz)	FC (outstrength) predicted better than chance the EZ and the RZ
Shah et al. (2019)	27 patients (18 TLE)	linear correlation	θ to high γ bands (5-105 Hz) + broadband	For all bands: Gradual decrease of FC (node strength): within RZ > between RZ-non RZ > within non RZ
Goodale et al. (2020)	15 patients (12 TLE)	imaginary coherence	δ to α bands (1-12 Hz)	Higher clustering coefficient, nodal betweenness centrality, and edge betweenness centrality in the clinically defined EZ compared to non-EZ tissue

Narasimhan et al. (2020)	25 patients (18 TLE)	mutual information, imaginary coherence, partial directed coherence, directed transfer entropy	α band (8-12 Hz)	Gradual decrease of FC (strength and inward strength): EZ > PZ > Irritative zone > NIZ
Paulo et al. (2022)	32 patients (18 TLE)	imaginary coherence, partial directed coherence	α band (8-12 Hz)	Increase of alpha inward strength in the EZ compared to non-EZ tissue
Jiang et al. (2022)	37 patients (23 TLE)	directed transfer function, cross-frequency directionality	broadband (1-250Hz)	Significantly higher inward information flow in the SOZ compared to non-SOZ
Rijal et al.. (2023)	31 patients (15 TLE)	Amplitude envelope correlation, orthogonalized amplitude envelope correlation, phase locking value	δ to high γ bands (2-90 Hz)	For all frequencies: Higher nodal strength inside resection compared to outside resection (only in good outcome patients). Same results for the SOZ, but only in δ, α, low γ, and high γ

EZ: epileptogenic zone; FC: functional connectivity; FCD: focal cortical dysplasia; HFOs: high frequency oscillations; irritative zone: area with interictal spikes but no seizures; NIZ: noninvolved zone; PZ: propagation zone; RZ: resection zone; SOZ: seizure onset zone; TLE: temporal lobe epilepsy; MTLE: mesial temporal lobe epilepsy.

3.2.2 Links between interictal iEEG FC and surgical outcome

Several studies have assessed the value of specific FC characteristics in predicting surgical outcome. First, Schevon et al.(2007) demonstrated that complete resection of local hypersynchrony regions improves clinical outcome [191], something that was challenged a year later in an ECoG study by Ortega et. al, who found no strong evidence that a complete resection of synchronisation clusters would result in a good surgical outcome [193]. Nevertheless, this could be due to the fact that the majority of the patients in this latter study were treated with anterior temporal lobectomy, while according to Lagarde et al., ECoG is mainly sensitive to the dynamics of the lateral temporal neocortex [34]. In another study, Antony et al. (2013) studied FC using linear correlation in recordings from both mesiotemporal

and neocortical structures of 23 TLE patients [201]. They found that good outcome patients had significantly lower mean strength values and lower variability of connections compared to poor outcome patients. Their FC-trained Support Vector Machine (SVM) classifier managed to predict surgical outcome with 87% accuracy. In contrast, Lagarde et al. (2018) showed that patients had worse outcomes if they exhibited high values of FC within the NIZ [183]. Similar findings have been reported the same year by Grobelny et al., in a study of 36 patients, who showed that individuals not seizure-free after surgery had a higher mean value of BC in the interictal period, while they also presented greater proportions of extreme-valued BC nodes [202].

Some studies have supported that higher FC inside the presumed EZ is associated with favourable surgical outcomes. In their work, Shah et al. (2019) found that high nodal strength values within the resection zone are linked with good surgical outcomes [38]. They additionally showed that the higher the overlap between the RZ and nodes with the highest strength, the better the outcome. In the same vein, Goodale et al. (2020) found a moderate relationship between high EZ connectivity and favourable outcome [36]. Interestingly, in a later study, the same group found no significant differences in FC of the EZ between good and poor outcome patients [199]. Moreover, larger within-frequency information flow asymmetry between SOZ and non-SOZ was associated with favourable seizure outcome in a study by Jiang et al. (2022) [41]. In their recent work, Rijal et al. (2023) found increased overlap of hubs (brain regions with high nodal strength) and resection in good patients, while they also showed that resection of highly connected hubs during the interictal period predicted outcome with an accuracy up to 81% [37]. Similar results were reported by Corona et al. (2023), who predicted postsurgical outcome based on hub resection with up to 68% accuracy [31].

The aforementioned studies are summarised in Table 5. Overall, existing literature indicates that higher FC within the EZ and more pronounced differences with the FC of NIZ are factors associated with favourable surgical outcomes.

Table 5: Summary of studies that link interictal functional connectivity and surgical outcome. Studies are presented in chronological order.

Authors	Patient population	FC method	Frequency range	Findings
Schevon et al. (2007)	9 neocortical patients	mean phase coherence	broadband (0.1-54 Hz or 0.5-65 Hz)	Complete resection of local hypersynchrony regions improves clinical outcome
Ortega et al. (2008)	29 patients with TLE	linear correlation, mutual information, and phase synchronisation	broadband (0.5-400 Hz)	No correlation between the complete resection of synchronisation clusters and good postsurgical outcome
Anthony et al. (2013)	23 patients with TLE	linear correlation	broadband (5-50 Hz)	Lower mean strength values and lower variability of connections are associated with good surgical outcome
Lagarde et al. (2018)	59 patients (20 TLE)	nonlinear correlation (h^2)	δ to γ bands (0.5-80 Hz) + broadband	Worse outcome if higher FC within NIZ
Grobelny et al. (2018)	36 patients	Directed Transfer Function	9 frequency ranges with centres at 2, 4, 7, 11, 13, 30, 50, 82, and 135 Hz	For frequencies above 11 Hz: Poor surgical outcome was associated with increased average BC and greater proportions of extreme-valued BC nodes
Shah et al. (2019)	27 patients (18 TLE)	linear correlation	θ to high γ bands (5-105 Hz) + broadband	For broadband and beta: High FC (high nodal strength) within the resection zone is associated with good surgical outcomes
Goodale et al. (2020)	15 patients (12 TLE)	imaginary coherence	δ to α bands (1-12 Hz)	For alpha: Possible moderate relationship between high epileptogenic zone functional connectivity and favorable outcome

Paulo et al. (2022)	32 patients (18 TLE)	imaginary coherence, partial directed coherence	α band (8-12 Hz)	No difference in the FC of the EZ of good outcome and the EZ of poor outcome patients
Jiang et al. (2022)	37 patients (23 TLE)	directed transfer function, cross-frequency directionality	broadband (1-250Hz)	Larger within-frequency information flow asymmetry between SOZ and non-SOZ is associated with favorable seizure outcome Weaker SOZ to non-SOZ information flow strength and stronger non-SOZ to SOZ information flow strength in seizure-free patients
Rijal et al.. (2023)	31 patients (15 TLE)	Amplitude envelope correlation, orthogonalized amplitude envelope correlation, phase locking value	δ to high γ bands (2-90 Hz)	For beta band: Increased overlap of hubs (nodes with high nodal strength) with resection in good- compared to poor-outcome patients For delta and low gamma band: Increased overlap of hubs with SOZ in good- compared to poor-outcome patients
Corona et al. (2024)	37 patients	Amplitude envelope correlation, phase locking value	δ to γ bands (1-50 Hz) + broadband	Resection of network hubs (nodes with high nodal strength) was associated with good surgical outcome

3.2.3 Interictal iEEG FC at high frequencies

Most of the studies discussed so far explored functional connectivity at either the broadband or specific sub-bands of the conventional frequency spectrum (0.5–80 Hz). The networking of the epileptic brain at the frequency range of HFOS

(80-500Hz) is of particular interest and can provide important insights, as high-frequency activity is highly connected to the epileptogenic process. However, very limited work has been done in this direction.

In an already mentioned study, Warren et al. (2010), found no significant differences in the FC between SOZ-NIZ, compared to within FC (SOS-SOZ or NIZ-NIZ) and the FC of control patients (implanted for facial pain) in the HFO band (75-500 Hz) [194]. In contrast, Shah et al. (2019), who studied FC at frequencies up to the lower end of the HFO band (90-105 Hz), found that FC within the RZ was significantly stronger than between RZ - nonRZ, and within nonRZ - nonRZ [38]. The same year, Zweiphening et al. used short-time direct directed transfer function (SdDTF) across different bands to study the connectivity in 18 patients with malformation of cortical development (MCD) or tumour [203]. Their results revealed that good outcome patients had significantly increased total strength and outstrength inside resection compared to outside, for the gamma and ripple bands. They also found that channels with interictal epileptiform events (spikes or HFOs) presented lower total strength and instrength and higher outstrength in the fast ripple (FR) band, a higher outstrength in the ripple band, and a higher total, instrength and outstrength in the gamma band. A recent work by Shen et al. (2023) studied the FC in the HFO band (80-500 Hz), using skewness-based functional connectivity in 59 patients [39]. Their results showed increased strength inside resection compared to outside, both in good and poor outcome patients, while they also reported that patients with poor outcome demonstrated increased strength in the non-resected tissue. Table 6 summarises the studies discussed above.

Table 6: Summary of studies that investigated interictal iEEG FC at the HFO band. Studies are presented in chronological order.

Authors	Patient population	FC method	Frequency range	Findings
Warren et al. (2010)	4 epilepsy vs. 2 chronic pain patients	linear correlation, mean phase coherence	HFOs (75- 500 Hz)	No significant differences in the FC between SOZ-NIZ, compared to within FC (SOS-SOZ or NIZ-NIZ) and the FC of control patients (refractory facial pain)
Shah et al. (2019)	27 patients (18 TLE)	linear correlation	high γ (90-105 Hz)	FC within the RZ was significantly stronger than between RZ - nonRZ, and within nonRZ - nonRZ
Zweiphening et al. (2019)	18 patients with MCD or tumour	short-time direct directed transfer function	θ (4–8 Hz), γ (30–80 Hz), ripples (80–250 Hz), fast ripples (250–500 Hz)	For γ and ripple bands: Increased total strength and outstrength inside resection compared to outside of good outcome patients. Channels with spikes or HFOs presented: i) lower total strength and instrength and higher outstrength in the FR band, ii) higher outstrength in the ripple band, ii) higher total, instrength and outstrength in the γ band
Shen et al. (2023)	59 patients (24 with TLE)	Time-varying skewness	HFO band (80-500 Hz)	Increased strength inside resection compared to outside, both in good and poor outcome patients. Increased connectivity in the non resected tissue of poor outcome compared to good outcome patietnes.

3.2.4 Knowledge gap

From the above discussion, it becomes evident that interictal FC at high frequencies (especially > 80 Hz) and its applications for the localisation of the EZ and the prediction of surgical outcome are greatly unexplored. Even less studied is the effect that HFOs have on FC computations, with very few works having approached this issue [197], [203], [204]. Here, I aim to address these research gaps by exploring FC at a wide spectrum of frequencies (from δ to fast ripples) while working with data both with and without HFOs. In the following chapter, I introduce the dataset and techniques used to generate the personalised functional networks, which will serve as the basis for my investigations during later chapters.

Chapter 4

Dataset and Network Construction

In this chapter, I start by introducing the iEEG dataset used in this work, from initial cohort selection to the acquisition of recordings. I discuss how these data were pre-processed and describe step-by-step the HFO detection pipeline followed in my work. Finally, I outline the different methodologies followed for the computation of functional connectivity matrices and show how these patterns transition to networks using graph theory principles.

4.1 iEEG dataset: Acquisition and Analysis

In order to have a pragmatic definition of the EZ, the analysis required knowledge on each patient's resected brain area and surgical outcome (reported at least one year post-surgery), information that only retrospective datasets could offer. As such, I looked in open-access repositories (CRCNS.org, OpenNeuro, IEEG.org, etc.) for iEEG datasets with the following specifications:

I. Interictal recordings acquired during non-rapid eye movement (non-REM) sleep for easier HFO event detection
II. Sampling rate > 2000 Hz to allow HFO analysis (due to the Nyquist theorem restriction) [118]
III. Resected electrodes identified and provided
IV. Patients with both good and poor surgical outcomes included.

I found and selected a single-centre dataset adhering to the above requirements, the details of which are presented in the following section.

4.1.1 Retrospective iEEG dataset

Long-term iEEG recordings from 20 DRE patients were obtained from CRCNS.org (iEEG Dataset-CRCNS.org, accessed on 28/10/2025), where they are

freely available and fully anonymous [205]. These data were acquired at the Neurosurgery Department of the University Hospital of Zurich from March 2012 to April 2016 [206], in the context of routine presurgical evaluations. Each of these patients underwent epilepsy surgery, and their postsurgical seizure outcome was determined in follow-up visits and classified according to the International League Against Epilepsy (ILAE) score ranking system [207].

4.1.1.1 Electrode implantation

The recordings were obtained using subdural strip and grid electrodes as well as depth electrodes, placed according to the findings of the non-invasive presurgical evaluation. In temporal lobe epilepsy (TLE) patients, depth electrodes (1.3 mm diameter, 8 contacts of 1.6 mm length, spacing between contact centres 5 mm, Ad-Tech) were implanted bilaterally into the amygdala, the entorhinal cortex, the anterior hippocampus, and the posterior hippocampus. In extratemporal epilepsy (ETE) patients, a combination of depth and subdural grid and strip electrodes (contact diameter 4 mm with a 2.3 mm exposure, spacing between contact centres 10 mm, Ad-Tech) was placed after craniotomy. Figure 10 depicts the iEEG implantation of an ETE patient in the dataset, with a combination of ECoG and SEEG electrodes.

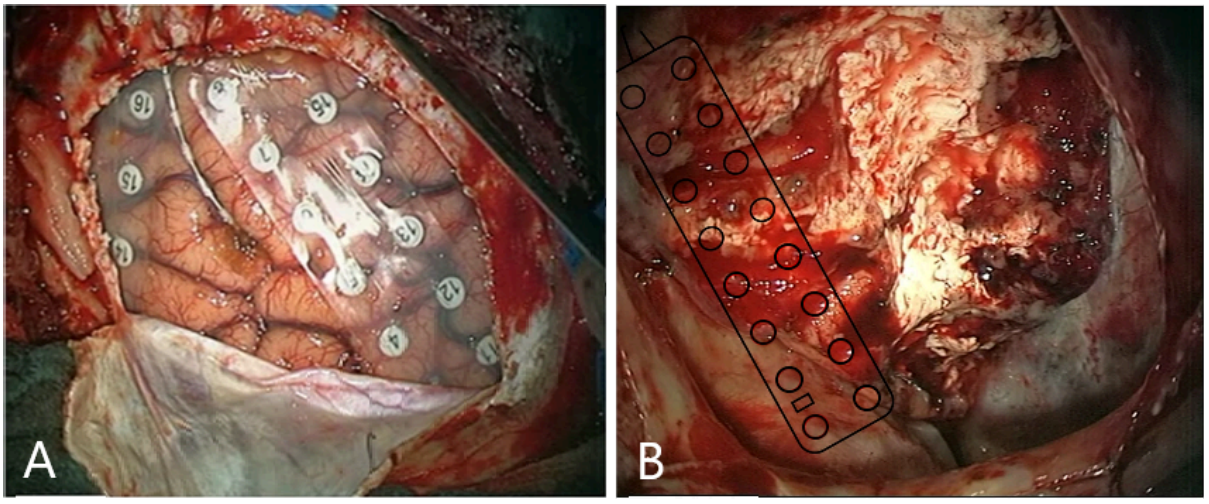

Figure 10: Combination of two subdural grid and one depth electrode implanted after open craniotomy in patient #17. The photographs were taken A) before resective surgery, B) after the surgery. Adapted from [206].

4.1.1.2 Data acquisition

Data was acquired at a sampling frequency of 4000 Hz with an ATLAS recording system (0.5-1000 Hz pass-band, NeuraLynx) and down-sampled to 2000 Hz. The iEEG of each patient was recorded against a common intracranial reference.

In addition, scalp EEG, according to the 10-20 system, with minor adaptations in order to avoid the surgical scalp lesions, and the submental electromyogram (EMG) were recorded. Pre-iEEG implantation and post-implantation MRIs were also taken. However, in the online publicly available dataset, the EEGs, EMGs and MRIs were not included for any patient. For further details on the drawbacks associated with the absence of MRIs, see Section 5.4.4.

4.1.1.3 Data selection

For every patient, from each night recording up to six sample intervals (depending on the recording's length), each containing five minutes of interictal slow-wave sleep, were selected by the initial authors for inclusion in the current data set. They performed sleep scoring based on scalp EEG, electro-oculogram, EMG and video recordings. Each segment had at least three hours distance from a seizure event to minimise the effects of ictal periods in the iEEG signals. The number of nights and intervals varied across patients.

4.1.1.4 Surgical resection

The decision for resection surgery was based on non-invasive investigations as well as on intracranial guidance [206]. After surgery, the electrodes that were resected were marked, and this information was included in the dataset, together with the type of surgical approach and surgical outcome of each patient (assessed at least 1 year post surgery) according to the ILAE ranking (ILAE1=Seizure Freedom, ILAE2-6=Recurrent Seizures).

4.1.1.5 Dataset demographics and statistics

In the cohort of 20 DRE patients, the mean age was 32.5 ± 11.7 years, with 68.4 % being males. Histopathological analysis revealed that the most common pathology was focal cortical dysplasia (FCD) (n=8, 40%), followed by hippocampal sclerosis

(HS) (n=7, 35%), tumour (n=2, 10%), cavernoma (n=1, 5%), gliosis (n=1, 5%), and a case of combined gliosis and HS (n=1, 5%). Of the 20 patients, 9 were diagnosed with TLE and 11 with ETE. All patients underwent iEEG implantation with either depth (n=8), subdural (n=5), or a combination of depth and subdural electrodes (n=7). After surgical resection, 13 patients had a good outcome (ILAE 1), while 7 patients presented recurrent seizures (ILAE 2-6) (average follow-up of 25 months). In total, 172 electrodes were located inside and 428 electrodes outside the surgical resection margins. Patient demographics are summarised in Table 7.

Table 7: Demographics of the patient cohort, adapted from [206].

Patient	Gender / Age	Histology/ Pathology	Epilepsy type	Electrode type	Surgery	# of bipolar elec. (# of resected)	Outcome / ILAE score
1	M / 25	HS and gliosis	TLE	Depth & Strip	sAHE; Les	43 (9)	1
2	M / 33	Glioma	TLE	Depth	sAHE; Les	56 (12)	1
3	F / 20	HS	TLE	Depth	sAHE	35 (12)	1
4	F / 20	HS	TLE	Depth	sAHE	56 (12)	1
5	M / 40	HS	TLE	Depth	sAHE	56 (12)	1
6	M / 48	HS	TLE	Depth	sAHE	56 (12)	1
7	M / 25	HS	TLE	Depth	sAHE	56 (12)	3
8	F / 21	HS	TLE	Depth	sAHE	56 (12)	3
9	M / 52	HS	TLE	Depth	sAHE	56 (12)	5
10	M / 37	FCD 2b	ETE	Grid & Strip	Les	37 (3)	1
11	M / 36	FCD 2b	ETE	Grid & Depth	Les	72 (3)	1
12	M / 49	Ganglioglioma	ETE	Grid & Depth	Les	40 (21)	1
13	M /17	FCD 1a	ETE	Grid & Depth	Les	60 (3)	1
14	F / 46	FCD 1b	ETE	Grid & Strip & Depth	Les	47 (1)	1
15	F / 31	Gliosis	ETE	Grid & Strip	Les	30 (4)	1
16	F / 17	FCD 2a	ETE	Grid & Depth	Les	40 (3)	1

17	M / 30	FCD 2a	ETE	Grid & Depth	Les	39 (30)	5
18	M / 40	FCD 2a	ETE	Strip & Depth	Les	23 (3)	5
19	M / 38	Cavernoma	ETE	Grid	Les	46 (6)	6
20	M / 17	FCD 3	ETE	Grid	Les	14 (5)	5

M=male: F=female; HS=hippocampal sclerosis; FCD=focal cortical dysplasia; TLE=temporal lobe epilepsy; ETE=extratemporal epilepsy; Les=lesionectomy; sAHE=selective amygdalahippocampectomy; ILAE=International League Against Epilepsy;

4.1.1.6 Ethical considerations

No ethical considerations were raised throughout the present study. The dataset used was already acquired at the Neurosurgery Department of the University Hospital of Zurich from 2012 to 2016, where ethical approval was obtained by the research ethics committee (Kantonale Ethikkommission KEK-ZHNr. 2012–0212) and collection of patients' written informed consent was waived [206]. I obtained the data from CRCNS.org (iEEG Dataset-CRCNS.org, accessed on 28/10/2025), where they were freely available for researchers and were also fully anonymous. Finally, this work is not meant in any way to be used for clinical purposes, but only to guide and propel future research.

4.2 Data preprocessing

4.2.1 Manual 3D modelling of iEEG implantations

For preprocessing the raw iEEG data, I worked in MATLAB and more specifically in the Brainstorm environment [208]. The first step was to create personalised 3D models for each patient's iEEG implantation, to enable visual representation of the networks generated later on. In the absence of anatomical data in the current dataset, each patient's brain anatomy was represented by the Montreal Neurological Institute (MNI) ICBM152 template, which included all the basic surfaces (head, outer skull, inner skull, and cortex). The co-registration of the iEEG electrodes was done in an approximating manner, with each electrode's position manually fixed on the 3D brain model according to 2D iEEG placement representations provided within the

dataset's documentation. Two representative examples of 3D representations of a purely SEEG (Patient #4) and a combined SEEG and ECOG implantation (Patient #16) can be seen in Figure 11. Similar figures for all patients can be found in Appendix 1.

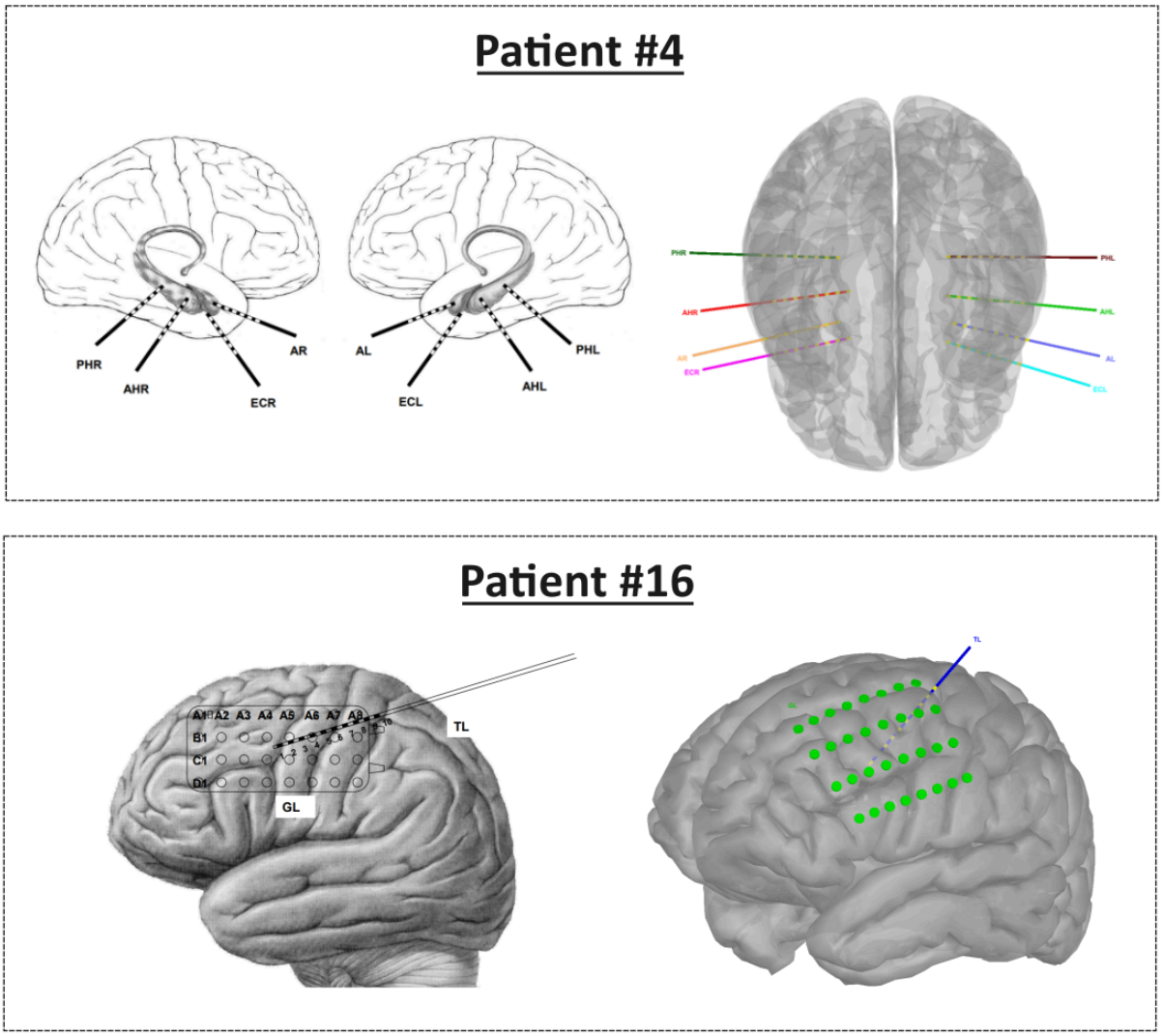

Figure 11: 3D representations (right), created manually in Brainstorm from the 2D implantation schemes provided in the dataset's documentation (left). A) Patient #4: purely SEEG implantation bilaterally into the hippocampus and parahippocampal areas. B) Patient #16: combined SEEG and ECOG implantation in the left frontocentral region.

4.2.2 iEEG data re-referencing and filtering

The raw iEEG data for each patient were transformed from the common intracranial reference into a single-spacing bipolar montage (Ch1-Ch2, Ch2-Ch3, Ch3-Ch4,...). This choice was made as, according to the literature, a bipolar montage is generally preferred over a monopolar when studying HFOs [118]. In addition, single spacing is commonly chosen over double spacing (Ch1-Ch2, Ch3-Ch4, Ch5-Ch6,...) when the patient is implanted with less than 150 electrodes [209], which is the case for all patients of the current dataset. Information on the resection status of the electrodes (resected or non-resected) was also provided in a bipolar format, which further pushed for the use of this montage in this work. In TLE patients (Patients 1-9), only the 3 most mesial bipolar channels were considered for further analysis, since no information was available on the resection status of the remaining (more lateral) SEEG contacts. As indicated in the dataset's documentation, channels in which electrical stimulation caused motor or language responses were marked as "important eloquent tissue" and were removed from further analysis. All raw data were subsequently notch filtered at 50Hz (2nd order IIR filter with zero lag phase), to control for line noise (50 Hz: line noise frequency in Switzerland).

4.2.3 Extraction of data segments with and without HFOs

For each night of iEEG recording of every patient, I extracted twenty non-overlapping 3-second segments of interictal data with HFOs and twenty segments without HFOs. As a segment with HFOs, I defined a 3-sec. data section which contained at least one HFO, either ripple (80-250 Hz) or fast ripple (250-500 Hz), at any of the intracranial bipolar electrodes. As a segment without HFOs, I defined a 3-sec. data section which did not contain any HFOs, at any of the electrodes. A total of 1 minute of data (20 x 3 sec.) was chosen since this data amount was found to generate stable FC networks [31], [37], [210], [211].

The detection of HFO events was performed manually inside the Brainstorm environment by a single reviewer of our group (Christos Stergiadis). In each patient, the following steps were carried out:

1. From every night of recording, I randomly chose one of the 5-minute iEEG intervals.
2. I projected all data (from all electrodes) simultaneously on the computer screen (24.8” LG monitor, 1980x1080), grouped by electrode (and hemisphere, in cases of bilateral SEEG implantation).
3. I applied a visual band-pass filter to the data, one time between 80 and 250 Hz (to detect ripples) and one time between 250 and 500 Hz (to detect fast ripples).
4. For ripples:
    I. I set the amplitude of the signals to 50μV/cm, following the suggestion of 5μV/mm in [118]
    II. I set the time scale to ~1.5 seconds per page (1050 pixels/second)
    III. I marked as a ripple an event with at least 4 oscillations clearly standing out from the background with a duration of up to ~100ms (Figure 12)
    IV. for each suspected event I switched to the raw (broadband) signal to ensure that the event is not the byproduct of filtering of an interictal spike (Figure 13)
    V. I discarded spike-ripples
5. For fast ripples:
    I. I set the amplitude to 25μV/cm
    II. I set the time scale to ~1.5 seconds per page (1050 pixels/second)
    III. I marked as a fast ripple an event with at least 4 oscillations clearly standing out from the background with a duration of up to ~40ms
6. HFO events (ripples or fast ripples) occurring less than 10 ms apart in the same electrode were considered a single event.

In cases where not enough HFOs could be identified from a single interval, then I chose an additional interval from the same night and followed the same procedure until I achieved the target of twenty in total non-overlapping 3-sec. segments with HFOs.

For the detection of segments without HFOs, twenty 3-sec. data segments were extracted, with each of them showing no high-frequency activity (stable HFA or HFO events) in the ripples and fast ripples bands simultaneously. I aimed for segments that were characterised by relatively stable, non-rapid EEG activity.

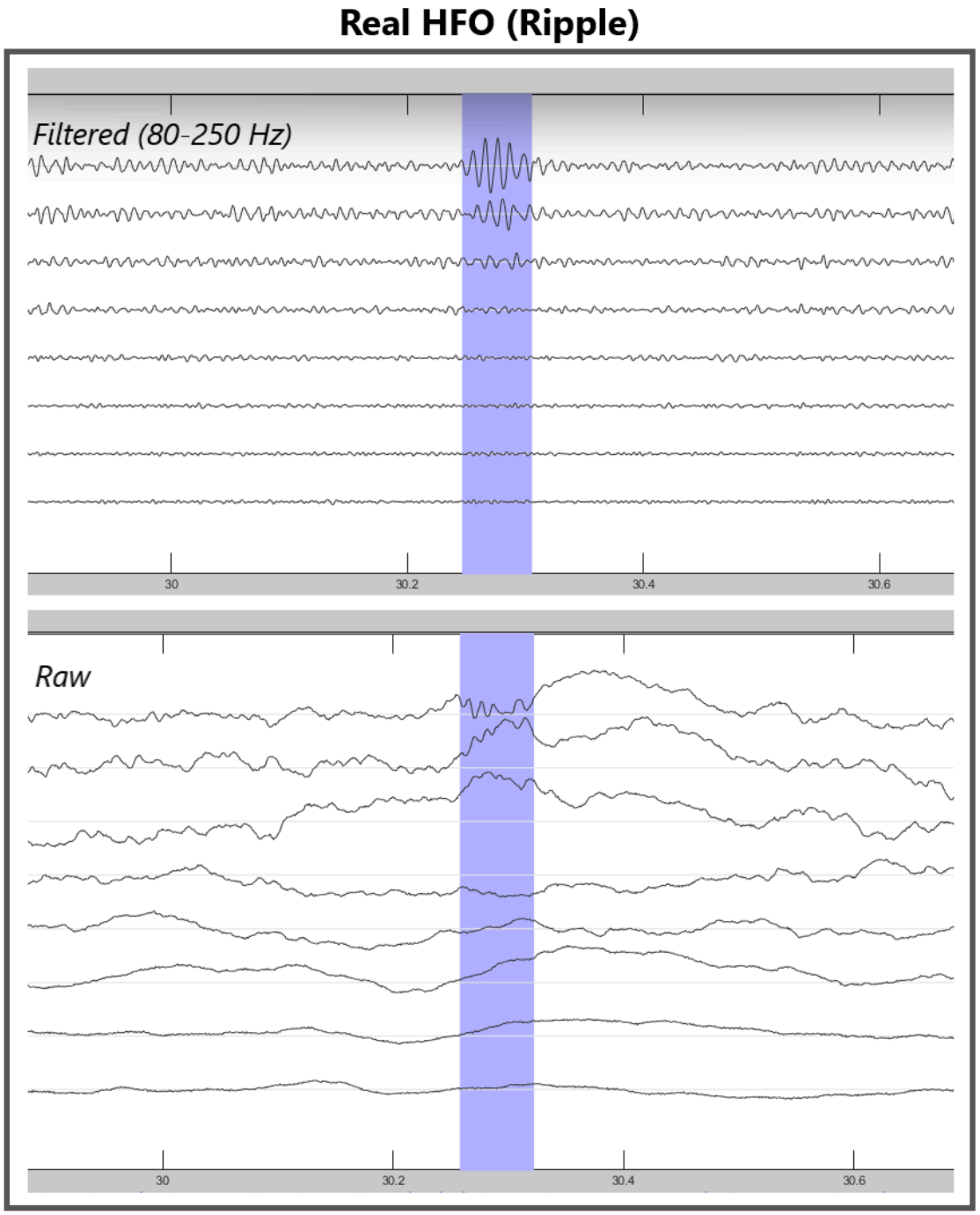

Figure 12: Detection of a High Frequency Oscillation (HFO) inside the Brainstorm environment. A representative HFO in the iEEG recording of patient #12 is depicted in the filtered (top) and raw/broadband signal (bottom).

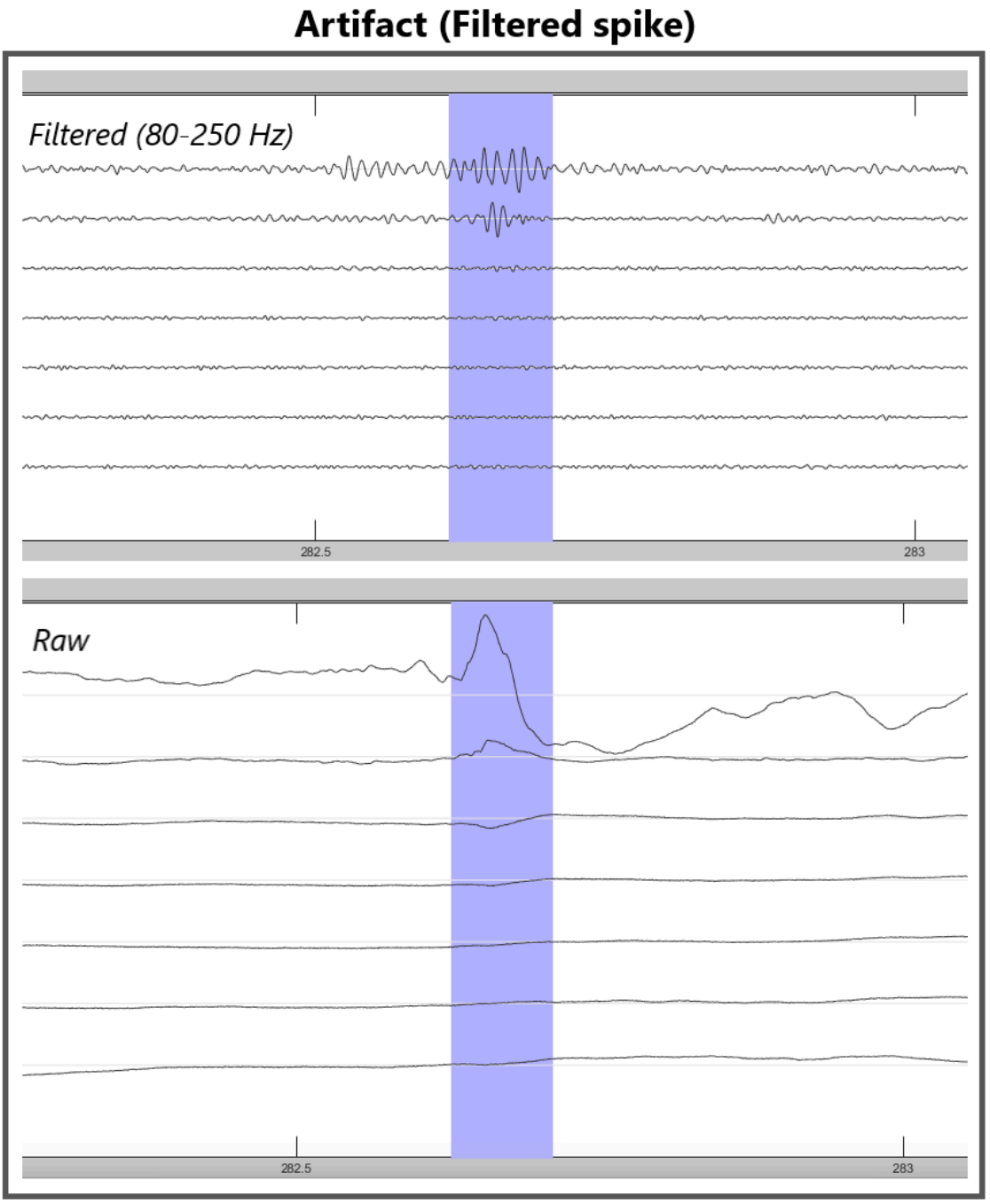

Figure 13: A representative HFO-like artifact (top) generated due to the filtering of an interictal spike (bottom).

By following the above pipeline, I ended up with 18 DRE patients having at least one night of recordings where 1 min. (20 x 3sec.) of data with HFOs and 1 min. of data without HFOs could be extracted. Patient 8 and Patient 15 were excluded from further analysis as the recordings of the former did not contain enough HFO events, while the data of the latter presented very frequent high-amplitude activity at the ripple band, making it impossible to clearly detect single HFO events on one hand and clean background activity on the other (Figure 14).

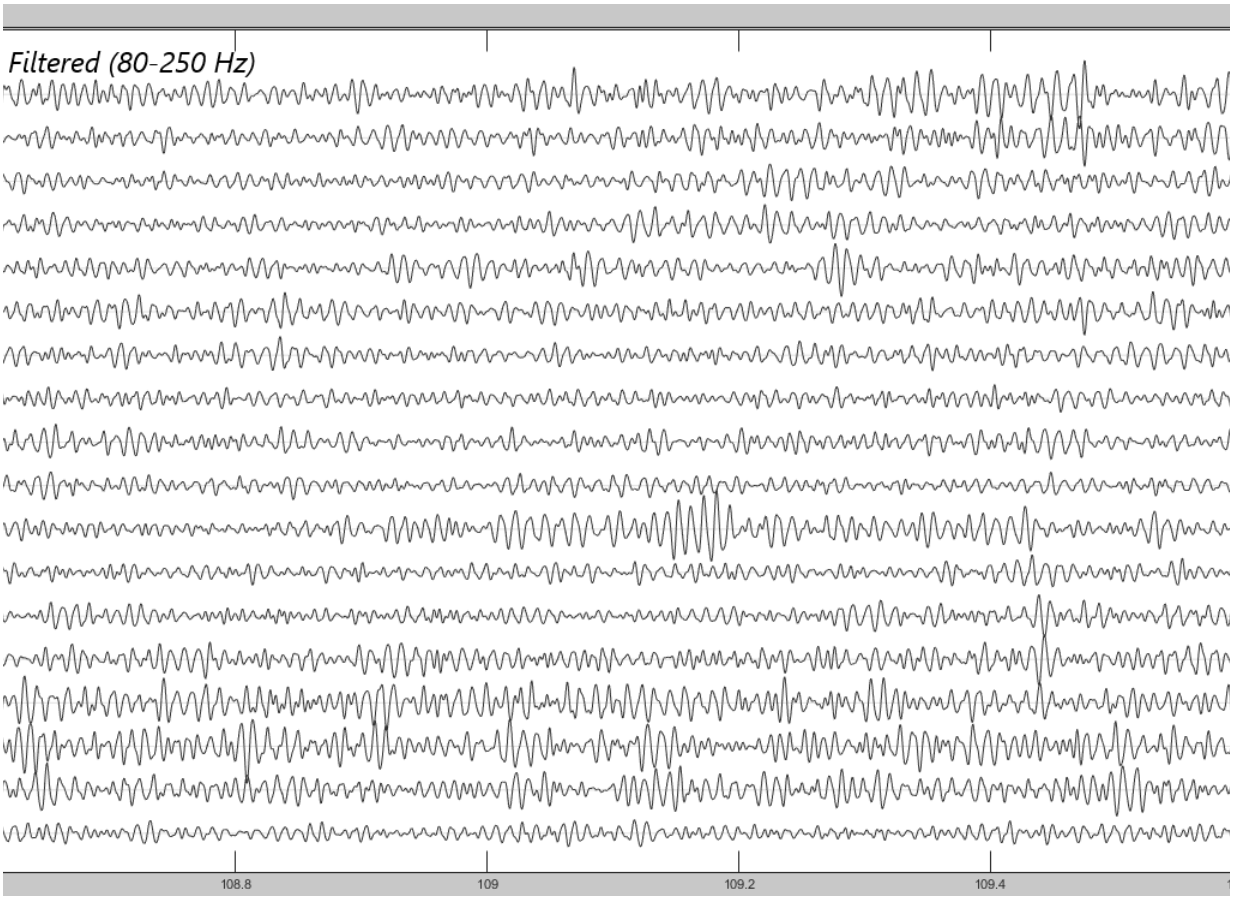

Figure 14: Continuous high-frequency activity observed in all intervals and nights of patient #15. The detection of HFOs in these recordings was deemed risky, and the exclusion of the patient from further analysis was decided.

4.3 Functional Connectivity computation

In the present work, I used several functional connectivity approaches for studying how the different brain areas are functionally interconnected. More specifically, the orthogonalized amplitude envelope correlation (oAEC) [212], the nonparametric directionality (NPD) [213], and the direct directed transfer function

(dDTF) [214] were utilised. oAEC and dDTF have been used in similar iEEG investigations of the EZ [37], [41], [203], while NPD was chosen for its potential to better capture connectivity than traditional parametric approaches [213]. As the nature of the study is exploratory, I wanted to investigate both directed (NPD and dDTF) and undirected (oAEC) connectivity techniques. Directed connections are defined as those that, besides quantifying the strength of the interaction, also convey information about the directionality of that interaction (who influences whom). On the other hand, undirected connectivity only provides information on how strongly or weakly two elements (brain regions in this case) are interacting with each other. This difference is embedded in the corresponding adjacency matrices (N x N), containing the pairwise connectivity between all electrodes (Figure 15). These matrices are symmetric in the case of undirected techniques and asymmetric in the case of directed ones.

All three techniques were computed separately in eight frequency bands. As already mentioned in the preceding chapters, one of the aims of this work is to extend FC analysis above the conventional frequencies (above gamma). For that reason, here, I explored functional connectivity in a wide frequency spectrum (from delta to fast ripples), to examine the transition of the connectivity patterns through increasing frequencies. More specifically, in this work, the studied frequency bands were: delta (2–4 Hz), theta (5–7 Hz), alpha (8–12 Hz), beta (15–29 Hz), low-gamma (30–59 Hz), high gamma (60-79 Hz), ripples (80-250 Hz), and fast ripples (251-500 Hz).

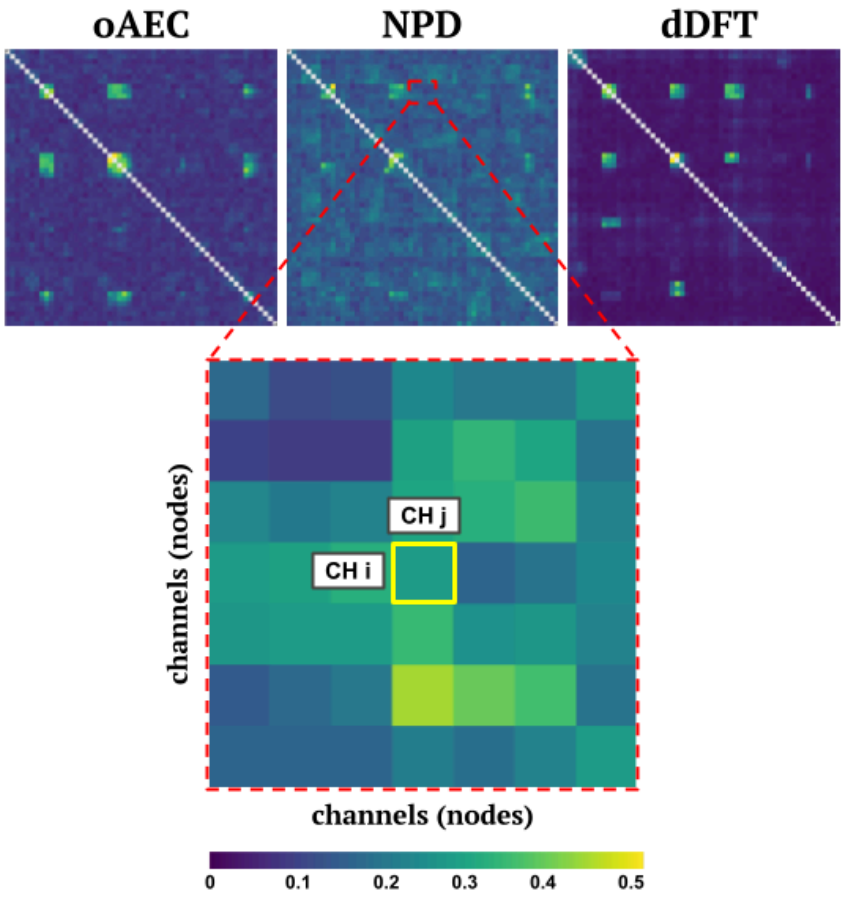

Figure 15: Adjacency matrix examples for the connectivity techniques used in this work (directed and undirected). Each element of an adjacency matrix represents the connectivity value between a specific pair of electrodes at a patient.

orthogonalized Amplitude Envelope Correlation (oAEC)

Assuming x(t) and y(t) are two iEEG time series, then $\bar{x}(t) = a_{\bar{x}}(t)e^{j\varphi_{\bar{x}}(t)}$ and $\bar{y}(t) = a_{\bar{y}}(t)e^{j\varphi_{\bar{y}}(t)}$ are their analytic signals after applying a Hilbert transform. The amplitude envelope correlation (AEC) is an undirected measure that quantifies the connectivity between the two time series x(t) and y(t), by measuring the linear (Pearson) correlation between their amplitude envelopes (defined as the absolute values of their analytic signals) [212]. An orthogonalisation step is commonly used to compensate for the spatial leakage and to remove all zero-lag signals between the studied brain regions (electrodes) [35]. In the present work oAEC was chosen as it is a measure able to detect signal coupling without phase coherence even between different frequencies [37], [212], [215], while it has also previously demonstrated the association between AEC-based networks and the EZ in drug-resistant epilepsy [31],

[35], [37], [216], [217], [218]. oAEC was computed with Brainstorm, and the adjacency matrices were extracted in MATLAB for further analysis.

Nonparametric Directionality (NPD)

Nonparametric directionality [213] uses a combination of time and frequency domain techniques to decompose the coherence function (Equation 1) by direction.

$$\left|R_{yx}(\omega)\right|^2 = \frac{\left|f_{yx}(\omega)\right|^2}{f_{yy}(\omega)f_{xx}(\omega)} \qquad \text{(Equation 1)}$$

Here $R_{yx}(\omega)$ is the coherence between two random processes x and y, where $f_{yx}(\omega)$ is the cross power spectral density (or cross-spectrum) between x and y, and $f_{yy}(\omega)$ and $f_{xx}(\omega)$ are the autospectra at frequency ω.

The total product moment correlation between (x, y), which is denoted as $R^2_{xy,}$

can be recovered by integration of the coherence [219].

$$R^2_{yx} = \frac{1}{2\pi}\int_{-\pi}^{+\pi}\left|R_{yx}(\omega)\right|^2 d\omega \qquad \text{(Equation 2)}$$

The decomposition of R^2_{xy} by direction is achieved using a novel form of filtering, which reduces the coherence to the cross spectrum. More specifically, the minimum mean square error (MMSE) whitening scheme is introduced, which, after being applied, results in the generation of two new (or derived) random processes x^w and y^w, which have spectra equal to 1 at all frequencies: $f^w_{xx}=1$, $f^w_{yy}=1$

As such, the coherence can be calculated from $\left|R^w_{yx}(\omega)\right|^2 = \left|f^w_{yx}(\omega)\right|^2$

However, the relationship between the variables is preserved, as coherence is insensitive to linear transformations of the original signals [220].

Thus, the coherence of the whitened and non-whitened processes are equal

$$\left|R^w_{yx}(\omega)\right|^2 = \left|R_{yx}(\omega)\right|^2$$

The scalar measure of dependence between x and y, R^2_{xy}, can now be written as

$$R^2_{yx} = \frac{1}{2\pi}\int_{-\pi}^{+\pi} \left| f^w_{yx}(\omega) \right|^2 d\omega \qquad \text{(Equation 3)}$$

and its final decomposition by direction is achieved through the introduction of a correlation measure in the time domain, $\rho_{xy}(\tau)$, with time lag τ , which forms a Fourier transform pair with the pre-whitened cross spectrum $f^w_{yx}(\omega)$, as

$$\rho_{yx}(\tau) = \frac{1}{2\pi}\int_{-\pi}^{+\pi} f^w_{yx}(\omega) e^{i\omega\tau}(\omega) d\omega \qquad \text{(Equation 4)}$$

Then R^2_{xy} can be decomposed by lag according to

$$R^2_{yx} = \int_{-\infty}^{+\infty} \left| \rho_{yx}(\tau) \right|^2 d\tau \qquad \text{(Equation 5)}$$

This equation can be proved using Parseval's theorem.

Further decomposition of R^2_{xy} by lag to obtain measures of directionality is achieved by selecting the required lag range in Equation 5.

Three measures which form a subset of R^2_{xy} are used, namely: R^2_{xy-}, R^2_{xy0} and $R^2_{xy+,}$ which measure the directionality: x ← y, x ↔ y and x → y, respectively. As such, R^2_{xy} is finally decomposed summatively into three components:

$$R^2_{yx} = \int_{\tau<0} \left| \rho_{yx}(\tau) \right|^2 d\tau + \left| \rho_{yx}(0) \right|^2 + \int_{\tau>0} \left| \rho_{yx}(\tau) \right|^2 d\tau$$

In the present work, I implemented NPD in MATLAB using the corresponding functions from the NeuroSpec GitHub repository (accessed on 28/10/2025).

direct Directed Transfer Function (dDTF)

Directed transfer function is rooted in the concept of Granger causality prediction modelling [198], transferred in the frequency domain. Signal y(t) has a Granger causal effect on x(t) when adding the past of y(t) improves the prediction of signal x(t) [221]. More specifically, trying to predict a value of x(t) using p previous values of the series x only, gives a prediction error e:

$$x(t) = \sum_{j=1}^{p} A_{11} x(t - j) + e(t)$$

At the same time, predicting a value of x(t) using p previous values of the series x and p previous values of y gives another prediction error e1:

$$x(t) = \sum_{j=1}^{p} A_{11} x(t - j) + \sum_{j=1}^{p} A_{12} y(t - j) + e1(t)$$

If the variance of e1 (after including series Y to the prediction) is lower than the variance of e, then Y causes X in the sense of Granger causality. To evaluate this causality in multichannel data (such as the iEEG data in this case), a multivariate autoregressive (MVAR) model is fitted to the recorded signals. Such a model assumes that the value of x at time t depends on the p past values of the signal itself, the p past values of signals at other electrodes and a random component [203]. The model order (p) determines the size of the prediction window. In my work, I used a model order of 10, as this configuration has been previously implemented in iEEG-based FC investigations of the EZ [198]. In addition, this choice is further justified by previous investigations that evaluated multiple multivariate models with orders between 2 and 22 [222].

The MVAR model was subsequently transformed to the frequency domain. The elements of the transfer matrix $H_{ij}(f)$ describe the causal flow from channel j to i at frequency f. The non-normalised DTF, which is directly related to the coupling strength [223], is defined as:

$$NDTF^{2}_{j->i}(f) = \left|H_{ij}(f)\right|^{2}$$

The normalised version of DTF, which takes values from 0 to 1, is defined as:

$$NDTF^{2}_{j->i}(f) = \frac{\left|H_{ij}(f)\right|^{2}}{\sum_{m=1}^{k} \left|H_{im}(f)\right|^{2}}$$

In the present study, I worked with direct Directed Transfer Function (dDTF), a variant of DTF which emphasises direct interactions by weighting DTF values with the partial coherence, thereby reducing the influence of indirect paths. Distinguishing direct from indirect transmission is essential in the case of signals from implanted electrodes [221]. I chose to work with dDTF over other directed connectivity techniques, since this method has been proven efficient for similar

interictal iEEG investigations at both lower [192], [196] and higher frequencies [41], [203]. Here, dDTF was computed in MATLAB using a group of specialised functions of the FieldTrip toolbox [224].

For each night, oAEC and dDTF were computed separately in every 3 sec. segment with HFOs and without HFOs across the eight different frequency bands. Subsequently, for each technique and segment type, the 20 adjacency matrices were averaged to produce the aggregate adjacency matrices (N x N) of the patient in the specific night (Figure 16A). On the other hand, the approach to calculate NPD measures was to construct spectral estimates using average periodograms across the twenty 3-second segments, from which the NPD measures were calculated as in [213].

For patients with only one night of iEEG recordings, these final adjacency matrices were the ones used in the rest of the work (Figure 16B). On the other hand, for patients with at least 2 nights of recordings, the aforementioned procedure was implemented separately for two random nights and a mean adjacency matrix across the nights was computed, to account for random confounders at specific nights (Figure 16C).

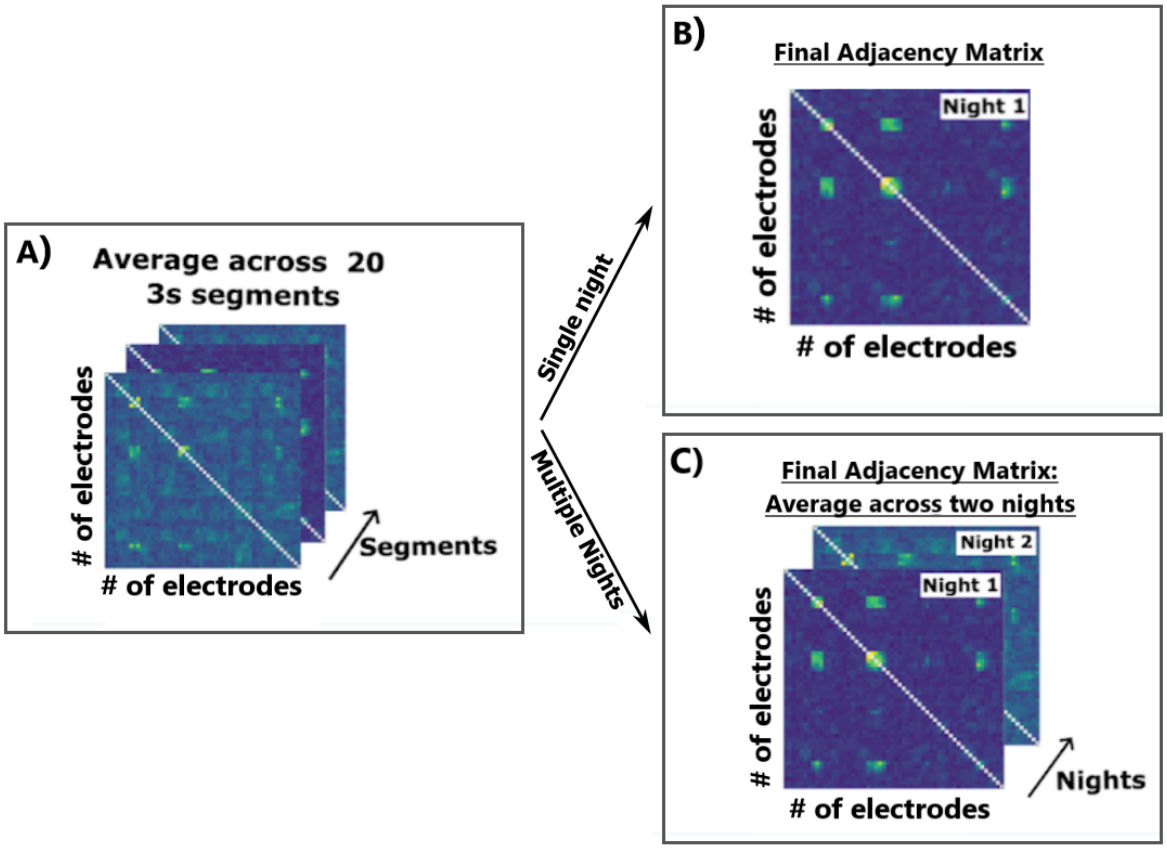

Figure 16: Final adjacency matrix construction in a patient. A) The connectivity matrices computed in every 3 sec. segment of iEEG data are averaged across all 20 segments for the specific night, resulting in an aggregate adjacency matrix. This procedure is implemented one time for data with HFOs and one time for data without HFOs. B) In patients with single night recordings, this aggregate matrix is the final adjacency matrix used for further network analysis. In multiple-night recordings, the procedure is implemented in two random nights, and the final adjacency matrix results from the mean of the two aggregate matrices (Night 1 and Night 2).

For each patient, the result of all of the aforementioned steps was the generation of 16 in total (2 HFO states x 8 frequency bands) final adjacency matrices for each connectivity technique (oAEC, NPD, dDTF).

4.4 Network generation

In order to transform the adjacency matrices (N x N), that contain information on the interconnectedness between pairs of iEEG electrodes, into quantifiable measurements of the role of each channel in the functional brain network (1 x N) I

utilised graph theory. Graph theory is a powerful mathematical tool that can graphically illustrate complex networks by modelling pairwise relations between objects. A graph (G) can be topographically represented by a set of nodes (V), which are interconnected by a collection of edges (E), which serve as the links between them. As a result, the mathematical representation of a graph is G=(V, E) (Figure 17).

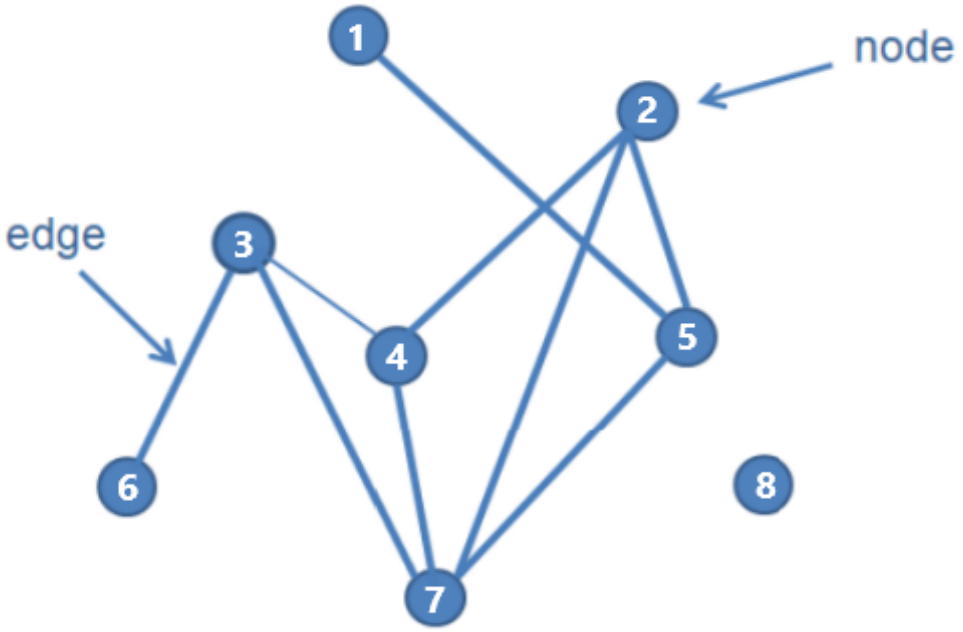

Figure 17: Graphical representation of a simple network containing eight nodes and nine edges.

In functional brain networks, we define nodes as the recording sites (discrete brain regions) and edges as the statistical measures of association between them. In my study, each bipolar iEEG electrode denoted a node, and the connectivity values between the electrodes (computed through oAEC, NPD, and dDTF) represented the edges. Since I did not apply any threshold for the connectivity values, the graphs are characterised as “weighted directed” (when based on NPD and dDTF) and “weighted undirected” (when based on oAEC). A graph can be characterised by a number of different measures, which can either be global, meaning that they account for the whole graph (network), or can be local, meaning that they quantify a property of a specific node [225]. Here, I worked with local measures as my main goal was to

identify specific localised network characteristics that could differentiate epileptogenic from non-epileptogenic brain tissue, something that was only possible at the local level. Four different local graph measures were computed, based on each final adjacency matrix, using the Brain Connectivity Toolbox (BCT) [226] in MATLAB. Prior to the computation of the measures, I curated each adjacency matrix to the proper format by first fixing common connection problems (BCT's weight_conversion.m function, 'autofix' option) and then normalising the fixed matrix between its maximum and minimum value (BCT's weight_conversion.m function, 'normalize' option). The set of chosen local measures that I computed is presented below:

1. **Betweenness centrality (BC)**: Local betweenness centrality is a measure of the importance of a node in a network based on the number of shortest paths that pass through it (Figure 18A). Specifically, it quantifies the fraction of all shortest paths between pairs of nodes in the network that include the given node. In weighted networks, the shortest path is defined as the path with the minimum total weight. A node with high BC contributes significantly to the efficient transfer of information across the network, as it lies on many of these shortest weighted paths. In the context of brain connectivity, such nodes may correspond to regions that facilitate the integration of information between different functional sub-systems. The BC of a node V can be calculated as:

$$g(V) = \sum_{s \neq V \neq t} \frac{\sigma_{st}(V)}{\sigma_{st}}$$

where σ_{st} is the total number of shortest paths from node s to node t and σ_{st} (V) is the number of those paths that pass through V. The sum is taken over all pairs of nodes (s,t), where s≠V≠t. Since I worked with weighted graphs, where the shortest path is determined based on the minimum total weight, the computation of BC (which is a distance measure) dictated the transformation of the adjacency matrices to a connection-length format. This was done using BCT's weight_conversion command with the 'lengths' option. This connection-length variant of the adjacency matrix was used only for the computation of BC and not the other three local measures.

2. **Clustering Coefficient (CC):** The local clustering coefficient of a node quantifies the tendency of its neighbouring nodes to also be connected with each other, forming a local cluster or triangle (Figure 18B). For a given node, CC is defined as the ratio between the number of existing connections among its neighbours and the maximum number of such connections that could possibly exist. In weighted networks, the clustering coefficient can be extended to account not only for the presence of connections but also for their strengths. A high local clustering coefficient indicates that a node is part of a tightly interconnected group, suggesting a locally specialised or segregated function. In brain networks, high clustering around a region may reflect localised processing or functional segregation within specific cortical areas.

3. **Strength:** Nodal strength is a measure that quantifies the total weight of all connections linked to a given node (Figure 18C). In other words, it is the sum of the weights of all edges connected to a node, reflecting the overall level of connectivity or interaction that the node has with the rest of the network. In the context of my work, a node/electrode with high strength is one that is strongly coupled with many other nodes/ electrodes, potentially indicating a key role in functional integration. Unlike degree, which counts the number of connections, strength incorporates the magnitude of those connections. For a node i, nodal strength S_i is defined as:

$$S_i = \sum_j w_{ij}$$

where w_{ij} is the weight of the edge between node i and node j.

In directed networks, like the ones generated with NPD and dDTF, I additionally computed inward strength (strength based on edges that flow towards the node), outward strength (strength based on edges that flow from the node towards other nodes), and total strength (sum of both incoming and outgoing edges).

4. **PageRank (PR):** PageRank is a centrality measure that reflects the influence of a node based on the importance of its neighbours (Figure 18D). Originally developed for ranking webpages, it has been adapted for brain networks to

identify nodes that are not only well-connected but also connected to other highly influential nodes. In a weighted network, PageRank considers both the number and the strength of established connections, distributing a node's importance proportionally across its neighbours. Unlike simple degree or strength measures, PageRank captures recursive importance (nodes are influential if they are connected to other influential nodes). In this work, I chose this measure over Eigenvector Centrality (EC), as BCT did not support EC computation for directed graphs (such as NPD and dDTF-based graphs). The damping factor, which represents the probability with which the influence flows through existing connections rather than randomly jumping to any node in the network, was set to 0.85, which is the most typical setting in brain studies.

I chose the specific set of measures (BC, CC, nodal strength, and PR) because together they capture complementary aspects of network integration and segregation, providing a more comprehensive understanding of brain network organisation.

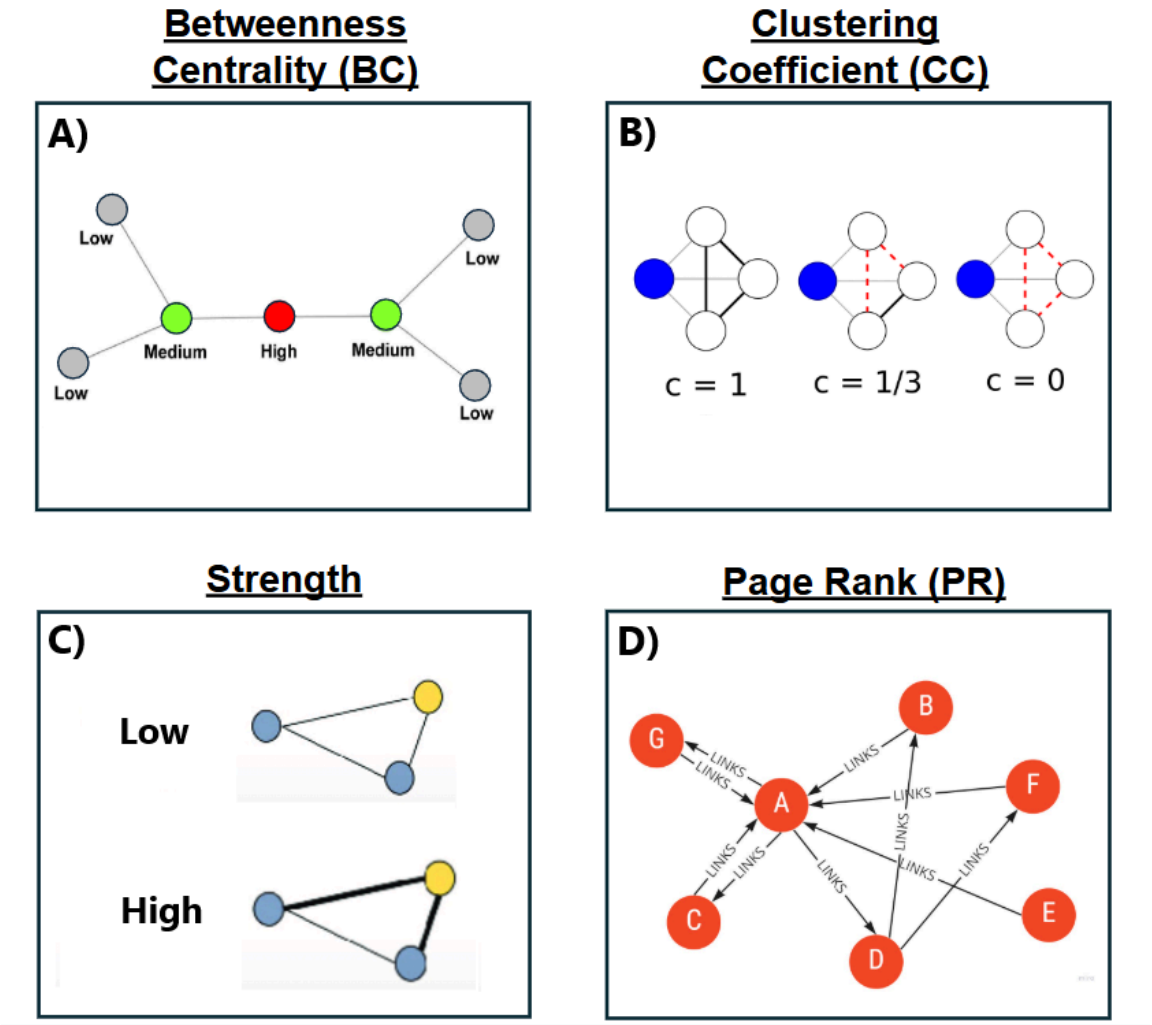

Figure 18: Local graph measures used to study the brain networks of the DRE patients of the present study. A) Betweenness centrality is high in nodes with an increased number of shortest paths passing through them. B) Clustering coefficient of a node increases when its immediate neighbours are also connected with each other. C) Strength of a node quantifies how strongly the node is interconnected in the network. D) PageRank is a measure that reflects the centrality and influence of a node based on the importance of its neighbours.

For each connectivity technique (oAEC, NPD, dDTF), I computed every local graph measure separately on each of the 16 (2 HFO states x 8 frequency bands) final adjacency matrices previously computed in 4.2. This resulted in 16 arrays (N x 1) containing the specific local measure's value in each electrode for the corresponding state and frequency. In the following chapter, I make use of these local graph measures to study the connectivity characteristics of epileptogenic and non-epileptogenic tissue, and assess their value in identifying the EZ and predicting the surgical outcome in the patients of our cohort.

A summary schematic representation depicting the overall processing pipeline, from electrode acquisition and modelling to the functional network generation, is presented in Figure 19 below.

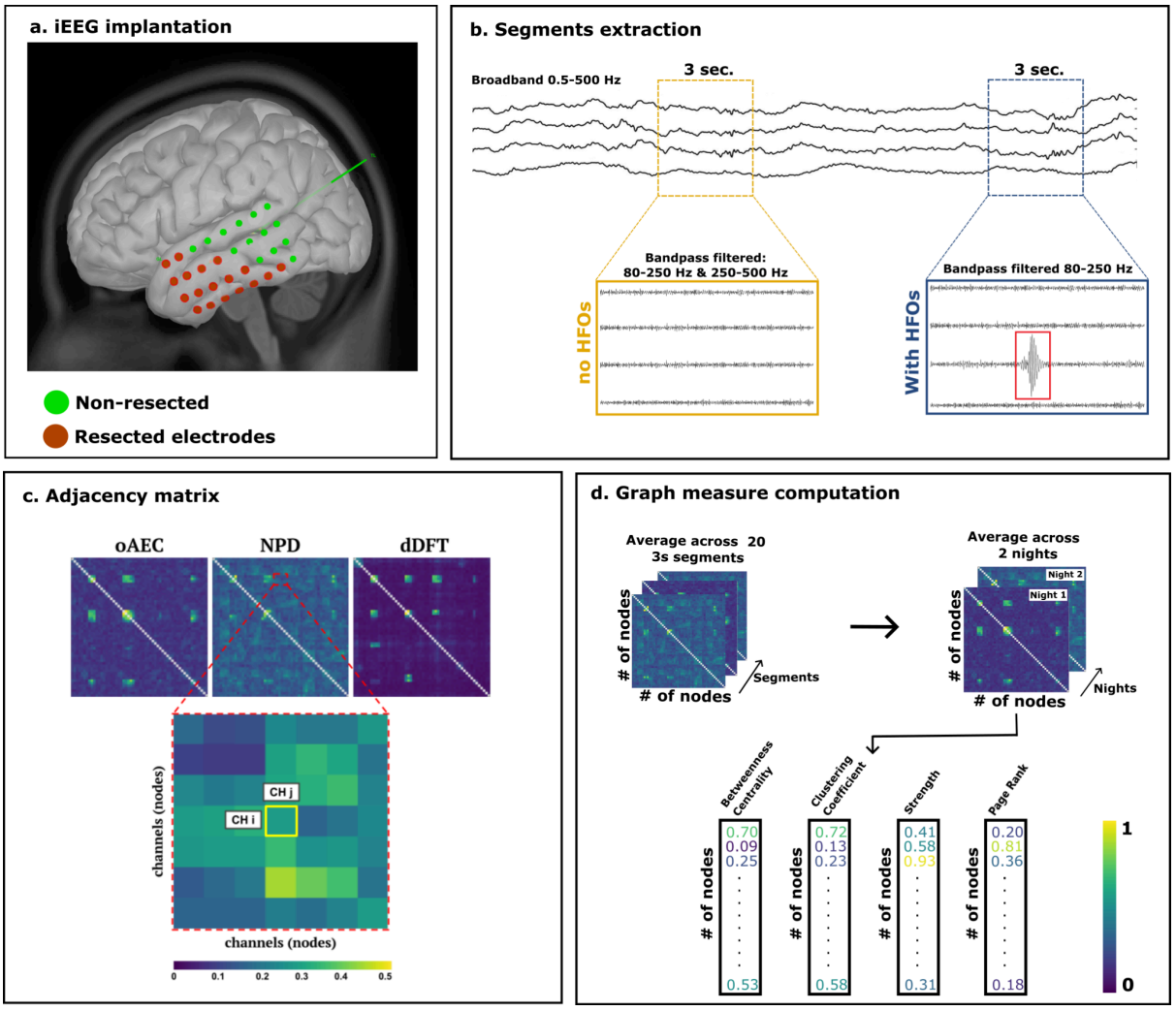

Figure 19: Overall processing pipeline. a) Schematic representation of the iEEG implantation (combined depth and subdural electrodes) in a patient: #12. b) Selection of 1 min. data (20 segments x 3 sec.), through visual review, for each HFO state: without HFOs with yellow, with HFOs with blue. c) Functional connectivity (FC) estimation using three different techniques: orthogonalized amplitude envelope correlation (oAEC), nonparametric directionality (NPD), and direct Directed Transfer Function (dDTF). Each element of the adjacency matrix represents the pairwise connectivity between two different channels (nodes) in the network. d) Averaging across the 20 segments and the two nights of recording (except cases of single-night recordings), followed by the computation of four local graph metrics: betweenness centrality (BC), clustering coefficient (CC), nodal strength, and PageRank (PR)].

4.5 Validation against power confounds

High-frequency FC can be influenced by local power [227]. To ensure that any observed differences in connectivity were not trivially explained by power, I repeated the entire analysis on prewhitened signals. Prewhitening was performed using autoregressive (AR) models, which removed predictable autocorrelations and thereby equalised spectral power across channels while preserving cross-channel dependencies. I tested model orders of 10 and 20 to confirm the robustness of the approach. Adjacency matrices and graph-theoretical measures were then recomputed from the whitened signals. This analysis served solely as a control, with the primary results reported later in this study being based on the original, non-whitened data.

Chapter 5

Interictal iEEG Functional Connectivity Identifies Epileptogenic Tissue and Predicts Outcome in DRE Patients

5.1 Introduction

The vast majority of existing literature links epileptogenic tissue with increased functional connectivity interictally (see 3.2.1). Many studies have utilised this network property to identify the EZ using different classification schemes [36], [41], [204], while others attempted to predict the surgical outcome of DRE patients based on the resection of highly connected areas (see 3.2.2) [37], [201], [228] All these works however, used FC and networks computed on conventional frequencies (from δ to γ), leaving connectivity at higher frequencies greatly unexplored. Moreover, very few studies have investigated the effect that HFOs have on FC and network measures, a factor that could be important when interpreting results.

In this chapter, I aim to address these gaps by exploring the influence of HFOs on FC computed using different techniques (oAEC, NPD, dDTF), and by assessing whether extending FC analysis to higher frequencies adds value to the identification of the EZ and the prediction of surgical outcome. In the following sections, I discuss the methodology and statistical tests used, present my results, and critically discuss them in light of the most recent literature.

5.2 Methodology and statistical analysis

The methodological approach for computing FC and generating the functional network in each patient is detailed in Chapter 4. As described, for each patient, I used 3 connectivity techniques (oAEC, NPD, and dDTF) (see 4.3) and computed 4 local graph measures (nodal strength, BC, CC, and PageRank) (see 4.4) across 8 frequency bands (delta to FRs) in 2 different data types (segments with HFOs, segments without HFOs). These networks form the basis for the investigations presented in the rest of this chapter. The methodological steps described below were implemented separately for each FC technique.

5.2.1 Functional connectivity differences between interictal data with and without HFOs

Here, I aim to investigate the effects that HFO events can have on FC estimates. In each patient, I normalised each graph measure (range: 0-1) using the measure's highest and lowest value in either of the two states (data with HFOs or data without HFOs), since I measuring from the same electrodes at different time points. Similar normalisation methodologies have been followed in previous works [31], [37]. I assessed the distribution of FC measures using the Shapiro-Wilk normality test and observed that the data followed a non-normal distribution. To assess the differences in FC between data types, I calculated, for each local graph measure and frequency band, its median value in each patient. I used median values since the number of electrodes was relatively small, so outliers would have a large impact when using the mean, while similar previous works have also used median instead of mean [37], [203]. I then compared pairwise (Wilcoxon matched samples test [singrank.m]) across all patients (N=18). Here, I did not investigate separately for good and poor outcome patients. The results from these comparisons are presented in section 5.3.1.

5.2.2 Functional connectivity inside vs. outside resection

Here, to assess whether FC differs between epileptogenic and non-epileptogenic tissue, I used the resection zone. To compare the FC between resected and non-resected electrodes, I first normalised (range: 0-1), at the patient level, each

graph measure using the measure's highest and lowest value for the specific frequency band and data type. Then, for each patient, I calculated the median value of each graph measure one time for electrodes inside resection and one time for electrodes outside. I subsequently compared pairwise these median graph measure values (inside vs. outside resection), separately for good- and poor-outcome patients, in all frequency bands (Wilcoxon matched samples test [singrank.m]). Results from these comparisons can be found in section 5.3.2.

5.2.3 FC-trained ML models for identifying the EZ

Here, I tested the ability of FC measures in predicting the EZ. I based on the assumption that in good outcome patients, the crucial epileptogenic areas were contained within the resection, while in poor outcome patients, they were not. In this sense, I trained ML models using data only from good outcome patients to have more objective margins between EZ areas (inside resection) and non-EZ areas (outside resection). MATLAB's Classification Learner App was used for training and testing the FC-based classifiers. Each classifier was trained only on the network measures that were found to significantly differ inside compared to outside the surgical resection during earlier investigations (see 5.3.2). I defined as true positive (TP) a resected electrode correctly identified as EZ, false positive (FP) a non-resected electrode identified as EZ, true negative (TN) a non-resected electrode correctly identified as non-EZ, and false negative (FN) a resected electrode identified as non-EZ. Based on these measures, sensitivity [TP/(TP+FN)] and specificity [TN/(TN+FP)] were computed, and the ROC curve was generated. The area under the curve (AUC), defined as the integral of the ROC curve, was then estimated. AUC ranges from 0 to 1 and represents overall classification performance. These AUC values were finally reported together with precision [TP/(TP + FP)] and recall (sensitivity).

An issue that arose was the greatly imbalanced number of instances in the two classes (# of resected electrodes << # of non-resected electrodes). To address this problem, similar works have used cost-sensitive learning models which assigned a high cost to the misclassification of the minority class [35]. Other studies used techniques that oversample the minority class or downsample the majority class (or both) [41]. Here, applying cost-sensitive parameters would be inefficient due to the

large number of factors under study (different FC methods, frequencies, and HFO states), which would require careful parametrisation in each combination of these factors to achieve the optimal classification. This would complicate the reporting and generalizability of the results, and would oppose my goals of a fully automatic pipeline. I also did not want to introduce synthetic data to the analysis by using techniques such as synthetic minority oversampling (SMOTE). As such, I decided to downsample the majority class. I ended up training the classifiers in 100 different random subsets of equal number of instances between the two classes (Class 1: resected, Class 2: non-resected) to increase the robustness of my approach. For each classification algorithm, I then calculated the mean AUC to assess its performance.

As my work is exploratory in nature, I evaluated 11 different classification models, all implemented inside MATLAB's Classification Learner App (with their default settings), to choose the best performing one (highest AUC). Namely, these algorithms were the: 1) Tree_Fine variant, 2) Tree_Medium variant, 3) Tree_Coarse variant, 4) Logistic Regression, 5) SVM_Linear, 6) SVM_Fine variant, 7) Naive Bayes_Gaussian, 8) kNN_Fine variant, 9) kNN_Cubic variant, 10) Ensemble_Bagged variant, and 11) Ensemble_Subspace Discriminant variant. I evaluated each model using 5-fold cross-validation, where the dataset was randomly divided into five equal-sized subsets, each used once as a test set. The ML results are presented in section 5.3.3.

5.2.4 Prediction of surgical outcome

Here, I assessed whether the removal of nodes with specific FC characteristics (nodes with FC above or below a threshold) can predict the surgical outcome of patients. For this purpose, I first chose the best performing classifier from 5.2.3 and trained it using only the local graph property that was found to be significantly higher or lower inside compared to outside resection in good outcome patients in 5.2.2. I then extracted the optimal graph measure threshold by finding the maximum Youden Index [229], which identifies the threshold that best separates classes by balancing sensitivity and specificity. After finding the threshold, I calculated for each patient the ratio (overlap) of resected "hubs" or "sinks" (nodes with FC above or below this

threshold) to the total number of clinically resected electrodes. This was called electrode overlap.

I then started a new classification based on these electrode overlap values. This classification was implemented manually, by generating overlap thresholds ranging from 0% overlap to 100% overlap with a 5% step, in accordance with previous works [37]. In each step, I checked in every patient if their electrode overlap value exceeded this threshold. Simultaneously, I checked the outcome of the patient and I calculated the following classification metrics: TP (Overlap above threshold and good outcome), FP (Overlap above threshold and poor outcome), TN (Overlap below threshold and poor outcome), and FN (Overlap below threshold and good outcome). After doing that for all patients, I then summed each metric and checked how many TPs, FPs, FNs, and TNs the specific threshold scored. Finally, based on these metrics, I calculated the positive predictive value (PPV)=TP/(TP+FP), the negative predictive value (NPV)=TN/(TN+FN), and the prediction accuracy=(TP+TN) / (TP+TN+FP+FN) for this overlap threshold. After following this procedure for all thresholds, I chose the optimal electrode overlap threshold by computing the maximum Youden index for the classification.

The last step was to run Fisher's exact test to assess whether resecting a certain percentage of hubs (or sinks) predicted good outcome. To run this test, I used the optimal overlap threshold found in the previous step and created a new set of TP, FP, FN and TN values. Now TP_Fisher: Patients with resected hubs who became seizure-free, FP_Fisher: Patients with resected hubs who continued having seizures, TN: Patients with missed hubs who continued having seizures, and FN_Fisher: Patients with missed hubs who still became seizure-free. Subsequently, I created a square 2x2 table: [TP_Fisher, FP_Fisher; FN_Fisher, TN_Fisher] and computed Fisher's test with the corresponding MATLAB command (fishertest.m). If the test generated statistically significant results, then removing hubs (or sinks) above the optimal overlap threshold could predict surgical outcome in DRE patients. The corresponding results are presented in section 5.3.4.

5.2.5 Statistical considerations

All analyses were performed in MATLAB 2019a. I considered a statistical significance for $p < 0.05$. Where appropriate, the False Discovery Rate (FDR) method was used to correct significance for multiple comparisons, in accordance with similar previous works [37], [199].

5.2.6 Overview of methodological steps and research questions

Overall, by following the methodological pipeline detailed above, I first seek to investigate the effects of HFOs in FC by answering RQ1: "*Does FC differ significantly when computed in data segments with and without HFOs?"*. Then I explore the characteristics of FC in the epileptic brain by answering RQ2: "*Can specific functional connectivity measures differentiate epileptogenic from non-epileptogenic tissue in DRE patients?"*. By finding specific patterns of FC, I assess the capabilities of machine learning models trained on FC properties in identifying the EZ, answering RQ3: "*Can machine learning algorithms, trained on different functional connectivity measures, predict channels that belong to the EZ?"*. Finally, I test whether resection of specific channel groups, determined by their connectivity profiles, can serve as a predictor of surgical outcome in DRE patients, by answering RQ4: "*Does resection of hub/sink nodes (channels) in the generated networks predict the surgical outcomes of DRE patients?"*.

5.3 Results

This section presents the results of the different investigations described in section 5.2, which are based on the network metrics defined in section 4.4. A discussion of the findings is provided in the subsequent section 5.4.

5.3.1 oAEC-based FC at high frequencies is significantly affected by the presence or absence of HFOs

To assess the effect of HFOs on FC computations, I assessed the differences of each local graph measure between networks generated from segments with and without HFOs. For oAEC, I observed lower nodal strength in interictal data with HFOs compared to data without HFOs ($p<0.05$) for the ripple band (HFOs: 0.27 ± 0.17, no HFOs: 0.53 ± 0.10, decrease: 95%) (Figure 20A). I also observed decreased clustering coefficient in data with HFOs for the high gamma (HFOs: 0.27 ± 0.20, no HFOs: 0.60 ± 0.27, decrease: 119%), and ripple bands (HFOs: 0.27 ± 0.20, no HFOs: 0.62 ± 0.12, decrease: 133%) (Figure 21A). No significant differences were observed between the two states in PR and BC.

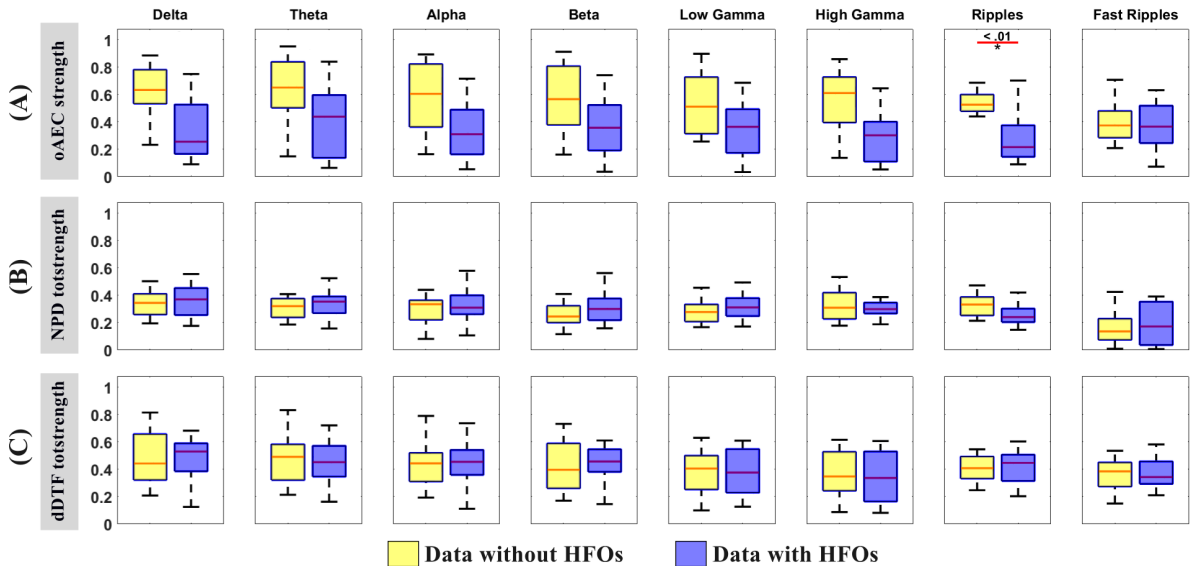

Figure 20: Nodal strength and total strength (totstrength) for segments with and without HFO events across all patients using: A) oAEC, B) NPD, and C) dDTF. Significant differences are marked with an asterisk ($p< 0.05$, Wilcoxon's signed-rank test).

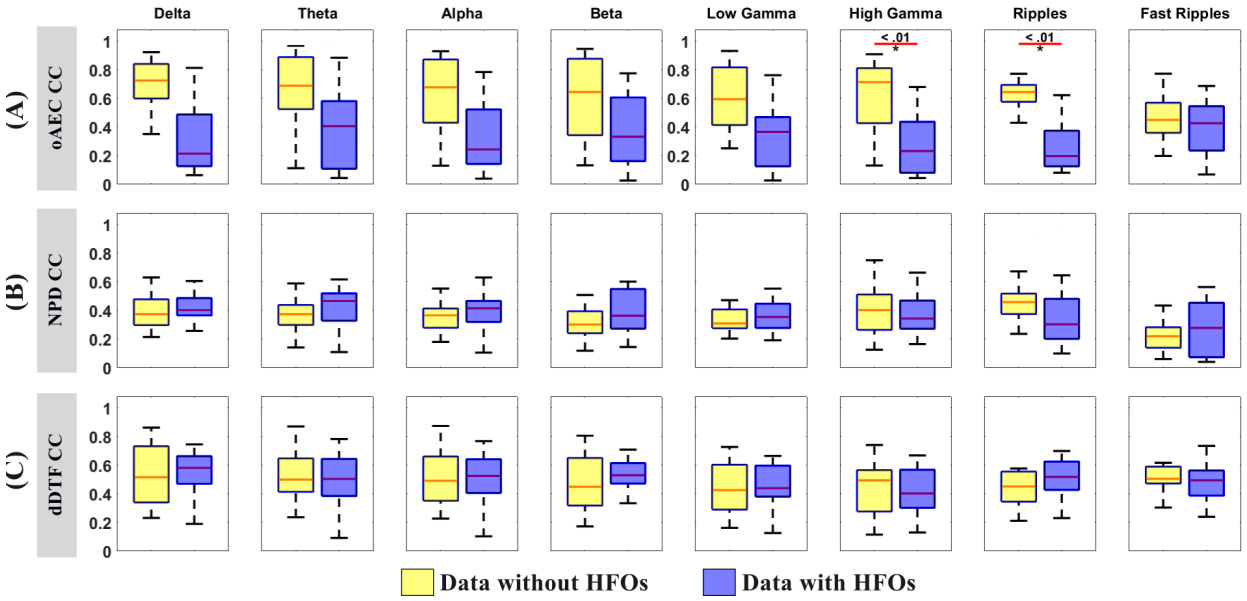

Figure 21: Local clustering coefficient for segments with and without HFO events across all patients using A) oAEC, B) NPD, C) dDTF. Significant differences are marked with an asterisk ($p<0.05$, Wilcoxon's signed-rank test).

For NPD and dDTF, I observed no significant differences in any local graph measure (BC, CC, PR, total strength, inward strength, outward strength) between networks derived from segments with and without HFOs. All findings from this section are discussed in 5.4.1.

5.3.2 FC differs between epileptogenic and non-epileptogenic tissue

In order to examine FC in the vicinity of the EZ, I compared the local network properties inside and outside the resection, separately for good and poor outcome patients.

5.3.2.1 oAEC

For oAEC computed in data with HFOs I observed increased nodal strength inside resection compared to outside, only in good outcome patients ($p<0.05$) for theta (in: 0.58 ± 0.16, out: 0.35 ± 0.18, increase: 67%), beta (in: 0.71 ± 0.18, out: 0.27 ± 0.20, increase: 158%), low gamma (in: 0.71 ± 0.21, out: 0.27 ± 0.19, increase: 160%), high gamma (in: 0.60 ± 0.21, out: 0.24 ± 0.16, increase: 150%), and ripples (in: 0.66 ± 0.25, out: 0.35 ± 0.18, increase: 87%) (Figure 22). The same pattern was

also observed for CC and PR for theta (CC increase: 66%, PR increase: 67%), beta (CC increase: 138%, PR increase: 154%), low gamma (CC increase: 141%, PR increase: 157%), high gamma (CC increase: 134%, PR increase: 148%), and ripples (CC increase: 65%, PR increase: 83%) (Suppl. Figures S5 and S6). On the other hand, BC showed no significant differences inside compared to outside the resection in any outcome group (Suppl. Figure S7).

For oAEC computed in segments without HFOs, I did not find significant differences inside (vs. outside) resection in any oAEC-based local graph measure. This held true for patients with both good and poor surgical outcomes (Suppl. Figures S8-S11).

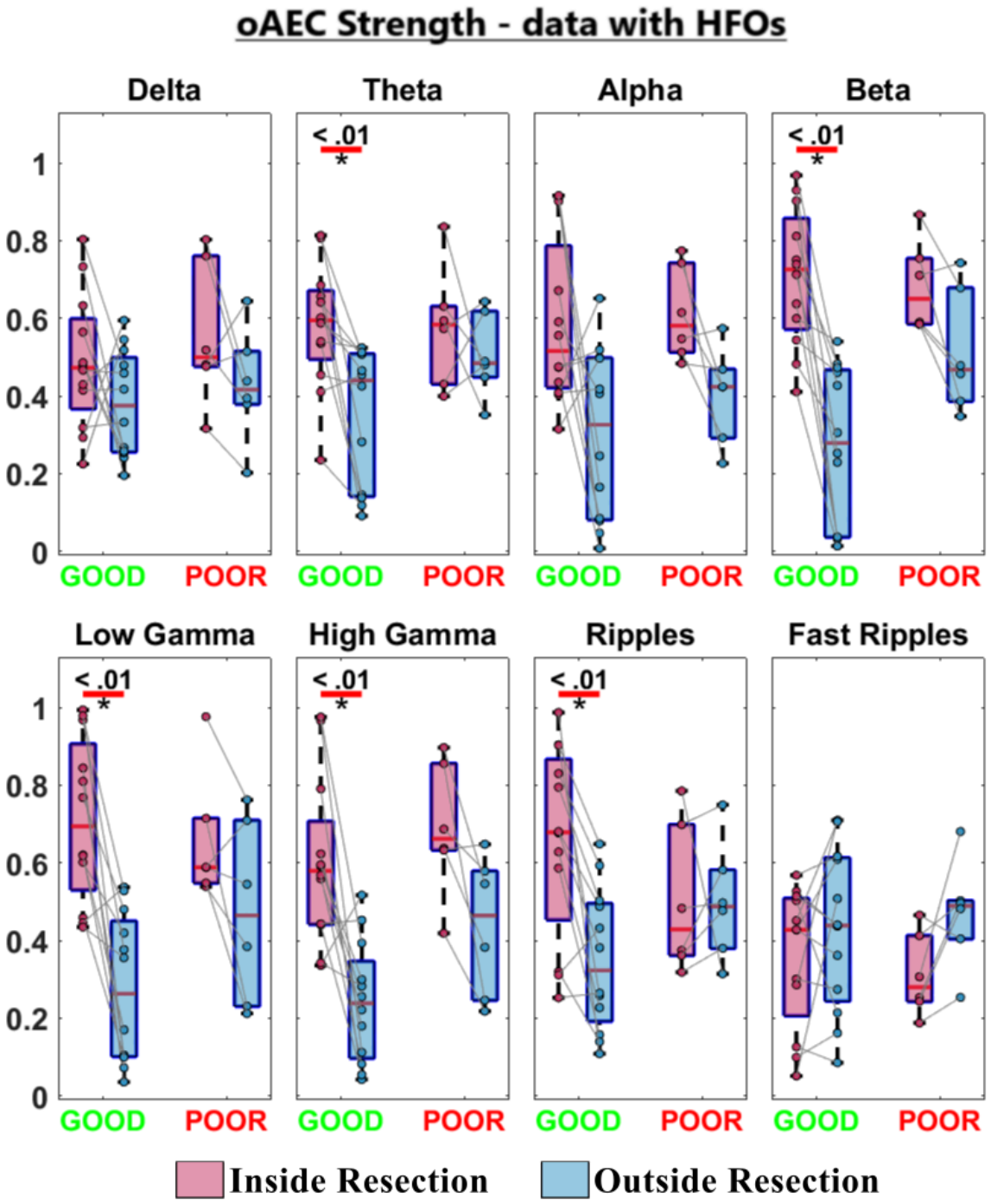

Figure 22: Orthogonalized amplitude envelope correlation (oAEC) nodal strength, for segments with HFOs, compared inside (pink) vs. outside (blue) resection separately for good (N=12) and poor (N=6) outcome patients. Significant differences are marked with an asterisk (*) ($p < 0.05$, pairwise Wilcoxon signed-rank test). In the box-plot diagrams, the horizontal line indicates the median value, the lower and upper edges represent the 25th and 75th percentiles, and the whiskers extend to the minimum and maximum values.

To emphasise the relationship of increased oAEC nodal strength with epileptogenic tissue during the presence of HFOs, I illustrated oAEC nodal strength one time for a good (Patient #4, ILAE 1) and one time for a poor outcome patient (Patient #9, ILAE 5), across all frequency bands (Figure 23). For the good outcome patient, electrodes (nodes) with increased nodal strength were observed inside the resection, which in this case includes the important epileptogenic tissue, while lower strength values are seen in distant (non-resected) brain regions. In contrast, nodes of increased nodal strength were scattered in both resected and non-resected areas in the poor outcome patient.

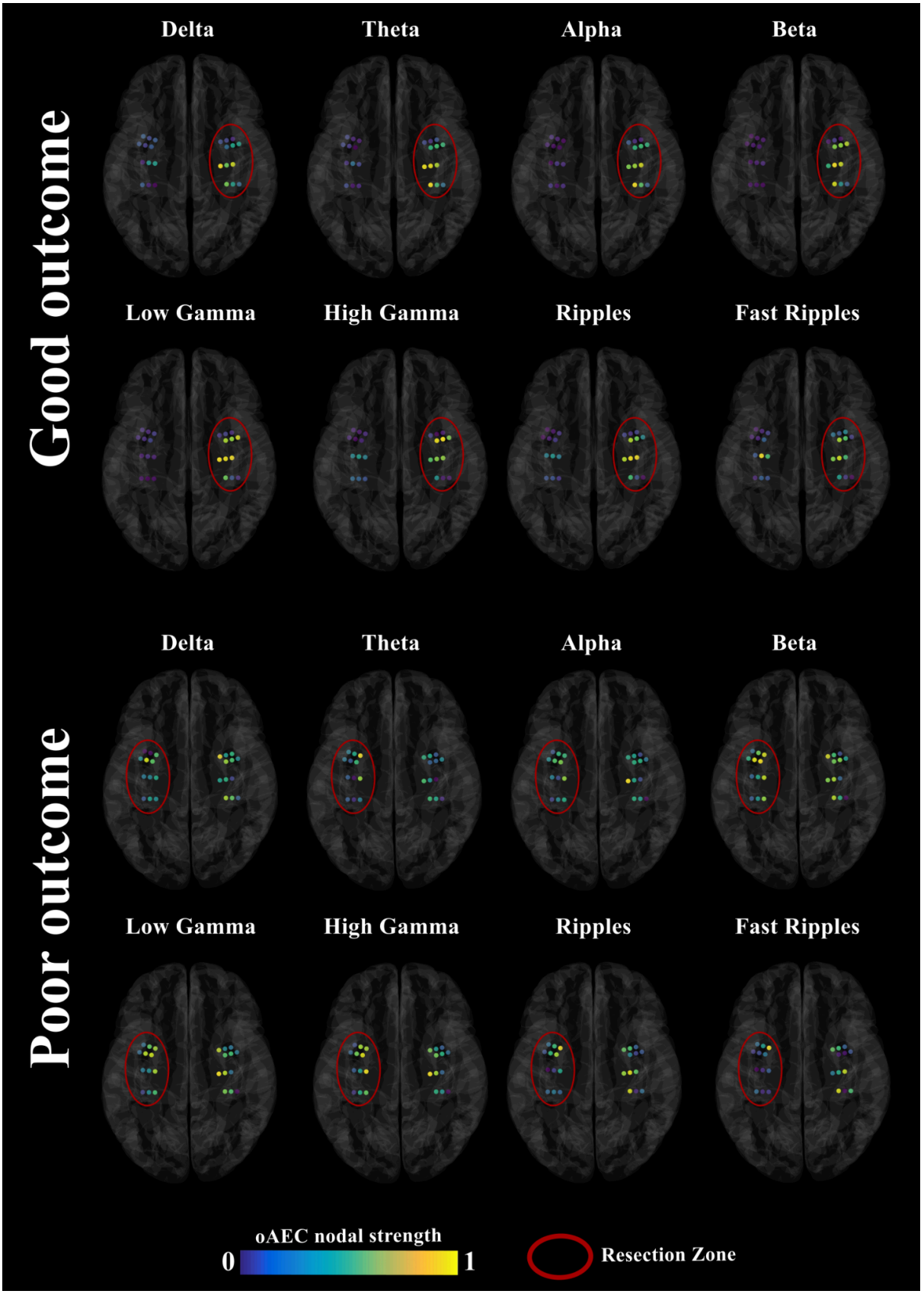

Figure 23: Orthogonalized amplitude envelope correlation (oAEC) nodal strength at the patient level across different frequency bands (from delta to fast ripples). The oAEC nodal strength value in each bipolar electrode (node) is depicted one time for a good outcome

(Patient #4, ILAE 1, *top*) and one time for a poor outcome patient (Patient #9, ILAE 5, *bottom*), using their 3D implantation models. Surgically resected electrodes are included in the resection zone, illustrated with a solid red line. The oAEC strength values are colour-coded: high oAEC nodal strength values are displayed in yellow; low oAEC nodal strength values are displayed in dark blue.

5.3.2.2 NPD

For NPD computed in data with HFOs, I found no significant differences in any local network measure (total strength, inward strength, outward strength, CC, PR, and BC) when comparing nodes inside and outside the resection area for both good and poor outcome patients (Suppl. Figures S12-S16). The same results were obtained for NPD computed in HFO-free segments (Suppl. Figures S17-S22). Figure 24 illustrates total strength in segments with HFOs at nodes inside and outside the resection areas, highlighting these non-significant variations.

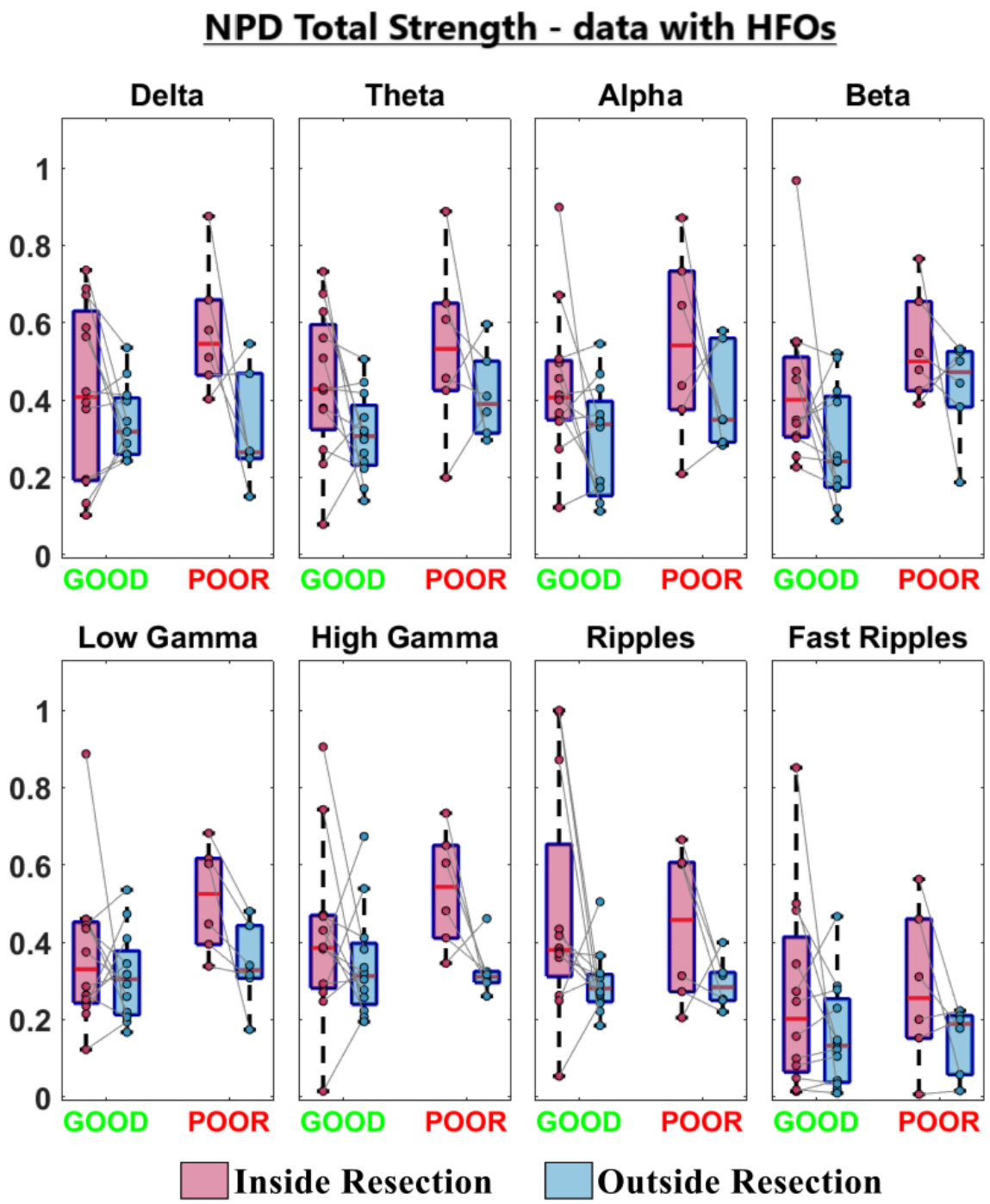

Figure 24: Nonparametric directionality (NPD) nodal total strength, for segments with HFOs, compared inside (pink) vs. outside (blue) resection separately for good (N=12) and poor (N=6) outcome patients. Significant differences are marked with an asterisk (*) ($p < 0.05$, pairwise Wilcoxon signed-rank test). In the box-plot diagrams, the horizontal line indicates the median value, the lower and upper edges represent the 25th and 75th percentiles, and the whiskers extend to the minimum and maximum values.

5.3.2.3 dDTF

For dDTF computed in data with HFOs, I found no significant differences between any local graph measure inside and outside resection in any surgical outcome group (Suppl. Figures S23-S27). Figure 25 depicts total strength values inside and outside the resection zone, illustrating the absence of statistically significant variations.

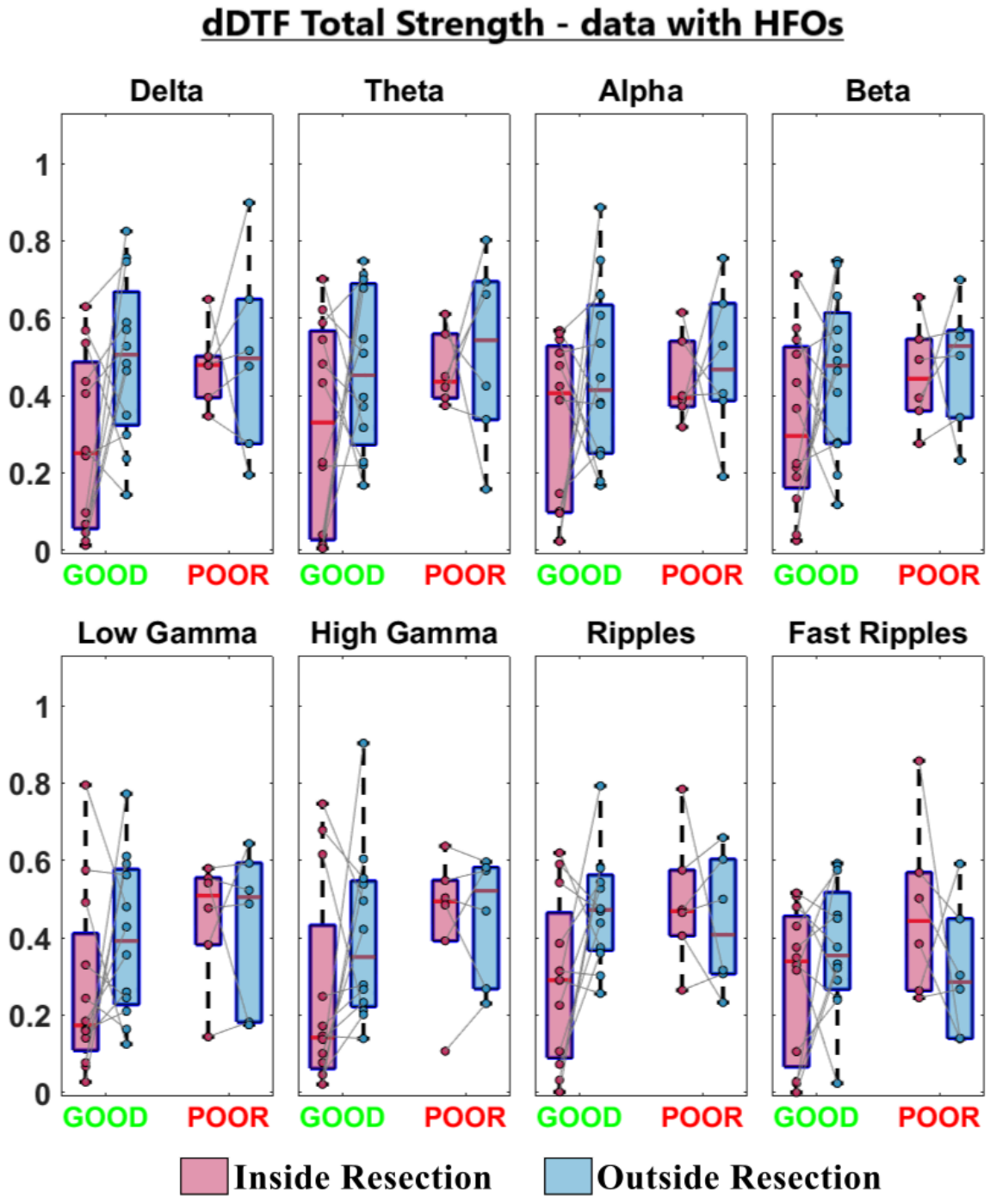

Figure 25: Direct directed transfer function (dDTF) nodal total strength, for segments without HFOs, compared inside (pink) vs. outside (blue) resection separately for good (N=12) and poor (N=6) outcome patients. Significant differences are marked with an asterisk (*) ($p < 0.05$, pairwise Wilcoxon signed-rank test). In the box-plot diagrams, the horizontal line indicates the median value, the lower and upper edges represent the 25th and 75th percentiles, and the whiskers extend to the minimum and maximum values.

For dDTF computed in data without HFO events, FC presented a different picture. Outward strength was significantly lower inside, compared to outside the resection of good outcome patients for beta (in: 0.24 ± 0.18, out: 0.5 ± 0.18, decrease: 122%), low gamma (in: 0.19 ± 0.16, out: 0.47 ± 0.20, decrease: 151%), high gamma (in: 0.17 ± 0.18, out: 0.47 ± 0.22, decrease: 182%), and ripples (in: 0.23 ± 0.18, out: 0.50 ± 0.17, decrease: 116%) (Figure 26). Inward strength did not differ significantly between the two areas in any frequency, for both outcome groups (Suppl. Figure S28). In line with outward strength, total strength was also decreased inside compared to outside the resection of good outcome patients for delta (decrease: 105%), theta (decrease: 94%), alpha (decrease: 102%), high gamma (decrease: 142%), and ripples (decrease: 82%) (Suppl. Figure S29). A similar pattern was observed for CC [alpha (decrease: 74%), beta (decrease: 89%), low gamma (decrease: 115%), high gamma (decrease: 161%), ripples (decrease: 107%)] (Figure 27), and PR [beta (decrease: 99%), low gamma (decrease: 112%), high gamma (decrease: 146%), ripples (decrease: 101%)] (Suppl. Figure S30). On the other hand, BC did not show any significant variations between nodes inside and outside resection for any outcome group (Suppl. Figure S31).

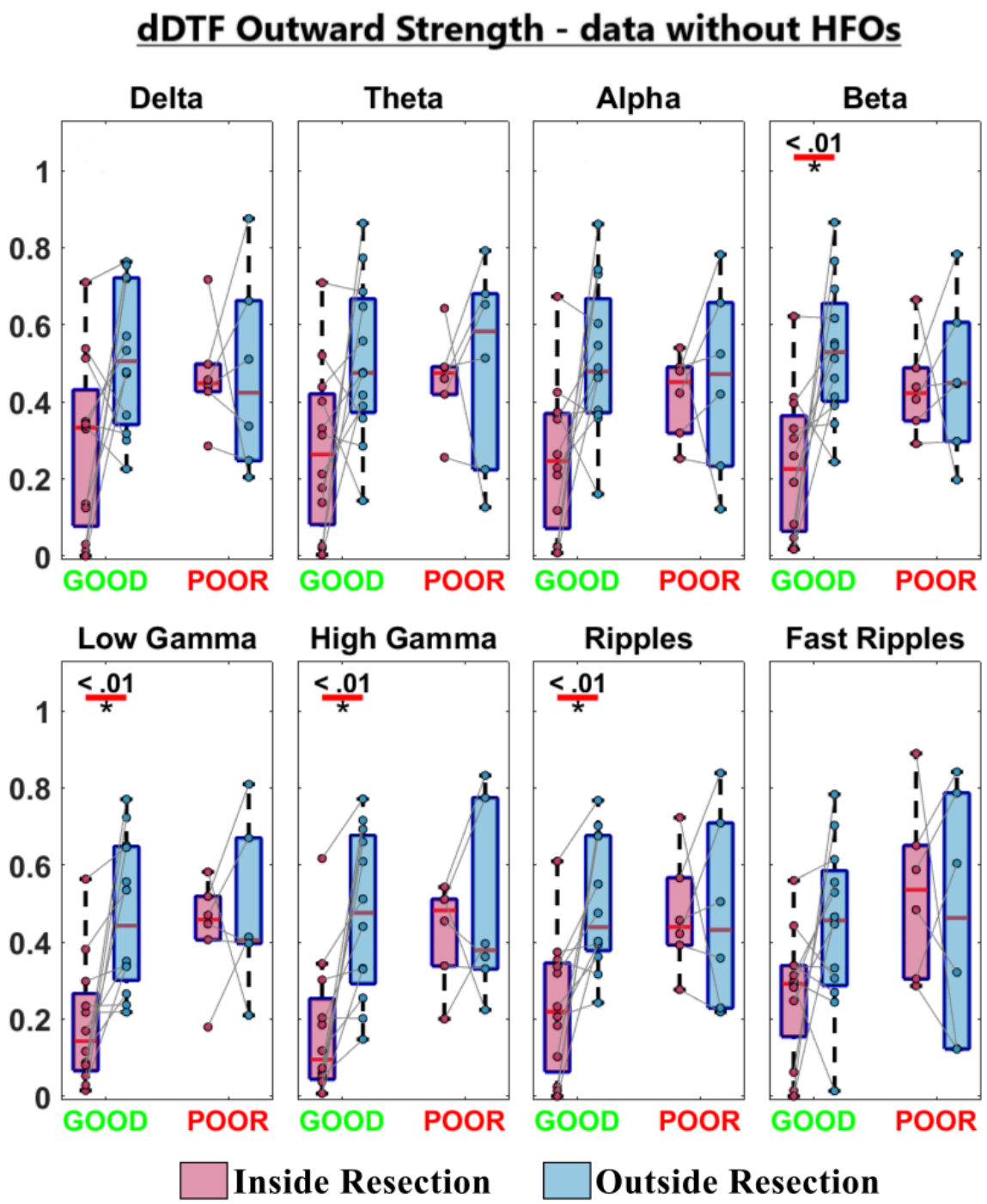

Figure 26: Direct directed transfer function (dDTF) nodal outward strength, for segments without HFOs, compared inside (pink) vs. outside (blue) resection separately for good (N=12) and poor (N=6) outcome patients. Significant differences are marked with an asterisk (*) ($p < 0.05$, Wilcoxon signed-rank test). In the box-plot diagrams, the horizontal line indicates the median value, the lower and upper edges represent the 25th and 75th percentiles, and the whiskers extend to the minimum and maximum values.

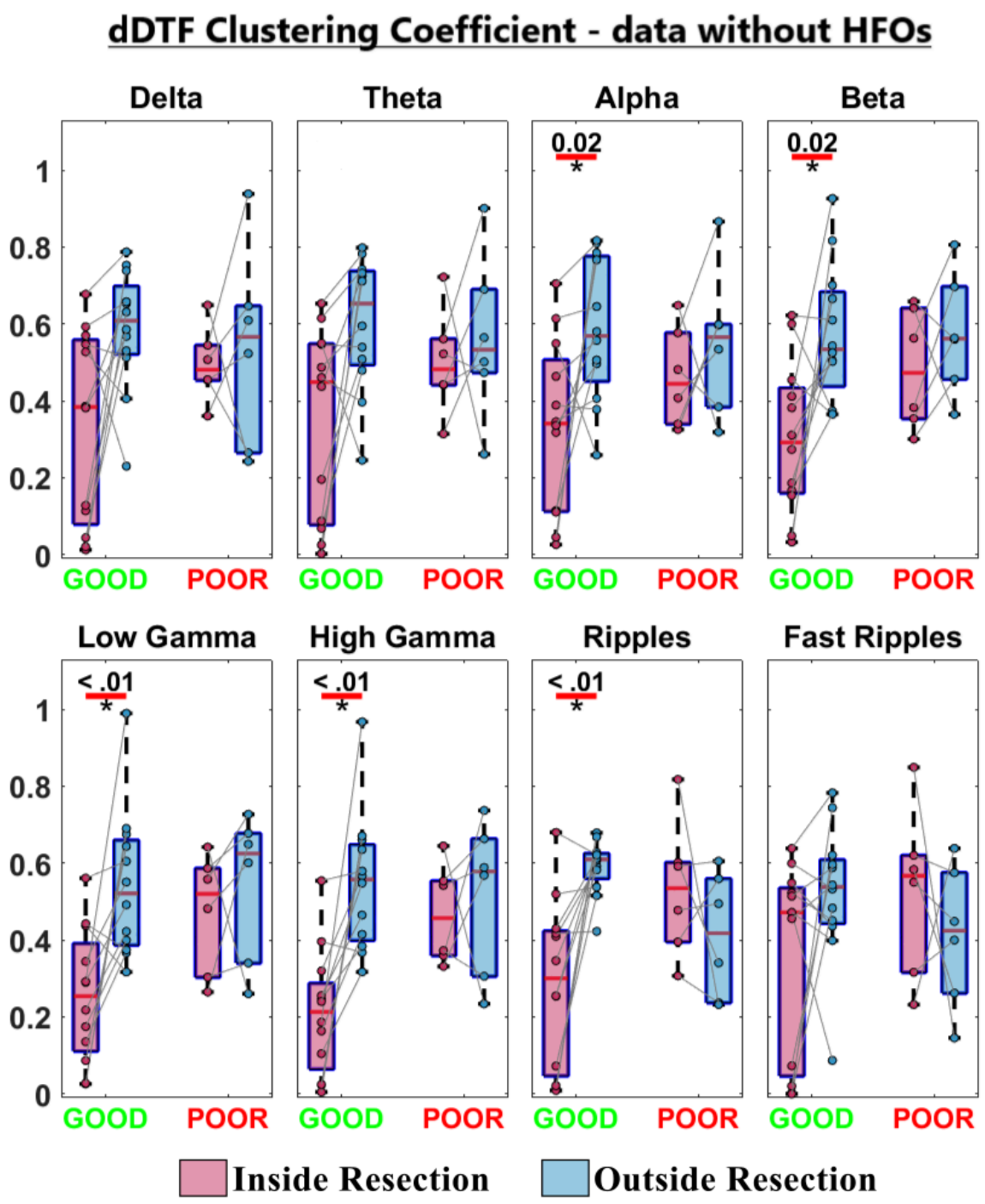

Figure 27: Direct directed transfer function (dDTF) clustering coefficient, for segments without HFOs, compared inside (pink) vs. outside (blue) resection separately for good (N=12) and poor (N=6) outcome patients. Significant differences are marked with an asterisk (*) ($p < 0.05$, Wilcoxon signed-rank test). In the box-plot diagrams, the horizontal line indicates the median value, the lower and upper edges represent the 25th and 75th percentiles, and the whiskers extend to the minimum and maximum values.

To highlight the relationship of decreased nodal outward strength and epileptogenic tissue during the absence of HFOs, I depicted dDTF outward strength across all frequency bands one time for a good outcome (Patient #16, ILAE 1) and one time for a poor outcome patient (Patient #19, ILAE 6) (Figure 28). For the good outcome patient, electrodes (nodes) of decreased outward strength are observed inside the resection, which in this case includes the important epileptogenic tissue, while higher outward strength values are seen in distant (non-resected) brain regions. In contrast, nodes of decreased outward strength were scattered in both resected and non-resected areas in the poor outcome patient.

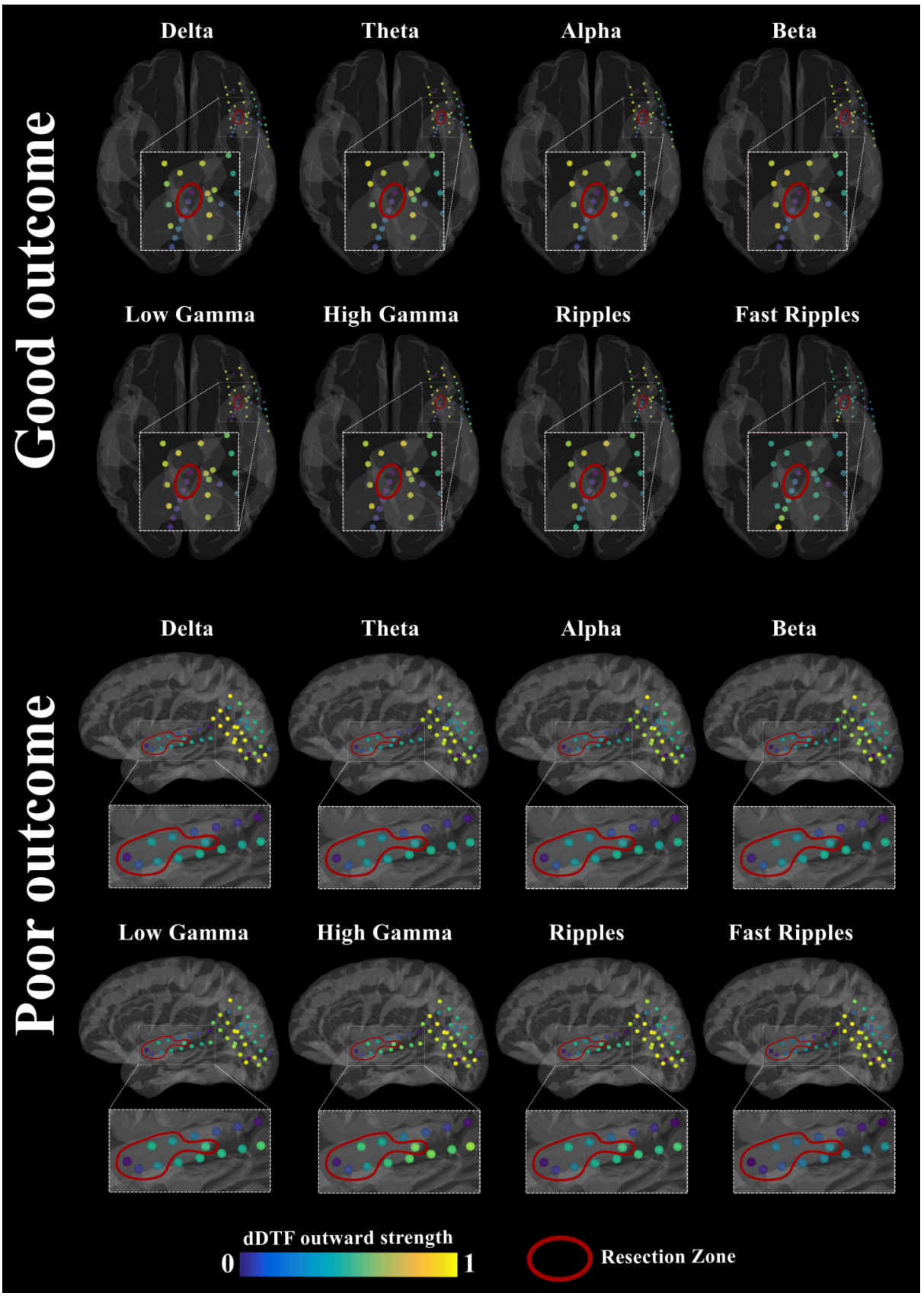

Figure 28: Direct directed transfer function (dDTF) outward strength at the patient level across different frequency bands (from delta to fast ripples). The dTDF outward strength in each bipolar electrode (node) is depicted one time for a good outcome (Patient #16, ILAE 1,

top) and one time for a poor outcome patient (Patient #19, ILAE 6, *bottom*), using their 3D implantation models. Surgically resected electrodes are included in the resection zone, illustrated with a solid red line. The dDTF outward strength values are colour-coded: high dDTF outward strength values are displayed in yellow; low dDTF outward strength values are displayed in dark blue.

Boxplots for all FC techniques (oAEC, NPD, dDTF), graph-theoretical measures, and experimental conditions (data with and without HFOs) are provided in Appendix 1 (Supplementary Figures S5-S31).

All findings from this section are discussed in detail in section 5.4.2.

5.3.3 FC-based ML classifiers can identify the EZ

Since specific local graph measures significantly differ between areas inside and outside the resection of good outcome patients, I assessed their value in identifying the EZ using ML classifiers (as described in section 5.2.3). NPD-based networks were excluded from further analysis, since no patterns of significant differences were found in good outcome patients in section 5.3.2.2.

I found that from the 11 different models trained (see section 5.2.3), Logistic Regression (LR) and Support Vector Machine (SVM) algorithms had the best performance in predicting the EZ. For oAEC-based networks, LR had superior performance over all other models across all frequencies, when data both with HFOs [(AUC=0.76, precision=0.71, recall=0.69] and without HFOs [AUC=0.67, precision=0.64, recall=0.63] were considered (Figure 29). For dDTF-based networks, LR [AUC=0.68, precision=0.64, recall=0.66] outperformed all other algorithms in data with HFOs, while SVM [AUC=0.70, precision=0.64, recall=0.76] was marginally better in data without HFOs (Figure 30).

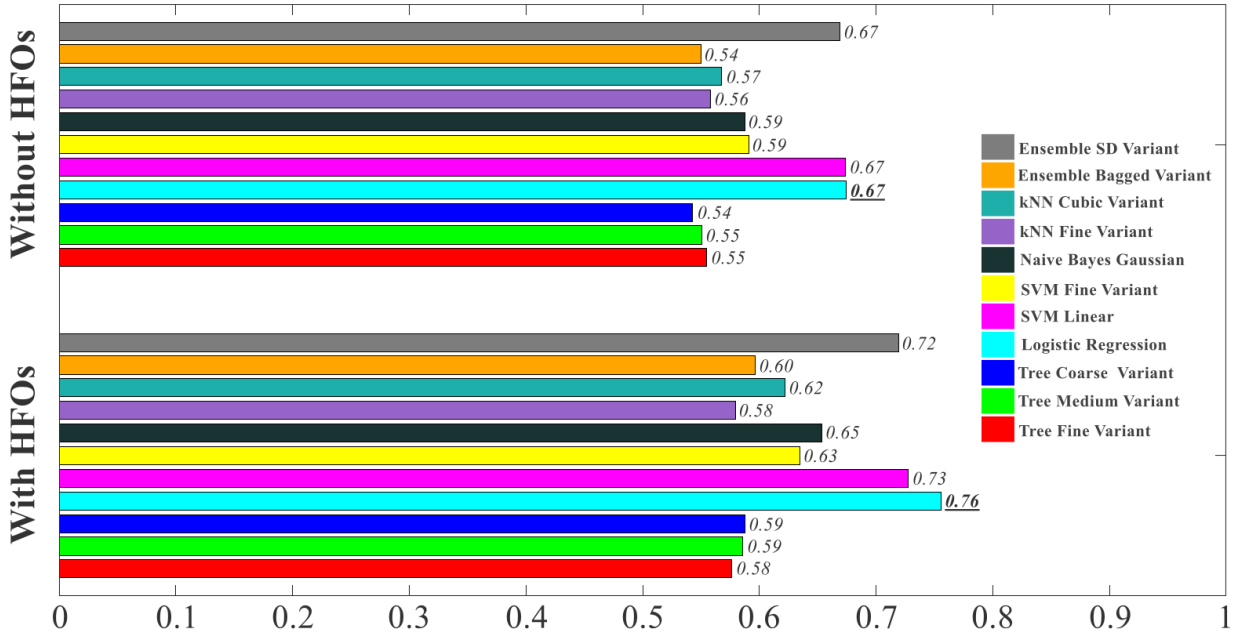

Figure 29: Performance (mean AUC across all frequencies) of 11 different ML algorithms, trained and tested on oAEC-based network measures (CC, PR, and nodal strength) of good outcome patients for predicting the EZ. The Logistic Regression algorithm had the best performance both in data with and without HFOs.

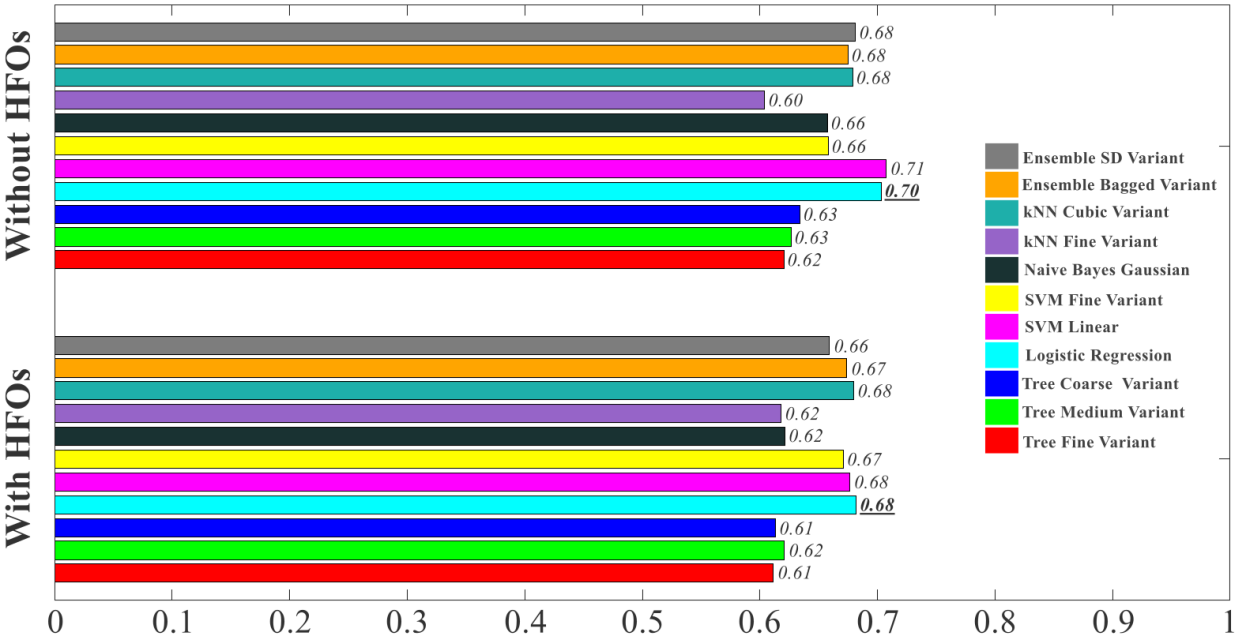

Figure 30: Performance (mean AUC across all frequencies) of 11 different ML algorithms, trained and tested on dDTF-based network measures (CC, PR, outward strength, and total strength) of good outcome patients for predicting the EZ. The Logistic Regression and Support Vector Machine (SVM) algorithms yielded the best results with closely matched performances.

The LR algorithm was chosen for all further analysis since it showed consistently superior performance in both connectivity techniques and data types. Figure 31 illustrates the performance of the LR algorithm across different frequencies for both oAEC and dDTF-based networks and for data with and without HFOs. Using oAEC connectivity in data with HFOs provided the best results in all but the fast ripples band, with beta (AUC=0.87, precision=0.80, recall=0.79) showing the best performance, followed by ripples (AUC=0.80, precision=0.76, recall=0.76).

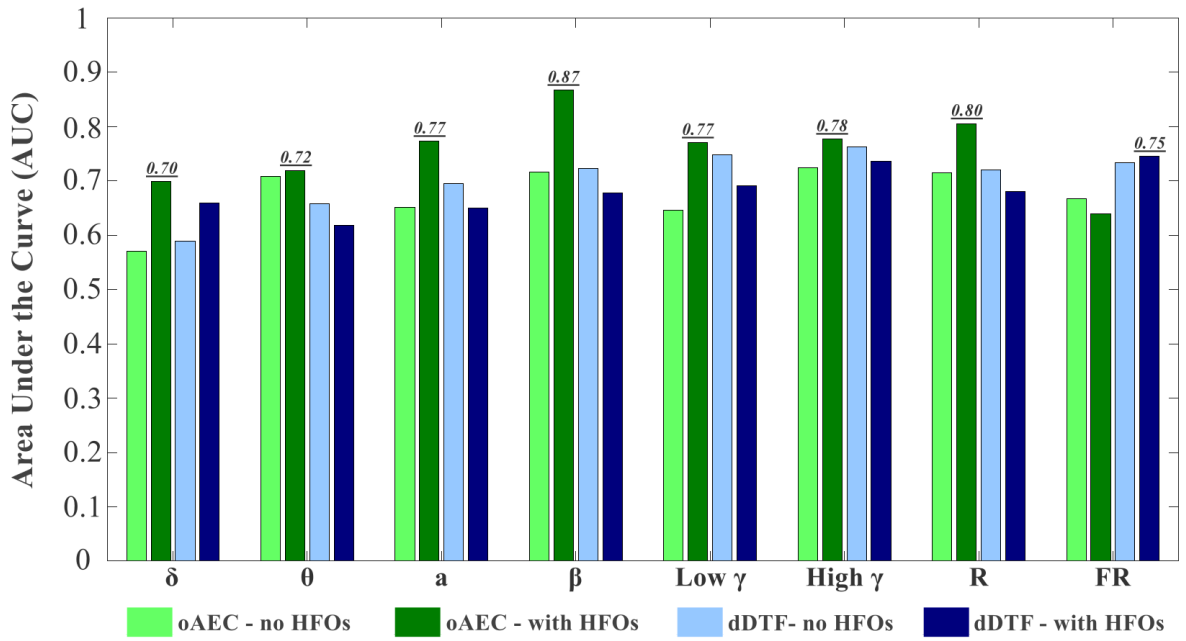

Figure 31: Performance (AUC values) of a Logistic Regression classifier trained and tested on oAEC-based and dDTF-based network measures of good outcome patients for predicting the EZ.

All models predicted the EZ, with moderate to good performances (AUC: 0.57-0.87), as can be seen in Figure 32.

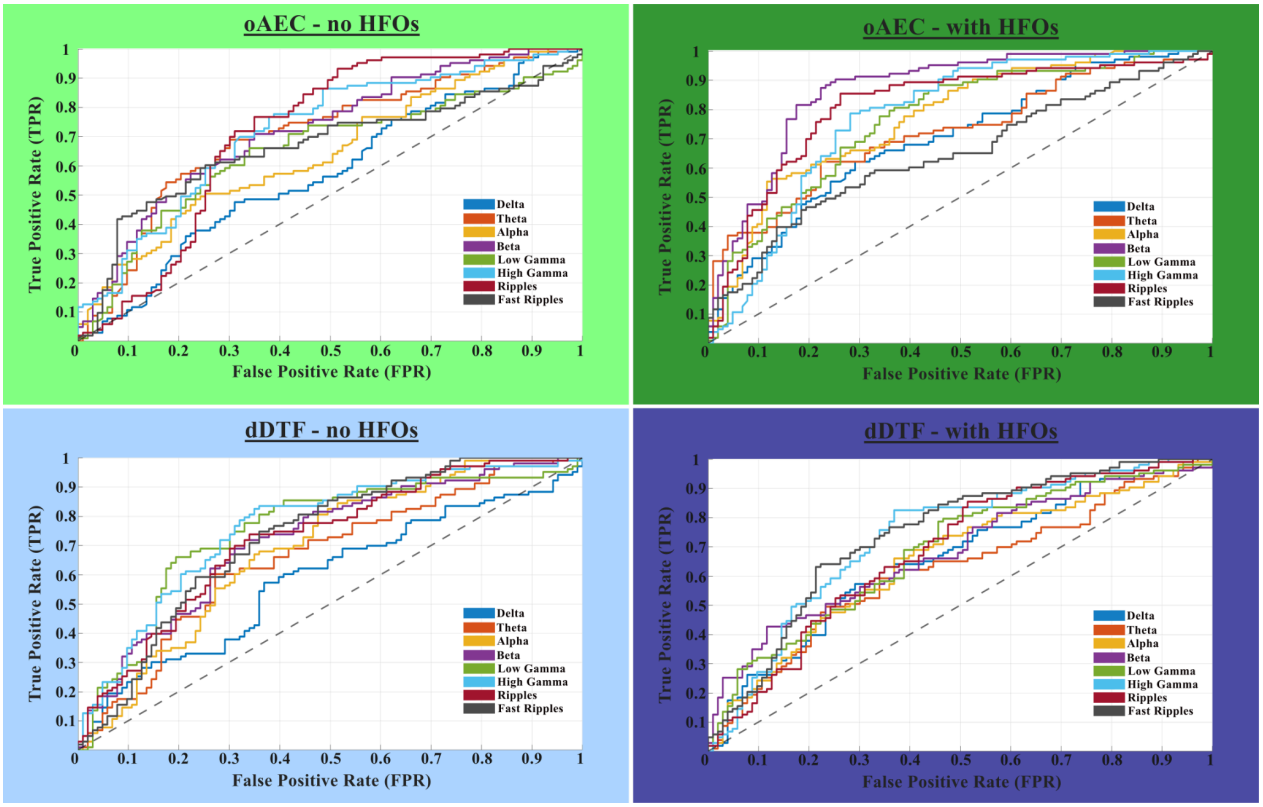

Figure 32: ROC curves representing the classification between EZ (inside resection) and non EZ electrodes (outside resection) in good outcome patients. A Logistic Regression classifier was trained and tested on: i) oAEC-based network measures computed on iEEG data without HFOs (top left), ii) oAEC-based network measures computed on iEEG data with HFOs (top right), iii) dDTF-based network measures computed on iEEG data without HFOs (bottom left), and iv) dDTF-based network measures computed on iEEG data with HFOs (bottom right).

The results from the ML analysis are discussed in detail in section 5.4.3.

5.3.4 Resection of “sink” nodes predicts surgical outcome

To test the prognostic value of resecting “hub” or “sink” nodes (nodes with FC above or below a certain threshold respectively) I assessed whether their overlap with resection was predictive of good surgical outcome or not. I chose oAEC nodal strength to define hub nodes, as this metric was found to be significantly increased inside resection of good outcome patients (see 5.3.2.1). I also chose dDTF outward strength to define sink nodes, as this measure was proven to be significantly lower inside the resection of the same patient population (see 5.3.2.3).

Resection of hub nodes did not predict outcome for any frequency band or data type ($p > 0.05$ in all, Fisher's exact test) (Figure 33).

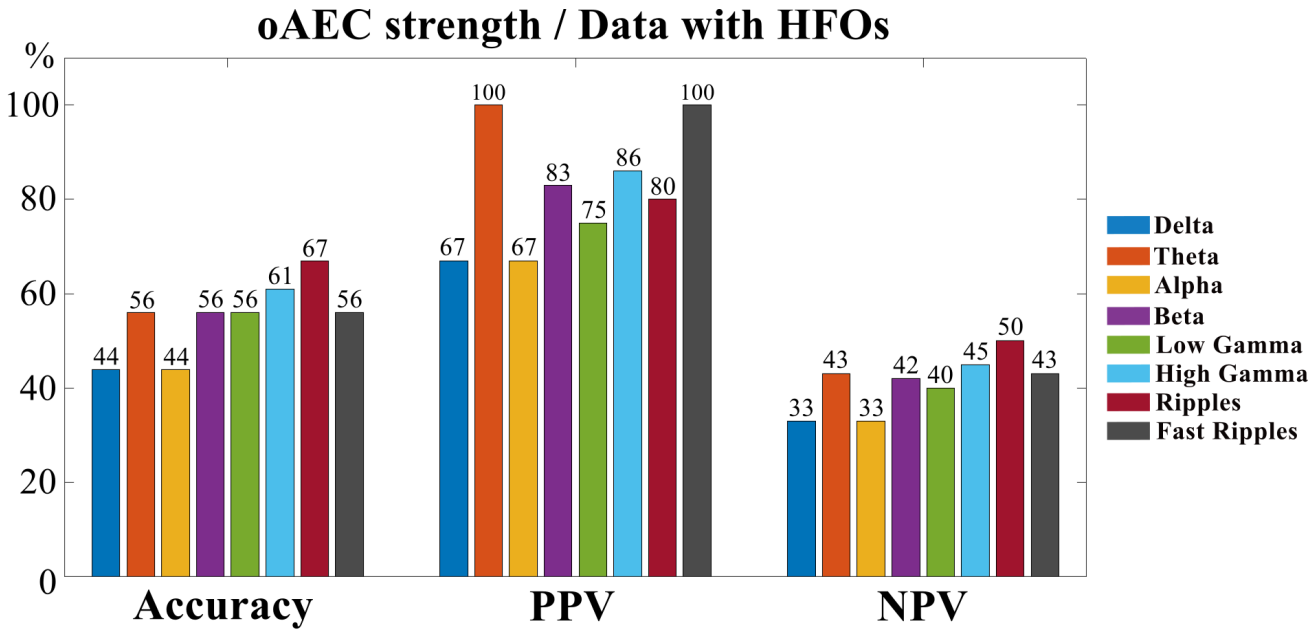

Figure 33: Prediction of surgical outcome across different frequency bands based on oAEC-derived nodal strength in iEEG data with HFO events. Resection of hub nodes (nodal strength > threshold) was not predictive of good surgical outcome for any frequency band ($p>0.05$, Fisher's exact test). PPV: positive predictive value, NPV: negative predictive value.

On the other hand, resection of sink nodes was predictive of outcome when dDTF was computed in data with HFOs, for low gamma [$p = 0.01$, optimal threshold = 0.51, overlap = 65%], high gamma [$p = 0.01$, optimal threshold = 0.55, overlap = 65%], and fast ripples [$p = 0.01$, optimal threshold = 0.51, overlap = 70%] (Figure 34).

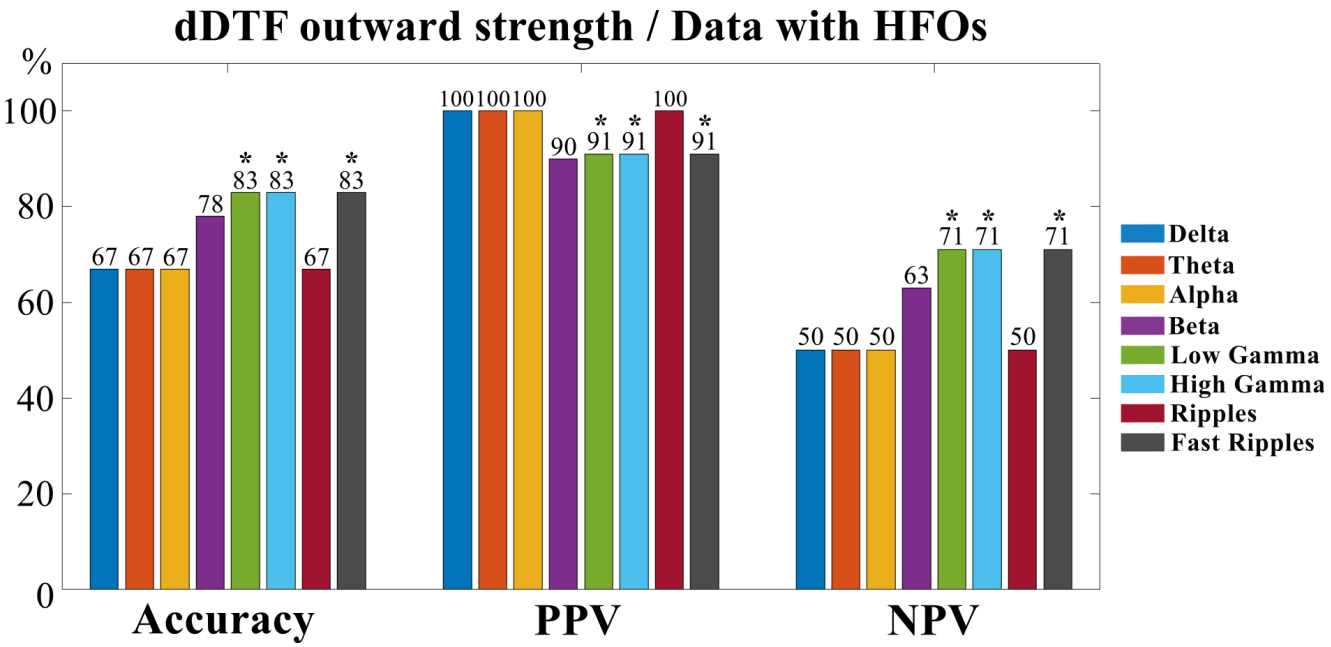

Figure 34: Prediction of surgical outcome across different frequency bands based on dDTF-derived nodal outward strength in iEEG data with HFO events. Resection of sink nodes (nodal outward strength < threshold) was predictive of good surgical outcome for the low gamma, high gamma, and fast ripples bands. Significant results are marked with an asterisk (*) ($p<0.05$, Fisher's exact test). PPV: positive predictive value, NPV: negative predictive value.

Similarly, when dDTF was computed in data without HFOs, resection of sink nodes was again predictive of outcome for beta [p = 0.01, optimal threshold = 0.50 , overlap = 70%], low gamma [p = 0.01, optimal threshold = 0.54 , overlap = 70%], high gamma [p = 0.02, optimal threshold = 0.53 , overlap = 65%], ripples [p = 0.01, optimal threshold = 0.50, overlap = 80%], and fast ripples [p = 0.02, optimal threshold = 0.49 , overlap = 55%] (Figure 35).

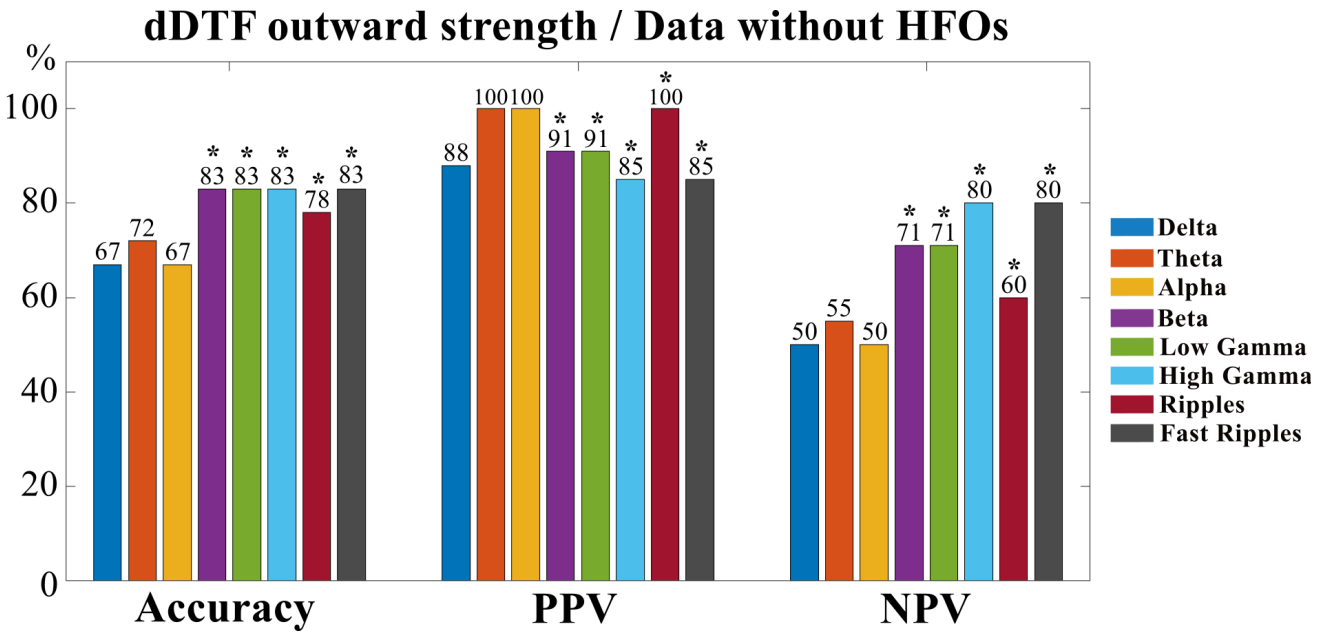

Figure 35: Prediction of surgical outcome across different frequency bands based on dDTF-derived nodal outward strength in iEEG data without HFO events. Resection of sink nodes (nodal outward strength < threshold) was predictive of good surgical outcome for the beta, low gamma, high gamma, ripples, and fast ripples bands. Significant results are marked with an asterisk (*) ($p<0.05$, Fisher's exact test). PPV: positive predictive value, NPV: negative predictive value.

In order to assess whether good outcome patients had greater overlap between sink nodes and the resection compared to poor outcome patients, I compared the percentage of overlap in each frequency between the two outcome groups using the Wilcoxon rank sum test. I found that, in data without HFOs, the overlap of sinks with resection was increased in good outcome patients, compared to patients with poor outcome for beta (good: 85%, poor:65%, $p=0.02$), high gamma (good: 87%, poor:61%, $p=0.02$), and ripple bands (good: 83%, poor:53%, $p<.01$). A visual representation of this overlap difference is presented in Figure 36, where the overlap of sink nodes with resection is depicted one time for a good outcome (Patient #16, ILAE 1) and one time for a poor outcome patient (Patient #20, ILAE 5) from low gamma to fast ripples.

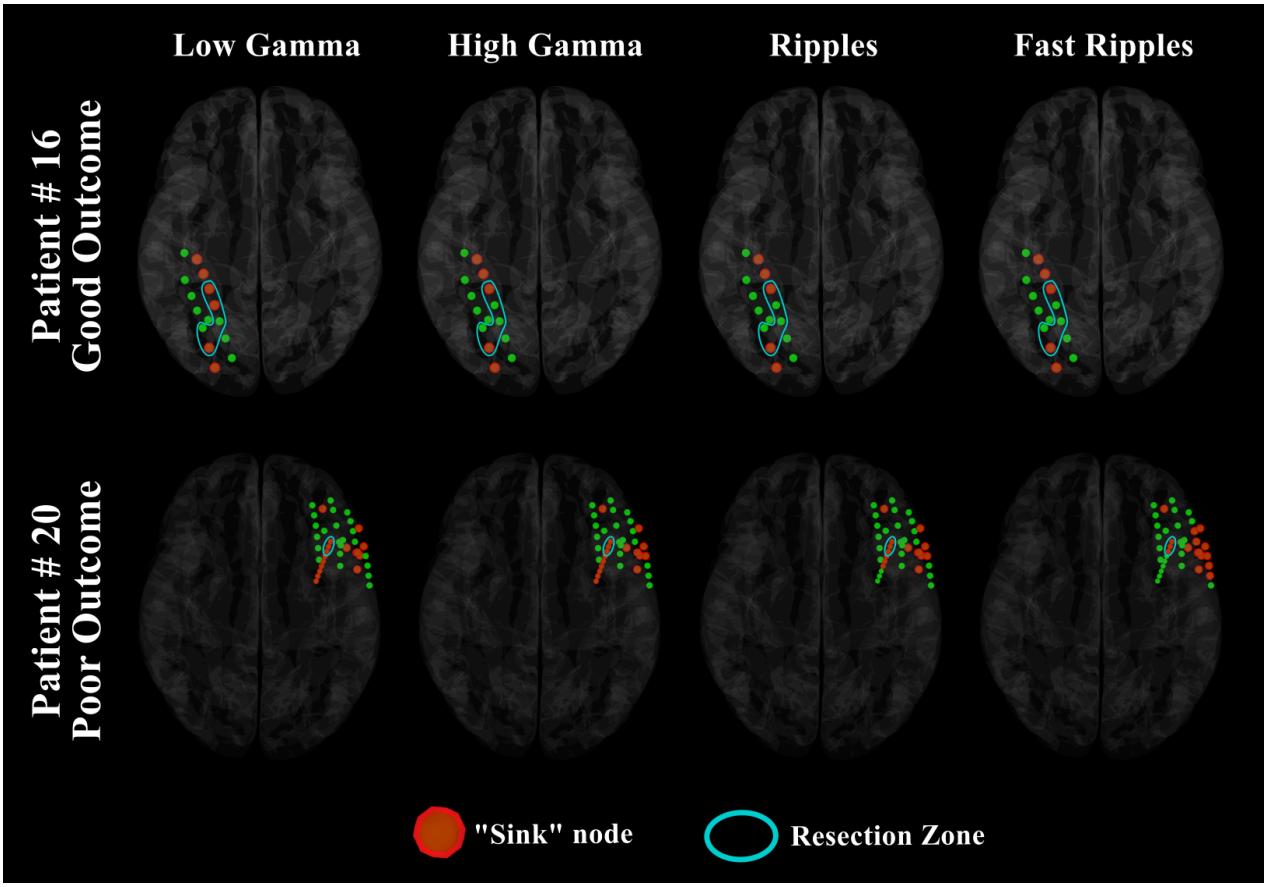

Figure 36: Overlap between sink nodes and the resection zone at the patient level across different frequency bands (from low gamma to fast ripples). Sink nodes, defined as nodes with dDTF outward strength below the optimal threshold, are visualised as red spheres, and are depicted one time for a good outcome patient (Patient #16, ILAE 1, *top*) and one time for a poor outcome patient (Patient #20, ILAE 5, *bottom*), using their 3D implantation models. The resected electrodes are included in the resection zone, illustrated with a solid light blue line.

All findings on FC-based prediction of surgical outcome are discussed in section 5.4.3.

5.3.5 FC results are not explained by local power

When repeating the entire analysis on whitened data (see 4.5), the main effects observed in the original signals were preserved, indicating that my findings are not explained solely by power dependences across electrodes.

5.4 Discussion and Conclusion

In this explorative network study I showcase that at higher frequencies interictal iEEG FC is affected by the presence of HFO events, can identify epileptogenic and non epileptogenic tissue, and can predict surgical outcome in DRE patients. This notion derives from my main findings:

I. Decreased oAEC nodal strength and clustering coefficient during interictal periods with HFOs compared to periods without HFOs for the high gamma and ripple bands.
II. Higher oAEC nodal strength, CC, and PR, and lower dDTF outward strength, total strength, CC, and PR inside compared to outside resection of good outcome patients for multiple frequencies.
III. ML classifiers trained on local network properties identified the EZ with AUCs up to 0.87 (optimal performance in the beta and ripple bands).
IV. Overlap of “sink” nodes (outward strength < threshold) with resection was predictive of good surgical outcome in data both with HFOs and without HFOs for frequency bands above beta.

In the following sections, I discuss these findings in detail and interpret them in light of the most recent literature.

5.4.1 The influence of HFOs on FC is method dependent

Despite several works having already assessed the effects of interictal spikes on FC [37], [40], [41], there is a lack of studies on the behaviour of the corresponding networks and their properties during the presence or absence of HFOs. Here, I attempted to fill this gap by extensively investigating FC separately in segments containing HFOs and segments that are HFO-free, across a wide range of frequency bands (from delta to FRs). My results reveal that in the presence of HFOs, oAEC-based FC (nodal strength and CC) decreases compared to HFO-free segments, with the most profound differences in the high gamma and ripple bands (see 5.3.1). These findings come to complement previous works which have demonstrated a negative correlation between the rate of HFOs and the value of different network measures at a node (strength, EC, and CC), at both the conventional (theta, alpha, low gamma) [230] and higher frequencies (ripples, fast

ripples) [204]. This decrease of FC at electrodes where HFOs are generated (or propagated to), could contribute to a lower overall FC at the patient level, something that is in line with my findings. Interestingly, the presence of interictal spikes has the opposite effects, as previous studies have found that the suppression of segments with spikes did not to change the results of FC [34], [40], [41], while other works reported increased overal FC during the occurrence or spead of spikes in the brain [37], [231], [232]. Although HFOs and spikes are both closely linked to epileptogenicity, there is evidence supporting that these events may engage distinct pathophysiological mechanisms that disrupt the resting brain [233], [234]. In this line, a possible explanation for my observations could be that spikes and HFOs alter network integration and functional connectivity in notably different ways. However, to confirm such a hypothesis, a future study should investigate the effects of spikes and HFOs on FC using the same patient cohort, FC technique, and frequency bands.

My results also revealed an increase in dDTF clustering coefficient in the ripple band during the presence of HFOs, which despite initially being significant did not survive correction for multiple comparisons (FDR method). The fact that dDTF quantifies causal influences based on phase relationships, and since HFOs are highly localised amplitude bursts with altered spectral content, could potentially explain why the overall dDTF-based network structure is not greatly influenced by their presence (stable total strength, PR and BC), while clustering might increase (especially in the HFO band) since a specific cluster of local hubs drives the activity of the network at times they occur. Following the same notion, envelope-based techniques such as oAEC would pick up these amplitude deviations as decreased global coupling, since few nodes would "take over" and result in decreased overall FC.

5.4.2 Decreased outward strength is a robust characteristic of the EZ

Assessing interictal iEEG functional connectivity, coupled with graph theory principles, has shown promise as a means of delineating the EZ in DRE patients [36], [37], [40], [41], [198], [235], [236], [237]. The vast majority of prior studies investigated connectivity at frequencies up to the high gamma band (~80 Hz). However, recent

research directions suggest that networks at higher frequency ranges (> 80 Hz) can help comprehend epileptic networks, serving as a reliable tool for assessing epileptogenic zones and predicting surgical outcomes [238]. Here, I extended FC analysis to a wider spectrum of frequencies, from delta to fast ripples, and investigated the network characteristics of epileptogenic and non-epileptogenic tissue. I followed the notion that in good outcome patients, resection included the critical epileptic targets, while in poor outcome patients these crucial epileptic foci could also be located in areas outside the resection margins.

Undirected FC results

At conventional frequencies, prior studies that used undirected FC consistently reported increased nodal strength [37], [198], [236], local clustering [36], [40], and centrality measures [36] in epileptogenic tissue. Similarly, in this work, I observed higher oAEC nodal strength, CC, and PageRank inside the resection of good outcome patients (and no differences for poor outcome) for the θ, β, low γ, and high γ bands, when using data with HFOs. This profound increase in connectivity at epileptogenic areas during periods of HFO presence further supports the value of HFOs as an indispensable component of epileptogenicity, while it also links microscale neuronal circuitry with mesoscale functional organisation of the brain in DRE patients.

For undirected FC at higher frequencies (> 80 Hz), the literature is very sparse. Isolated reports support higher FR band eigenvector centrality at brain areas with spikes [239], higher ripple band nodal strength inside (vs. outside) the SOZ [237], and higher HFO band nodal strength inside (vs. outside) the resection of both good and poor outcome patiens [39]. My results show increased oAEC ripple band FC (nodal strength, CC, and PR) inside compared to outside resection of good outcome patients, and no differences in any FC measure for the fast ripples band. The fact that only ripple band FC is increased implies that the observed differences are not driven by amplitude-based dependencies due to the presence of HFOs, since then FR connectivity would also be altered. Rather, my results suggest that ripple band FC could also hold valuable information about the underlying functional motif of the network and assist in the identification of epileptogenic tissue.

Directed FC results

Directed functional connectivity has been demonstrated to provide more accurate EZ localization compared to undirected connectivity [198], [240], [241]. In the electrographic network, inward and outward connections of the EZ are related to the concept of inhibition and excitation, which is indispensably associated with epilepsy [242], [243]. Recent studies suggest increased inward connectivity in EZ areas [36], [41], [198], [237], [244], while others report increased outward connectivity from the EZ to the rest of the network [203], [235], [245]. This heterogeneity of results has been attributed to the variable methods used for FC estimation [34]. However, another explanation may lie in the influence of interictal spikes on the directionality of FC [34], [43], as studies using the same connectivity method have produced conflicting results, with some analysing data containing spikes and others not. In response to the existing variety of observations and interpretations, here I explored two different directed connectivity techniques, which I tested both on data with and without HFOs to assess their impact on FC directionality.

I observed decreased dDTF outward strength inside (vs. outside) the resection of only good outcome patients in data without HFOs (for beta, low γ, high γ, and ripples). This result is consistent with the recently proposed concept of the “Interictal Suppression Hypothesis (IHS)”, which posits that during the interictal period, the SOZ is tonically suppressed by other areas of the brain to prevent seizure initiation [237]. The electrographic network signature of this concept is increased inward strength and decreased outward strength in the SOZ [237]. My results are only partly in line with this notion, since dDTF inward strength did not present significant differences between areas inside and outside resection in good outcome patients. Interestingly, I also found decreased dDTF CC and PR inside the resection of only good outcome patients, indicating that the nodes within epileptogenic tissue are less cohesive and have diminished overall influence between the broader network. These observations fit well within the concept of the ISH, which wants epileptogenic tissue to be in a suppressed, isolated, and low-influence state during interictal periods. However, we need to keep in mind alternative interpretations that could still explain the results. For example, reduced outward connectivity of epileptogenic tissue could reflect a functional segregation that may permit seizure generation, in contrast to a more integrated configuration with surrounding brain regions which could exert

suppressive control [237]. Also, decreased CC and PR might also arise from structural damage or network reorganisation due to the long-standing disease burden, although the selective occurrence in good outcome patients supports the ISH interpretation.

This connectivity pattern vanished when the same network measures were computed on segments with HFOs. This observation is in line with previous reports on the effects that other interictal epileptiform events, such as spikes, might have on the directionality of connectivity in the epileptic brain [43]. In addition, observing such patterns of decreased EZ connectivity primarily during HFO-free data further supports the idea that interictal suppression mechanisms are present mostly at times of no epileptiform activity interictally.

This functional isolation of the EZ, that my results support, has been demonstrated in the literature [203], [230], and especially for higher frequencies it is believed to act as a compensatory mechanism to thwart seizure initiation and halt ictal propagation [238].

5.4.3 FC can identify epileptogenic tissue and predict surgical outcome

To test the biomarker value that FC differences observed between epileptogenic and non-epileptogenic tissue hold, several studies assessed the performance of ML models trained on network properties in identifying EZ areas [36], [41], [198], [204], [237]. Similarly, my Logistic Regression (LR) model showed that FC can identify the presumed EZ (resected nodes in good outcome patients) in all frequencies, using both oAEC and dDTF-based measures. The performance of oAEC-based models was greatly dependent on the presence or absence of HFOs (with-HFOs AUC: 0.64-0.87, without-HFOs AUC: 0.57-0.72), while dDTF-based models were less affected (with HFOs AUC: 0.62-0.75, no HFOs AUC: 0.59-0.76). Interestingly, FC at higher frequencies (low γ, high γ, ripples, and fast ripples) was found to provide better classification results compared to lower frequencies (δ, θ, and α) for both FC techniques (see Figure 32 in 5.3.3). Most previous similar studies have also used LR [36], [198], whereas others have employed SVM classification schemes for the

identification of the EZ [237]. In my data driven approach, I found SVM models to have equally good performance to LR, however, I chose to move forward with the later as I belive LR models are more likely to be trusted and adopted by clinicians, given their simplicity and widespread use in medical literature.

Moreover, only a limited number of studies have evaluated the applicability of interictal iEEG FC for predicting the surgical outcome of DRE patients [31], [37], [41], [201], [202]. Here, I showed that resection of dDTF-derived sink nodes can predict good surgical outcome ($p<0.05$, Fisher's exact test). This finding held true for data both with and without HFOs, with higher frequencies (> beta) presenting the most consistent results. Contrarily, resection of oAEC-derived hub nodes was not predictive of outcome in any of the HFO states or frequencies. Being able to predict the surgical outcome of a patient using FC computed on brief interictal segments of data, regardless of the presence of epileptiform events such as HFOs, enhances the potential value of FC applications during the presurgical evaluation of DRE patients. The predictive relevance of pre-operative brain networks for surgical outcomes has also been demonstrated in structural studies using tractography MRI, which suggest that heightened limbic and extralimbic connectivity may underlie less favorable postoperative seizure outcomes [246], [247].

5.4.4 Limitations and future considerations

My work has several limitations, which I classify into two categories:

I. Data- and theory-related limitations, stemming from the characteristics of the dataset or conceptual constraints.
II. Methodological limitations, resulting from specific analytical choices in my study.

Data- and theory-related limitations

The relatively small cohort size (18 patients: 12 good outcome, 6 poor outcome) limits the generalizability of the results, especially those related to poor outcome patients. Future works should investigate larger, multicentre datasets to increase the reliability of the proposed analysis. In addition, a concern inherent to all iEEG data analyses is the partial sampling of the brain, since electrode placement is based on

clinical necessity [236]. Therefore, critical network components might not be adequately covered, especially in patients with poor outcomes. The problem of incomplete sampling or over-sampling of some structures can introduce bias during the computation of centrality measures, with simpler metrics, such as nodal strength, being more robust [34] Future works could overcome such limitations by analysing noninvasive high-density recordings (HD-EEG, HD-MEG) using source modelling and virtual sensors, with several recent studies already reporting promising results [31], [35], [248], [249], [250]. Moreover, it is established that electrodes that are physically closer are more likely to be highly connected [34], with previous studies addressing this issue by normalising FC values, usually through the Euclidean distance between electrodes [37], [183], [251]. In the absence of anatomical information (MRIs, CTs), my work did not account for inter-electrode distance effects on FC, something that could potentially have affected the results. Similarly, SEEG contacts within the white matter could not be identified and removed from further analysis, something that was deemed important in previous works [36], [37], [198], [199], mainly due to the uncertainty of the origin of the signals in these areas . Finally, since the dataset did not include information about the drug load of each patient at the time of monitoring, I could not account for the effects that antizeizure medication might have on FC [199].

Methodological limitations

The choice of reference is an important point of discussion in FC studies. Here I worked with a bipolar montage, as this configuration is generally preferred when studying HFOs [118], and also because all relevant information about the iEEG channels, such as the resection status, was provided in bipolar format inside the dataset's documentation. Moreover, in a previous study on interictal iEEG FC at higher frequencies, the authors assessed the influence of reference choice (bipolar vs. common average reference) on MVAR model fitting, revealing that rereferencing to common average made FC fade at conventional frequency bands and disappear in the FR band [203]. Nevertheless, future investigations should address the impact that other referencing techniques might have on FC estimates. Another confounder in this work, could be the fact that the detection of HFOs (ripples and fast ripples) was performed only by a single reviewer, in comparison to most other studies where at least two separate experts mark the events and an inter-observer agreement is

calculated using Cohen's kappa coefficient to accomplish a consensus, increasing accuracy and reducing bias. Moreover, a methodological consideration that needs careful interpretation is the choice of model order in dDTF computations. Various criteria can be applied to determine the optimal order, with Akaike's Information Criterion (AIC) being among the most widely used [200], [252]. In practise, factors such as the sampling rate and the length of the data segments influence the estimation of the optimal model order [253], [254], [255]. Traditional model order selection paradigms build on the model fit to the data, and high-frequency activity has very small impact on the residuals [203]. In our case, where both parameters are stable across patients, I chose to use a model order of 10 based on previous litterature and emprical findings [198], [203], [222]. A previous work has shown that, despite different model orders yielded similar results at conventional frequencies, at fast ripples outward strength was significantly influenced by the model order, with lower orders resulting in decreased outward strength in the resected area, and higher orders leading to increased outward strength [203]. This may suggest that for short prediction windows, the model struggles to capture the stochastic propagation of epileptic activity but can effectively model the background signal in non-epileptic channels, leading to stronger connectivity among those channels [203]. Future works should use data-driven approaches to determine the optimal model order at the patient level to increase the robustness of FC estimations. Finally, an inherent requirement that came with the exploratory nature of my work, in terms of the number of frequencies and network measures studied, was the need for correction for multiple statistical comparisons. By correcting for such a large number of statistical tests I may have increased the risk of false negatives (missing real effects) in the statistical tests. Exploratory works, such as this one, should be interpreted with this in mind and ideally followed by confirmatory analysis, where the present statistical results can be followed up with fewer, more targeted tests.

5.5 Conclusion

In summary, the present exploratory work demonstrates that, by extending to higher frequencies, interictal iEEG FC can trace the epileptogenic process in the brain of DRE patients. I show that HFO events can significantly affect FC analysis depending on the chosen technique, while I also highlight the robustness of directed connectivity methods, such as the dDTF, in identifying epileotogenic tissue and predicting surgical outcome. By showcasing that epileptogenic tissue acts as a “sink” area in the network, my results support the recently proposed Interictal Suppression Hypothesis and the notion that the epileptogenic foci are functionally isolated from the rest of the network interictally. Overall, I believe these findings may serve as a stepping stone for more targeted research on high-frequency FC in epilepsy, helping to bridge the gap between promising FC tools and their potential clinical application.

Chapter 6

Temporal Stability of Interictal iEEG Functional Connectivity Across Multiple Levels of Analysis

6.1 Introduction

In Chapter 5, I provided evidence that interictal FC and network analysis at higher frequencies can identify epileptogenic tissue and predict surgical outcome in DRE patients. These results further support recent literature proposing the development and use of FC-based biomarkers of the EZ. However, several confounders influencing FC can limit the transition of network-based applications in clinical settings. The effect of time on FC measurements falls under this category and needs to be carefully studied, since the temporal stability of network patterns would strengthen the confidence in their use for EZ delineation in practice [34]. However, this topic remains underrepresented in the literature. Previous works have shown stability of FC results when using different recordings from the same day [41], [191], [192], or across different days [41], [184], [191], [192], [199], [256]. It has also been demonstrated that FC remains stable over iEEG data of different lengths (from 10 seconds to 1 hour long) recorded on the same day [251]. In this chapter, I aim to contribute to this growing body of research by assessing the temporal stability of FC measures across different days of iEEG monitoring, using cohort-, patient-, and electrode-level analysis.

In addition, very few studies have investigated temporal robustness of FC separately in EZ and non-EZ tissue [199], [257], and these did not discriminate

between good and poor outcome patients. Such a distinction could provide a clearer picture of the stability of epileptogenic and non-epileptogenic tissue separately. Through the patient- and electrode-level analyses, I aim to examine potential differences in the stability of the presumed EZ (resection area) and non-EZ regions (non-resected area) in patients with good and poor outcomes, and assess whether these differences could provide added value for delineating epileptogenic tissue.

6.2 Methodology and statistical analysis

This section discusses the patient cohort and the different types of methodological and statistical analyses followed to comprehensively study the temporal stability of FC across several days.

The FC and network measures studied in the rest of this chapter are described in detail in sections 4.3 and 4.4. The only difference compared to the methodological pipeline described in these sections is that here I compute FC and network measures separately at each recording day (night) rather than aggregating across nights. Due to the more informative nature of dDTF, compared to oAEC and NPD, in characterizing the FC of epileptogenic tissue (see 5.3.2), and based on its superiority in predicting surgical outcome (see 5.3.4), I decided to investigate the stability of only dDTF outward strength and CC at data segments without HFOs. I also restricted the analysis at the higher frequencies (low gamma, high gamma, ripples and fast ripples bands), since FC at these bands provided the best results both in identifying epileptogenic tissue (see 5.3.3) and predicting surgical outcome (see 5.3.4) in Chapter 5.

6.2.1 Patient sub-cohort

From the cohort of 18 DRE patients (see 4.1 and 4.2) I identified individuals that had at least four separate nights of iEEG monitoring in the epilepsy unit. I selected this specific number of nights to strengthen my temporal stability analysis, as most previous studies have only examined two [184], [256] or three [41], [191], [199] different days. More specifically the sub-cohort of patients studied in this chapter consists of: patient #1 (TLE, good outcome), patient #3 (TLE, good outcome), patient #4 (TLE, good outcome), patient #5 (TLE, good outcome), patient #6 (TLE, good outcome),

and patient #20 (ETE, poor outcome). Patient demographics for this sub-cohort are summarised in Table 8.

Table 8: Demographics of patients with at least 4 nights of iEEG recordings in the epilepsy unit.

Patient #	Gender / Age	Histology/ Pathology	Epilepsy type	Electrode type	Surgery type	# of bipolar elec. (# of resected)	ILAE score
1	M / 25	HS and gliosis	TLE	Depth & Strip	sAHE; Les	43 (9)	1
3	F / 20	HS	TLE	Depth	sAHE	35 (12)	1
4	F / 20	HS	TLE	Depth	sAHE	56 (12)	1
5	M / 40	HS	TLE	Depth	sAHE	56 (12)	1
6	M / 48	HS	TLE	Depth	sAHE	56 (12)	1
20	M / 17	FCD 3	ETE	Grid	Les	14 (5)	5

M=male: F=female; HS=hippocampal sclerosis; FCD=focal cortical dysplasia; TLE=mesial temporal lobe epilepsy; ETE=extratemporal lobe epilepsy; Les=lesionectomy; sAHE=selective amygdalahippocampectomy; ILAE=International League Against Epilepsy

6.2.2 Cohort-level temporal stability analysis

To investigate the stability of FC patterns across the four nights at the cohort level, I first separated good outcome from poor outcome patients. Since there is only one patient with poor surgical outcome in the sub-cohort (patient #20), I continued the analysis in this section (6.2.2) concerning only the good outcome group (patients #1, #3, #4, #5, #6).

I normalised each patient's dDTF-based network measures (outward strength and CC) within each night to the 0–1 range using that night's minimum and maximum values, similar to the methodology in 5.2 and in accordance to previous works [31], [37]. This procedure was performed separately for each frequency band (low γ, high γ, ripples, and fast ripples). Next, for each patient, I calculated the median value of each measure one time for electrodes inside resection and one time for electrodes outside. Finally, I plotted the graph measures inside vs. outside the resection to visually assess their variation across different nights.

6.2.3 Patient-level temporal stability analysis

To analyze FC robustness across nights at the patient level I included all 6 patients of the sub-cohort (5 good outcome + 1 poor outcome). Here, I normalised each graph measure at the 0-1 range using its maximum and minimum value across all 4 nights. For each patient I computed the median graph measure value in each night separately for electrodes inside and outside the resection. I assessed the temporal stability of each measure using a linear mixed-effects (LME) model. For a specific area (inside or outside resection) and frequency band, I computed the median FC value per patient and night, leading to a 6 (patients) × 4 (nights) model. The model was specified with nights as the fixed effect, representing the effect of recording night on the specific measure. In addition I introduced a random effect accounting for inter-individual baseline differences in the measure's overall value, ensuring that variability between patients does not inflate the estimated effect of night. The model could be mathematicaly expressed as:

$$LME = \beta_0 + \beta_{Night_j} + u_i + e_{ij}$$

where, β_0 is the grand intercept, β_{Nightj} are fixed effects of night j, u_i is the random intercept fot patient i, and e_{ij} is the residual error. The effect of night was assessed using an analysis of variance (ANOVA) on the LME model [anova.m].

6.2.4 Electrode-level temporal stability analysis

In order to investigate the temporal stability at the electrode level I studied each patient seperately, in a case-study like analysis. The normalization procedure followed was the same as in 6.2.3. I again distinguished resected from non-resected electrodes to study the corresponding areas individually. For each patient separately, I generated an LME model (N electrodes x 4 nights). The number of electrodes (N) both inside and outside the resection varied from patient to patient. Similarly to 6.2.3, here, nights were specified as the fixed effect, and a random effect was introduced to capture electrode-level variability. The effect of nights in the stability of FC measures across the different electrodes was assessed using ANOVA.

Through the above investigations, I aimed to address RQ5: "*Are functional connectivity patterns stable across four different days of recording?"*. Furthermore, based on the patient- and electrode level analyses, I sought to answer RQ6: "*Does*

the stability of FC across separate days differ between epileptogenic and non-epileptogenic tissue?".

6.3 Results

In this section I present the results of the FC stability analysis for the three levels of interest: cohort, patient, and electrode. Each level is presented separately.

6.3.1 Functional connectivity is stable across nights at the cohort level

When assessing the stability of FC at the cohort level (see 6.2.2), I found that outward strength and CC were relatively stable both inside and outside resection for all frequency bands (Figure 37, Figure 38). Across the four different nights, both measures were consistently decreased inside compared to outside resection for the low gamma, high gamma, and ripple bands (Figure 37A-C, Figure 38A-C). For fast ripples, I observed no obvious differences in outward strength (Figure 37D), and interestingly, I found CC to be increased inside resection compared to outside (Figure 38D).

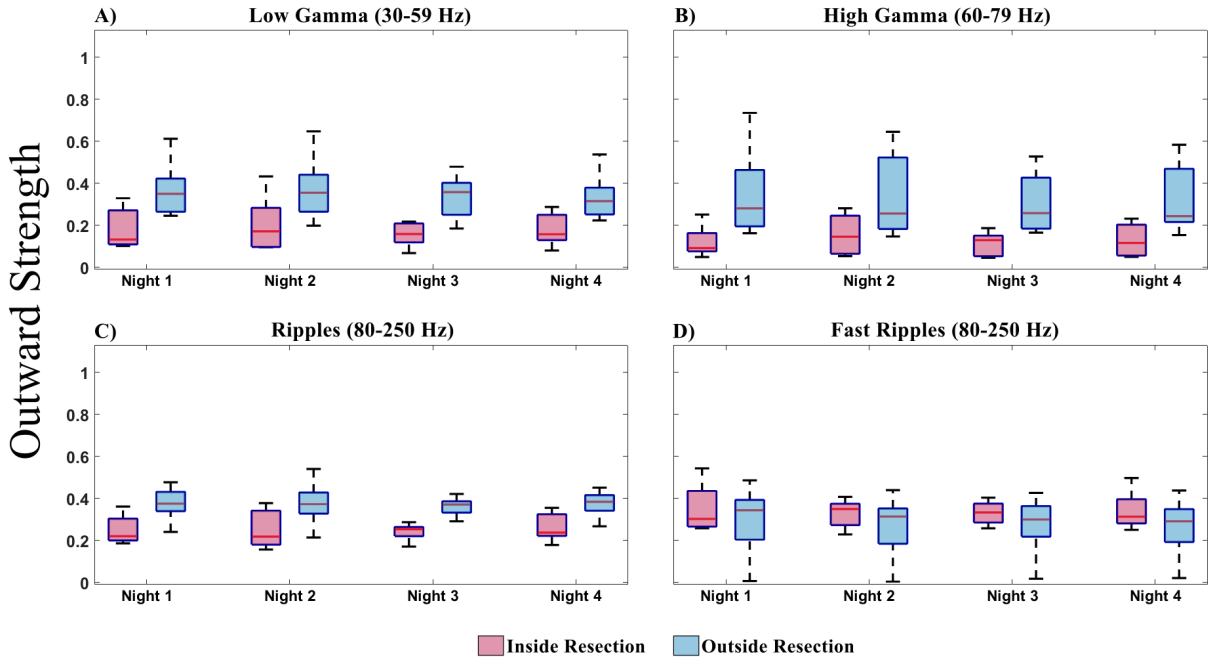

Figure 37: Direct directed transfer function (dDTF) nodal outward strength illustrated inside (pink) and outside (blue) the surgical resection across four different nights of recording for: A) low gamma, B) high gamma, C) ripples, and D) fast ripples. In the box-plot diagrams, the

horizontal line indicates the median value, the lower and upper edges represent the 25th and 75th percentiles, and the whiskers extend to the minimum and maximum values.

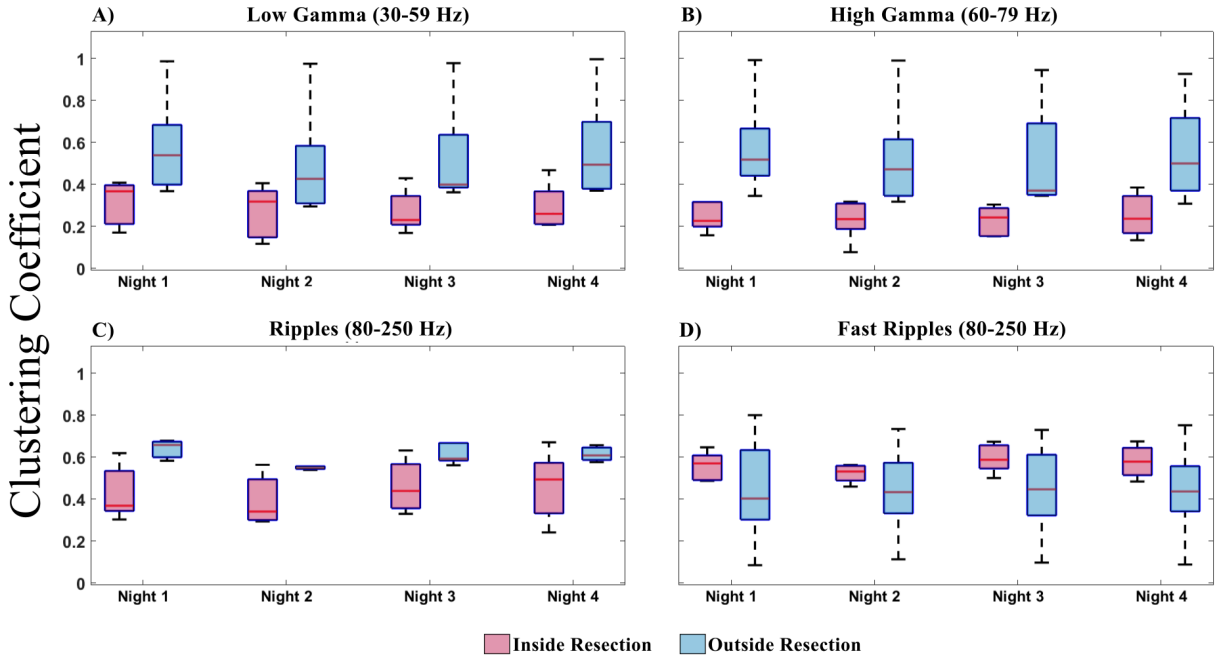

Figure 38: Direct directed transfer function (dDTF) clustering coefficient illustrated inside (pink) and outside (blue) the surgical resection across four different nights of recording for: A) low gamma, B) high gamma, C) ripples, and D) fast ripples. In the box-plot diagrams, the horizontal line indicates the median value, the lower and upper edges represent the 25th and 75th percentiles, and the whiskers extend to the minimum and maximum values.

6.3.2 Functional connectivity is stable across nights at the patient level

When the stability of FC was assessed at the patient level (see 6.2.3), I found that outward strength appeared stable both inside and outside resection (Figure 39), and did not statistically differ from night to night (LME model, ANOVA p = 0.97–0.99). Similarly, CC also proved relatively stable across nights both inside and outside resection (LME model, ANOVA p = 0.20–0.99).

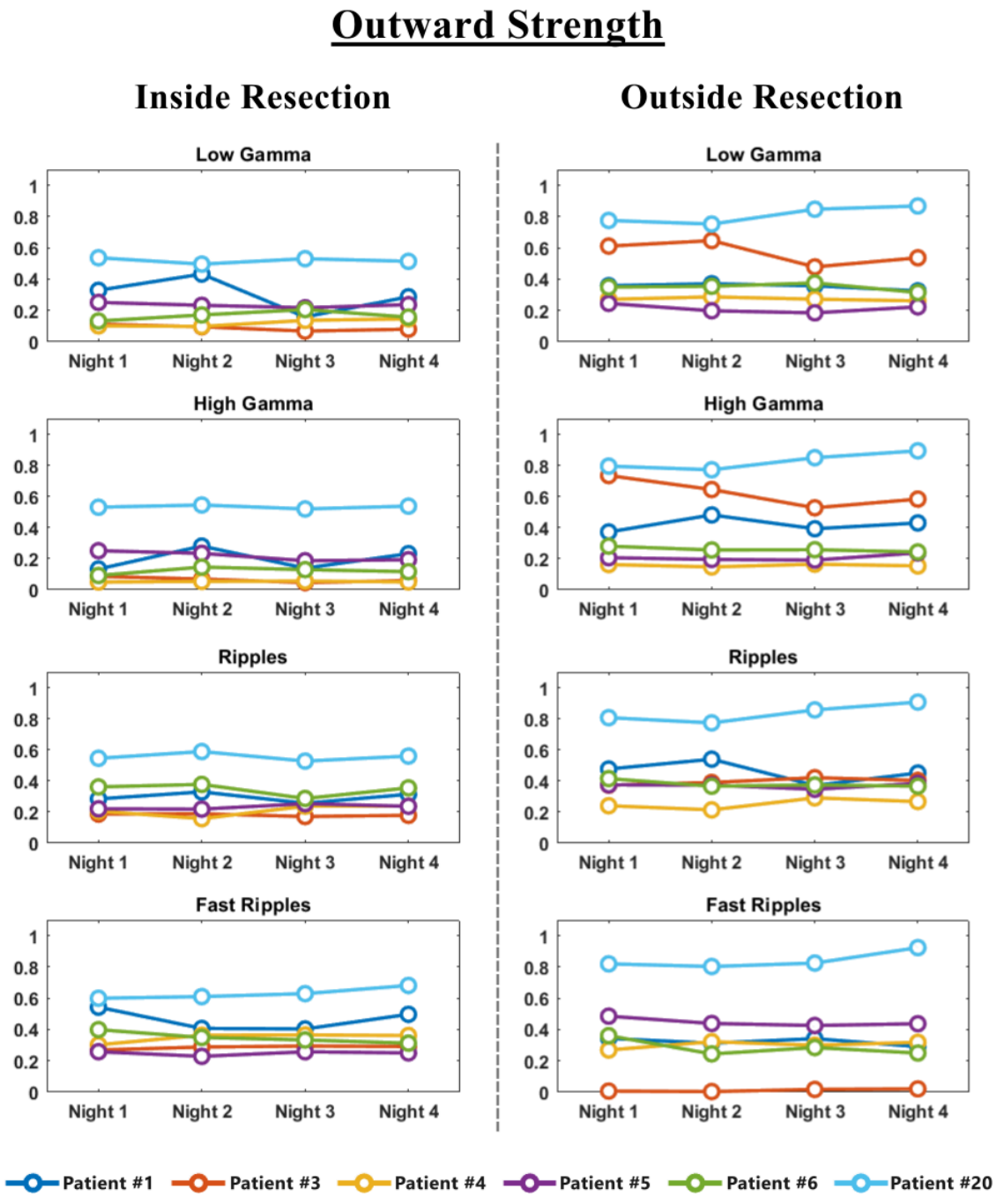

Figure 39: Variation of the mean dDTF nodal outward strength in each patient across four different nights of recording, separately for nodes (electrodes) inside and outside resection.

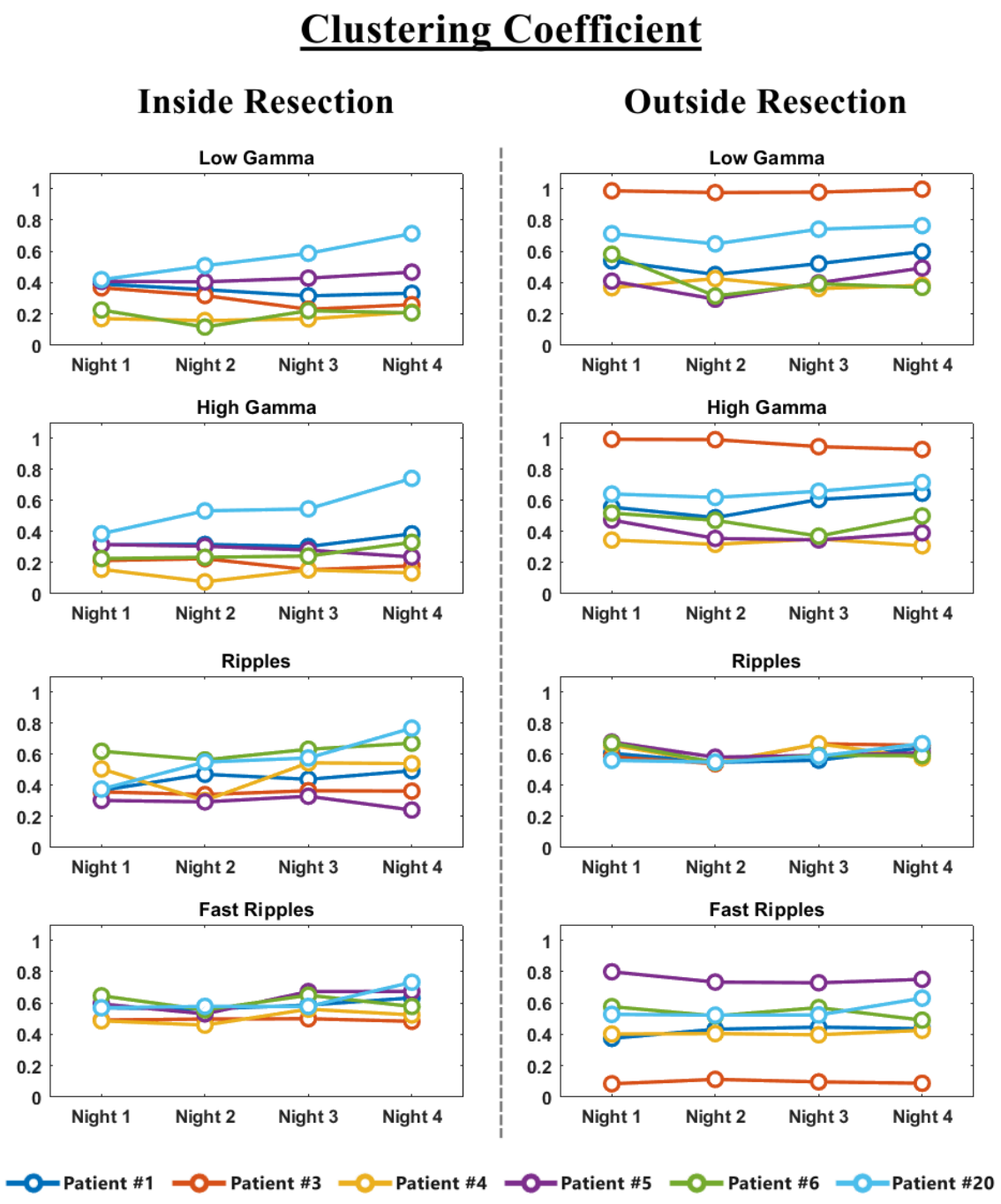

Figure 40: Variation of the mean dDTF clustering coefficient in each patient across four different nights of recording, separately for nodes (electrodes) inside and outside resection.

6.3.3 Functional connectivity is stable across nights at the electrode level

To investigate the stability of FC at the level of individual electrodes I studied each patient separately (see 6.2.4). I found that for all patients and frequency bands, the effect of the different recording nights on outward strength was not significant (LME model, ANOVA p>0.05) both inside and outside the surgical resection: Patient #1 [inside: p=0.11-0.62, outside: p=0.78-0.95], Patient #3 [inside: p=0.17-0.99, outside: p=0.68-0.98], Patient #4 [inside: p=0.47-0.98, outside: p=0.96-0.99], Patient #5 [inside: p=0.79-0.98, outside: p=0.96-0.98], Patient #6 [inside: p=0.68-0.99, outside: p=0.50-0.98], and Patient #20 [inside: p=0.97-0.99, outside: p=0.98-0.99]. Figure 41 illustrates the temporal robustness of outward strength across the four different nights, both inside and outside the resection of each patient for the low gamma band. Additional figures for the rest of the frequencies (high gamma, ripples, and fast ripples) are provided in Appendix 1.

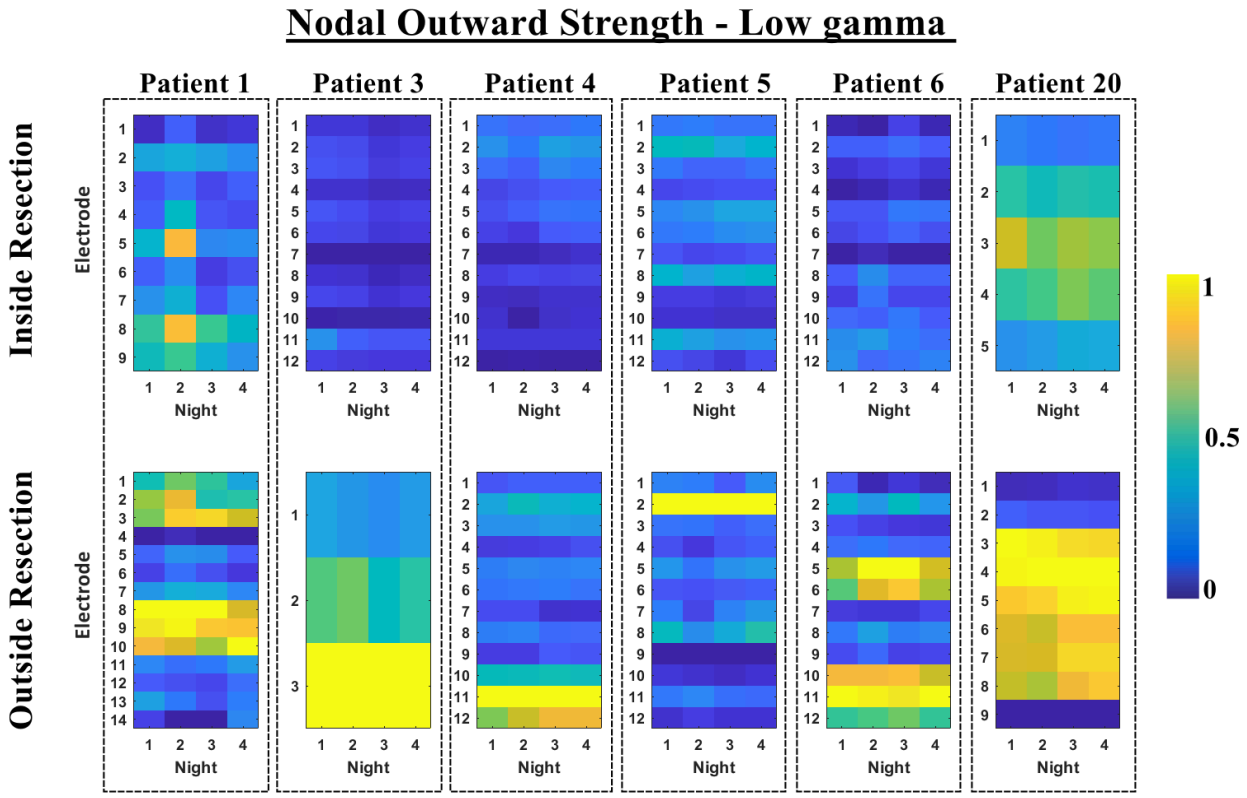

Figure 41: Variation of dDTF nodal outward strength in each electrode of every patient across four different nights of iEEG recording for the low gamma band.

Similar results were obtained for the stability of CC across nights. Again, the effect of the recording night was not significant both inside and outside resection, for all frequency bands: Patient 1 [inside: p=0.76-0.90, outside: p=0.48-0.92], Patient 3 [inside: p=0.37-0.99, outside: p=0.46-0.99], Patient 4 [inside: p=0.50-0.99, outside: p=0.94-0.99], Patient 5 [inside: p=0.76-0.96, outside: p=0.74-0.96], Patient 6 [inside: p=0.18-0.93, outside: p=0.51-0.88], and Patient 20 [inside: p=0.78-0.87, outside: p=0.94-0.97]. Figure 42 demostrates the variation of CC accross different recording nights for electrodes inside and outside resection for the high gamma band. Similar figures for the rest of the frequencies (low gamma, ripples, and fast ripples) can be found in Appendix 1.

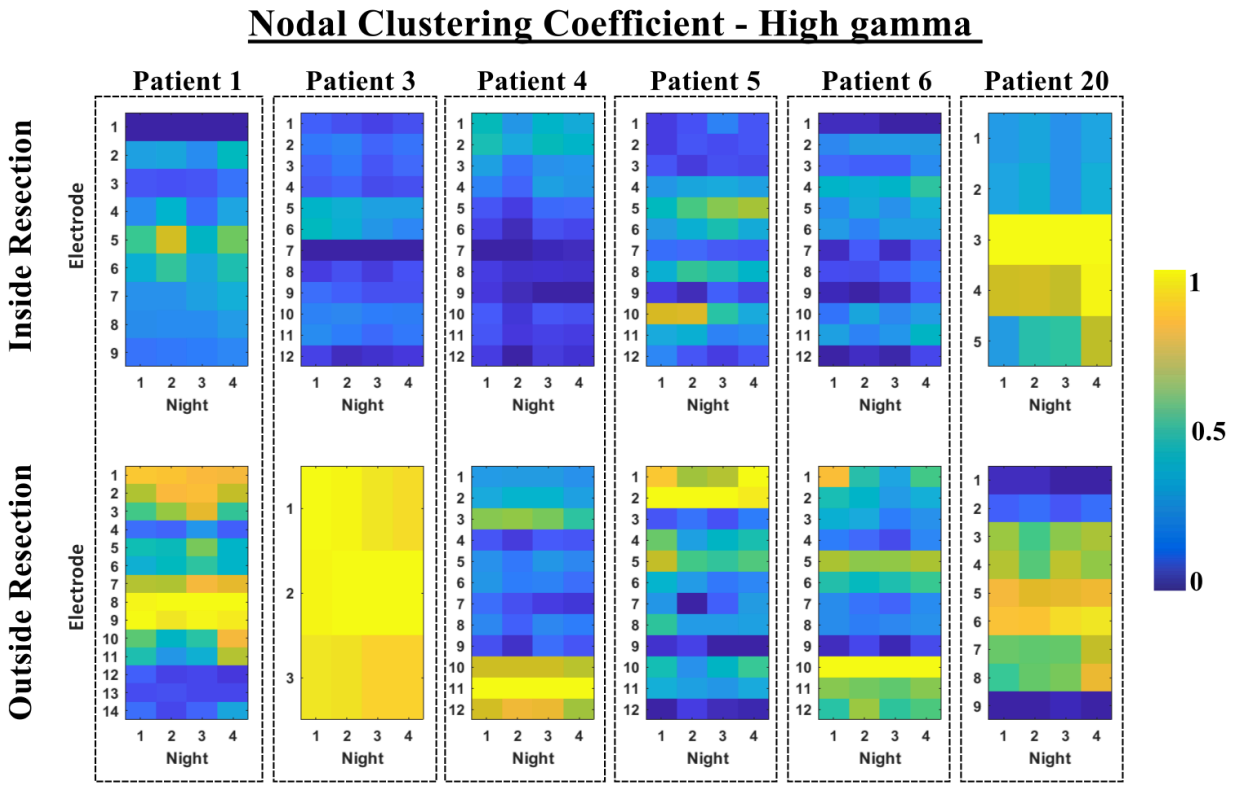

Figure 42: Variation of dDTF clustering coefficient in each electrode of every patient across four different nights of iEEG recording for the high gamma band.

Overall, FC showcases stability across different days of recording at the electrode level. Even though stability of outward strength and CC are statistically similar, visual inspection of the heatmaps reveals slightly more stable patterns of outward strength compared to CC. Moreover, no differences in the stability patterns are observed between patients with good (Patients #1, #3, #4, #5, #6) and poor surgical outcome (Patient #20).

6.4 Discussion and Conclusion

My findings demonstrate consistent stability of FC measures across different recording days and across multiple levels of analysis.

Over the course of four nights, dDTF outward strength and CC proved to be consistently decreased inside compared to outside resection of good outcome patients for the majority of higher frequencies (low γ, high γ, and ripples). These results built upon previous works on iEEG FC, which have demonstrated that directed FC measures at conventional frequencies consistently exhibit significant differences in epileptogenic compared to non-epileptogenic tissue across three different days [41], [199]. Höller et al. [258] pointed out that directed measures are more robust across longer time spans, and suggested this is because they take previous signals into account, whereas nondirected metrics do not. In addition, recent studies have proposed that during the interictal period the EZ is tonically inhibited from the rest of the network through increased inward strength and decreased outward strength [198], [237], and that robustness of directerd measures across days may reflect the importance of signal directionality [199].

In Chapter 5, I showed that, based on FC estimates averaged across different recording days, epileptogenic tissue exhibits decreased FC relative to surrounding regions and functions as a “sink” area within the network. Here, I demonstrate that this pattern is also present when analyzing networks separately, across four distinct days. This consistency, strengthens the robustness of my Chapter 5 findings and supports the notion that these effects are not a results of averaging, but rather reflect persistent interictal mechanisms driving the network into this specific state.

Moreover, in standard clinical practice antiseizure medications are gradually withdrawn to facilitate seizure occurance during iEEG implantation, rising questions on whether FC results change with respect to ASM withdrawal strategy. In our dataset, lack of information on ASM drug load at the time of recordings has already been identified as a limitation of the present work (see 5.4.4). The findings on the temporal stability of FC across four different nights, irrespective of ASM dosage, further strengthen the robustness of my Chapter 5 results.

I showed that dDTF outward strength and CC presented stable values across four separate nights in both resected and non-resected tissue, consistently at the patient- and electrode- levels, which held true for all frequency bands. Paulo et al. [199] has also studied temporal stability at the patient level across three days, and showed robustness of directed FC both inside and outside the EZ for the alpha band. To the best of our knowledge, the stability of FC measures at the electrode level has not been addressed before, with only some early works reporting that electrodes of local hypersynchrony (increased connectivity) remained relatively stable across different recording days [184], [192]. I opted to identify potential differences between the stability of epileptogenic and non-epileptogenic tissue in patients with different outcomes in an attempt to assess the added value that stability analysis could bring to EZ localisation. This notion was further encouraged by the results of a study from Geier and Lehnertz [257], which found higher percentage of variation at the clinically defined SOZ compared to the non-SOZ regions using broadband data. Nevertheless, my findings showed that FC was stable across nights at both resected and non resected areas, and for both good and poor outcome patients. Although non significant, a trend for more variation (in terms of lower p-values) was noted for areas inside the surgical resection in patients with good surgical outcome, especially for outward strength (see 6.3.3). With this case study-like approach I show that, during the interictal period, both epileptogenic and non-epileptigenic tissue has a specific and consistent role in the functional network, which could stem from biological changes aiming to maintain the epileptic brain in specific states (i.e to suppress the epileptogenic tissue through tonic inhibition to prevent seizure generation).

In terms of the limitations of the FC stability investigations, the most profound one is the very small cohort size (N=6), especially for the poor outcome group comprising of a single patient, which greatly limits the generalizabilty of my results. My work aimed to serve as a starting point for future investigations with larger datasets, necessary for validating temporal stability of FC during the interictal period. In addition, here, I did not investigate the effect that circadian rythms might have on FC, as according to previous works daily rhythms can have strong contribution to the temporal variability of FC in the timescale of hours to days [257].

6.5 Conclusion

In conclusion, I provide evidence that FC at higher frequencies (from low γ to fast ripples) remains stable across different days of recording, at both epileptogenic and non-epileptogenic tissue. I hope these findings will contribute to reducing ambiguity surrounding FC tools and promote their translation from research settings to clinical practice.

Chapter 7

Summary and Discussion

The overarching aim of this thesis has been to explore the potential of interictal iEEG functional connectivity in identifying epileptogenic tissue and predicting surgical outcome in patients with DRE. A substantial portion of this work is dedicated to exploring how HFO events affect functional connectivity in different frequency bands, and to examining whether high-frequency FC patterns could hold value for the presurgical workup. This concluding chapter offers a summary of the key findings, discusses their practical implications, and identifies future research directions.

7.1 High-frequency FC tools are not meant to replace HFOs

I would first like to make a quick note on the intention of some of my investigations. Despite a large portion of my work focused on FC at higher frequencies, I do not propose at any point for these high-frequency FC tools to act as substitutes for HFO events and their classical interpretation as biomarkers of epileptogenicity. Rather, I aim to expand our knowledge around FC-based biomarkers by extending the analysis to higher frequencies, with the hope that they will provide additional insights into the organisation of epileptogenicity and improve surgical treatment outcomes.

7.2 Practical implications

My results reveal that when FC is quantified and analyzed using network theory, especially at higher frequencies, it represents a conceptually powerful tool for identifying epileptogenic tissue and distinguishing it from surrounding non-epileptogenic areas. By complementing and reinforcing existing literature that has also demonstrated similar results, my work helps lay another brick in the foundation of FC-based biomarkers in epilepsy research. The key barrier is not scientific potential but clinical translation.

A central consideration has to do with the word “biomarker” itself. Many studies directly refer to “biomarkers of the EZ” or indirectly imply that the EZ is a directly measurable quantity. While locating the epileptogenic zone holds clear academic appeal, asserting the existence of a definitive biomarker for it remains problematic. First, even the term “epileptogenic zone” is poorly defined and continues to change [16]. Second, the epileptogenic zone is a theoretical concept that cannot be directly measured or validated. In this sense, regulatory approval of a clinical biomarker, which requires validation to demonstrate sensitivity and specificity, is particularly challenging in the case of the EZ [259]. Thus, a gap exists between the language commonly used in academia and the requirements of governmental agencies responsible for translating academic projects into clinical practice.

BEST Resource and Guidelines

A first step towards bridging this gap could be for future studies to follow the guidelines of the BEST (Biomarkers, EndpointS, and other Tools) Resource [260], a collaborative initiative between the National Institute of Health (NIH) and the FDA, with the overarching goal of getting biomarkers out of the research lab and into clinical practice, with one of the essential steps being proper validation. An important advantage of the BEST guidelines is standardizing the presentation of information, so that each study contains enough information to help facilitate future comparison across studies. According to the Resource, biomarkers should have two key points:

I. Biomarker Description: Clearly defined name, source (urine, blood, EEG, etc.), type (e.g., molecular, histologic, electrophysiologic, etc.), measurement method, and biologic plausibility (association of the biomarker with the disease or condition of interest).
II. Intended Use: The specific clinical circumstance or purpose that the biomarker is sought to inform, which clarifies the clinical actions that might be taken based on the biomarker information. The intended use should also clearly indicate its category, which at present consists of 8 types: Diagnostic, Monitoring, Response, Predictive, Prognostic, Safety, Susceptibility/Risk, and Surrogate End Points.

Since in the present work I propose a FC-based biomarker, I first need to accurately describe it. Based on my results, I can use the “sinkness” of a brain area, defined as “sink-like behavior based on high-frequency dDTF outward strength”, as the biomarker under study. The outward strength threshold that determines whether a node is a “sink” is dependent on the frequency for which dDTF is computed each time, so I will not define a single value here. The source of the “sinkness” biomarker could be defined as: “*Interictal intracranial EEG”*. As the measurement method, I can use the specific techniques followed to extract the biomarker from the source, which in my case translates to: *“Outward strength (BCT toolbox) computed on direct Directed Transfer Function (FieldTrip toolbox)”*. The biological plausibility here reads: *“In patients with good surgery outcome, sink nodes are associated with the resected volume”*. Equally important to describing the characteristics of “sinkness” is defining its intended use. As mentioned above, proposing “sinkness” as a biomarker of the EZ is extremely problematic, since it would be practically impossible to prove it to the FDA. Taking this into account, I propose that a clinically useful and validatable context of use for “sinkness” would be to prognosticate outcome by measuring how much of the biomarker is resected during surgery, with seizure relief as a measurable outcome.

Table 9 presents the “Sinkness” Description Table, which summarizes the proposed biomarker. I propose that similar tables should be included in any future study on FC-based biomarkers (or any other biomarker of epilepsy).

Table 9: “Sinkness” Description Table

Biomarker Name	“Sinkness”
Source	Interictal intracranial EEG
Type	Electrographic
Biological plausibility	In patients with good surgery outcome, sink nodes are associated with the resected volume
Measurement method	Outward strength (BCT toolbox) computed on direct Directed Transfer Function (FieldTrip toolbox)
Intended use	Prognosticate surgery outcome

EEG=electroenchephalography; BCT= Brain Connectivity Toolbox

Since there is an increasing number of studies that propose FC-based biomarkers for investigating epileptogenicity in the brain, it is important for the epilepsy research community to be aware of the BEST guidelines and incorporate them into future research. This will hopefully get these new promising biomarkers a step closer to their intended purpose: use in real clinical practice.

7.3 Future research directions

Beyond considerations that come with the placement of FC-based tools in the context of a biomarker, future works should focus on practical research efforts to alleviate the ambiguity around the value of FC tools as valuable markers of epileptogenicity in the brain.

Research on FC-based biomarkers is currently limited by the heterogeneity of analytical methods and the lack of standardised protocols. To move beyond encouraging but largely retrospective and single-centre findings, large-scale multicentre prospective validation will be required to ensure robustness, reproducibility, and generalizability across patient cohorts and clinical environments. Such validation efforts should ultimately culminate in prospective clinical trials to test whether adding FC measures to the presurgical evaluation influences surgical decisions and improves patient outcomes.

As further steps, dedicated software platforms need to be developed that will integrate smoothly with existing presurgical workflows and deliver results in a format that is transparent and easily interpretable for clinicians. Beyond the technical implementation, comprehensive training initiatives, workshops, and consensus guidelines will be necessary to equip epileptologists, neurosurgeons, and neurophysiology teams with the knowledge and confidence to interpret FC-derived measures and incorporate them into complex surgical decision-making. Only through this combination of standardised methods, clinical validation, and user-friendly tools can FC-based biomarkers progress from research applications to everyday presurgical evaluation tools.

Appendix 1

Supplementary Figures

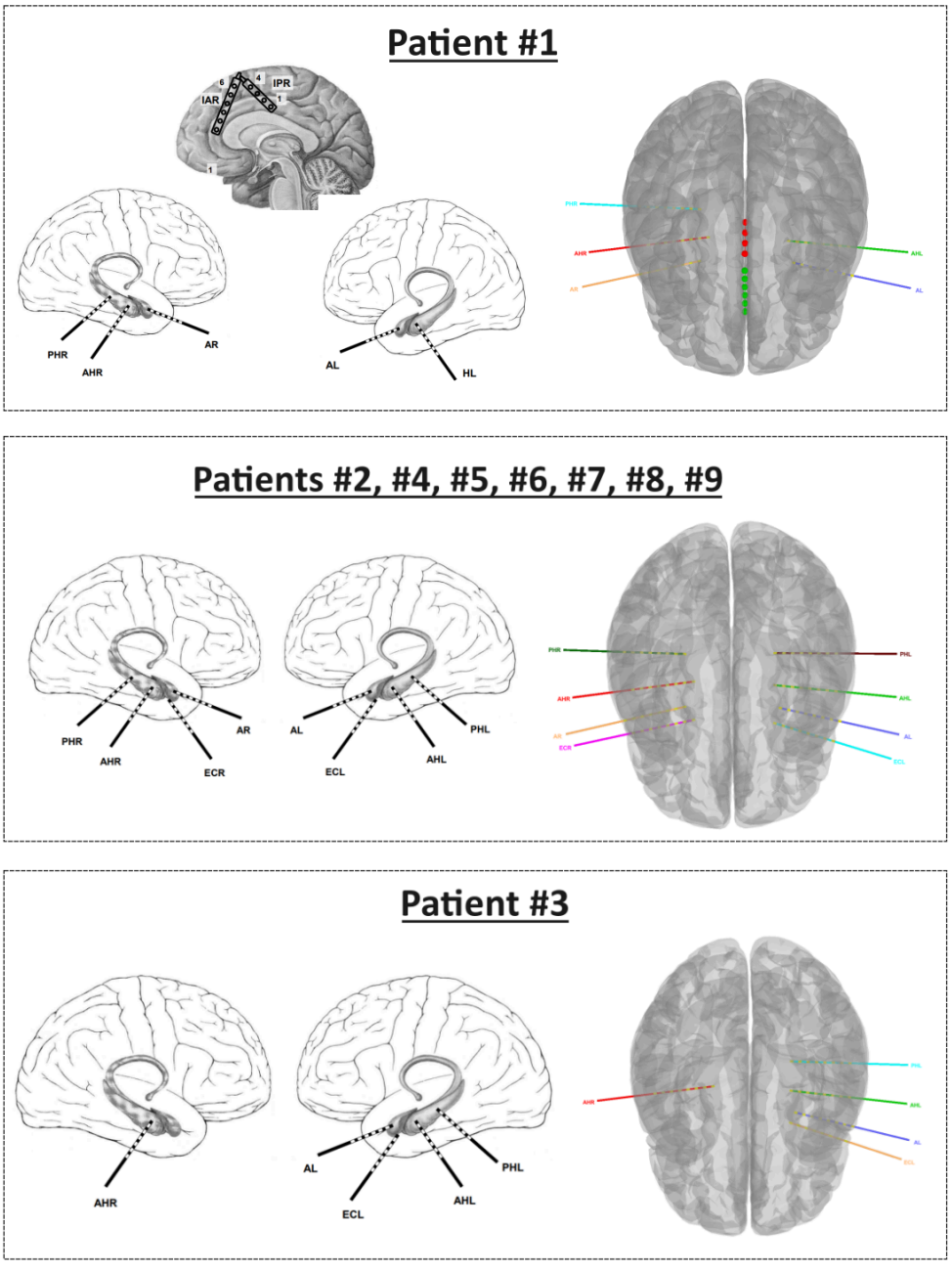

Supplementary Figure S1: 2D and 3D implantation schemes for TLE patients

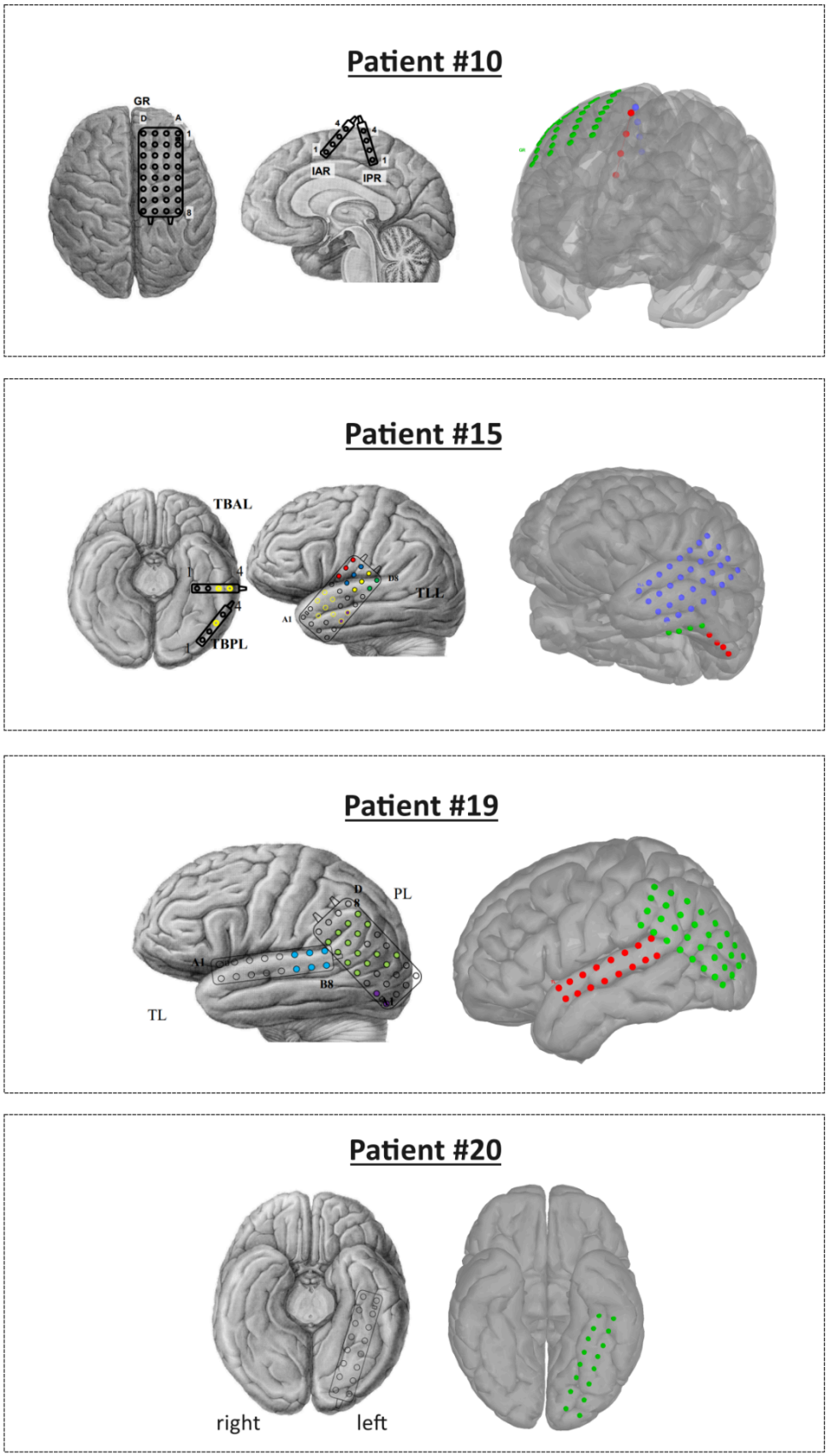

Supplementary Figure S2: 2D and 3D implantation schemes for ETE patients undergoing ECoG only

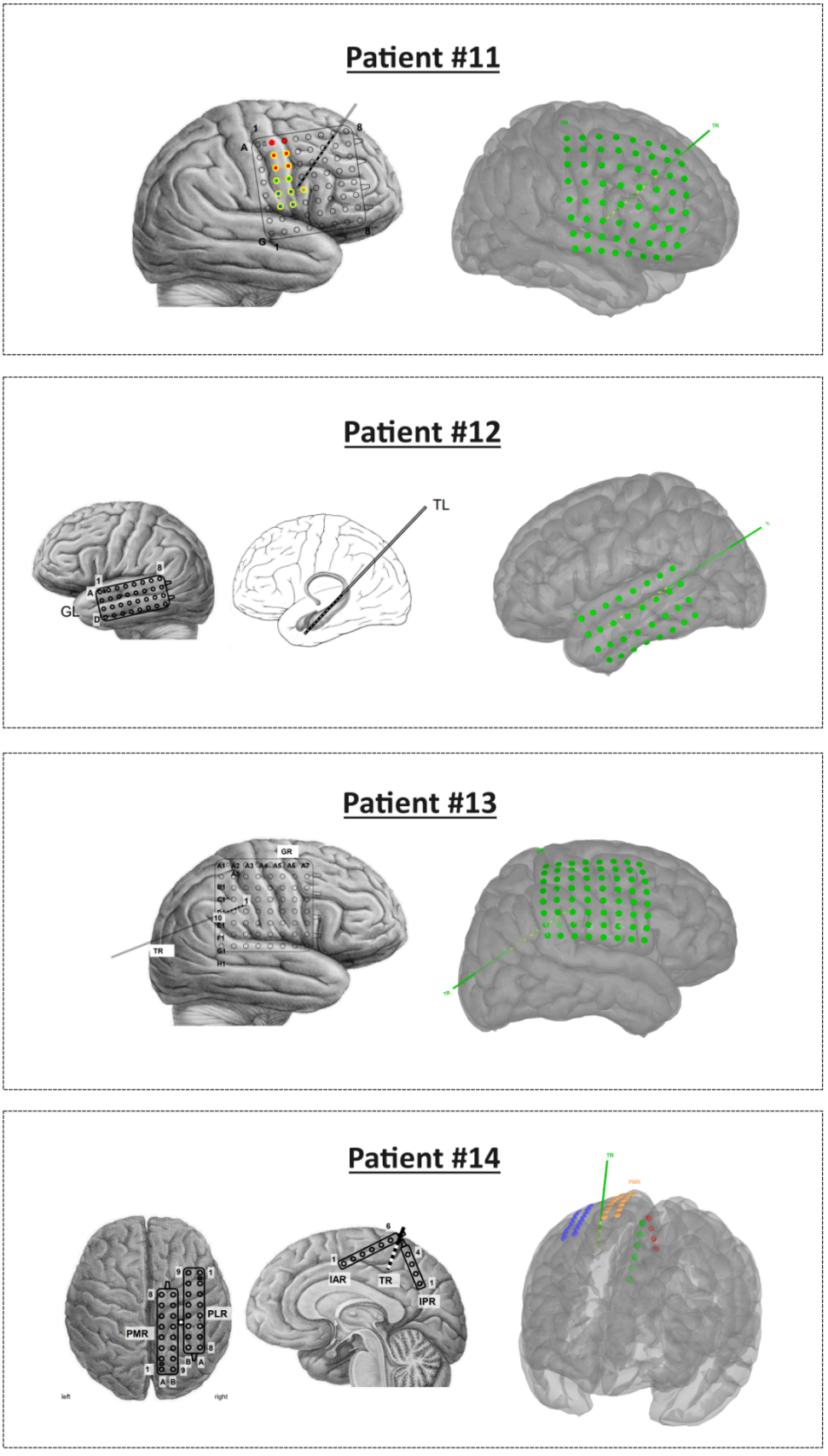

Supplementary Figure S3: 2D and 3D implantation schemes for ETE patients undergoing combined SEEG and ECOG (Patients #11, #12, #13, #14)

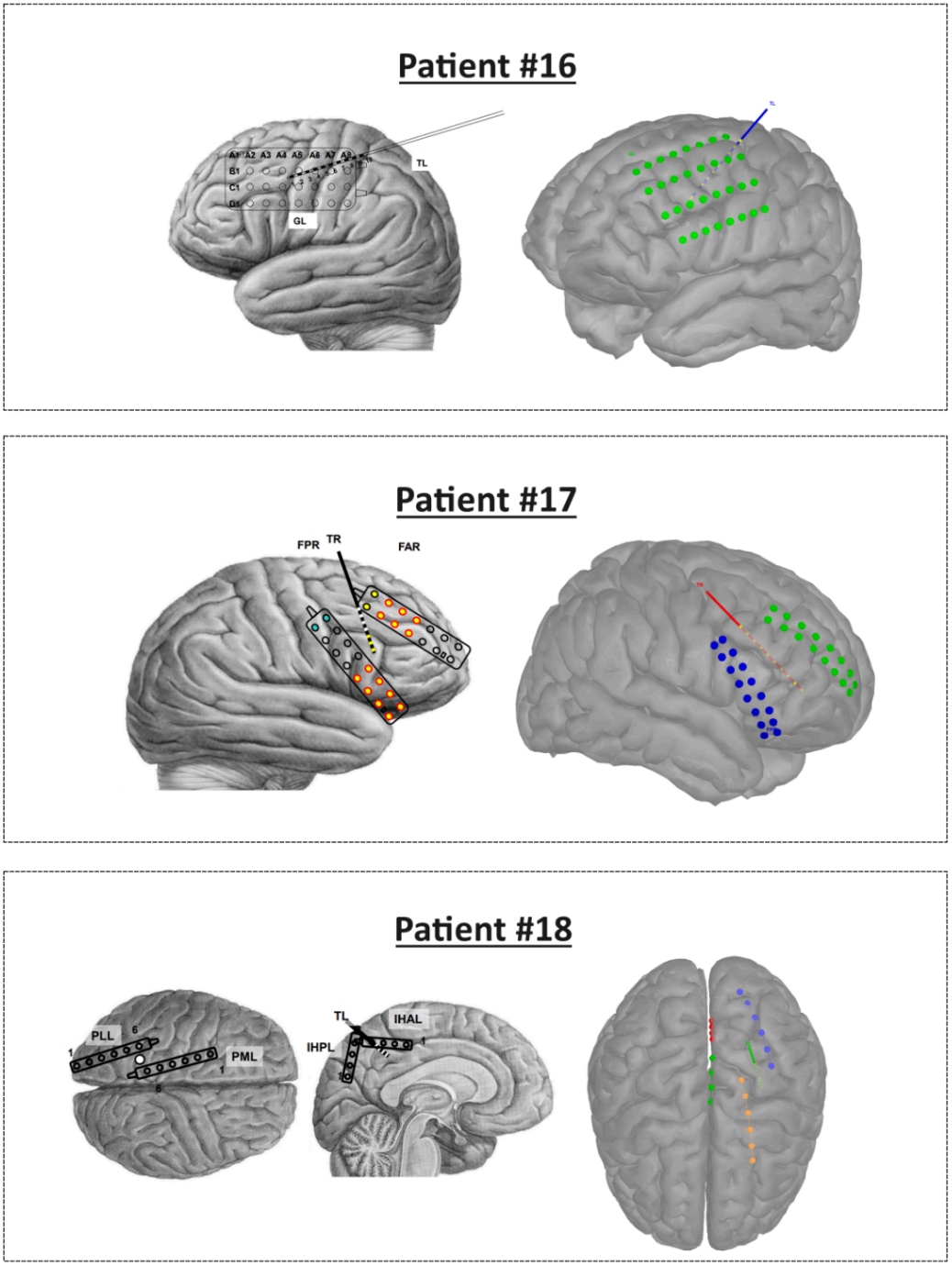

Supplementary Figure S4: 2D and 3D implantation schemes for ETE patients undergoing combined SEEG and ECOG (Patients #16, #17, #18)

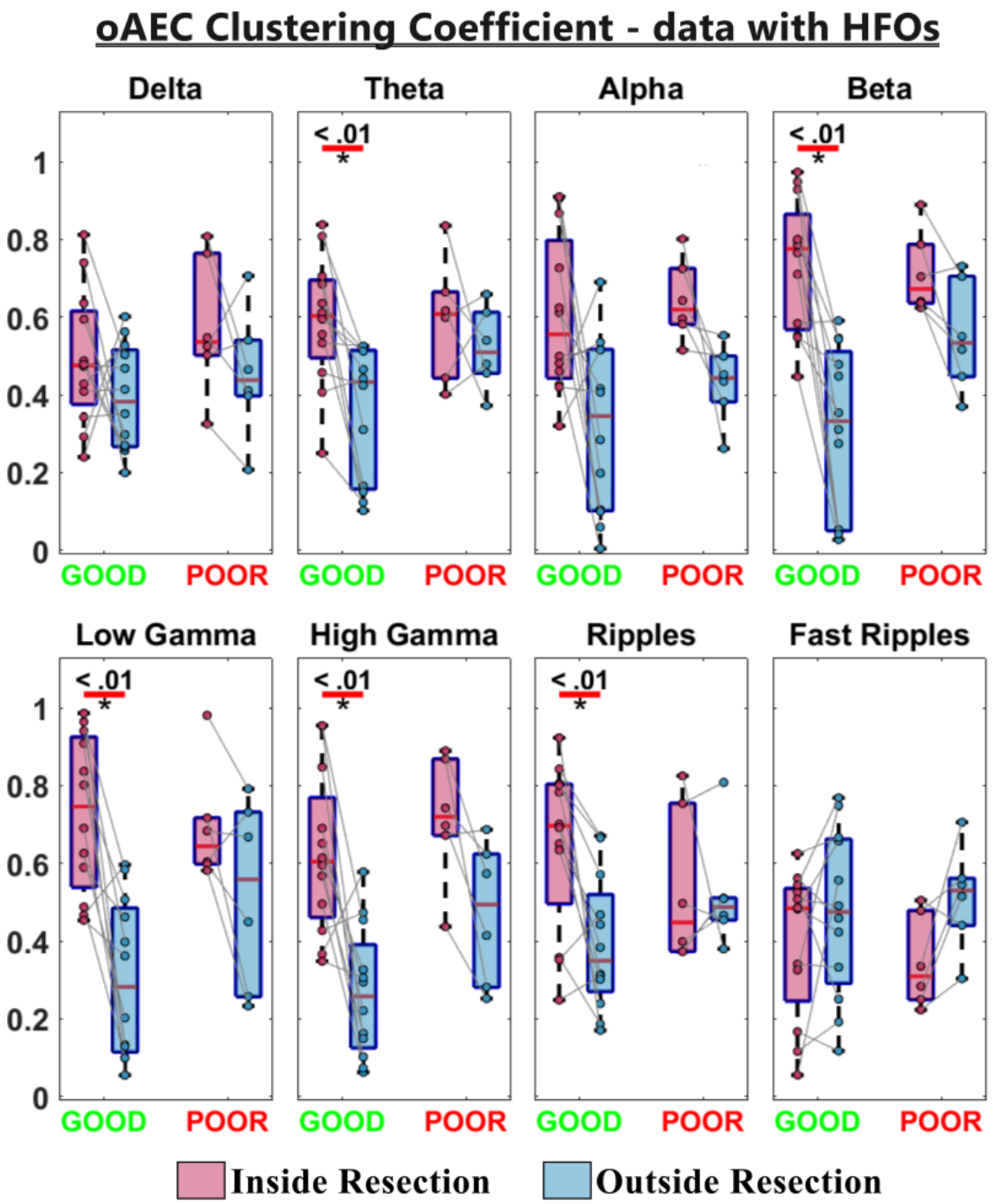

Supplementary Figure S5: Orthogonalized amplitude envelope correlation (oAEC) clustering coefficient, for segments with HFOs, compared inside (pink) vs. outside (blue) resection separately for good (N=12) and poor (N=6) outcome patients.

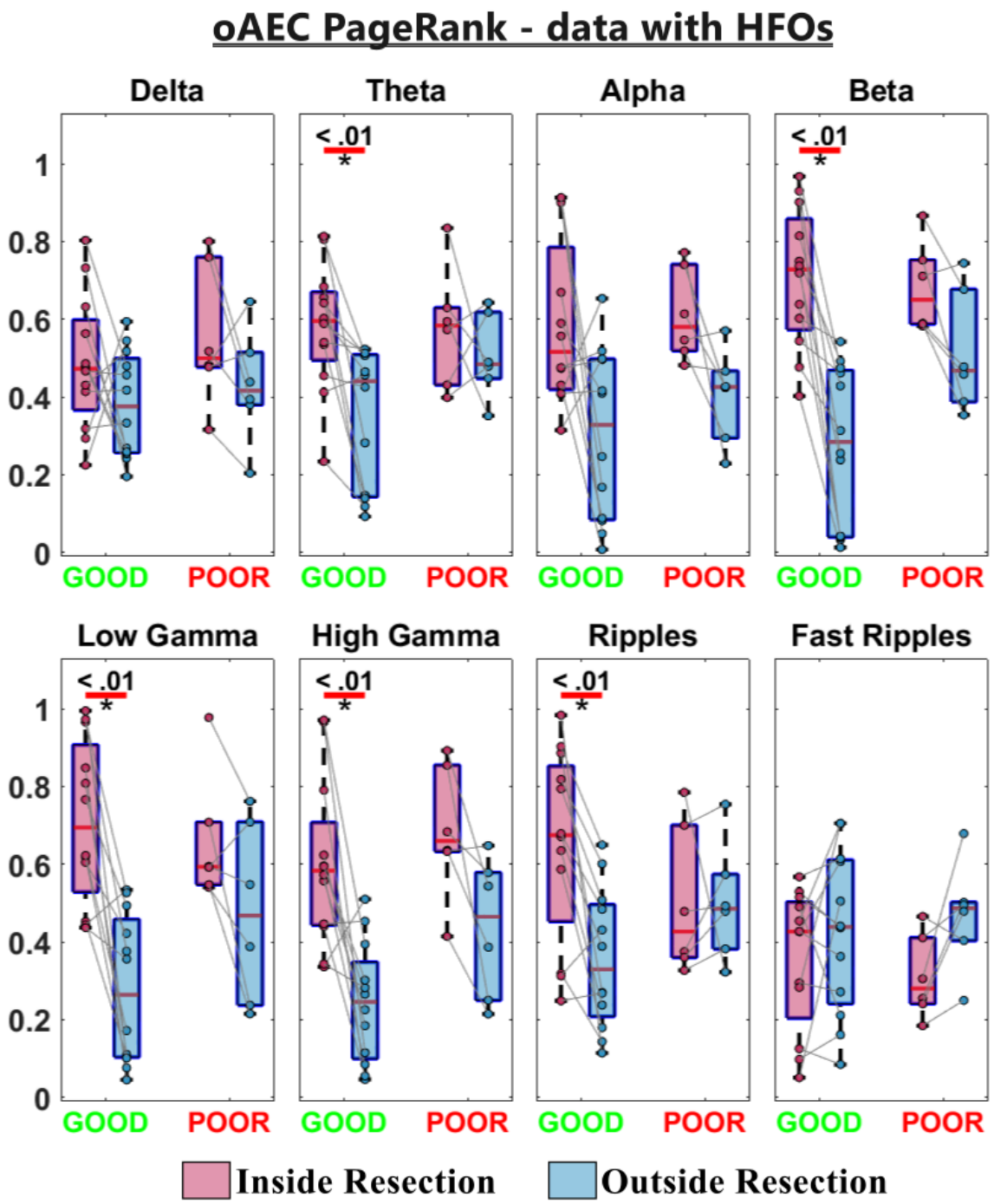

Supplementary Figure S6: Orthogonalized amplitude envelope correlation (oAEC) PageRank, for segments with HFOs, compared inside (pink) vs. outside (blue) resection separately for good (N=12) and poor (N=6) outcome patients.

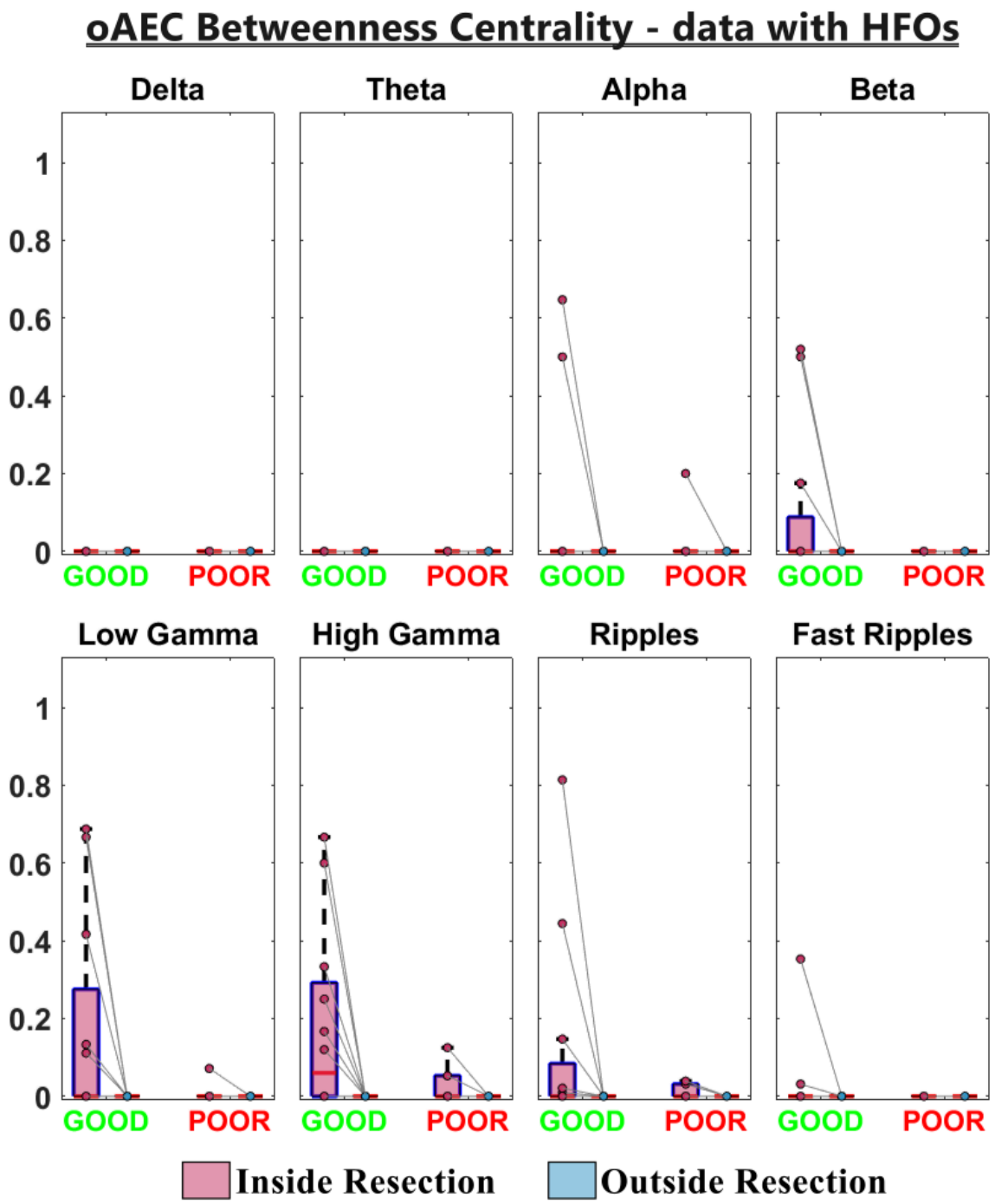

Supplementary Figure S7: Orthogonalized amplitude envelope correlation (oAEC) betweenness centrality, for segments with HFOs, compared inside (pink) vs. outside (blue) resection separately for good (N=12) and poor (N=6) outcome patients.

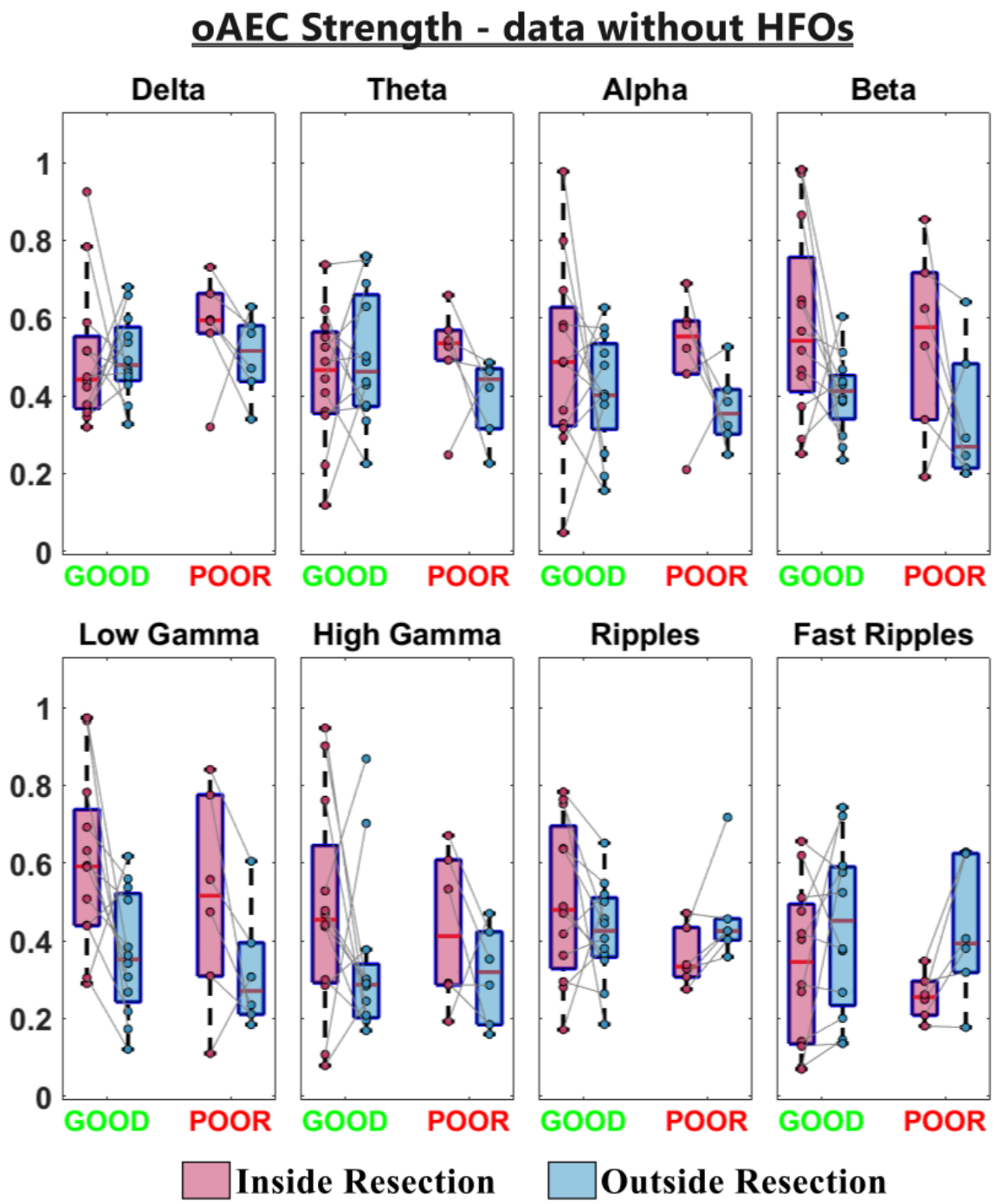

Supplementary Figure S8: Orthogonalized amplitude envelope correlation (oAEC) nodal strength, for segments without HFOs, compared inside (pink) vs. outside (blue) resection separately for good (N=12) and poor (N=6) outcome patients.

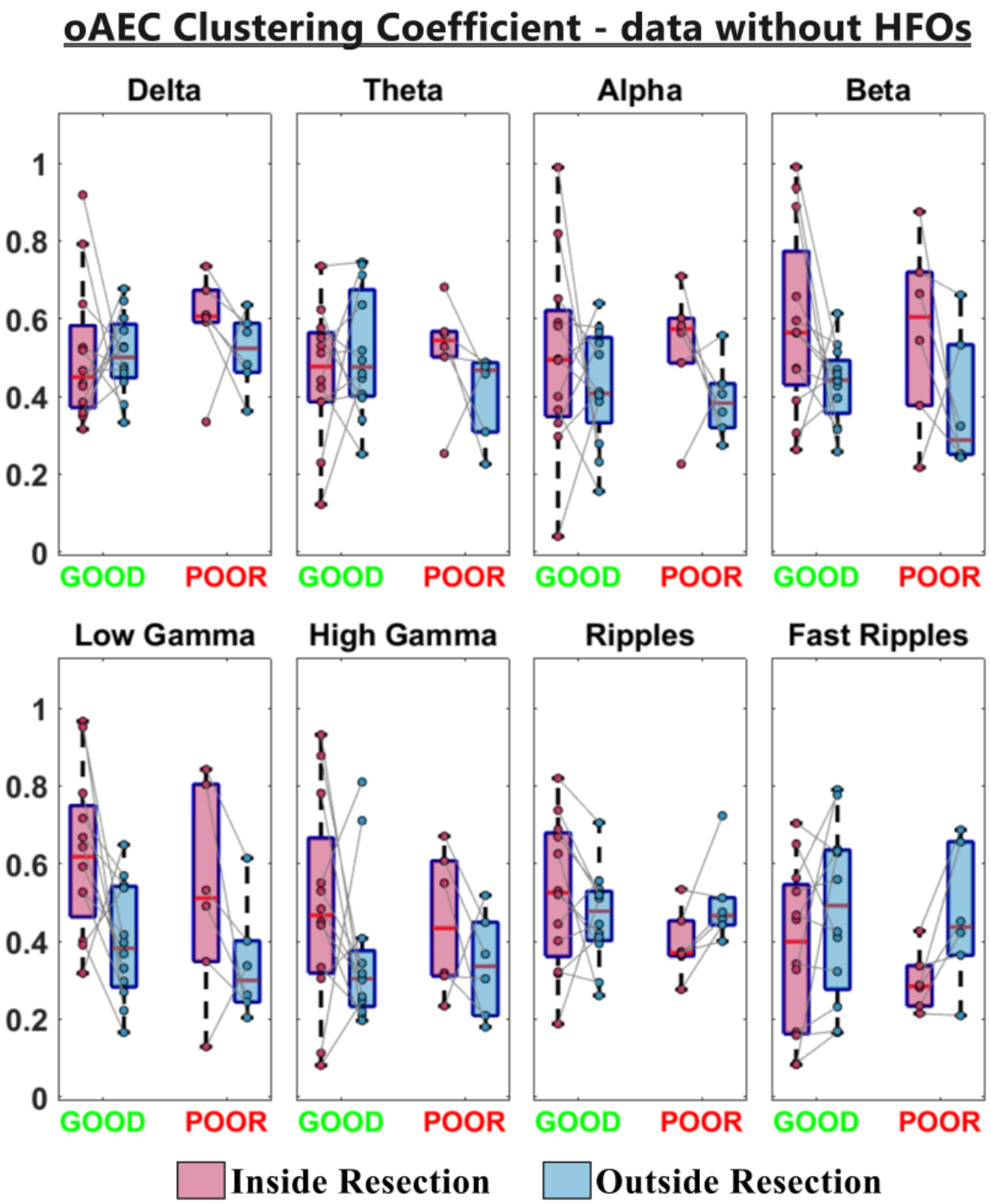

Supplementary Figure S9: Orthogonalized amplitude envelope correlation (oAEC) clustering coefficient, for segments without HFOs, compared inside (pink) vs. outside (blue) resection separately for good (N=12) and poor (N=6) outcome patients.

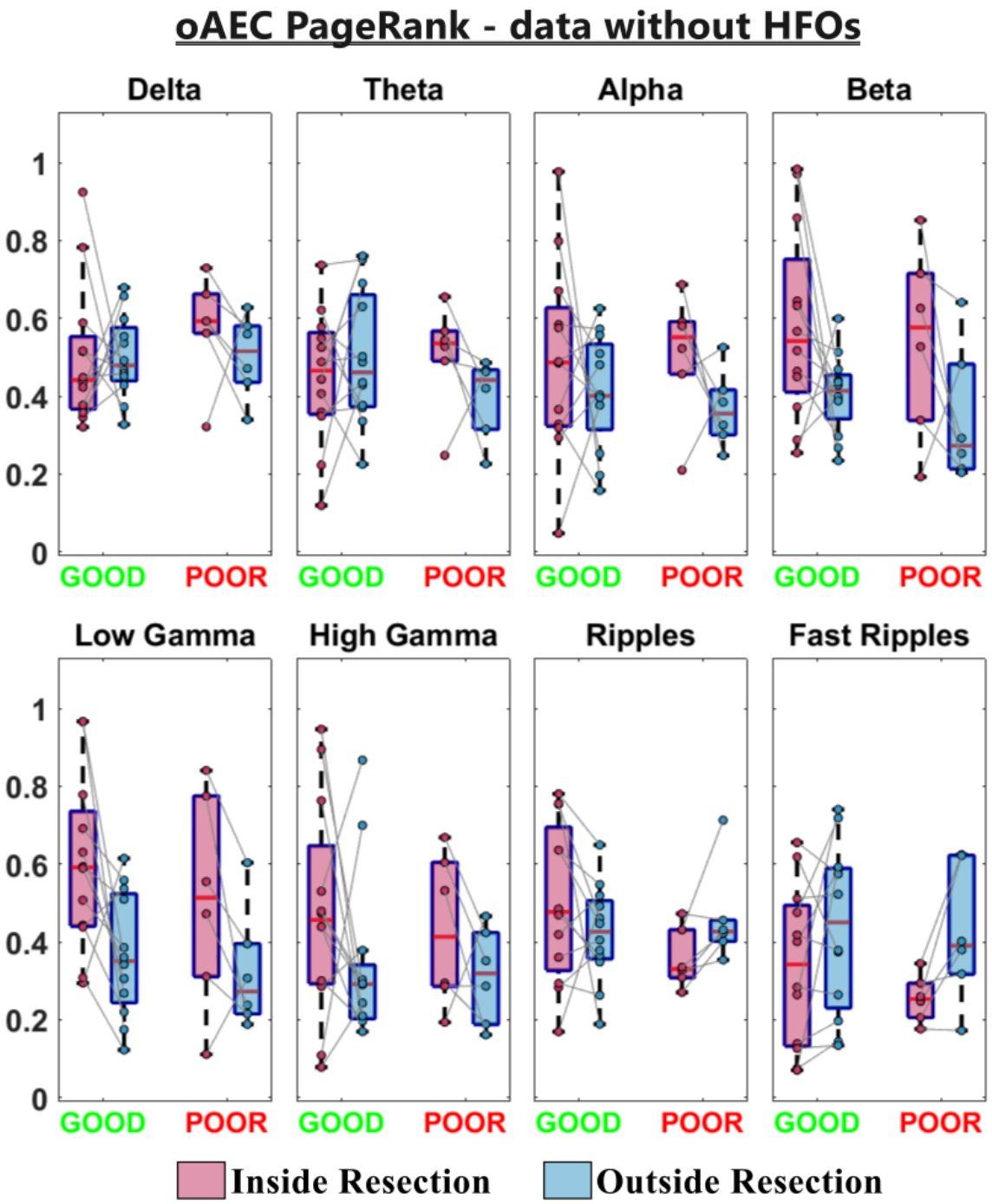

Supplementary Figure S10: Orthogonalized amplitude envelope correlation (oAEC) PageRank, for segments without HFOs, compared inside (pink) vs. outside (blue) resection separately for good (N=12) and poor (N=6) outcome patients.

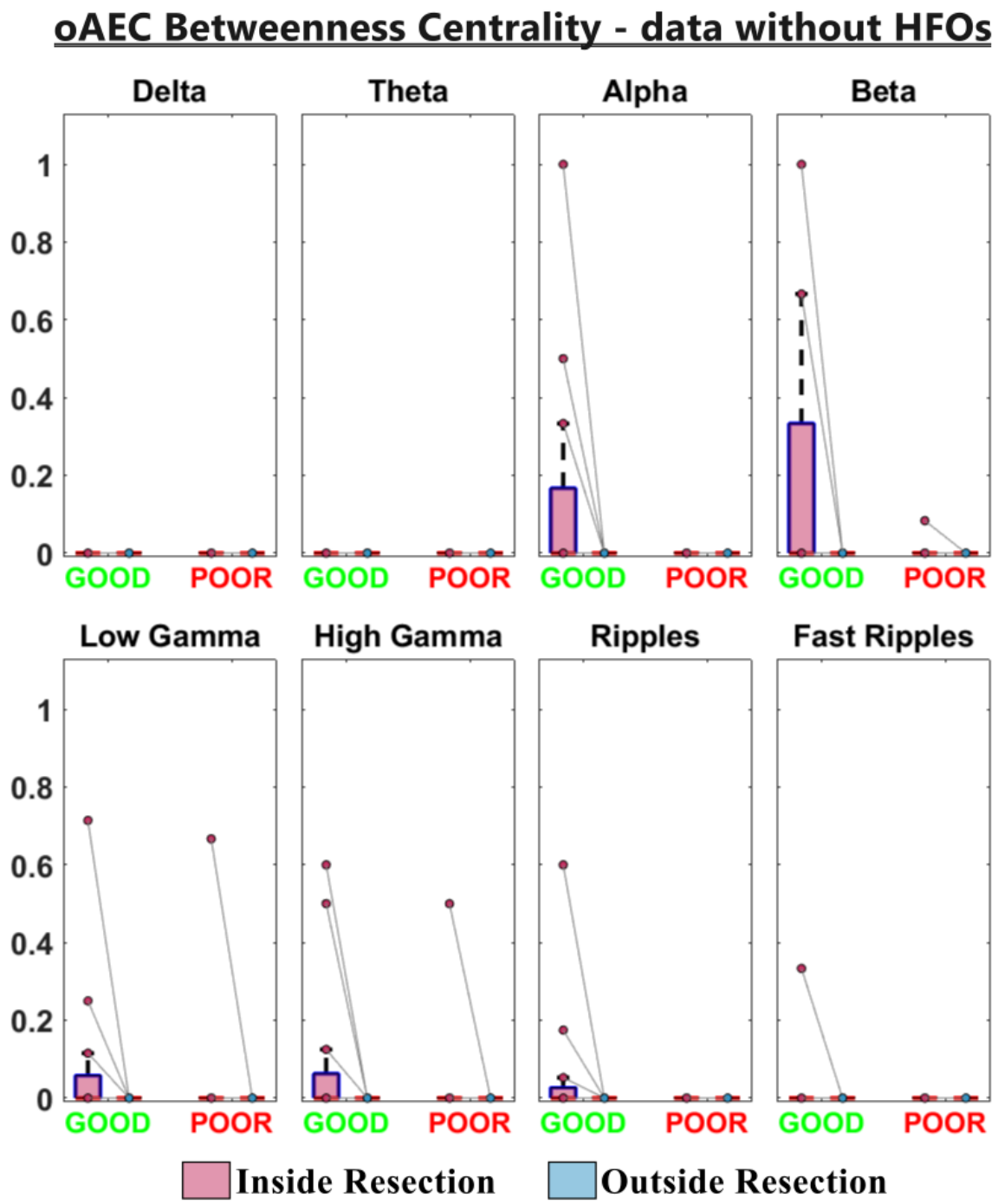

Supplementary Figure S11: Orthogonalized amplitude envelope correlation (oAEC) betweenness centrality, for segments without HFOs, compared inside (pink) vs. outside (blue) resection separately for good (N=12) and poor (N=6) outcome patients.

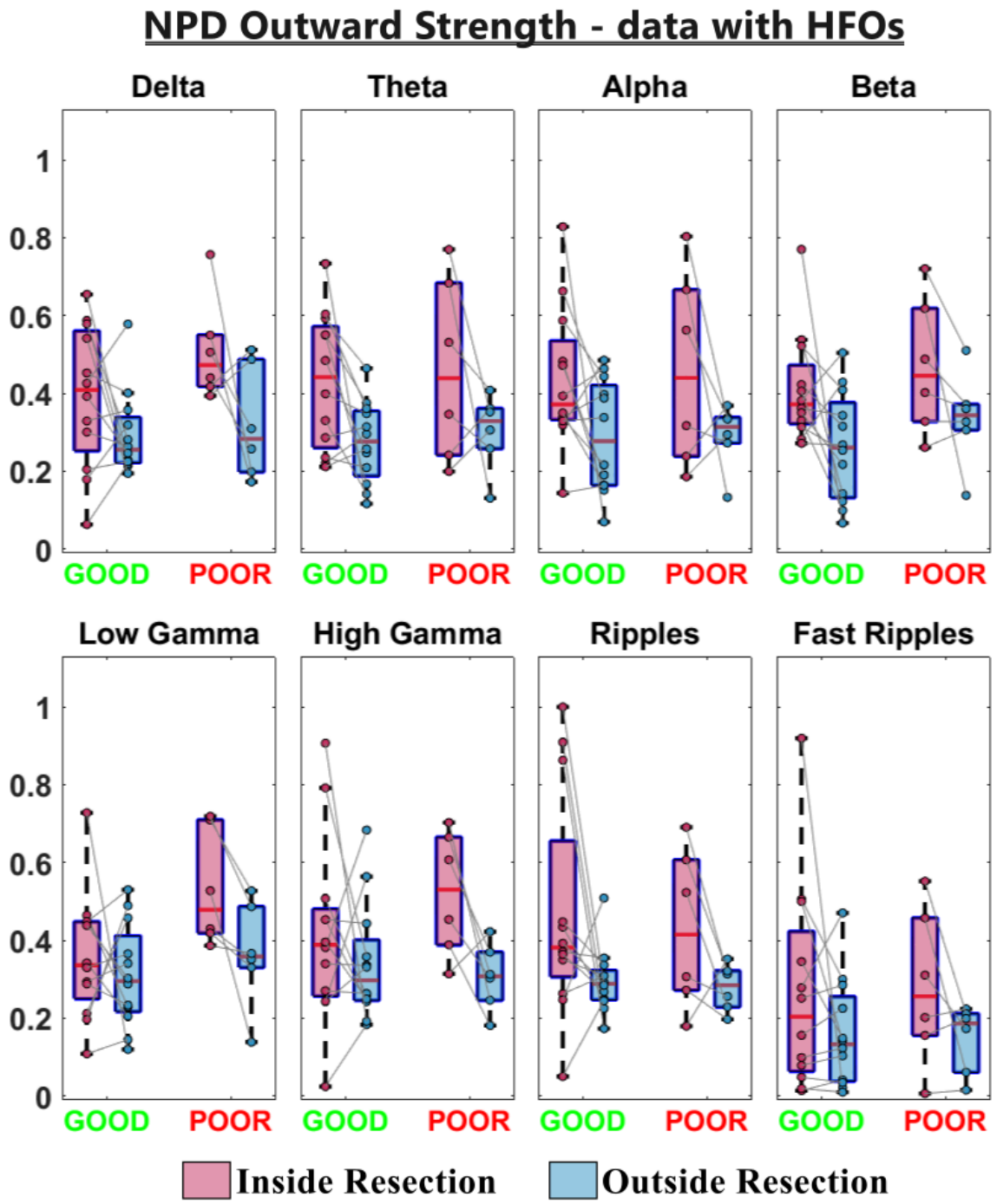

Supplementary Figure S12: Nonparametric directionality (NPD) outward strength, for segments with HFOs, compared inside (pink) vs. outside (blue) resection separately for good (N=12) and poor (N=6) outcome patients.

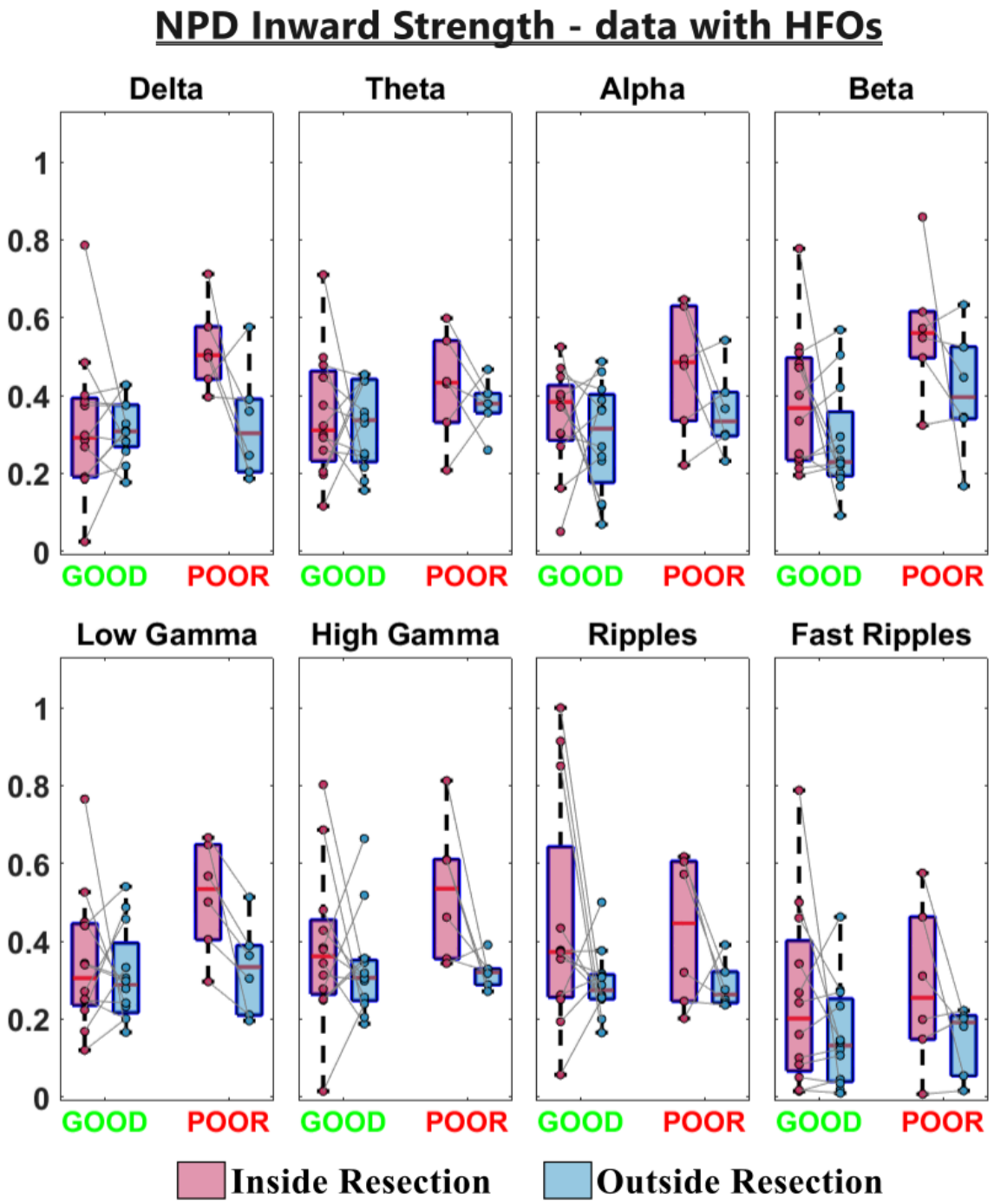

Supplementary Figure S13: Nonparametric directionality (NPD) inward strength, for segments with HFOs, compared inside (pink) vs. outside (blue) resection separately for good (N=12) and poor (N=6) outcome patients.

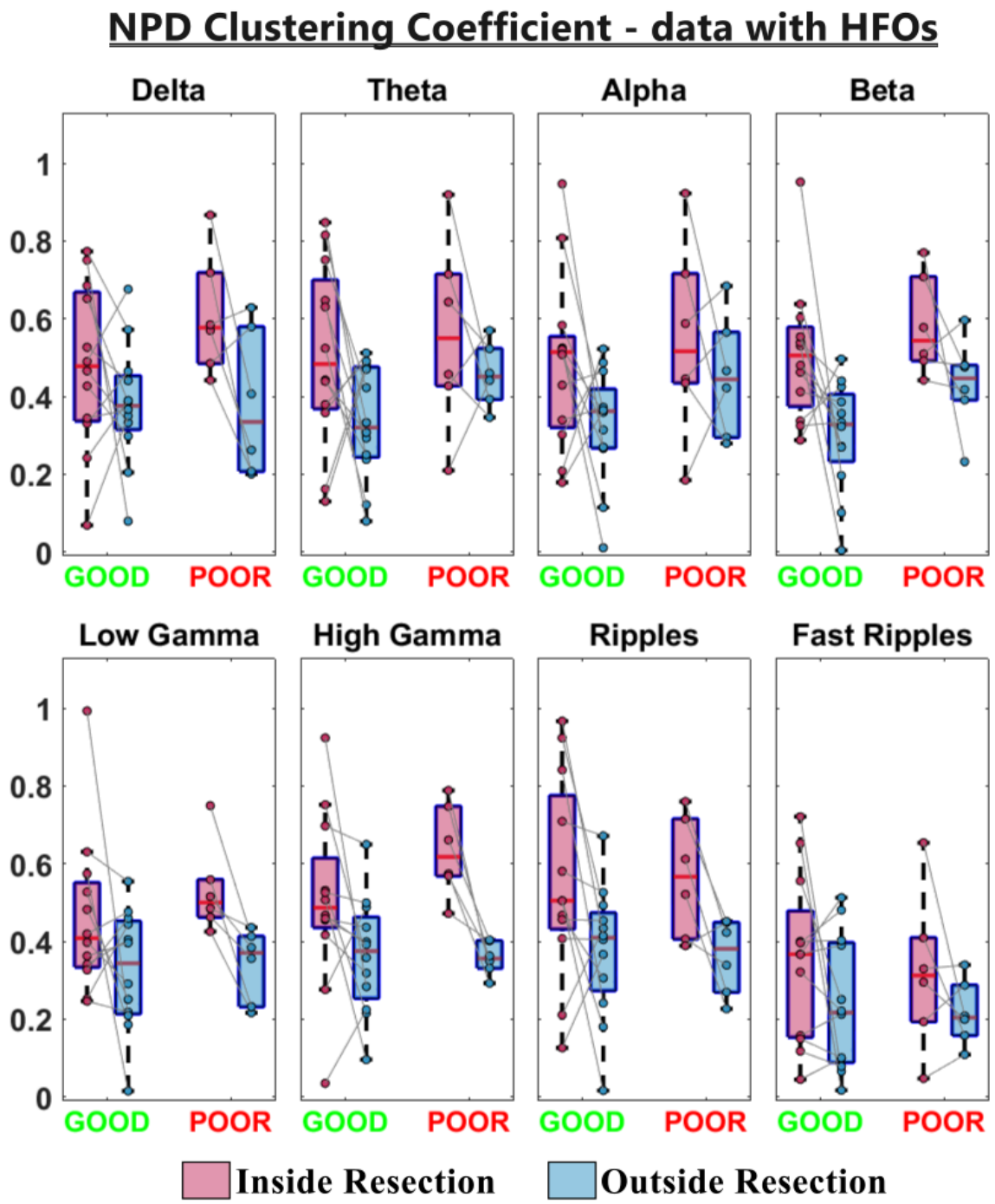

Supplementary Figure S14: Nonparametric directionality (NPD) clustering coefficient, for segments with HFOs, compared inside (pink) vs. outside (blue) resection separately for good (N=12) and poor (N=6) outcome patients.

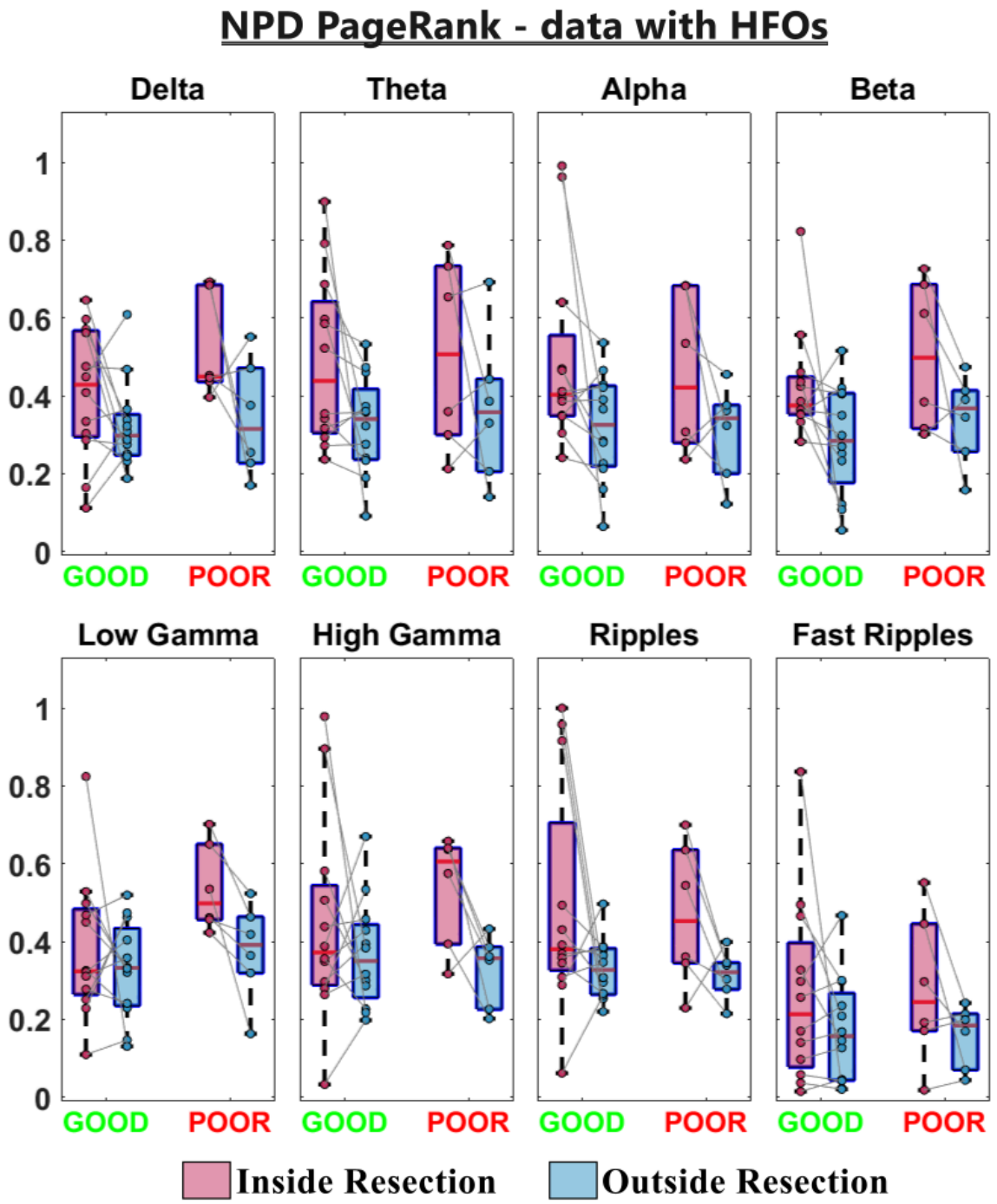

Supplementary Figure S15: Nonparametric directionality (NPD) PageRank, for segments with HFOs, compared inside (pink) vs. outside (blue) resection separately for good (N=12) and poor (N=6) outcome patients.

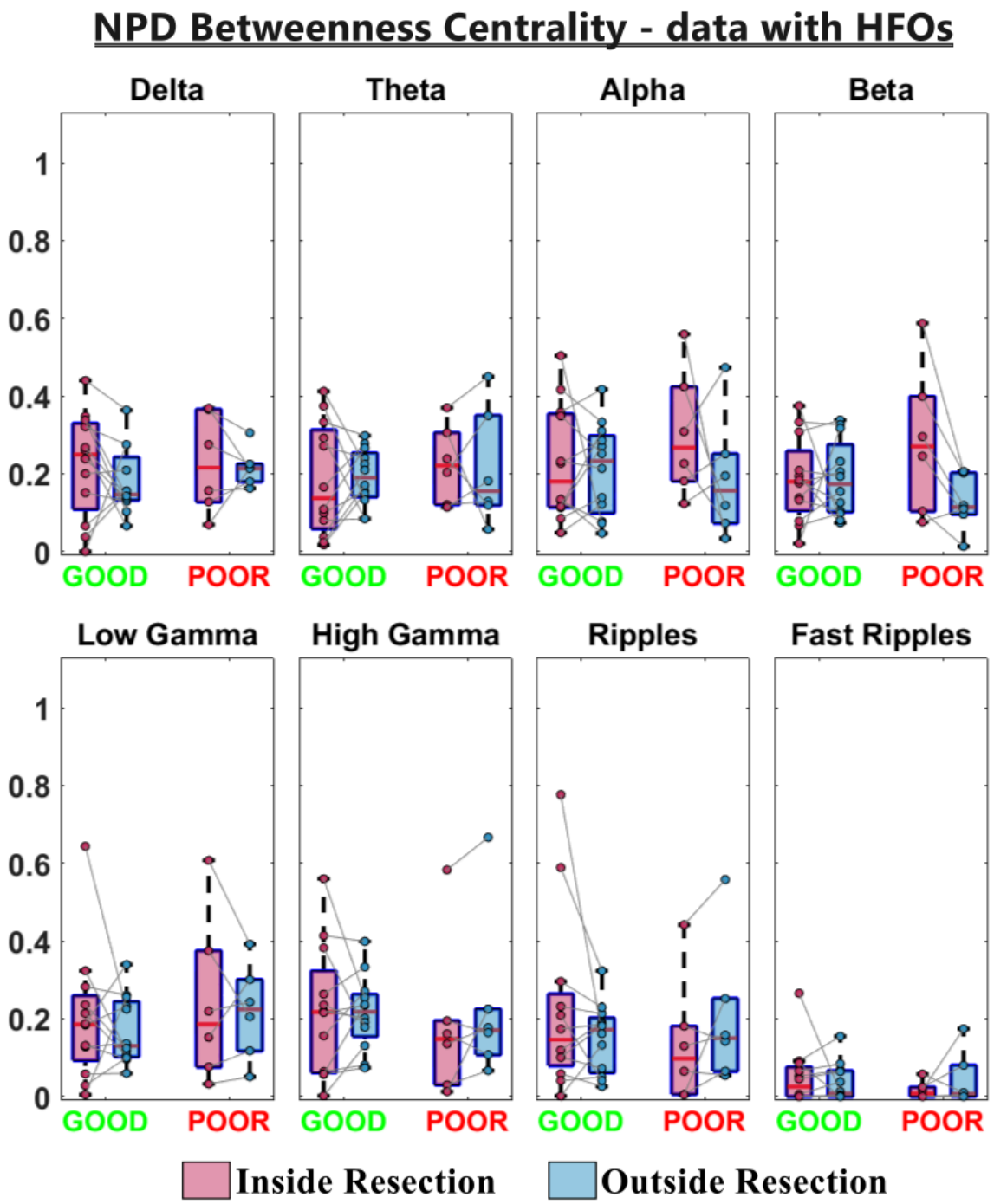

Supplementary Figure S16: Nonparametric directionality (NPD) betweenness centrality, for segments with HFOs, compared inside (pink) vs. outside (blue) resection separately for good (N=12) and poor (N=6) outcome patients.

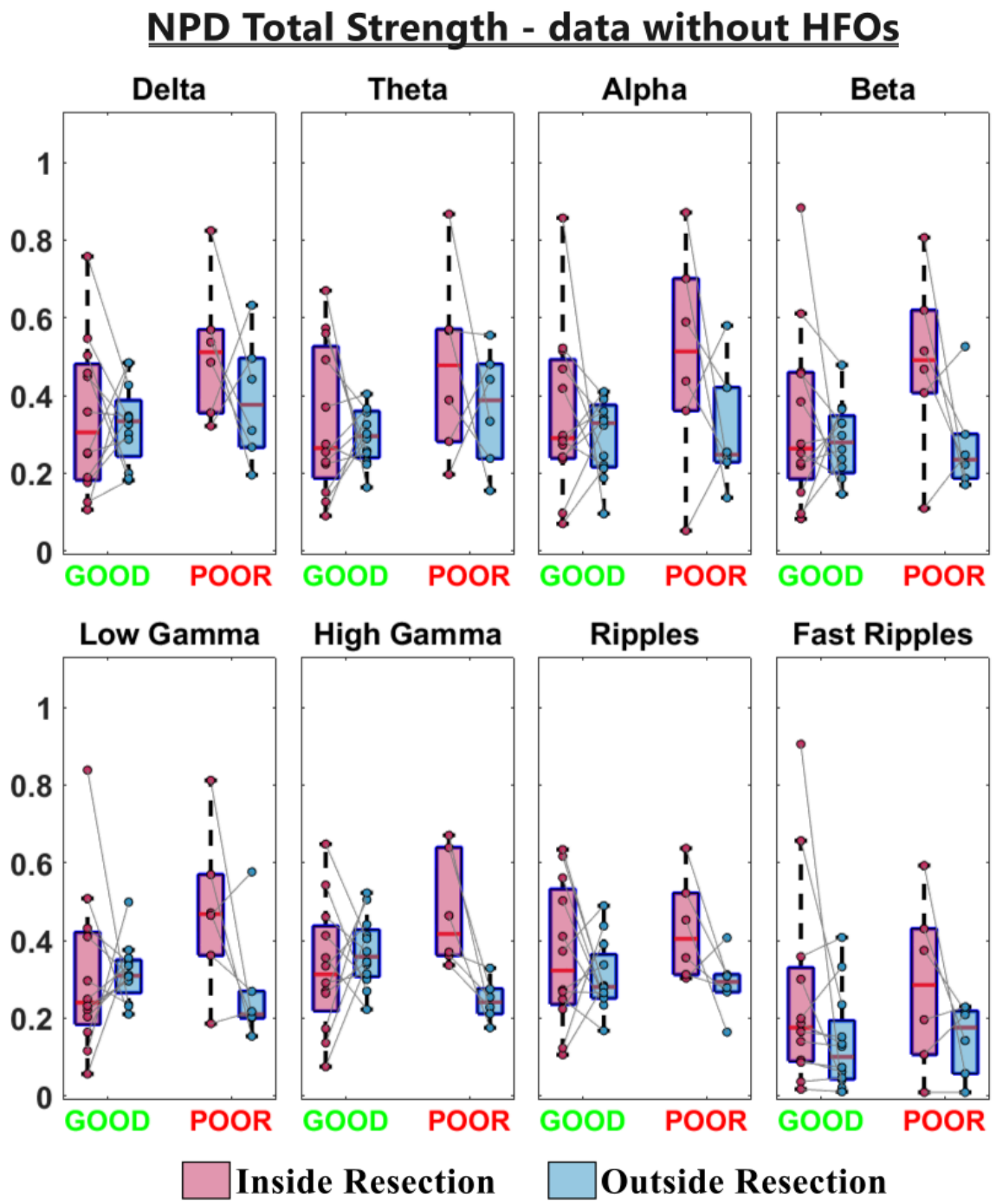

Supplementary Figure S17: Nonparametric directionality (NPD) total strength, for segments without HFOs, compared inside (pink) vs. outside (blue) resection separately for good (N=12) and poor (N=6) outcome patients.

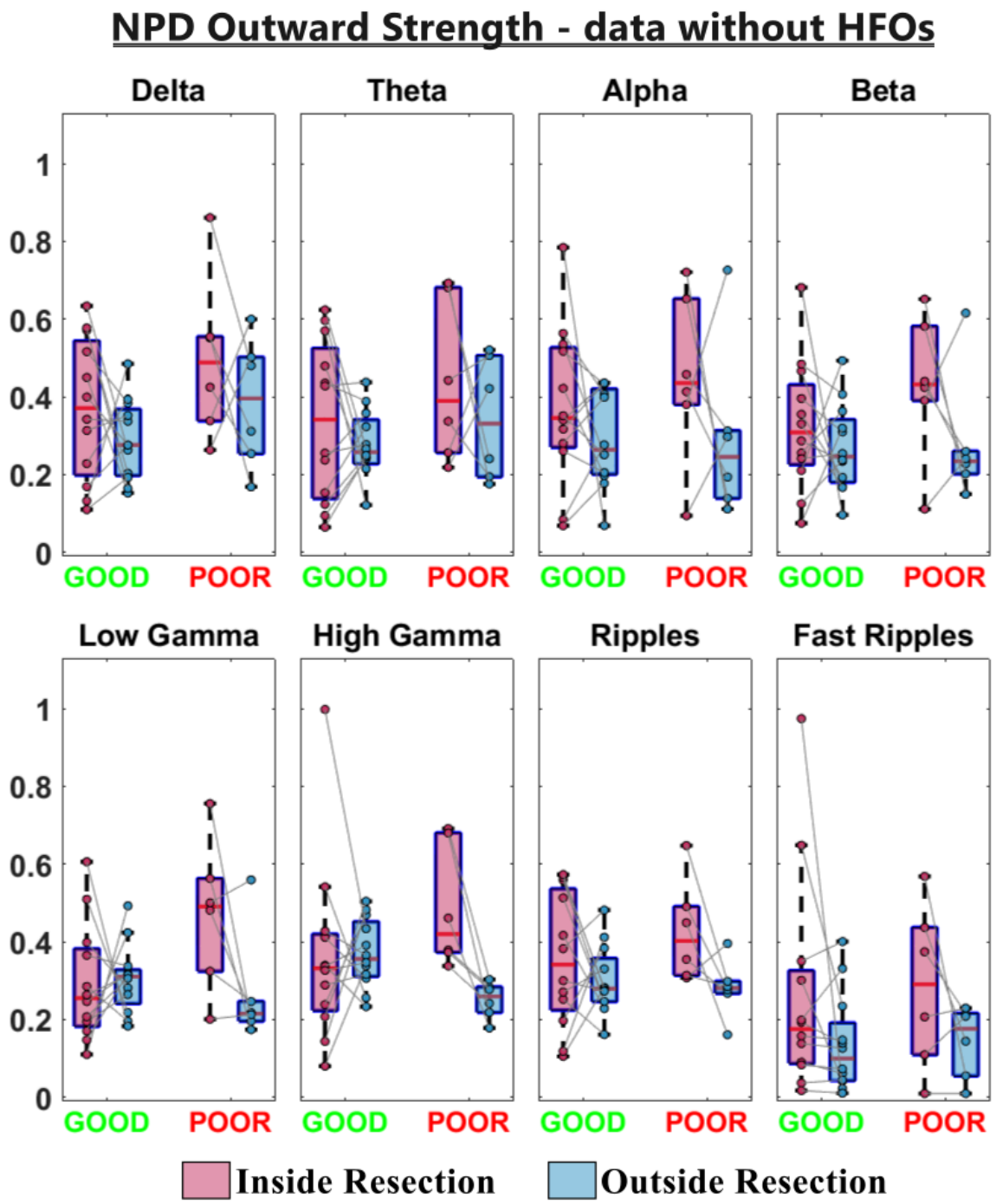

Supplementary Figure S18: Nonparametric directionality (NPD) outward strength, for segments without HFOs, compared inside (pink) vs. outside (blue) resection separately for good (N=12) and poor (N=6) outcome patients.

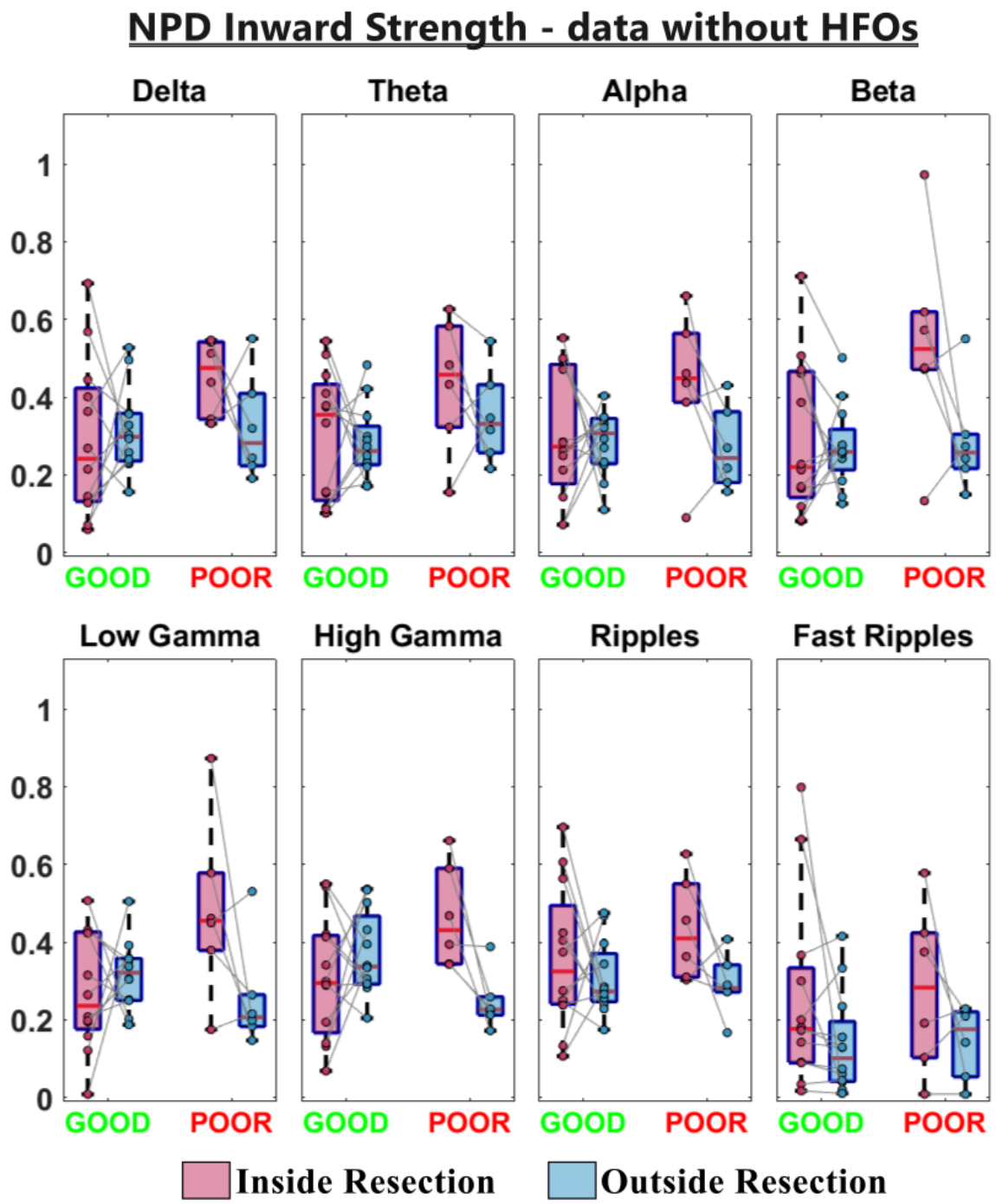

Supplementary Figure S19: Nonparametric directionality (NPD) inward strength, for segments without HFOs, compared inside (pink) vs. outside (blue) resection separately for good (N=12) and poor (N=6) outcome patients.

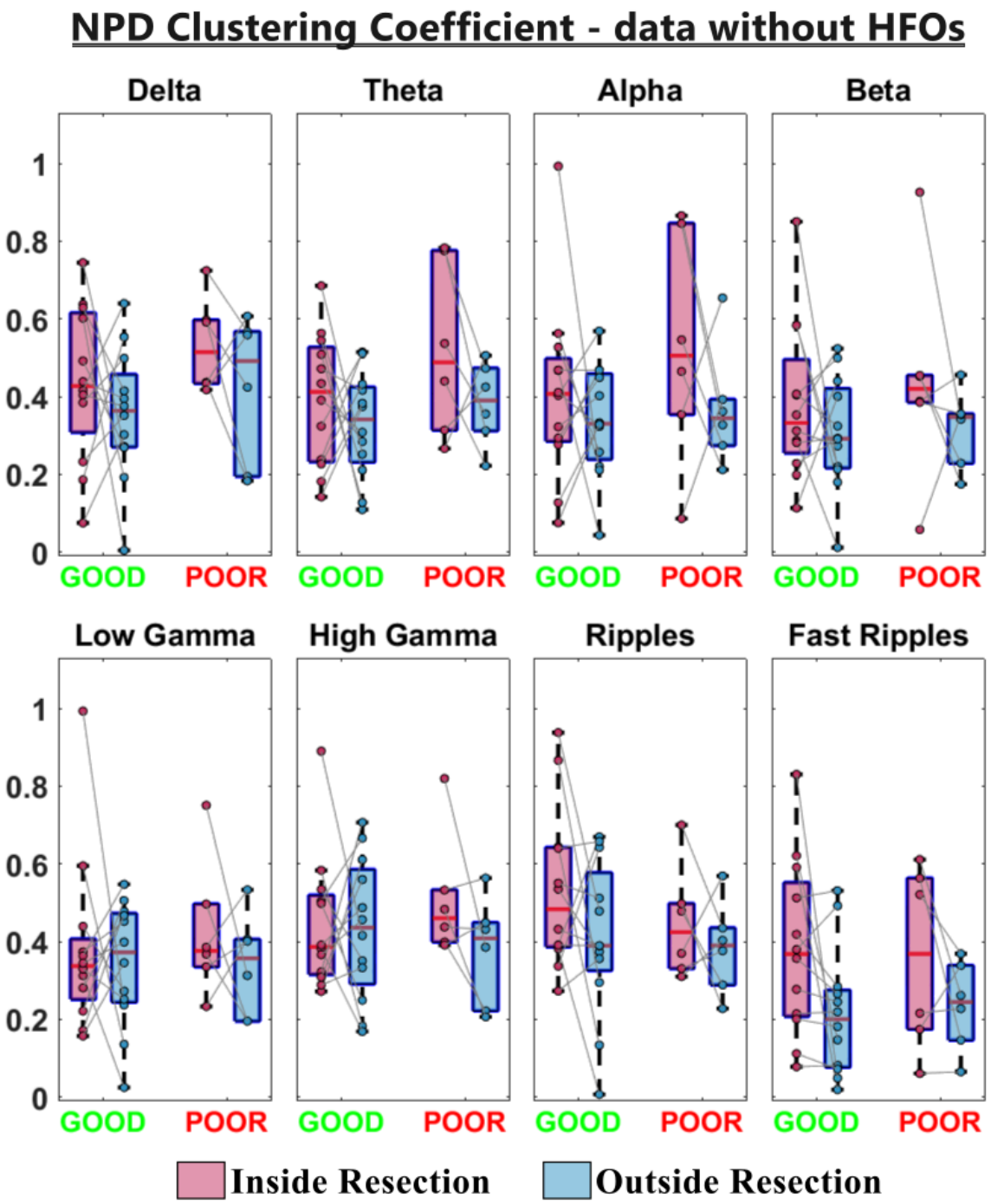

Supplementary Figure S20: Nonparametric directionality (NPD) clustering coefficient, for segments without HFOs, compared inside (pink) vs. outside (blue) resection separately for good (N=12) and poor (N=6) outcome patients.

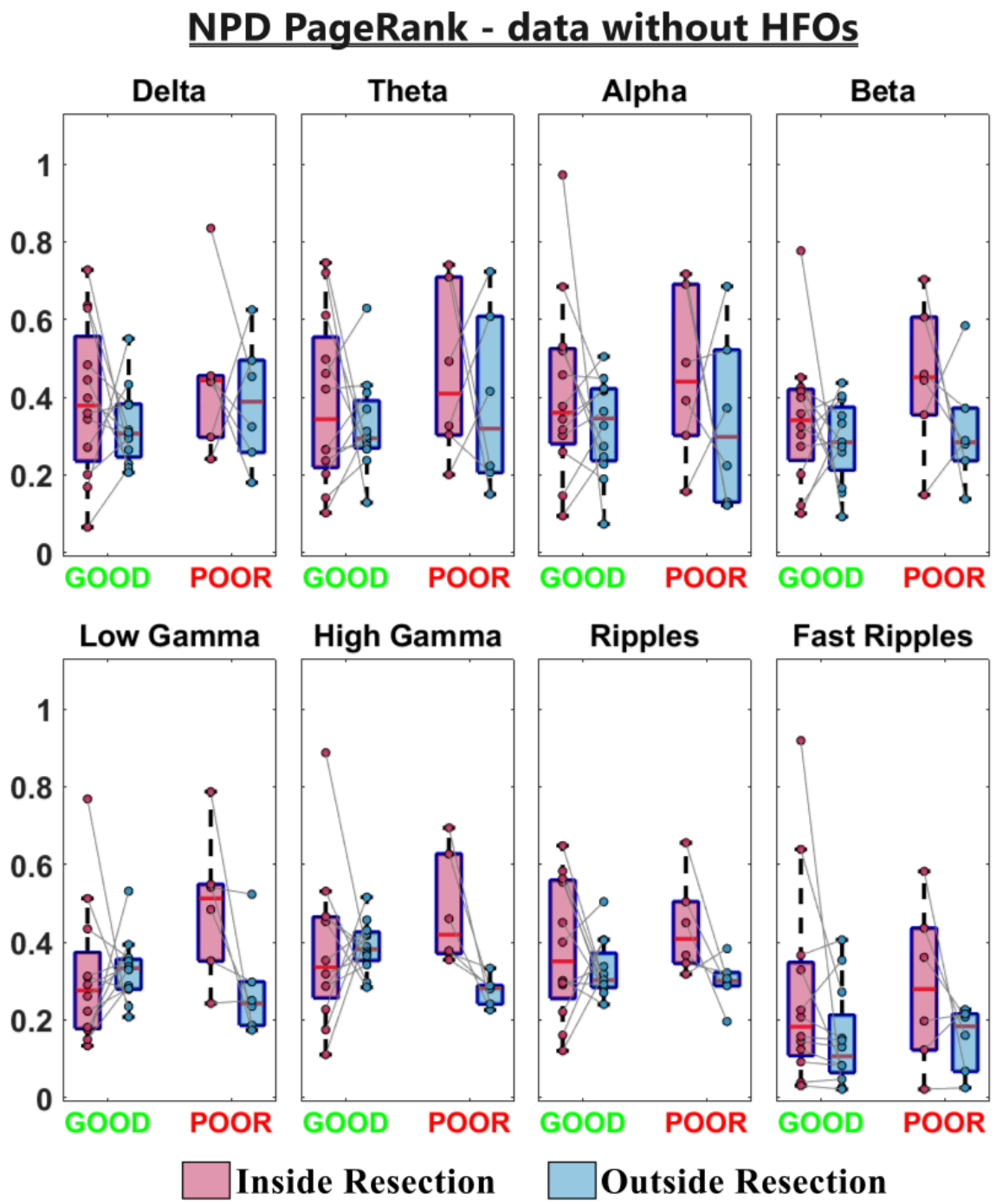

Supplementary Figure S21: Nonparametric directionality (NPD) PageRank, for segments without HFOs, compared inside (pink) vs. outside (blue) resection separately for good (N=12) and poor (N=6) outcome patients.

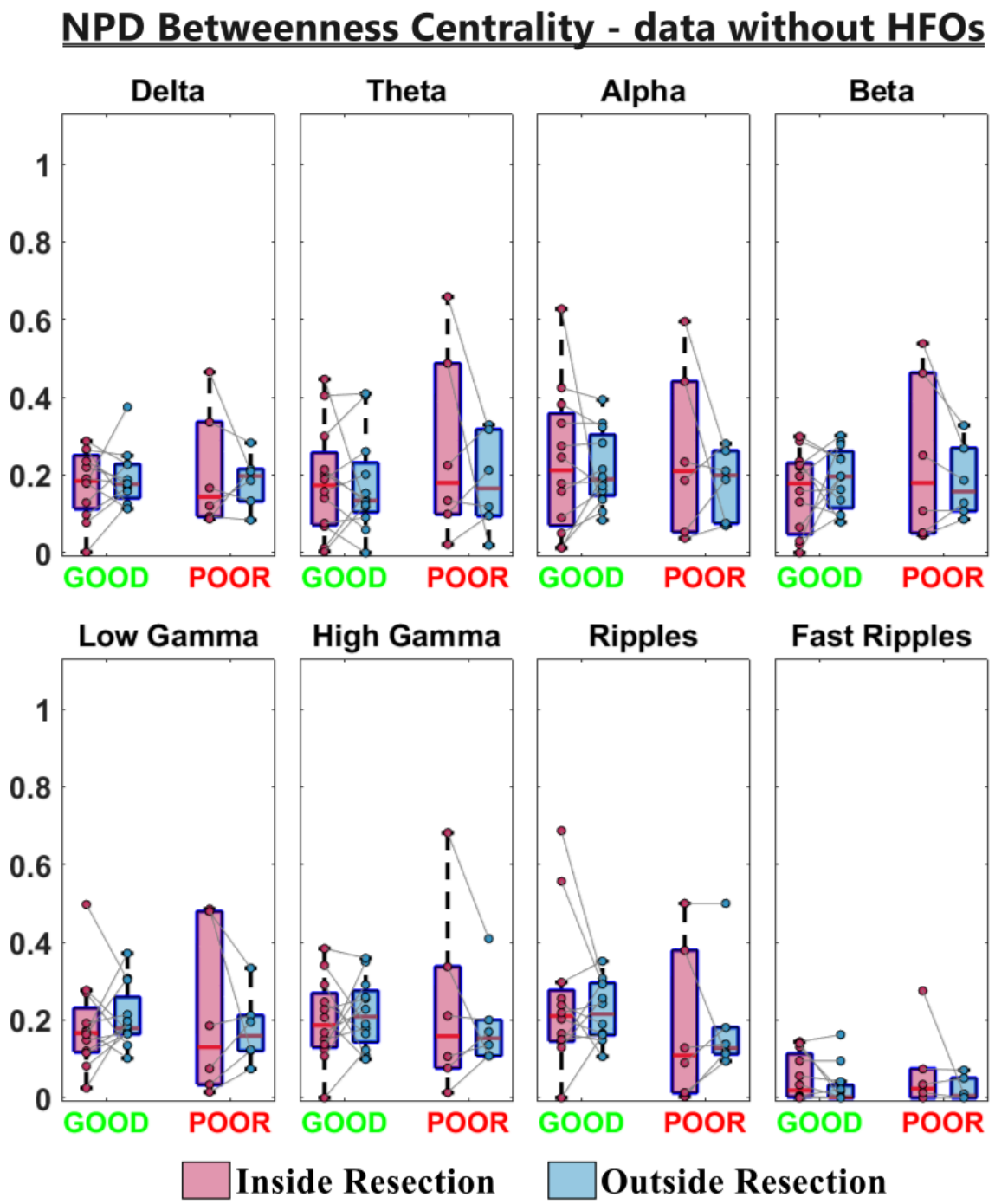

Supplementary Figure S22: Nonparametric directionality (NPD) betweenness centrality, for segments without HFOs, compared inside (pink) vs. outside (blue) resection separately for good (N=12) and poor (N=6) outcome patients.

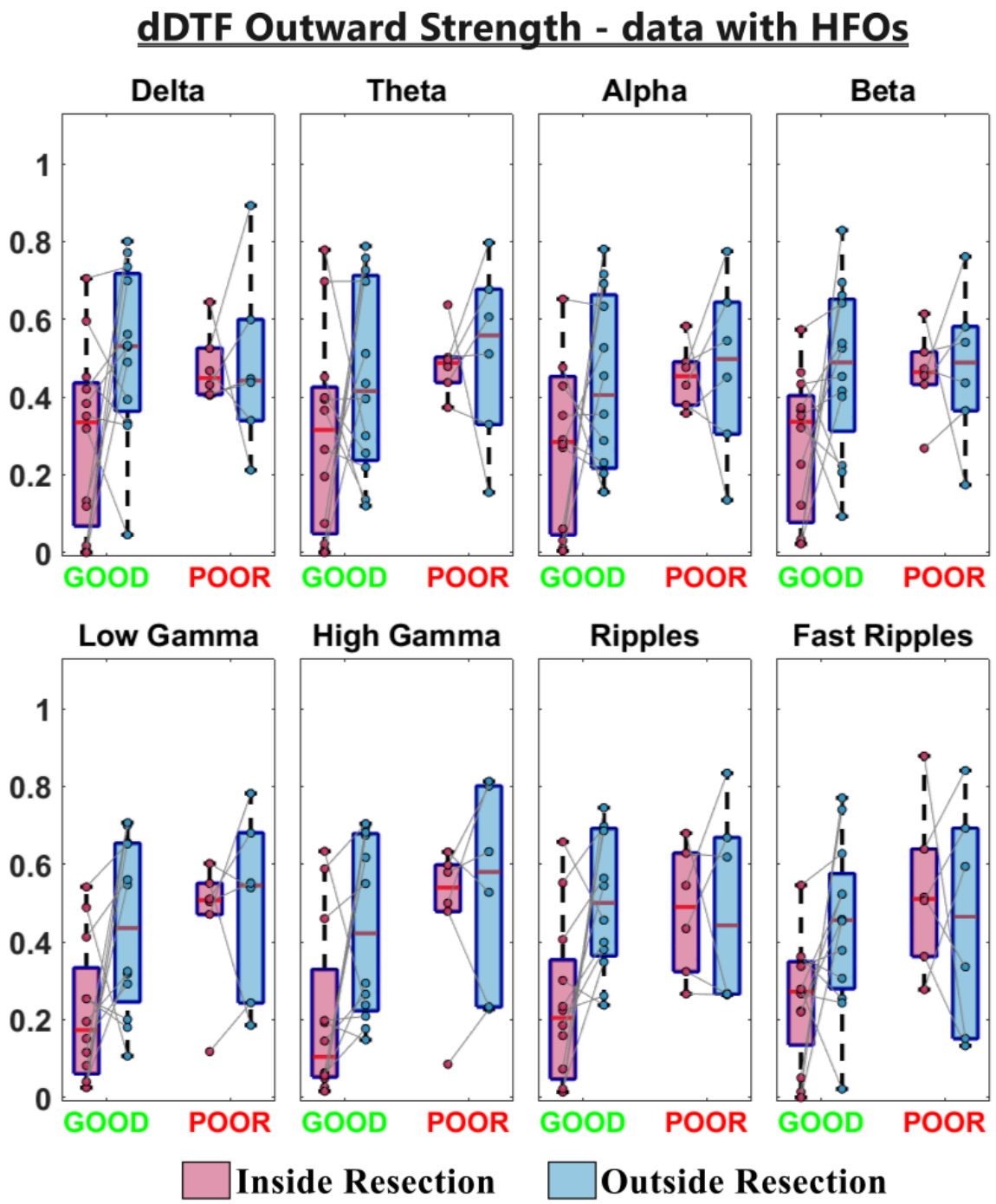

Supplementary Figure S23: Direct directed transfer function (dDTF) outward strength, for segments with HFOs, compared inside (pink) vs. outside (blue) resection separately for good (N=12) and poor (N=6) outcome patients.

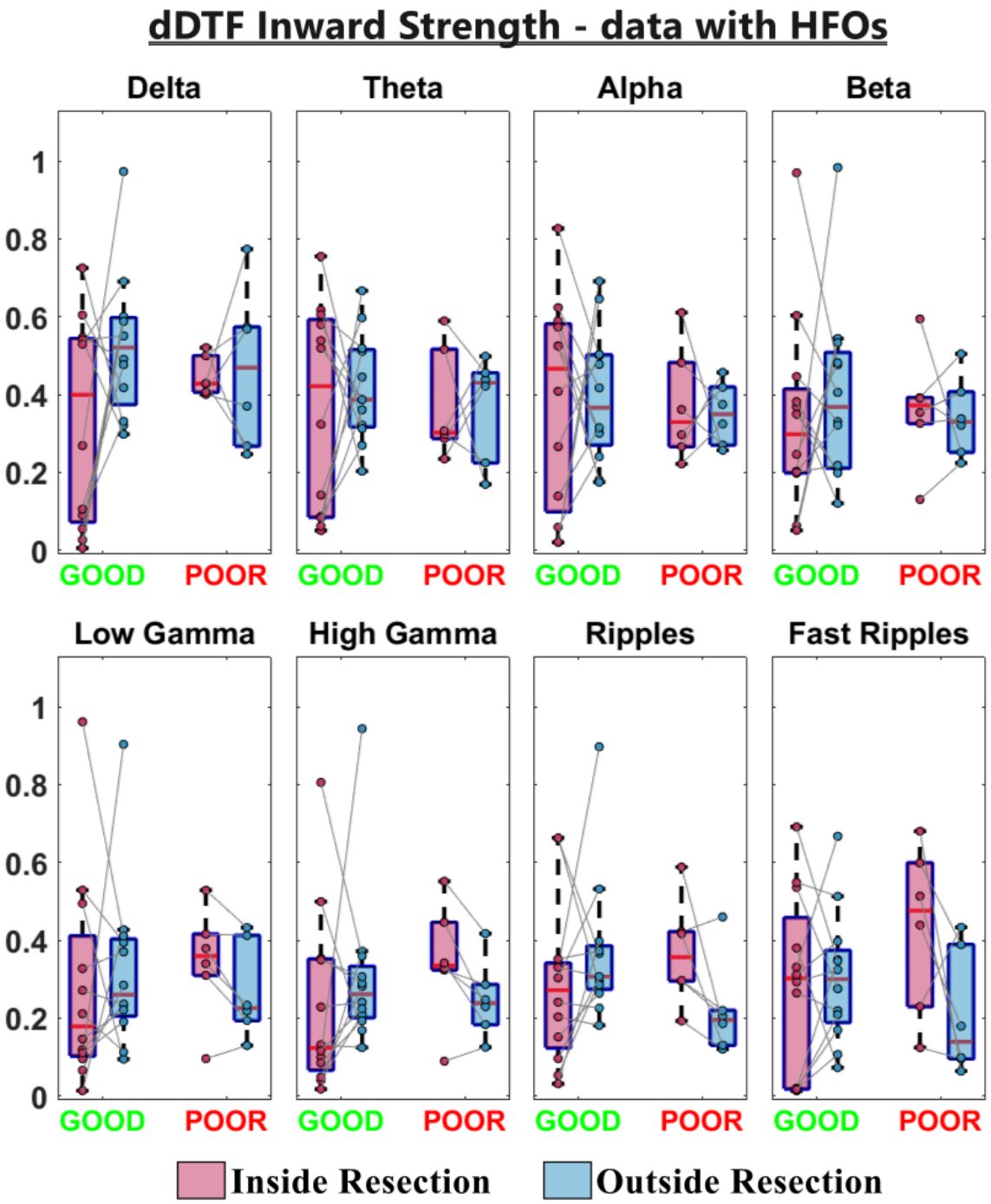

Supplementary Figure S24: Direct directed transfer function (dDTF) inward strength, for segments with HFOs, compared inside (pink) vs. outside (blue) resection separately for good (N=12) and poor (N=6) outcome patients.

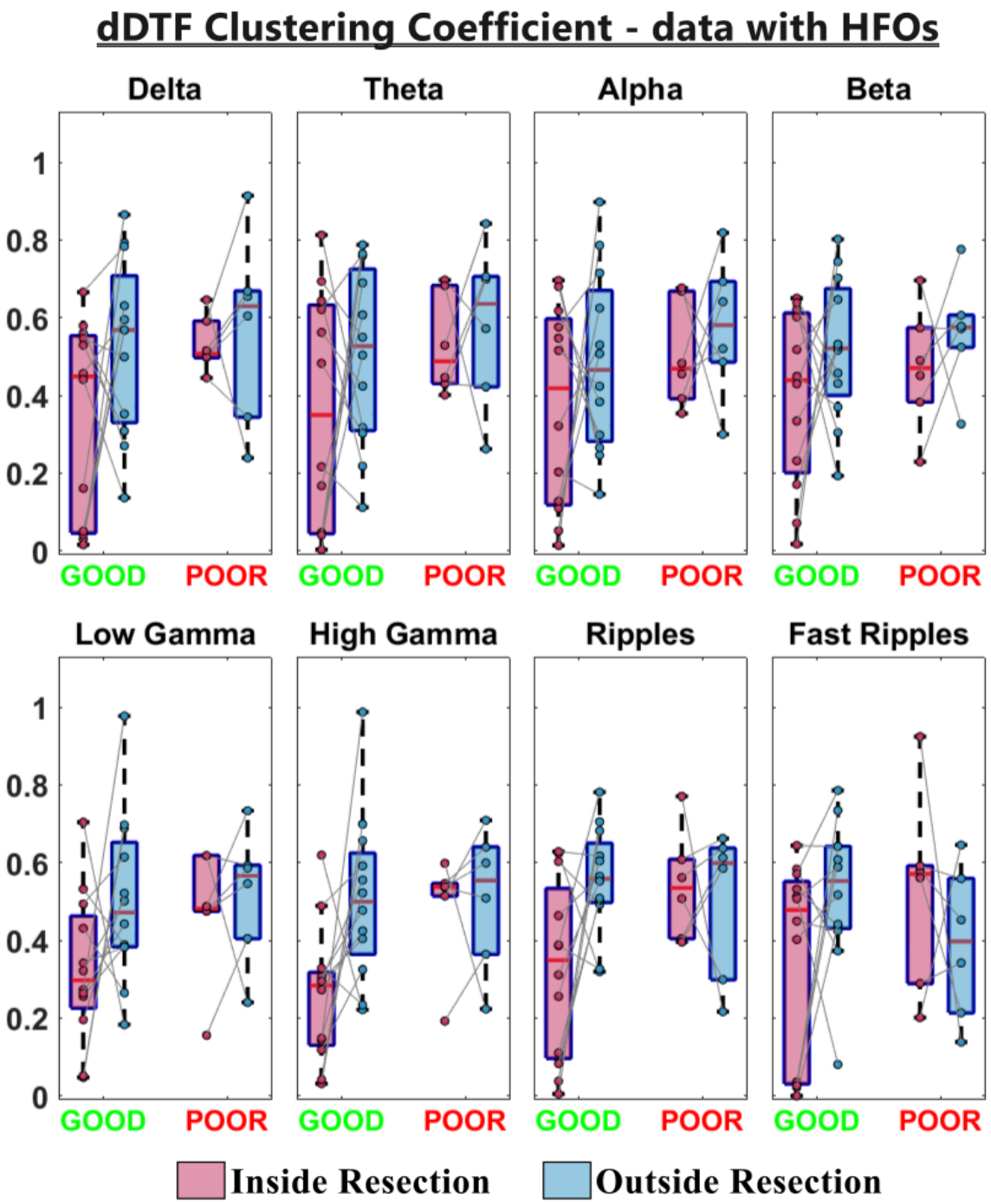

Supplementary Figure S25: Direct directed transfer function (dDTF) clustering coefficient, for segments with HFOs, compared inside (pink) vs. outside (blue) resection separately for good (N=12) and poor (N=6) outcome patients.

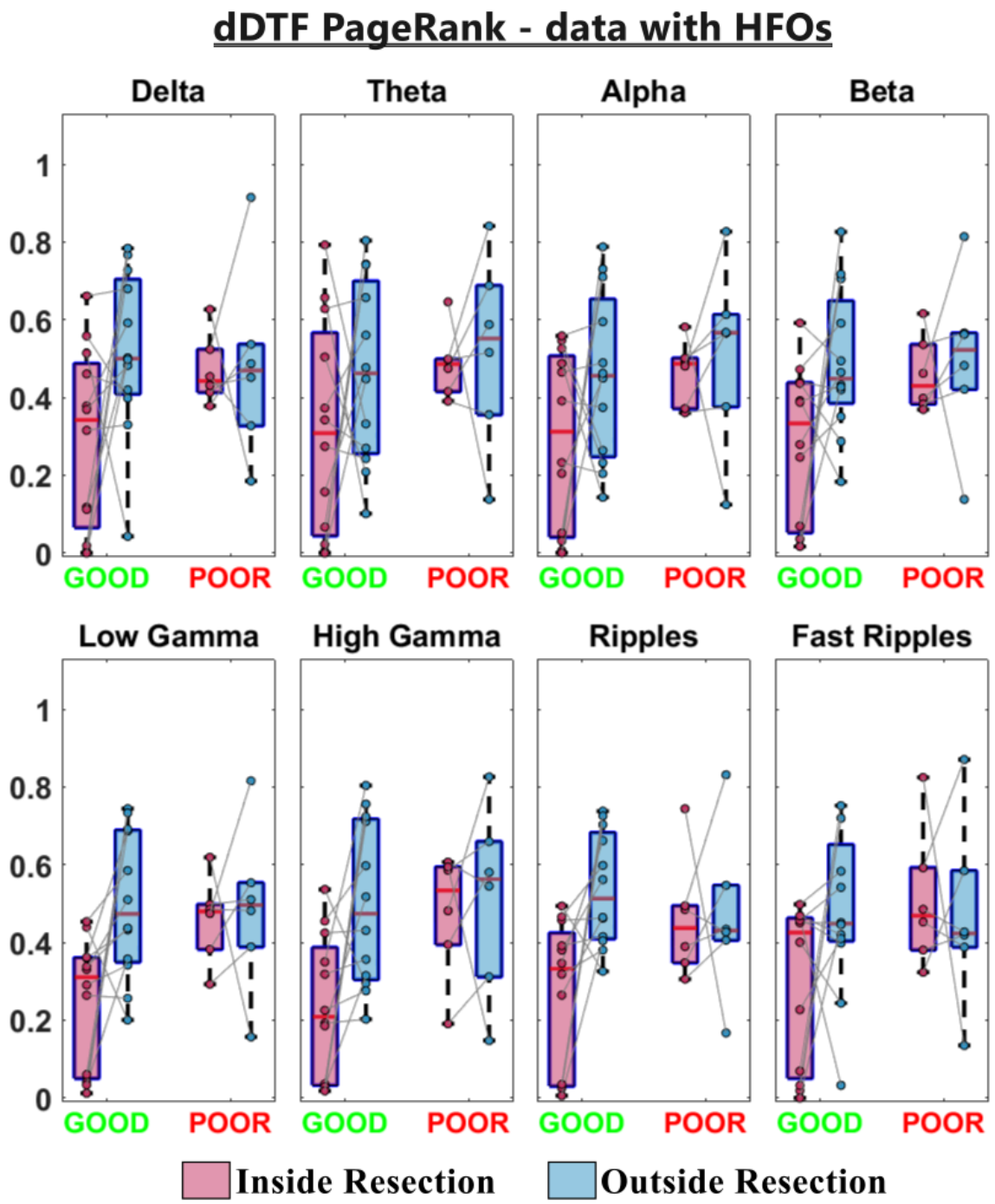

Supplementary Figure S26: Direct directed transfer function (dDTF) PageRank, for segments with HFOs, compared inside (pink) vs. outside (blue) resection separately for good (N=12) and poor (N=6) outcome patients.

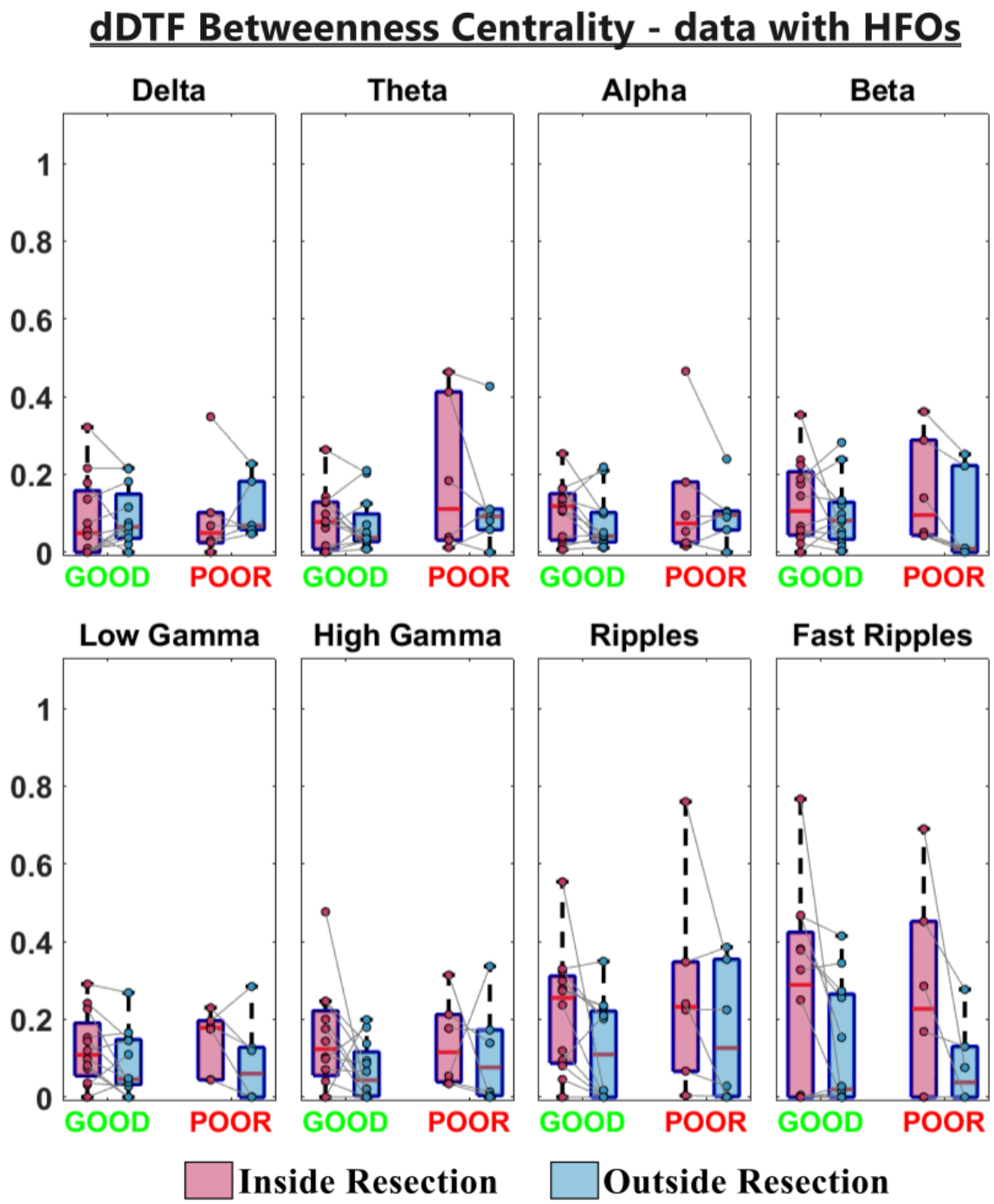

Supplementary Figure S27: Direct directed transfer function (dDTF) betweenness centrality, for segments with HFOs, compared inside (pink) vs. outside (blue) resection separately for good (N=12) and poor (N=6) outcome patients.

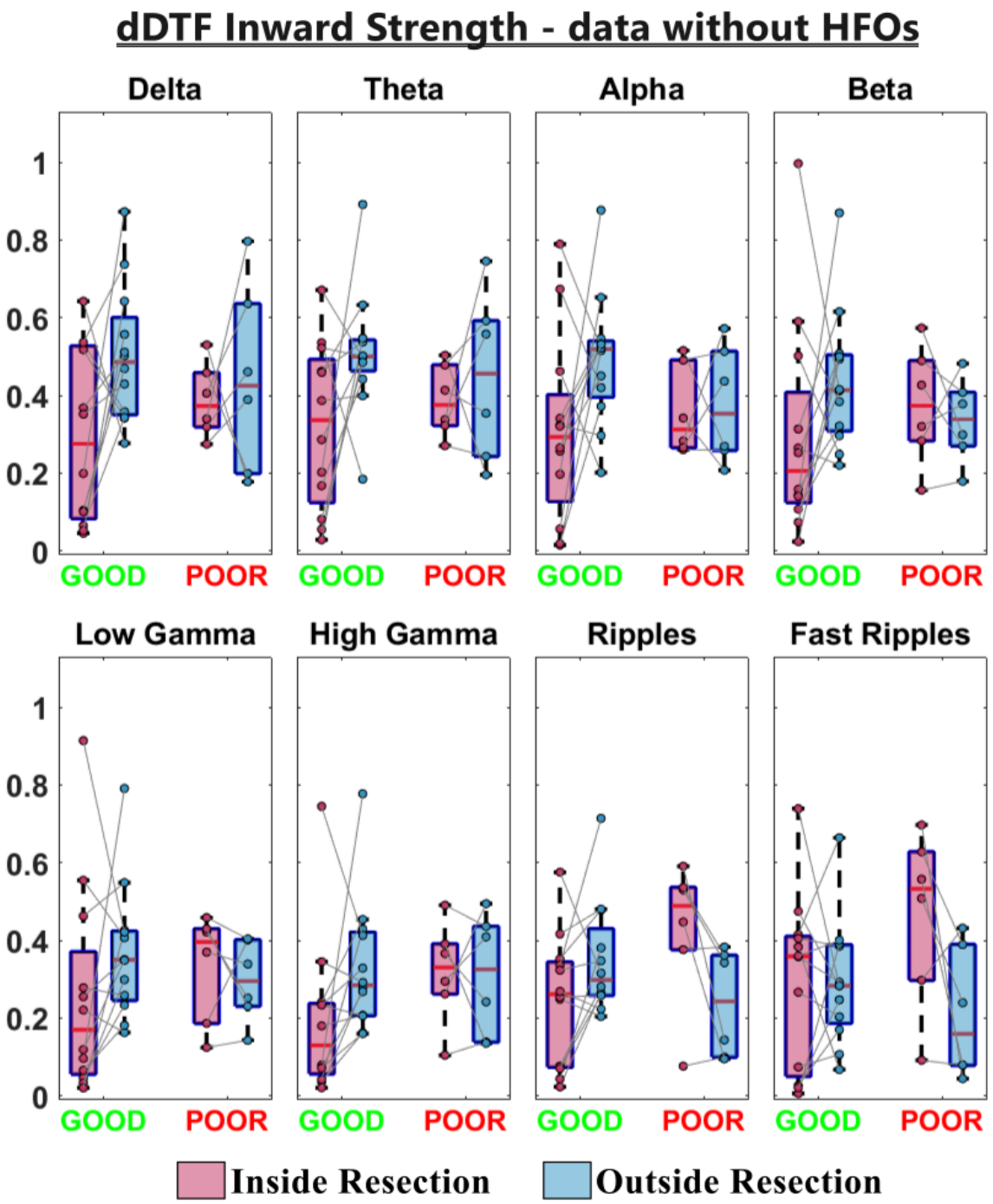

Supplementary Figure S28: Direct directed transfer function (dDTF) inward strength, for segments without HFOs, compared inside (pink) vs. outside (blue) resection separately for good (N=12) and poor (N=6) outcome patients.

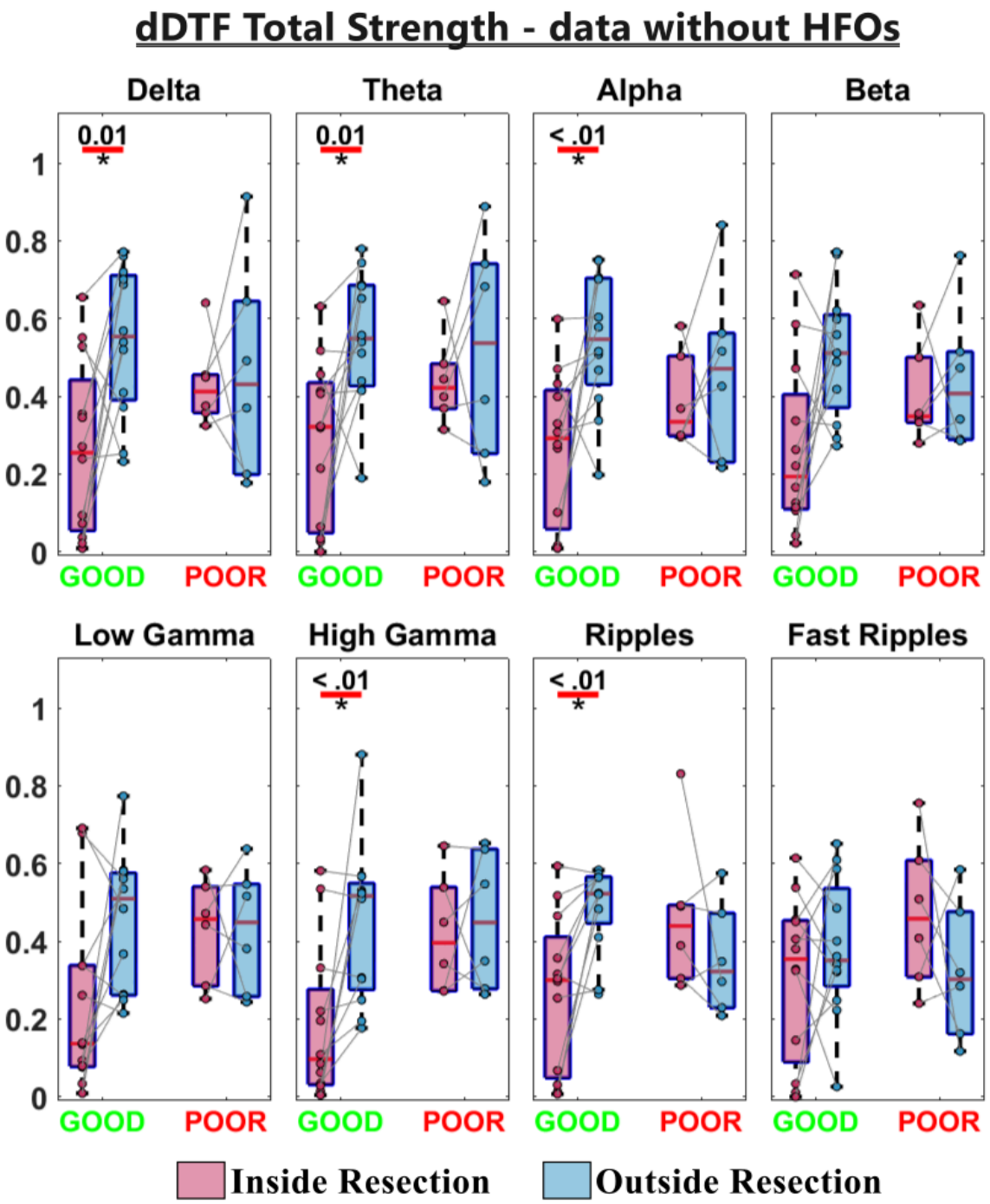

Supplementary Figure S29: Direct directed transfer function (dDTF) total strength, for segments without HFOs, compared inside (pink) vs. outside (blue) resection separately for good (N=12) and poor (N=6) outcome patients.

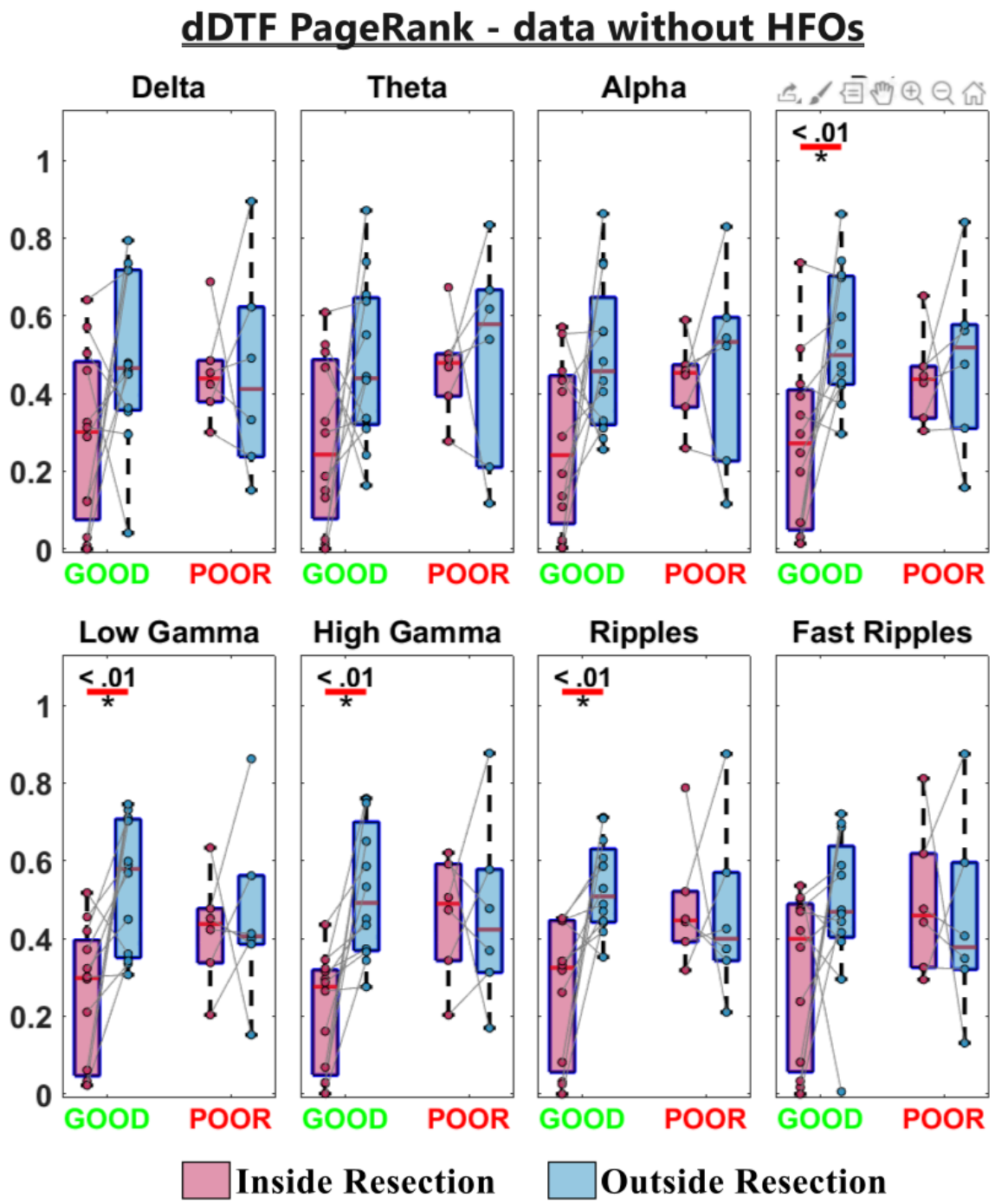

Supplementary Figure S30: Direct directed transfer function (dDTF) PageRank, for segments without HFOs, compared inside (pink) vs. outside (blue) resection separately for good (N=12) and poor (N=6) outcome patients.

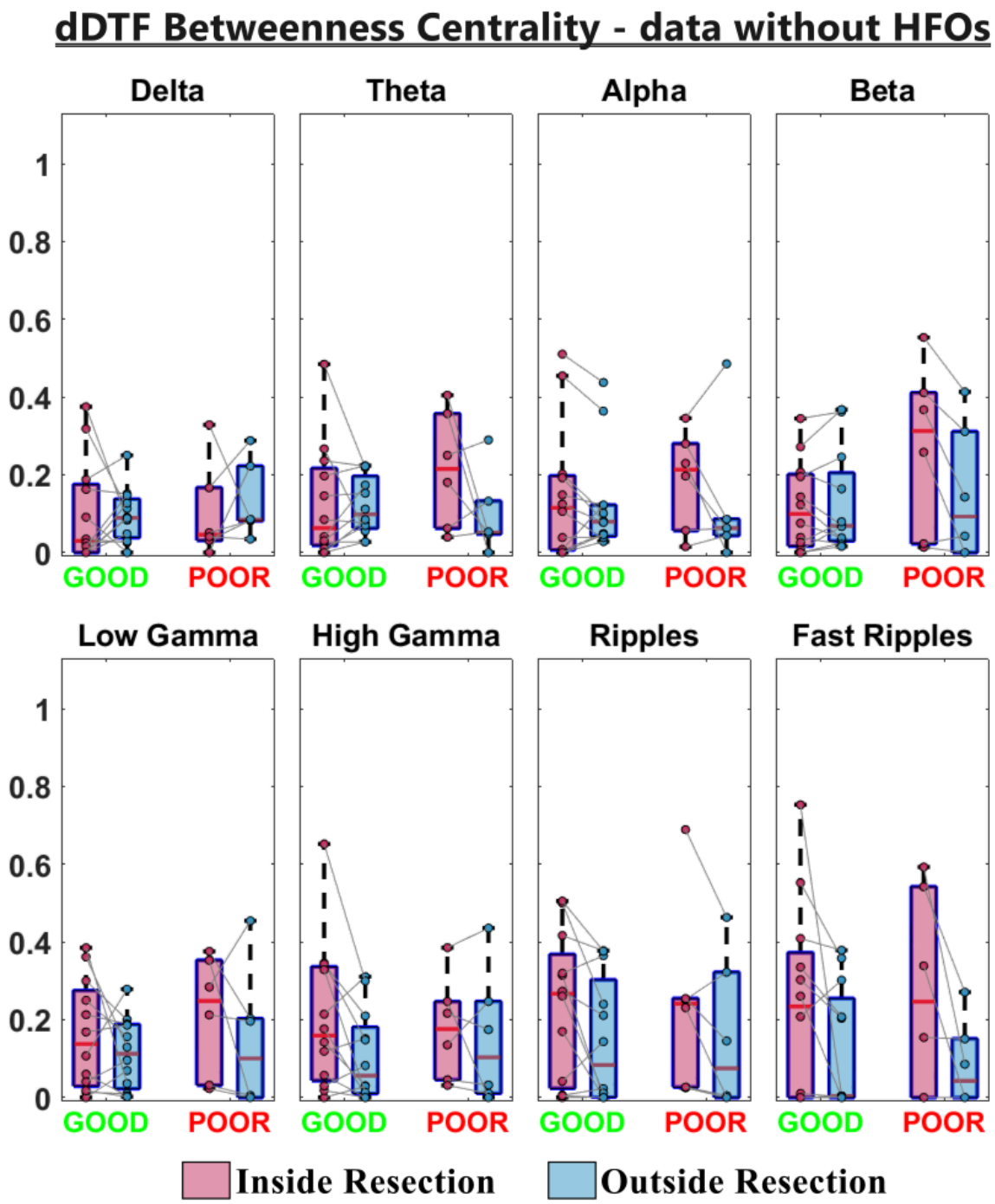

Supplementary Figure S31: Direct directed transfer function (dDTF) betweenness centrality, for segments without HFOs, compared inside (pink) vs. outside (blue) resection separately for good (N=12) and poor (N=6) outcome patients.

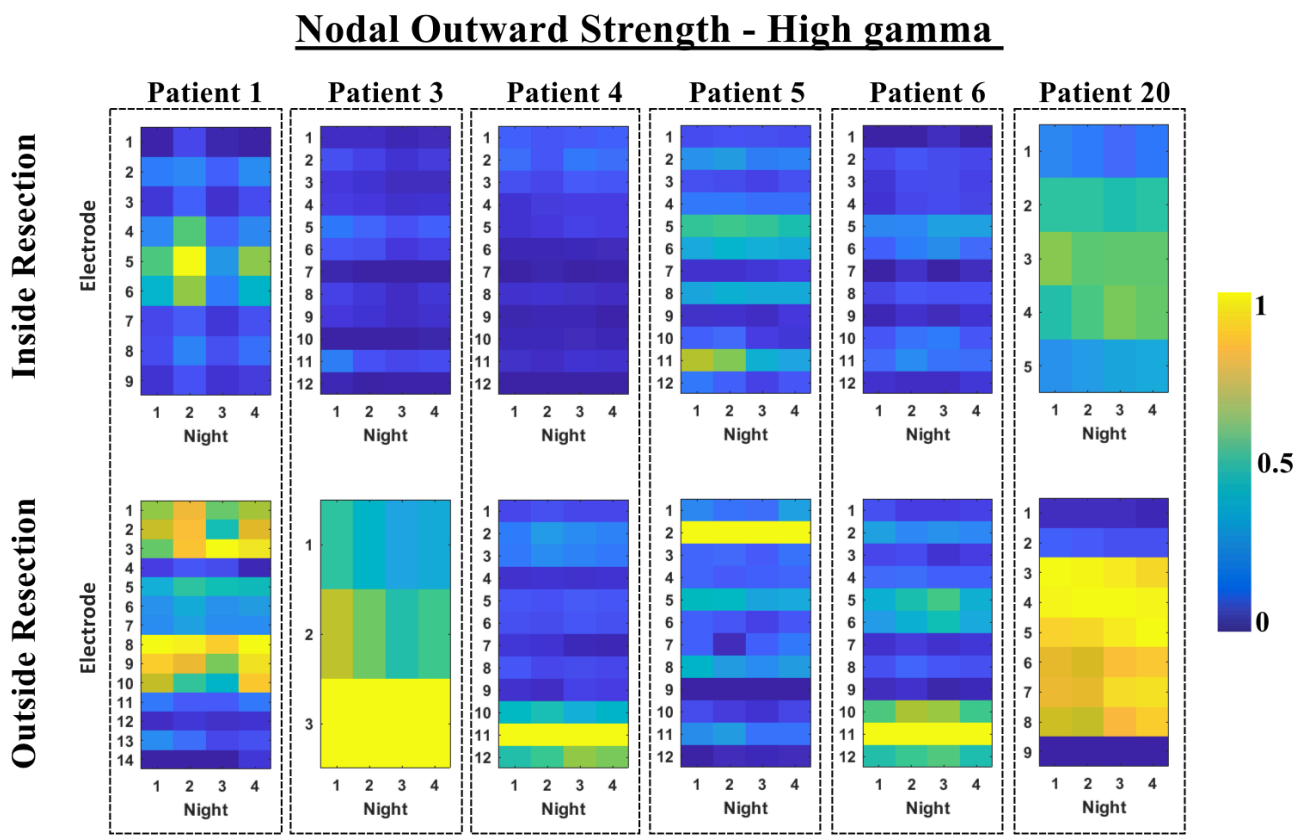

Supplementary Figure S32: Variation of nodal outward strength in each electrode of every patient across four different nights of iEEG recording for the high gamma band.

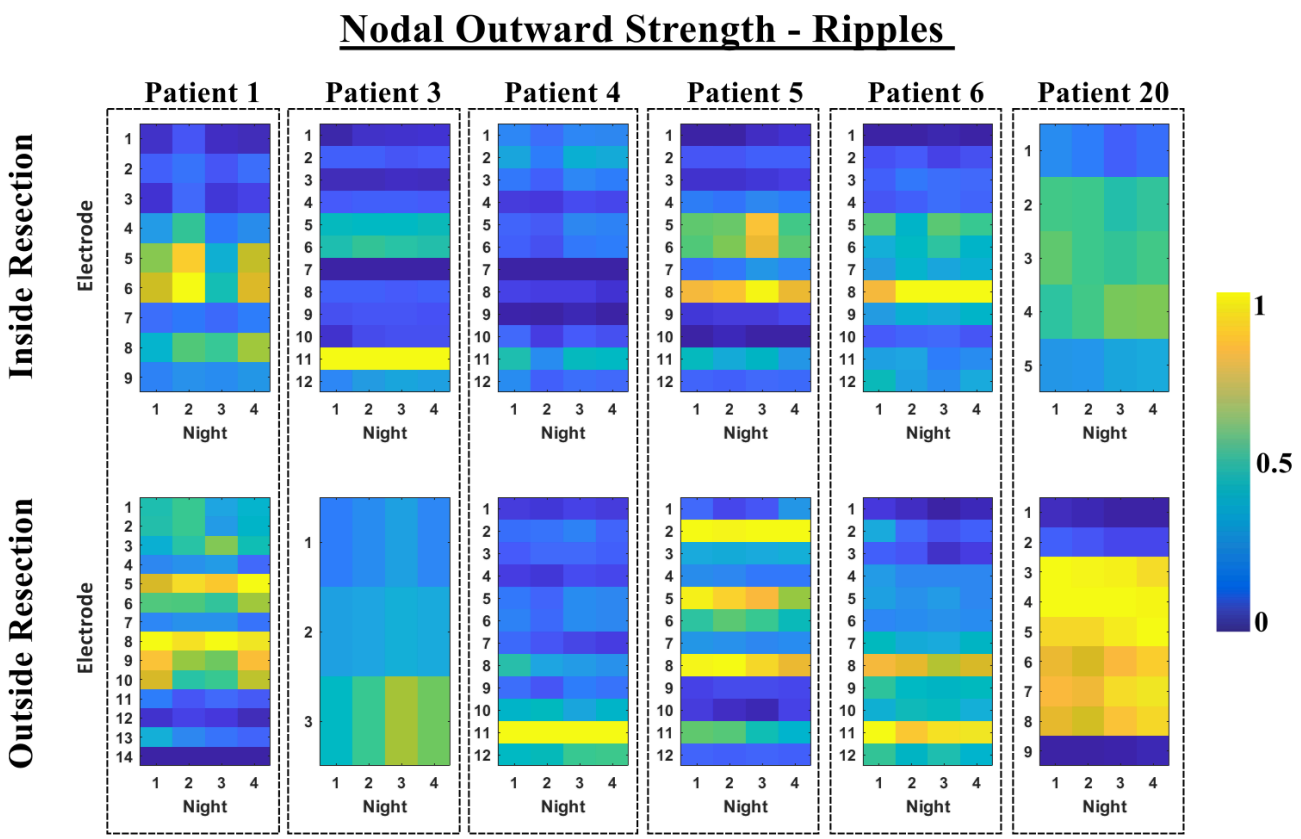

Supplementary Figure S33: Variation of nodal outward strength in each electrode of every patient across four different nights of iEEG recording for the ripple band.

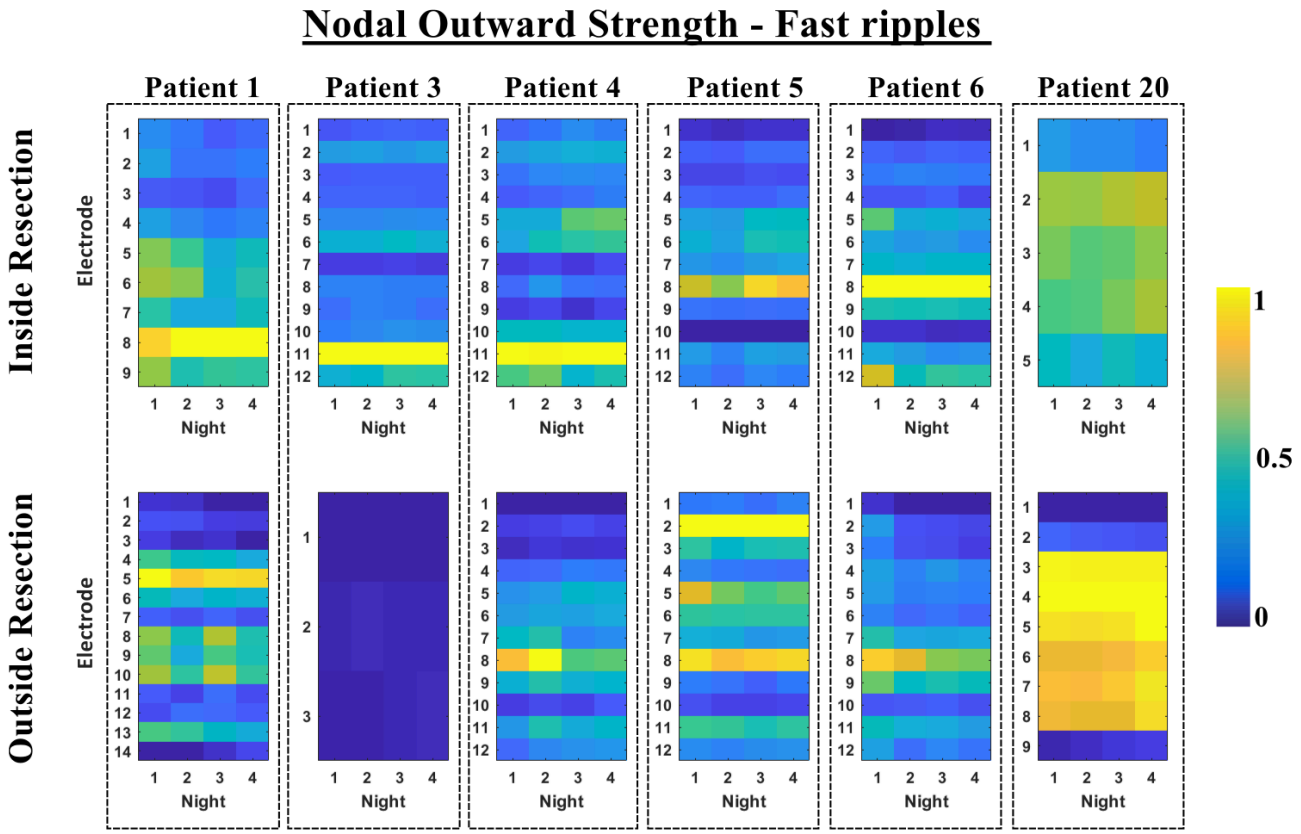

Supplementary Figure S34: Variation of nodal outward strength in each electrode of every patient across four different nights of iEEG recording for the fast ripples band.

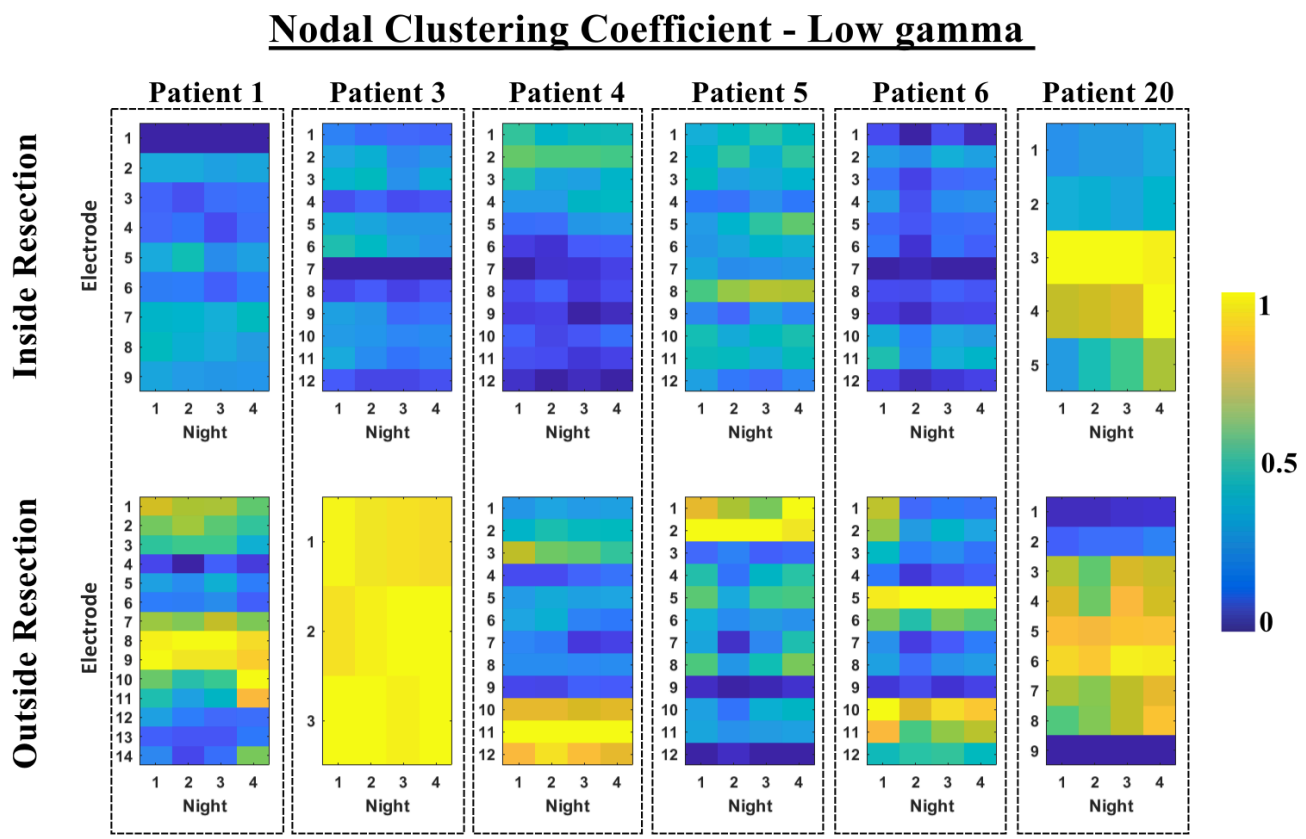

Supplementary Figure S35: Variation of nodal clustering coefficient in each electrode of every patient across four different nights of iEEG recording for the low gamma band.

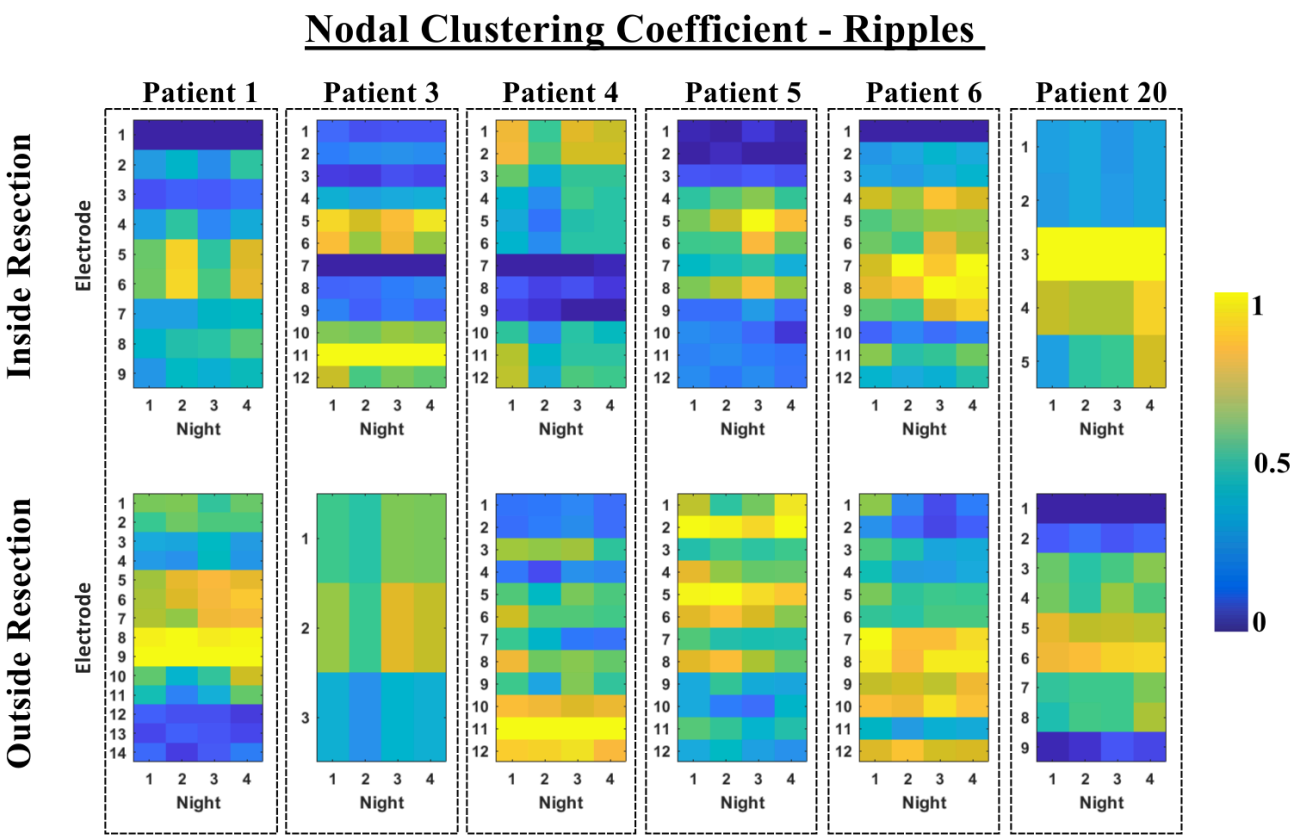

Supplementary Figure S36: Variation of nodal clustering coefficient in each electrode of every patient across four different nights of iEEG recording for the ripple band.

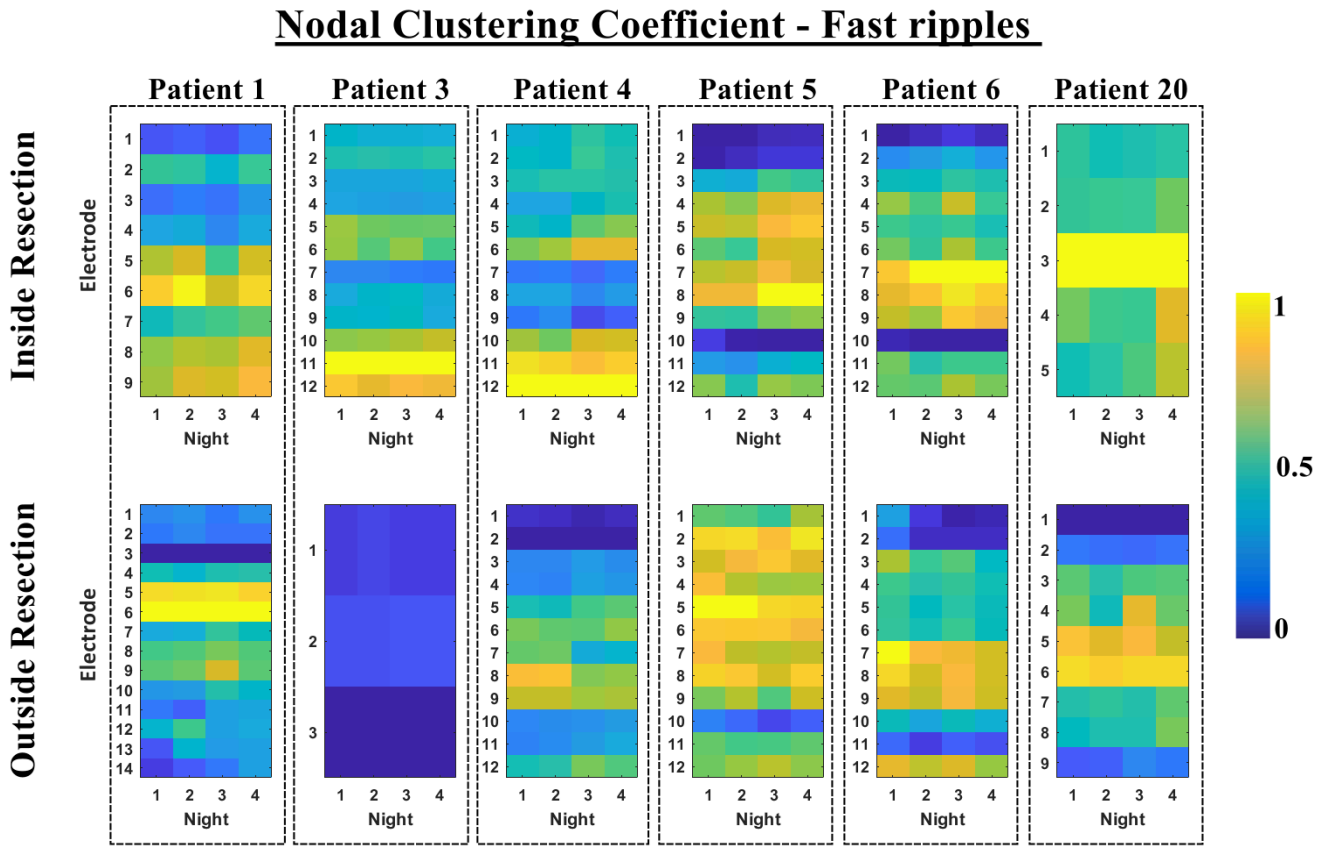

Supplementary Figure S37: Variation of nodal clustering coefficient in each electrode of every patient across four different nights of iEEG recording for the fast ripples band.

List of abbreviations

AEC	Amplitude Envelove Correlation
AI	Artificial Intelligence
AIC	Akaike’s Information Criterion
ANOVA	Analysis of Variance
AR	Autoregressive
ASMs	Antiseizure Medications
AUC	Area Under the Curve
BC	Betweenness Centrality
BCT	Brain Connectivity Toolbox
CC	Clustering Coefficient
CNS	Central Nervous System
CT	Computerized Tomography
DC	Direct Current
DRE	Drug-Resistant Epilepsy
DTF	Direted Transfer Function
dDTF	direct Directed Transfer Function
EC	Eigenvector Centrality
ECOG	Electrocorticography
EEG	Electroencephalography
EMG	Electromyogram
ETE	Extratemporal Epilepsy
ES	Epilepsy Surgery
EZ	Epileptogenic Zone
FC	Functional Connectivity
FCD	Focal Cortical Displasia
FDR	False Discovery Rate

FR	Fast Ripple
GABA	Gamma-Amino-Butyric Acid
FDA	Food and Drug Administration
fMRI	functional Magnetic Resonance Imaging
FN	False Negative
FP	False Positive
HD-EEG	High-Density Electroencephalography
HD-MEG	High-Density Magnetoencephalography
HFA	High-Frequency Activity
HFOs	High-Frequency Oscillations
HS	Hippocampal Sclerosis
IEDS	Interictal Epileptiform Discharges
iEEG	Intracranial Electroenchephalography
IIR	Infinite Impulse Response
ILAE	International League Against Epilepsy
ISH	Interictal Suppression Hypothesis
IZ	Irritative Zone
kNN	k-Nearest Neighbors
LME	Linear Mixed-Effects
LR	Logistic Regression
MCD	Malformation of Cortical Development
MEG	Magnetoencephalography
MI	Modulation Index
MMSE	Minimum Mean Square Error
ML	Machine Learning
MNI	Montreal Neurological Institute
MPC	Mean Phase Coherence
MRI	Magnetic Resonance Imaging

MTLE	Mesial Temporal Lobe epilepsy
MVAR	Multivariate Autoregressive
NIH	National Institute of Health
NIZ	Non-Involved Zone
NMDA	N-methyl-D-aspartate
NREM	Non-Rapid Eye Movement
NPD	Nonparametric Directionality
NPV	Negative Predictive Value
oAEC	orthogonalized Amplitude Envelope Correlation
PET	Photon Emision Tomography
PLV	Phase Locking Value
PPV	Positive Predictive Value
PR	PageRank
PZ	Propagation Zone
RZ	Resection Zone
SdDTF	Short-Time Direct Directed Transfer Function
SEEG	Stereoenchephalography
SMOTE	Synthetic Minority Over-sampling Technique
SOZ	Seizure Onset Zone
SPECT	SIngle-Photon Emission Computed Tomography
SUDEP	Sudden Unexpected Death in Epilepsy
SVM	Support Vector Machine
TBI	Traumatic Brain Injury
TLE	Temporal Lobe Epilepsy
TN	True Negative
TP	True Positive
WHO	World Health Organization

References

[1] R. S. Fisher *et al.*, “ILAE Official Report: A practical clinical definition of epilepsy,” *Epilepsia*, vol. 55, no. 4, pp. 475–482, 2014, doi: 10.1111/epi.12550.

[2] H. Kumar, S. Debnath, and A. Sharma, “Can epilepsy be cured? A review,” *Health Sci. Rev.*, vol. 5, p. 100062, Dec. 2022, doi: 10.1016/j.hsr.2022.100062.

[3] *Epilepsy: a Public Health Imperative*. World Health Organization, 2019. [Online]. Available: https://books.google.gr/books?id=rSiMzQEACAAJ

[4] G. L. Holmes, “Consequences of Epilepsy Through the Ages: When Is the Die Cast?,” *Epilepsy Curr.*, vol. 12, no. Suppl 3, pp. 4–6, 2012, doi: 10.5698/1535-7511-12.4s.4.

[5] C. E. Stafstrom and L. Carmant, “Seizures and Epilepsy: An Overview for Neuroscientists,” *Cold Spring Harb. Perspect. Med.*, vol. 5, no. 6, p. a022426, June 2015, doi: 10.1101/cshperspect.a022426.

[6] L. Ochoa-Gómez *et al.*, “A study of epilepsy according to the age at onset and monitored for 3 years in a regional reference paediatric neurology unit,” *An. Pediatría Engl. Ed.*, vol. 86, no. 1, pp. 11–19, Jan. 2017, doi: 10.1016/j.anpede.2016.05.003.

[7] E. Beghi, “The Epidemiology of Epilepsy,” *Neuroepidemiology*, vol. 54, no. 2, pp. 185–191, 2020, doi: 10.1159/000503831.

[8] E. Beghi *et al.*, “Global, regional, and national burden of epilepsy, 1990–2016: a systematic analysis for the Global Burden of Disease Study 2016,” *Lancet Neurol.*, vol. 18, no. 4, pp. 357–375, Apr. 2019, doi: 10.1016/S1474-4422(18)30454-X.

[9] M. Mula, A. M. Kanner, N. Jetté, and J. W. Sander, “Psychiatric Comorbidities in People With Epilepsy,” *Neurol. Clin. Pract.*, vol. 11, no. 2, pp. e112–e120, Apr. 2021, doi: 10.1212/CPJ.0000000000000874.

[10] P. Kwan *et al.*, “Definition of drug resistant epilepsy: consensus proposal by the ad hoc Task Force of the ILAE Commission on Therapeutic Strategies,” *Epilepsia*, vol. 51, no. 6, pp. 1069–1077, June 2010, doi: 10.1111/j.1528-1167.2009.02397.x.

[11] J. W. Sander, “The epidemiology of epilepsy revisited,” *Curr. Opin. Neurol.*, vol. 16, no. 2, pp. 165–170, Apr. 2003.

[12] P. Ryvlin, J. H. Cross, and S. Rheims, “Epilepsy surgery in children and adults,” *Lancet Neurol.*, vol. 13, no. 11, pp. 1114–1126, Nov. 2014, doi: 10.1016/S1474-4422(14)70156-5.

[13] H. O. Lüders, I. Najm, D. Nair, P. Widdess-Walsh, and W. Bingman, “The epileptogenic zone: general principles,” *Epileptic Disord. Int. Epilepsy J. Videotape*, vol. 8 Suppl 2, pp. S1-9, Aug. 2006.

[14] F. Rosenow and H. Lüders, “Presurgical evaluation of epilepsy,” *Brain*, vol. 124, no. 9,

pp. 1683–1700, Sept. 2001, doi: 10.1093/brain/124.9.1683.

[15] S. S. Balaji and K. K. Parhi, “Seizure Onset Zone Identification From iEEG: A Review,” *IEEE Access*, vol. 10, pp. 62535–62547, 2022, doi: 10.1109/ACCESS.2022.3182716.

[16] L. Jehi, “The Epileptogenic Zone: Concept and Definition,” *Epilepsy Curr.*, vol. 18, no. 1, pp. 12–16, 2018, doi: 10.5698/1535-7597.18.1.12.

[17] C.-H. Lee, S.-N. Lim, F. Lien, and T. Wu, “Duration of electroencephalographic recordings in patients with epilepsy,” *Seizure*, vol. 22, no. 6, pp. 438–442, July 2013, doi: 10.1016/j.seizure.2013.02.016.

[18] M. A. G. Matarrese *et al.*, “Spike propagation mapping reveals effective connectivity and predicts surgical outcome in epilepsy,” *Brain J. Neurol.*, p. awad118, Apr. 2023, doi: 10.1093/brain/awad118.

[19] J. Jacobs *et al.*, “High-frequency oscillations (HFOs) in clinical epilepsy,” *Prog. Neurobiol.*, vol. 98, no. 3, pp. 302–315, Sept. 2012, doi: 10.1016/j.pneurobio.2012.03.001.

[20] M. Zijlmans, P. Jiruska, R. Zelmann, F. S. S. Leijten, J. G. R. Jefferys, and J. Gotman, “High-frequency oscillations as a new biomarker in epilepsy,” *Ann. Neurol.*, vol. 71, no. 2, pp. 169–178, 2012, doi: 10.1002/ana.22548.

[21] J. Jacobs *et al.*, “High-frequency electroencephalographic oscillations correlate with outcome of epilepsy surgery,” *Ann. Neurol.*, vol. 67, no. 2, pp. 209–220, Feb. 2010, doi: 10.1002/ana.21847.

[22] J. Jacobs, P. LeVan, R. Chander, J. Hall, F. Dubeau, and J. Gotman, “Interictal high-frequency oscillations (80-500 Hz) are an indicator of seizure onset areas independent of spikes in the human epileptic brain,” *Epilepsia*, vol. 49, no. 11, pp. 1893–1907, Nov. 2008, doi: 10.1111/j.1528-1167.2008.01656.x.

[23] E. Tamilia *et al.*, “Surgical resection of ripple onset predicts outcome in pediatric epilepsy,” *Ann. Neurol.*, vol. 84, no. 3, pp. 331–346, Sept. 2018, doi: 10.1002/ana.25295.

[24] X. Liu *et al.*, “An Automatic HFO Detection Method Combining Visual Inspection Features with Multi-Domain Features,” *Neurosci. Bull.*, vol. 37, no. 6, pp. 777–788, Mar. 2021, doi: 10.1007/s12264-021-00659-y.

[25] C. J. Park and S. B. Hong, “High Frequency Oscillations in Epilepsy: Detection Methods and Considerations in Clinical Application,” *J. Epilepsy Res.*, vol. 9, no. 1, pp. 1–13, June 2019, doi: 10.14581/jer.19001.

[26] J. Engel Jr, A. Bragin, R. Staba, and I. Mody, “High-frequency oscillations: What is normal and what is not?,” *Epilepsia*, vol. 50, no. 4, pp. 598–604, 2009, doi: 10.1111/j.1528-1167.2008.01917.x.

[27] S. S. Spencer, “Neural networks in human epilepsy: evidence of and implications for treatment,” *Epilepsia*, vol. 43, no. 3, pp. 219–227, Mar. 2002, doi:

10.1046/j.1528-1157.2002.26901.x.

[28] H. Stefan and F. H. Lopes da Silva, “Epileptic neuronal networks: methods of identification and clinical relevance,” *Front. Neurol.*, vol. 4, p. 8, 2013, doi: 10.3389/fneur.2013.00008.

[29] F. Wendling, P. Chauvel, A. Biraben, and F. Bartolomei, “From intracerebral EEG signals to brain connectivity: identification of epileptogenic networks in partial epilepsy,” *Front. Syst. Neurosci.*, vol. 4, p. 154, 2010, doi: 10.3389/fnsys.2010.00154.

[30] T. Bröhl, T. Rings, J. Pukropski, R. von Wrede, and K. Lehnertz, “The time-evolving epileptic brain network: concepts, definitions, accomplishments, perspectives,” *Front. Netw. Physiol.*, vol. 3, Jan. 2024, doi: 10.3389/fnetp.2023.1338864.

[31] L. Corona *et al.*, “Non-invasive mapping of epileptogenic networks predicts surgical outcome,” *Brain J. Neurol.*, vol. 146, no. 5, pp. 1916–1931, Dec. 2023, doi: 10.1093/brain/awac477.

[32] S. A. Weiss *et al.*, “Graph theoretical measures of fast ripples support the epileptic network hypothesis,” *Brain Commun.*, vol. 4, no. 3, p. fcac101, June 2022, doi: 10.1093/braincomms/fcac101.

[33] C. Stergiadis, D. M. Halliday, D. Kazis, and M. A. Klados, “Functional connectivity of interictal iEEG and the connectivity of high-frequency components in epilepsy,” *Brain Organoid Syst. Neurosci. J.*, vol. 1, pp. 3–12, Dec. 2023, doi: 10.1016/j.bosn.2023.11.001.

[34] S. Lagarde, C.-G. Bénar, F. Wendling, and F. Bartolomei, “Interictal Functional Connectivity in Focal Refractory Epilepsies Investigated by Intracranial EEG,” *Brain Connect.*, vol. 12, no. 10, pp. 850–869, Dec. 2022, doi: 10.1089/brain.2021.0190.

[35] G. Ntolkeras *et al.*, “Interictal EEG source connectivity to localize the epileptogenic zone in patients with drug-resistant epilepsy: A machine learning approach,” *Epilepsia*, vol. 65, no. 4, pp. 944–960, Apr. 2024, doi: 10.1111/epi.17898.

[36] S. E. Goodale *et al.*, “Resting-State SEEG May Help Localize Epileptogenic Brain Regions,” *Neurosurgery*, vol. 86, no. 6, pp. 792–801, June 2020, doi: 10.1093/neuros/nyz351.

[37] S. Rijal *et al.*, “Functional connectivity discriminates epileptogenic states and predicts surgical outcome in children with drug resistant epilepsy,” *Sci. Rep.*, vol. 13, no. 1, p. 9622, June 2023, doi: 10.1038/s41598-023-36551-0.

[38] P. Shah *et al.*, “High interictal connectivity within the resection zone is associated with favorable post-surgical outcomes in focal epilepsy patients,” *NeuroImage Clin.*, vol. 23, p. 101908, 2019, doi: 10.1016/j.nicl.2019.101908.

[39] M. Shen, L. Zhang, Y. Gong, L. Li, and X. Liu, “Epileptic Tissue Localization through Skewness-Based Functional Connectivity in the High-Frequency Band of Intracranial

EEG," *Bioeng. Basel Switz.*, vol. 10, no. 4, p. 461, Apr. 2023, doi: 10.3390/bioengineering10040461.

[40] F. Bartolomei, G. Bettus, C. J. Stam, and M. Guye, "Interictal network properties in mesial temporal lobe epilepsy: a graph theoretical study from intracerebral recordings," *Clin. Neurophysiol. Off. J. Int. Fed. Clin. Neurophysiol.*, vol. 124, no. 12, pp. 2345–2353, Dec. 2013, doi: 10.1016/j.clinph.2013.06.003.

[41] H. Jiang *et al.*, "Interictal SEEG Resting-State Connectivity Localizes the Seizure Onset Zone and Predicts Seizure Outcome," *Adv. Sci. Weinh. Baden-Wurtt. Ger.*, vol. 9, no. 18, p. e2200887, June 2022, doi: 10.1002/advs.202200887.

[42] G. Bettus *et al.*, "Enhanced EEG functional connectivity in mesial temporal lobe epilepsy," *Epilepsy Res.*, vol. 81, no. 1, pp. 58–68, Sept. 2008, doi: 10.1016/j.eplepsyres.2008.04.020.

[43] S. Karunakaran *et al.*, "The interictal mesial temporal lobe epilepsy network," *Epilepsia*, vol. 59, no. 1, pp. 244–258, 2018, doi: 10.1111/epi.13959.

[44] G. Salvatici, G. Pellegrino, M. Perulli, A. Danieli, P. Bonanni, and G. M. Duma, "Electroencephalography derived connectivity informing epilepsy surgical planning: Towards clinical applications and future perspectives," *NeuroImage Clin.*, vol. 44, p. 103703, Nov. 2024, doi: 10.1016/j.nicl.2024.103703.

[45] H. Spitzer *et al.*, "Interpretable surface-based detection of focal cortical dysplasias: a Multi-centre Epilepsy Lesion Detection study," *Brain*, vol. 145, no. 11, pp. 3859–3871, Nov. 2022, doi: 10.1093/brain/awac224.

[46] G. Susi *et al.*, "Interictal epileptic network hubs as a biomarker for automatic localization of the epileptogenic zone: a connectivity and machine learning based analysis of stereo-EEG," Jan. 26, 2024, *medRxiv*. doi: 10.1101/2024.01.25.24301659.

[47] N. Makaram *et al.*, "Deep Learning-Based Visual Complexity Analysis of Electroencephalography Time-Frequency Images: Can It Localize the Epileptogenic Zone in the Brain?," *Algorithms*, vol. 16, no. 12, p. 567, Dec. 2023, doi: 10.3390/a16120567.

[48] B. Wang *et al.*, "Decreased Complexity in Alzheimer's Disease: Resting-State fMRI Evidence of Brain Entropy Mapping," *Front. Aging Neurosci.*, vol. 9, Nov. 2017, doi: 10.3389/fnagi.2017.00378.

[49] D. Chang *et al.*, "Older is order: entropy reduction in cortical spontaneous activity marks healthy aging," *BMC Neurosci.*, vol. 25, no. 1, p. 74, Dec. 2024, doi: 10.1186/s12868-024-00916-6.

[50] V. M. Saenger, A. Ponce-Alvarez, M. Adhikari, P. Hagmann, G. Deco, and M. Corbetta, "Linking Entropy at Rest with the Underlying Structural Connectivity in the Healthy and Lesioned Brain," *Cereb. Cortex N. Y. N 1991*, vol. 28, no. 8, pp. 2948–2958, Aug. 2018,

doi: 10.1093/cercor/bhx176.

[51] D. Purves *et al.*, “Electrical Signals of Nerve Cells,” in *Neuroscience. 2nd edition*, Sinauer Associates, 2001. Accessed: Apr. 02, 2025. [Online]. Available: https://www.ncbi.nlm.nih.gov/books/NBK11053/

[52] E. B. Bromfield, J. E. Cavazos, and J. I. Sirven, “Basic Mechanisms Underlying Seizures and Epilepsy,” in *An Introduction to Epilepsy [Internet]*, American Epilepsy Society, 2006. Accessed: Apr. 01, 2025. [Online]. Available: https://www.ncbi.nlm.nih.gov/books/NBK2510/

[53] J. A. Cardin, “Inhibitory interneurons regulate temporal precision and correlations in cortical circuits,” *Trends Neurosci.*, vol. 41, no. 10, pp. 689–700, Oct. 2018, doi: 10.1016/j.tins.2018.07.015.

[54] M. Pradip Chauhan, M. Shalom Elsy Philip, M. D. S. Girish Chauhan, and M. Simmi Mehra, “The Anatomical Basis of Seizures,” *Exon Publ.*, pp. 15–23, Apr. 2022, doi: 10.36255/exon-publications-epilepsy-anatomical-basis.

[55] K. Łukawski, M. Andres-Mach, M. Czuczwar, J. J. Łuszczki, K. Kruszyński, and S. J. Czuczwar, “Mechanisms of epileptogenesis and preclinical approach to antiepileptogenic therapies,” *Pharmacol. Rep.*, vol. 70, no. 2, pp. 284–293, Apr. 2018, doi: 10.1016/j.pharep.2017.07.012.

[56] W. Löscher and C. Brandt, “Prevention or modification of epileptogenesis after brain insults: experimental approaches and translational research,” *Pharmacol. Rev.*, vol. 62, no. 4, pp. 668–700, Dec. 2010, doi: 10.1124/pr.110.003046.

[57] R. Mani, J. Pollard, and M. A. Dichter, “Human clinical trials in antiepileptogenesis,” *Neurosci. Lett.*, vol. 497, no. 3, pp. 251–256, June 2011, doi: 10.1016/j.neulet.2011.03.010.

[58] F. A. Lado and S. L. Moshé, “How do seizures stop?,” *Epilepsia*, vol. 49, no. 10, pp. 1651–1664, Oct. 2008, doi: 10.1111/j.1528-1167.2008.01669.x.

[59] F. Zubler, A. Steimer, H. Gast, and K. A. Schindler, “Seizure termination,” *Int. Rev. Neurobiol.*, vol. 114, pp. 187–207, 2014, doi: 10.1016/B978-0-12-418693-4.00008-X.

[60] “Types of Seizures.” Accessed: Mar. 10, 2025. [Online]. Available: https://www.hopkinsmedicine.org/health/conditions-and-diseases/epilepsy/types-of-seizures

[61] S. Beniczky *et al.*, “Updated classification of epileptic seizures: Position paper of the International League Against Epilepsy,” *Epilepsia*, vol. 66, no. 6, pp. 1804–1823, June 2025, doi: 10.1111/epi.18338.

[62] P. Ioannou *et al.*, “The burden of epilepsy and unmet need in people with focal seizures,” *Brain Behav.*, vol. 12, no. 9, p. e2589, Aug. 2022, doi: 10.1002/brb3.2589.

[63] J. Alvarez-Linera, “Temporal Lobe Epilepsy (TLE) and Neuroimaging,” in *Clinical*

Neuroradiology: The ESNR Textbook, F. Barkhof, H. R. Jäger, M. M. Thurnher, and À. Rovira, Eds., Cham: Springer International Publishing, 2019, pp. 891–914. doi: 10.1007/978-3-319-68536-6_50.

[64] C. S. Nayak and S. Bandyopadhyay, “Mesial Temporal Lobe Epilepsy,” in *StatPearls*, Treasure Island (FL): StatPearls Publishing, 2025. Accessed: Mar. 11, 2025. [Online]. Available: http://www.ncbi.nlm.nih.gov/books/NBK554432/

[65] S. Bauer and H. M. Hamer, “Chapter 15 - Extratemporal epilepsies,” in *Handbook of Clinical Neurology*, vol. 107, H. Stefan and W. H. Theodore, Eds., in Epilepsy, vol. 107. , Elsevier, 2012, pp. 241–256. doi: 10.1016/B978-0-444-52898-8.00015-X.

[66] S. F. Malamed and D. L. Orr, “Chapter 21 - Seizures,” in *Medical Emergencies in the Dental Office (Seventh Edition)*, S. F. Malamed and D. L. Orr, Eds., St. Louis (MO): Mosby, 2015, pp. 314–335. doi: 10.1016/B978-0-323-17122-9.00021-4.

[67] A. Trebuchon *et al.*, “The different patterns of seizure-induced aphasia in temporal lobe epilepsies,” *Epilepsy Behav.*, vol. 78, pp. 256–264, Jan. 2018, doi: 10.1016/j.yebeh.2017.08.022.

[68] R. S.-K. Chang, C. Y. W. Leung, C. C. A. Ho, and A. Yung, “Classifications of seizures and epilepsies, where are we? - A brief historical review and update,” *J. Formos. Med. Assoc. Taiwan Yi Zhi*, vol. 116, no. 10, pp. 736–741, Oct. 2017, doi: 10.1016/j.jfma.2017.06.001.

[69] C. P. Panayiotopoulos, “Epileptic seizures and their classification,” in *A Clinical Guide to Epileptic Syndromes and their Treatment*, C. P. Panayiotopoulos, Ed., London: Springer, 2010, pp. 21–63. doi: 10.1007/978-1-84628-644-5_2.

[70] R. S. Fisher *et al.*, “Operational classification of seizure types by the International League Against Epilepsy: Position Paper of the ILAE Commission for Classification and Terminology,” *Epilepsia*, vol. 58, no. 4, pp. 522–530, 2017, doi: 10.1111/epi.13670.

[71] J. Engel, “Epileptic Seizures,” in *Seizures and Epilepsy*, Jr. Engel Jerome, Ed., Oxford University Press, 2013, p. 0. doi: 10.1093/med/9780195328547.003.0006.

[72] E. K. St. Louis, W. E. Rosenfeld, and T. Bramley, “Antiepileptic Drug Monotherapy: The Initial Approach in Epilepsy Management,” *Curr. Neuropharmacol.*, vol. 7, no. 2, pp. 77–82, June 2009, doi: 10.2174/157015909788848866.

[73] S. Ghosh *et al.*, “Pharmacological and Therapeutic Approaches in the Treatment of Epilepsy,” *Biomedicines*, vol. 9, no. 5, Art. no. 5, May 2021, doi: 10.3390/biomedicines9050470.

[74] C. L. Gunasekera, J. I. Sirven, and A. M. Feyissa, “The evolution of antiseizure medication therapy selection in adults: Is artificial intelligence -assisted antiseizure medication selection ready for prime time?,” *J. Cent. Nerv. Syst. Dis.*, vol. 15, p. 11795735231209209, Oct. 2023, doi: 10.1177/11795735231209209.

[75] T. Tieu and M. Barker-Haliski, “Pharmacological Profiling of Conventional Antiseizure Medicines Against Acute Focal Seizures and Corneal Kindling Acquisition in Female Mice (Abstract ID: 161550),” *J. Pharmacol. Exp. Ther.*, vol. 392, no. 3, Mar. 2025, doi: 10.1016/j.jpet.2024.101329.

[76] T. Tomson, J. Zelano, Y. L. Dang, and P. Perucca, “The pharmacological treatment of epilepsy in adults,” *Epileptic. Disord.*, vol. 25, no. 5, pp. 649–669, 2023, doi: 10.1002/epd2.20093.

[77] K. Bolin, B. Patric, and T. Tomson, “Trends in Antiseizure Medication Initiation, Switch, or Termination in Patients With Newly Diagnosed Epilepsy: A Nationwide Study,” *Neurology*, vol. 103, no. 2, p. e209500, July 2024, doi: 10.1212/WNL.0000000000209500.

[78] J. A. French and E. Perucca, “Time to Start Calling Things by Their Own Names? The Case for Antiseizure Medicines,” *Epilepsy Curr.*, vol. 20, no. 2, pp. 69–72, Mar. 2020, doi: 10.1177/1535759720905516.

[79] J. D. Sánchez, J. Gómez-Carpintero, J. F. González, and J. C. Menéndez, “Twenty-first century antiepileptic drugs. An overview of their targets and synthetic approaches,” *Eur. J. Med. Chem.*, vol. 272, p. 116476, June 2024, doi: 10.1016/j.ejmech.2024.116476.

[80] B. Mesraoua, F. Brigo, S. Lattanzi, B. Abou-Khalil, H. A. Hail, and A. A. Asadi-Pooya, “Drug-resistant epilepsy: Definition, pathophysiology, and management,” *J. Neurol. Sci.*, vol. 452, Sept. 2023, doi: 10.1016/j.jns.2023.120766.

[81] L. Dalic and M. J. Cook, “Managing drug-resistant epilepsy: challenges and solutions,” *Neuropsychiatr. Dis. Treat.*, vol. 12, pp. 2605–2616, 2016, doi: 10.2147/NDT.S84852.

[82] P. Kwan and M. J. Brodie, “Refractory epilepsy: a progressive, intractable but preventable condition?,” *Seizure*, vol. 11, no. 2, pp. 77–84, Mar. 2002, doi: 10.1053/seiz.2002.0593.

[83] D. J. Dlugos, M. D. Sammel, B. L. Strom, and J. T. Farrar, “Response to first drug trial predicts outcome in childhood temporal lobe epilepsy,” *Neurology*, vol. 57, no. 12, pp. 2259–2264, Dec. 2001, doi: 10.1212/wnl.57.12.2259.

[84] L. Czornyj, J. Auzmendi, and A. Lazarowski, “Transporter hypothesis in pharmacoresistant epilepsies. Is it at the central or peripheral level?,” *Epilepsia Open*, vol. 7 Suppl 1, no. Suppl 1, pp. S34–S46, Aug. 2022, doi: 10.1002/epi4.12537.

[85] S. M. Sisodiya, W.-R. Lin, B. N. Harding, M. V. Squier, and M. Thom, “Drug resistance in epilepsy: expression of drug resistance proteins in common causes of refractory epilepsy,” *Brain J. Neurol.*, vol. 125, no. Pt 1, pp. 22–31, Jan. 2002, doi: 10.1093/brain/awf002.

[86] E. D. Bazhanova, A. A. Kozlov, and A. V. Litovchenko, “Mechanisms of Drug Resistance in the Pathogenesis of Epilepsy: Role of Neuroinflammation. A Literature Review,” *Brain*

Sci., vol. 11, no. 5, p. 663, Dec. 2021, doi: 10.3390/brainsci11050663.

[87] J. Engel, “What can we do for people with drug-resistant epilepsy? The 2016 Wartenberg Lecture,” *Neurology*, vol. 87, no. 23, pp. 2483–2489, Dec. 2016, doi: 10.1212/WNL.0000000000003407.

[88] R. Mohanraj, J. Norrie, L. J. Stephen, K. Kelly, N. Hitiris, and M. J. Brodie, “Mortality in adults with newly diagnosed and chronic epilepsy: a retrospective comparative study,” *Lancet Neurol.*, vol. 5, no. 6, pp. 481–487, June 2006, doi: 10.1016/S1474-4422(06)70448-3.

[89] C. Baumgartner, J. P. Koren, M. Britto-Arias, L. Zoche, and S. Pirker, “Presurgical epilepsy evaluation and epilepsy surgery,” *F1000Research*, vol. 8, p. F1000 Faculty Rev-1818, 2019, doi: 10.12688/f1000research.17714.1.

[90] B. C. Jobst and G. D. Cascino, “Resective epilepsy surgery for drug-resistant focal epilepsy: a review,” *JAMA*, vol. 313, no. 3, pp. 285–293, Jan. 2015, doi: 10.1001/jama.2014.17426.

[91] A. G. Baroumand *et al.*, “Automated EEG source imaging: A retrospective, blinded clinical validation study,” *Clin. Neurophysiol. Off. J. Int. Fed. Clin. Neurophysiol.*, vol. 129, no. 11, pp. 2403–2410, Nov. 2018, doi: 10.1016/j.clinph.2018.09.015.

[92] C. Papadelis and M. S. Perry, “Localizing the Epileptogenic Zone with Novel Biomarkers,” *Semin. Pediatr. Neurol.*, vol. 39, p. 100919, Oct. 2021, doi: 10.1016/j.spen.2021.100919.

[93] J. Parvizi and S. Kastner, “Promises and limitations of human intracranial electroencephalography,” *Nat. Neurosci.*, vol. 21, no. 4, pp. 474–483, Apr. 2018, doi: 10.1038/s41593-018-0108-2.

[94] L. Jehi *et al.*, “Comparative Effectiveness of Stereotactic Electroencephalography Versus Subdural Grids in Epilepsy Surgery,” *Ann. Neurol.*, vol. 90, no. 6, pp. 927–939, Dec. 2021, doi: 10.1002/ana.26238.

[95] N. Tandon *et al.*, “Analysis of Morbidity and Outcomes Associated With Use of Subdural Grids vs Stereoelectroencephalography in Patients With Intractable Epilepsy,” *JAMA Neurol.*, vol. 76, no. 6, pp. 672–681, June 2019, doi: 10.1001/jamaneurol.2019.0098.

[96] J. S. Duncan, G. P. Winston, M. J. Koepp, and S. Ourselin, “Brain imaging in the assessment for epilepsy surgery,” *Lancet Neurol.*, vol. 15, no. 4, pp. 420–433, Apr. 2016, doi: 10.1016/S1474-4422(15)00383-X.

[97] I. Wang *et al.*, “MRI essentials in epileptology: a review from the ILAE Imaging Taskforce,” *Epileptic. Disord.*, vol. 22, no. 4, pp. 421–437, 2020, doi: 10.1684/epd.2020.1174.

[98] S. J. Gascoigne *et al.*, “Incomplete resection of the intracranial electroencephalographic seizure onset zone is not associated with postsurgical outcomes,” *Epilepsia*, vol. 65, no.

9, pp. e163–e169, Sept. 2024, doi: 10.1111/epi.18061.

[99] M. Khan *et al.*, “Proportion of resected seizure onset zone contacts in pediatric stereo-EEG-guided resective surgery does not correlate with outcome,” *Clin. Neurophysiol.*, vol. 138, pp. 18–24, June 2022, doi: 10.1016/j.clinph.2022.03.012.

[100] C. Rummel *et al.*, “Resected Brain Tissue, Seizure Onset Zone and Quantitative EEG Measures: Towards Prediction of Post-Surgical Seizure Control,” *PLOS ONE*, vol. 10, no. 10, p. e0141023, Oct. 2015, doi: 10.1371/journal.pone.0141023.

[101] M. Pesce *et al.*, “WE-184. From ‘irritative zone’ to ‘irritative network’: a novel interictal estimate of the epileptogenic zone using invasive EEG,” *Clin. Neurophysiol.*, vol. 141, p. S86, Sept. 2022, doi: 10.1016/j.clinph.2022.07.228.

[102] G. Ramantani *et al.*, “Passive and active markers of cortical excitability in epilepsy,” *Epilepsia*, vol. 64, no. Suppl 3, pp. S25–S36, Dec. 2023, doi: 10.1111/epi.17578.

[103] J. Thomas *et al.*, “A Subpopulation of Spikes Predicts Successful Epilepsy Surgery Outcome,” *Ann. Neurol.*, vol. 93, no. 3, pp. 522–535, Mar. 2023, doi: 10.1002/ana.26548.

[104] E. D. Marsh *et al.*, “Interictal EEG spikes identify the region of seizure onset in some, but not all pediatric epilepsy patients,” *Epilepsia*, vol. 51, no. 4, pp. 592–601, Apr. 2010, doi: 10.1111/j.1528-1167.2009.02306.x.

[105] F. E. Abd El-Samie, T. N. Alotaiby, M. I. Khalid, S. A. Alshebeili, and S. A. Aldosari, “A Review of EEG and MEG Epileptic Spike Detection Algorithms,” *IEEE Access*, vol. 6, no. 8489863, pp. 60673–60688, 2018, doi: 10.1109/ACCESS.2018.2875487.

[106] S. B. Tomlinson, C. Bermudez, C. Conley, M. W. Brown, B. E. Porter, and E. D. Marsh, “Spatiotemporal Mapping of Interictal Spike Propagation: A Novel Methodology Applied to Pediatric Intracranial EEG Recordings,” *Front. Neurol.*, vol. 7, p. 229, 2016, doi: 10.3389/fneur.2016.00229.

[107] A. Hufnagel, M. Dümpelmann, J. Zentner, O. Schijns, and C. E. Elger, “Clinical Relevance of Quantified Intracranial Interictal Spike Activity in Presurgical Evaluation of Epilepsy,” *Epilepsia*, vol. 41, no. 4, pp. 467–478, 2000, doi: 10.1111/j.1528-1157.2000.tb00191.x.

[108] Y. Lai, W. van Drongelen, K. Hecox, D. Frim, M. Kohrman, and B. He, “Cortical activation mapping of epileptiform activity derived from interictal ECoG spikes,” *Epilepsia*, vol. 48, no. 2, pp. 305–314, Feb. 2007, doi: 10.1111/j.1528-1167.2006.00936.x.

[109] G. Alarcon *et al.*, “Origin and propagation of interictal discharges in the acute electrocorticogram. Implications for pathophysiology and surgical treatment of temporal lobe epilepsy,” *Brain J. Neurol.*, vol. 120 (Pt 12), pp. 2259–2282, Dec. 1997, doi: 10.1093/brain/120.12.2259.

[110] W. Zweiphenning *et al.*, “Intraoperative electrocorticography using high-frequency

oscillations or spikes to tailor epilepsy surgery in the Netherlands (the HFO trial): a randomised, single-blind, adaptive non-inferiority trial," *Lancet Neurol.*, vol. 21, no. 11, pp. 982–993, Nov. 2022, doi: 10.1016/S1474-4422(22)00311-8.

[111] W. Shi *et al.*, "Spike ripples localize the epileptogenic zone best: an international intracranial study," *Brain J. Neurol.*, vol. 147, no. 7, pp. 2496–2506, July 2024, doi: 10.1093/brain/awae037.

[112] L. Fabbri *et al.*, "Spikes on ripples are better interictal biomarkers of epilepsy than spikes or ripples," *Brain Commun.*, vol. 7, no. 1, p. fcaf056, Feb. 2025, doi: 10.1093/braincomms/fcaf056.

[113] A. Bragin, J. Engel, C. L. Wilson, I. Fried, and G. Buzsáki, "High-frequency oscillations in human brain," *Hippocampus*, vol. 9, no. 2, pp. 137–142, 1999, doi: 10.1002/(SICI)1098-1063(1999)9:2%3C137::AID-HIPO5%3E3.0.CO;2-0.

[114] M. A. van 't Klooster *et al.*, "Residual fast ripples in the intraoperative corticogram predict epilepsy surgery outcome," *Neurology*, vol. 85, no. 2, pp. 120–128, July 2015, doi: 10.1212/WNL.0000000000001727.

[115] K. Remakanthakurup Sindhu, R. Staba, and B. A. Lopour, "Trends in the use of automated algorithms for the detection of high-frequency oscillations associated with human epilepsy," *Epilepsia*, vol. 61, no. 8, pp. 1553–1569, 2020, doi: 10.1111/epi.16622.

[116] L. Noorlag, N. E. C. van Klink, K. Kobayashi, J. Gotman, K. P. J. Braun, and M. Zijlmans, "High-frequency oscillations in scalp EEG: A systematic review of methodological choices and clinical findings," *Clin. Neurophysiol.*, vol. 137, pp. 46–58, May 2022, doi: 10.1016/j.clinph.2021.12.017.

[117] J. Jacobs, R. Zelmann, J. Jirsch, R. Chander, C.-É. C. F. Dubeau, and J. Gotman, "High frequency oscillations (80–500 Hz) in the preictal period in patients with focal seizures," *Epilepsia*, vol. 50, no. 7, pp. 1780–1792, 2009, doi: 10.1111/j.1528-1167.2009.02067.x.

[118] M. Zijlmans *et al.*, "How to record high-frequency oscillations in epilepsy: A practical guideline," *Epilepsia*, vol. 58, no. 8, pp. 1305–1315, Aug. 2017, doi: 10.1111/epi.13814.

[119] C. Cepeda *et al.*, "Pathological high frequency oscillations associate with increased GABA synaptic activity in pediatric epilepsy surgery patients," *Neurobiol. Dis.*, vol. 134, p. 104618, Feb. 2020, doi: 10.1016/j.nbd.2019.104618.

[120] A. Bragin, J. Engel, and R. J. Staba, "High-frequency oscillations in epileptic brain," *Curr. Opin. Neurol.*, vol. 23, no. 2, pp. 151–156, Apr. 2010, doi: 10.1097/WCO.0b013e3283373ac8.

[121] P. Jiruska *et al.*, "Update on the mechanisms and roles of high-frequency oscillations in seizures and epileptic disorders," *Epilepsia*, vol. 58, no. 8, pp. 1330–1339, Aug. 2017, doi: 10.1111/epi.13830.

[122] M. Le Van Quyen, A. Bragin, R. Staba, B. Crépon, C. L. Wilson, and J. Engel, “Cell type-specific firing during ripple oscillations in the hippocampal formation of humans,” *J. Neurosci. Off. J. Soc. Neurosci.*, vol. 28, no. 24, pp. 6104–6110, June 2008, doi: 10.1523/JNEUROSCI.0437-08.2008.

[123] J. R. Cho *et al.*, “Resection of individually identified high-rate high-frequency oscillations region is associated with favorable outcome in neocortical epilepsy,” *Epilepsia*, vol. 55, no. 11, pp. 1872–1883, 2014, doi: 10.1111/epi.12808.

[124] Y. Höller *et al.*, “High-frequency oscillations in epilepsy and surgical outcome. A meta-analysis,” *Front. Hum. Neurosci.*, vol. 9, p. 574, Oct. 2015, doi: 10.3389/fnhum.2015.00574.

[125] V. Dimakopoulos *et al.*, “Multicentre analysis of seizure outcome predicted by removal of high frequency oscillations,” *Brain J. Neurol.*, p. awae361, Nov. 2024, doi: 10.1093/brain/awae361.

[126] Z. Wang, J. Guo, M. van ’t Klooster, S. Hoogteijling, J. Jacobs, and M. Zijlmans, “Prognostic Value of Complete Resection of the High-Frequency Oscillation Area in Intracranial EEG,” *Neurology*, vol. 102, no. 9, p. e209216, May 2024, doi: 10.1212/WNL.0000000000209216.

[127] J. Y. Wu, R. Sankar, J. T. Lerner, J. H. Matsumoto, H. V. Vinters, and G. W. Mathern, “Removing interictal fast ripples on electrocorticography linked with seizure freedom in children,” *Neurology*, vol. 75, no. 19, pp. 1686–1694, Nov. 2010, doi: 10.1212/WNL.0b013e3181fc27d0.

[128] Z. Chen, M. I. Maturana, A. N. Burkitt, M. J. Cook, and D. B. Grayden, “High-Frequency Oscillations in Epilepsy: What Have We Learned and What Needs to be Addressed,” *Neurology*, vol. 96, no. 9, pp. 439–448, Mar. 2021, doi: 10.1212/WNL.0000000000011465.

[129] J. Jacobs *et al.*, “Removing high-frequency oscillations: A prospective multicenter study on seizure outcome,” *Neurology*, vol. 91, no. 11, pp. e1040–e1052, Sept. 2018, doi: 10.1212/WNL.0000000000006158.

[130] G. Buzsáki and F. L. da Silva, “High frequency oscillations in the intact brain,” *Prog. Neurobiol.*, vol. 98, no. 3, pp. 241–249, Sept. 2012, doi: 10.1016/j.pneurobio.2012.02.004.

[131] G. Buzsáki, Z. Horváth, R. Urioste, J. Hetke, and K. Wise, “High-frequency network oscillation in the hippocampus,” *Science*, vol. 256, no. 5059, pp. 1025–1027, May 1992, doi: 10.1126/science.1589772.

[132] M. T. Kucewicz *et al.*, “High frequency oscillations are associated with cognitive processing in human recognition memory,” *Brain*, vol. 137, no. 8, pp. 2231–2244, Aug. 2014, doi: 10.1093/brain/awu149.

[133] N. E. Crone, A. Korzeniewska, and P. J. Franaszczuk, “Cortical gamma responses: Searching high and low,” *Int. J. Psychophysiol.*, vol. 79, no. 1, pp. 9–15, Jan. 2011, doi: 10.1016/j.ijpsycho.2010.10.013.

[134] J. Cimbalnik *et al.*, “Physiological and pathological high frequency oscillations in focal epilepsy,” *Ann. Clin. Transl. Neurol.*, vol. 5, no. 9, pp. 1062–1076, Aug. 2018, doi: 10.1002/acn3.618.

[135] L. Fabbri *et al.*, “Noninvasive classification of physiological and pathological high frequency oscillations in children,” *Brain Commun.*, vol. 7, no. 3, p. fcaf170, June 2025, doi: 10.1093/braincomms/fcaf170.

[136] N. von Ellenrieder, B. Frauscher, F. Dubeau, and J. Gotman, “Interaction with slow waves during sleep improves discrimination of physiologic and pathologic high-frequency oscillations (80-500 Hz),” *Epilepsia*, vol. 57, no. 6, pp. 869–878, June 2016, doi: 10.1111/epi.13380.

[137] A. Matsumoto *et al.*, “Pathological and physiological high-frequency oscillations in focal human epilepsy,” *J. Neurophysiol.*, vol. 110, no. 8, pp. 1958–1964, Oct. 2013, doi: 10.1152/jn.00341.2013.

[138] K. Charupanit, I. Sen-Gupta, J. J. Lin, and B. A. Lopour, “Amplitude of high frequency oscillations as a biomarker of the seizure onset zone,” *Clin. Neurophysiol. Off. J. Int. Fed. Clin. Neurophysiol.*, vol. 131, no. 11, pp. 2542–2550, Nov. 2020, doi: 10.1016/j.clinph.2020.07.021.

[139] R. Alkawadri *et al.*, “The spatial and signal characteristics of physiologic high frequency oscillations,” *Epilepsia*, vol. 55, no. 12, pp. 1986–1995, 2014, doi: 10.1111/epi.12851.

[140] B. Frauscher *et al.*, “High-frequency oscillations: The state of clinical research,” *Epilepsia*, vol. 58, no. 8, pp. 1316–1329, Aug. 2017, doi: 10.1111/epi.13829.

[141] N. Sciaraffa, M. A. Klados, G. Borghini, G. Di Flumeri, F. Babiloni, and P. Aricò, “Double-Step Machine Learning Based Procedure for HFOs Detection and Classification,” *Brain Sci.*, vol. 10, no. 4, Art. no. 4, Apr. 2020, doi: 10.3390/brainsci10040220.

[142] A. Thomschewski *et al.*, “Automatic vs. Manual Detection of High Frequency Oscillations in Intracranial Recordings From the Human Temporal Lobe,” *Front. Neurol.*, vol. 11, Oct. 2020, doi: 10.3389/fneur.2020.563577.

[143] L. R. Quitadamo, R. Mai, F. Gozzo, V. Pelliccia, F. Cardinale, and S. Seri, “Kurtosis-Based Detection of Intracranial High-Frequency Oscillations for the Identification of the Seizure Onset Zone,” *Int. J. Neural Syst.*, vol. 28, no. 07, p. 1850001, Sept. 2018, doi: 10.1142/S0129065718500016.

[144] S. M. Wong *et al.*, “Detection of high-frequency oscillations in

electroencephalography: A scoping review and an adaptable open-source framework," *Seizure*, vol. 84, pp. 23–33, Jan. 2021, doi: 10.1016/j.seizure.2020.11.009.

[145] S. V. Gliske, Z. T. Irwin, K. A. Davis, K. Sahaya, C. Chestek, and W. C. Stacey, "Universal automated high frequency oscillation detector for real-time, long term EEG," *Clin. Neurophysiol. Off. J. Int. Fed. Clin. Neurophysiol.*, vol. 127, no. 2, pp. 1057–1066, Feb. 2016, doi: 10.1016/j.clinph.2015.07.016.

[146] G. Birot, A. Kachenoura, L. Albera, C. Bénar, and F. Wendling, "Automatic detection of fast ripples," *J. Neurosci. Methods*, vol. 213, no. 2, pp. 236–249, Mar. 2013, doi: 10.1016/j.jneumeth.2012.12.013.

[147] M. Dümpelmann, J. Jacobs, K. Kerber, and A. Schulze-Bonhage, "Automatic 80-250Hz 'ripple' high frequency oscillation detection in invasive subdural grid and strip recordings in epilepsy by a radial basis function neural network," *Clin. Neurophysiol. Off. J. Int. Fed. Clin. Neurophysiol.*, vol. 123, no. 9, pp. 1721–1731, Sept. 2012, doi: 10.1016/j.clinph.2012.02.072.

[148] M. Pail *et al.*, "Intracerebrally recorded high frequency oscillations: simple visual assessment versus automated detection," *Clin. Neurophysiol. Off. J. Int. Fed. Clin. Neurophysiol.*, vol. 124, no. 10, pp. 1935–1942, Oct. 2013, doi: 10.1016/j.clinph.2013.03.032.

[149] S. Liu *et al.*, "Detection of high frequency oscillations in epilepsy with k-means clustering method," *Int. IEEEEMBS Conf. Neural Eng. NER*, vol. 2015, pp. 934–937, July 2015, doi: 10.1109/NER.2015.7146779.

[150] K. Charupanit and B. A. Lopour, "A Simple Statistical Method for the Automatic Detection of Ripples in Human Intracranial EEG," *Brain Topogr.*, vol. 30, no. 6, pp. 724–738, Nov. 2017, doi: 10.1007/s10548-017-0579-6.

[151] R. Zuo *et al.*, "Automated Detection of High-Frequency Oscillations in Epilepsy Based on a Convolutional Neural Network," *Front. Comput. Neurosci.*, vol. 13, 2019, Accessed: Jan. 18, 2022. [Online]. Available: https://www.frontiersin.org/article/10.3389/fncom.2019.00006

[152] M. Wu, T. Wan, X. Wan, Y. Du, and J. She, "Fast, Accurate Localization of Epileptic Seizure Onset Zones Based on Detection of High-Frequency Oscillations Using Improved Wavelet Transform and Matching Pursuit Methods," *Neural Comput.*, vol. 29, no. 1, pp. 194–219, Jan. 2017, doi: 10.1162/NECO_a_00899.

[153] S. Liu *et al.*, "Exploring the time-frequency content of high frequency oscillations for automated identification of seizure onset zone in epilepsy," *J. Neural Eng.*, vol. 13, no. 2, p. 026026, Apr. 2016, doi: 10.1088/1741-2560/13/2/026026.

[154] T. Fedele *et al.*, "Automatic detection of high frequency oscillations during epilepsy surgery predicts seizure outcome," *Clin. Neurophysiol. Off. J. Int. Fed. Clin.*

Neurophysiol., vol. 127, no. 9, pp. 3066–3074, Sept. 2016, doi: 10.1016/j.clinph.2016.06.009.

[155] C. Haegelen *et al.*, “High-frequency oscillations, extent of surgical resection, and surgical outcome in drug-resistant focal epilepsy,” *Epilepsia*, vol. 54, no. 5, pp. 848–857, 2013, doi: 10.1111/epi.12075.

[156] U. Malinowska, G. K. Bergey, J. Harezlak, and C. C. Jouny, “Identification of seizure onset zone and preictal state based on characteristics of high frequency oscillations,” *Clin. Neurophysiol. Off. J. Int. Fed. Clin. Neurophysiol.*, vol. 126, no. 8, pp. 1505–1513, Aug. 2015, doi: 10.1016/j.clinph.2014.11.007.

[157] K. Charupanit, I. Sen-Gupta, J. J. Lin, and B. A. Lopour, “Detection of anomalous high-frequency events in human intracranial EEG,” *Epilepsia Open*, vol. 5, no. 2, pp. 263–273, June 2020, doi: 10.1002/epi4.12397.

[158] M. Pail, P. Řehulka, J. Cimbálník, I. Doležalová, J. Chrastina, and M. Brázdil, “Frequency-independent characteristics of high-frequency oscillations in epileptic and non-epileptic regions,” *Clin. Neurophysiol. Off. J. Int. Fed. Clin. Neurophysiol.*, vol. 128, no. 1, pp. 106–114, Jan. 2017, doi: 10.1016/j.clinph.2016.10.011.

[159] A. H. Mooij, B. Frauscher, J. Gotman, and G. J. M. Huiskamp, “A skew-based method for identifying intracranial EEG channels with epileptic activity without detecting spikes, ripples, or fast ripples,” *Clin. Neurophysiol. Off. J. Int. Fed. Clin. Neurophysiol.*, vol. 131, no. 1, pp. 183–192, Jan. 2020, doi: 10.1016/j.clinph.2019.10.025.

[160] S. A. Weiss *et al.*, “Ictal high frequency oscillations distinguish two types of seizure territories in humans,” *Brain J. Neurol.*, vol. 136, no. Pt 12, pp. 3796–3808, Dec. 2013, doi: 10.1093/brain/awt276.

[161] G. M. Ibrahim *et al.*, “Dynamic modulation of epileptic high frequency oscillations by the phase of slower cortical rhythms,” *Exp. Neurol.*, vol. 251, pp. 30–38, Jan. 2014, doi: 10.1016/j.expneurol.2013.10.019.

[162] H. Motoi *et al.*, “Quantitative analysis of intracranial electrocorticography signals using the concept of statistical parametric mapping,” *Sci. Rep.*, vol. 9, no. 1, p. 17385, Nov. 2019, doi: 10.1038/s41598-019-53749-3.

[163] F. Bartolomei *et al.*, “Defining epileptogenic networks: Contribution of SEEG and signal analysis,” *Epilepsia*, vol. 58, no. 7, pp. 1131–1147, 2017, doi: 10.1111/epi.13791.

[164] J. Bancaud and J. Talairach, *La stéréo-électroencéphalographie dans l’épilepsie: informations neurophysiopathologiques apportées par l’investigation fonctionnelle stéreotaxique*. in Travail du service de neurochirurgie fonctionnelle de l’hôpital Sainte-Anne. Paris: Masson, 1965.

[165] F. Bartolomei *et al.*, “Entorhinal cortex involvement in human mesial temporal lobe epilepsy: an electrophysiologic and volumetric study,” *Epilepsia*, vol. 46, no. 5, pp.

677–687, Dec. 2005, doi: 10.1111/j.1528-1167.2005.43804.x.

[166] V. K. Jirsa *et al.*, “The Virtual Epileptic Patient: Individualized whole-brain models of epilepsy spread,” *NeuroImage*, vol. 145, no. Pt B, pp. 377–388, Jan. 2017, doi: 10.1016/j.neuroimage.2016.04.049.

[167] T. Proix, F. Bartolomei, P. Chauvel, C. Bernard, and V. K. Jirsa, “Permittivity coupling across brain regions determines seizure recruitment in partial epilepsy,” *J. Neurosci. Off. J. Soc. Neurosci.*, vol. 34, no. 45, pp. 15009–15021, Nov. 2014, doi: 10.1523/JNEUROSCI.1570-14.2014.

[168] M. Guye *et al.*, “The role of corticothalamic coupling in human temporal lobe epilepsy,” *Brain J. Neurol.*, vol. 129, no. Pt 7, pp. 1917–1928, July 2006, doi: 10.1093/brain/awl151.

[169] S. C. Ponten, F. Bartolomei, and C. J. Stam, “Small-world networks and epilepsy: graph theoretical analysis of intracerebrally recorded mesial temporal lobe seizures,” *Clin. Neurophysiol. Off. J. Int. Fed. Clin. Neurophysiol.*, vol. 118, no. 4, pp. 918–927, Apr. 2007, doi: 10.1016/j.clinph.2006.12.002.

[170] G. Varotto, L. Tassi, S. Franceschetti, R. Spreafico, and F. Panzica, “Epileptogenic networks of type II focal cortical dysplasia: a stereo-EEG study,” *NeuroImage*, vol. 61, no. 3, pp. 591–598, July 2012, doi: 10.1016/j.neuroimage.2012.03.090.

[171] P. Jiruska, M. de Curtis, J. G. R. Jefferys, C. A. Schevon, S. J. Schiff, and K. Schindler, “Synchronization and desynchronization in epilepsy: controversies and hypotheses,” *J. Physiol.*, vol. 591, no. 4, pp. 787–797, Feb. 2013, doi: 10.1113/jphysiol.2012.239590.

[172] K. Schindler, H. Leung, C. E. Elger, and K. Lehnertz, “Assessing seizure dynamics by analysing the correlation structure of multichannel intracranial EEG,” *Brain J. Neurol.*, vol. 130, no. Pt 1, pp. 65–77, Jan. 2007, doi: 10.1093/brain/awl304.

[173] J. Gotman and V. Levtova, “Amygdala-hippocampus relationships in temporal lobe seizures: a phase-coherence study,” *Epilepsy Res.*, vol. 25, no. 1, pp. 51–57, Sept. 1996, doi: 10.1016/0920-1211(96)00021-6.

[174] S. Courtens, B. Colombet, A. Trébuchon, A. Brovelli, F. Bartolomei, and C. G. Bénar, “Graph Measures of Node Strength for Characterizing Preictal Synchrony in Partial Epilepsy,” *Brain Connect.*, vol. 6, no. 7, pp. 530–539, Sept. 2016, doi: 10.1089/brain.2015.0397.

[175] P. van Mierlo *et al.*, “Ictal-onset localization through connectivity analysis of intracranial EEG signals in patients with refractory epilepsy,” *Epilepsia*, vol. 54, no. 8, pp. 1409–1418, Aug. 2013, doi: 10.1111/epi.12206.

[176] J. S. Barlow and M. A. B. Brazier, “A note on a correlator for electroencephalographic work,” *Electroencephalogr. Clin. Neurophysiol.*, vol. 6, pp. 321–325, Jan. 1954, doi:

10.1016/0013-4694(54)90036-X.

[177] J. Gotman, “Measurement of small time differences between EEG channels: Method and application to epileptic seizure propagation,” *Electroencephalogr. Clin. Neurophysiol.*, vol. 56, no. 5, pp. 501–514, Nov. 1983, doi: 10.1016/0013-4694(83)90235-3.

[178] K. Ansari-Asl, L. Senhadji, J.-J. Bellanger, and F. Wendling, “Quantitative evaluation of linear and nonlinear methods characterizing interdependencies between brain signals,” *Phys. Rev. E Stat. Nonlin. Soft Matter Phys.*, vol. 74, no. 3 Pt 1, p. 31916, Sept. 2006, doi: 10.1103/PhysRevE.74.031916.

[179] H. E. Wang, C. G. Bénar, P. P. Quilichini, K. J. Friston, V. K. Jirsa, and C. Bernard, “A systematic framework for functional connectivity measures,” *Front. Neurosci.*, vol. 8, p. 405, 2014, doi: 10.3389/fnins.2014.00405.

[180] B. He *et al.*, “Electrophysiological Brain Connectivity: Theory and Implementation,” *IEEE Trans. Biomed. Eng.*, p. 10.1109/TBME.2019.2913928, May 2019, doi: 10.1109/TBME.2019.2913928.

[181] F. Bartolomei *et al.*, “Seizures of temporal lobe epilepsy: identification of subtypes by coherence analysis using stereo-electro-encephalography,” *Clin. Neurophysiol. Off. J. Int. Fed. Clin. Neurophysiol.*, vol. 110, no. 10, pp. 1741–1754, Oct. 1999, doi: 10.1016/s1388-2457(99)00107-8.

[182] A. M. Bastos and J.-M. Schoffelen, “A Tutorial Review of Functional Connectivity Analysis Methods and Their Interpretational Pitfalls,” *Front. Syst. Neurosci.*, vol. 9, p. 175, 2015, doi: 10.3389/fnsys.2015.00175.

[183] S. Lagarde *et al.*, “Interictal stereotactic-EEG functional connectivity in refractory focal epilepsies,” *Brain J. Neurol.*, vol. 141, no. 10, pp. 2966–2980, Oct. 2018, doi: 10.1093/brain/awy214.

[184] M. A. Kramer, U. T. Eden, K. Q. Lepage, E. D. Kolaczyk, M. T. Bianchi, and S. S. Cash, “Emergence of persistent networks in long-term intracranial EEG recordings,” *J. Neurosci. Off. J. Soc. Neurosci.*, vol. 31, no. 44, pp. 15757–15767, Nov. 2011, doi: 10.1523/JNEUROSCI.2287-11.2011.

[185] E. C. Conrad *et al.*, “The sensitivity of network statistics to incomplete electrode sampling on intracranial EEG,” *Netw. Neurosci.*, vol. 4, no. 2, pp. 484–506, May 2020, doi: 10.1162/netn_a_00131.

[186] M. Müller, K. Schindler, M. Goodfellow, C. Pollo, C. Rummel, and A. Steimer, “Evaluating resective surgery targets in epilepsy patients: A comparison of quantitative EEG methods,” *J. Neurosci. Methods*, vol. 305, pp. 54–66, July 2018, doi: 10.1016/j.jneumeth.2018.04.021.

[187] J. M. Bernabei *et al.*, “Electrocorticography and stereo EEG provide distinct

measures of brain connectivity: implications for network models," *Brain Commun.*, vol. 3, no. 3, p. fcab156, 2021, doi: 10.1093/braincomms/fcab156.

[188] V. L. Towle *et al.*, "Identification of the sensory/motor area and pathologic regions using ECoG coherence," *Electroencephalogr. Clin. Neurophysiol.*, vol. 106, no. 1, pp. 30–39, Jan. 1998, doi: 10.1016/s0013-4694(97)00082-5.

[189] J. Arnhold, P. Grassberger, K. Lehnertz, and C. E. Elger, "A robust method for detecting interdependences: application to intracranially recorded EEG," *Phys. Nonlinear Phenom.*, vol. 134, no. 4, pp. 419–430, Dec. 1999, doi: 10.1016/S0167-2789(99)00140-2.

[190] F. Mormann, K. Lehnertz, P. David, and C. E. Elger, "Mean phase coherence as a measure for phase synchronization and its application to the EEG of epilepsy patients," *Phys. Nonlinear Phenom.*, vol. 144, pp. 358–369, Oct. 2000, doi: 10.1016/S0167-2789(00)00087-7.

[191] C. Schevon *et al.*, "Cortical Abnormalities in Epilepsy Revealed by Local EEG Synchrony," *NeuroImage*, vol. 35, no. 1, pp. 140–148, Mar. 2007, doi: 10.1016/j.neuroimage.2006.11.009.

[192] J. Dauwels, E. Eskandar, and S. Cash, "Localization of seizure onset area from intracranial non-seizure EEG by exploiting locally enhanced synchrony," *Annu. Int. Conf. IEEE Eng. Med. Biol. Soc. IEEE Eng. Med. Biol. Soc. Annu. Int. Conf.*, vol. 2009, pp. 2180–2183, 2009, doi: 10.1109/IEMBS.2009.5332447.

[193] G. J. Ortega, L. Menendez de la Prida, R. G. Sola, and J. Pastor, "Synchronization clusters of interictal activity in the lateral temporal cortex of epileptic patients: intraoperative electrocorticographic analysis," *Epilepsia*, vol. 49, no. 2, pp. 269–280, Feb. 2008, doi: 10.1111/j.1528-1167.2007.01266.x.

[194] C. P. Warren, S. Hu, M. Stead, B. H. Brinkmann, M. R. Bower, and G. A. Worrell, "Synchrony in Normal and Focal Epileptic Brain: The Seizure Onset Zone is Functionally Disconnected," *J. Neurophysiol.*, vol. 104, no. 6, pp. 3530–3539, Dec. 2010, doi: 10.1152/jn.00368.2010.

[195] G. Bettus *et al.*, "Interictal functional connectivity of human epileptic networks assessed by intracerebral EEG and BOLD signal fluctuations," *PloS One*, vol. 6, no. 5, p. e20071, 2011, doi: 10.1371/journal.pone.0020071.

[196] C. Wilke, G. Worrell, and B. He, "Graph analysis of epileptogenic networks in human partial epilepsy," *Epilepsia*, vol. 52, no. 1, pp. 84–93, Jan. 2011, doi: 10.1111/j.1528-1167.2010.02785.x.

[197] E. van Diessen *et al.*, "Are high frequency oscillations associated with altered network topology in partial epilepsy?," *NeuroImage*, vol. 82, pp. 564–573, Nov. 2013, doi: 10.1016/j.neuroimage.2013.06.031.

[198] S. Narasimhan *et al.*, “Seizure-onset regions demonstrate high inward directed connectivity during resting-state: An SEEG study in focal epilepsy,” *Epilepsia*, vol. 61, no. 11, pp. 2534–2544, Nov. 2020, doi: 10.1111/epi.16686.

[199] D. L. Paulo *et al.*, “SEEG Functional Connectivity Measures to Identify Epileptogenic Zones: Stability, Medication Influence, and Recording Condition,” *Neurology*, vol. 98, no. 20, pp. e2060–e2072, Dec. 2022, doi: 10.1212/WNL.0000000000200386.

[200] E.-H. Park and J. R. Madsen, “Granger Causality Analysis of Interictal iEEG Predicts Seizure Focus and Ultimate Resection,” *Neurosurgery*, vol. 82, no. 1, pp. 99–109, Jan. 2018, doi: 10.1093/neuros/nyx195.

[201] A. R. Antony *et al.*, “Functional connectivity estimated from intracranial EEG predicts surgical outcome in intractable temporal lobe epilepsy,” *PloS One*, vol. 8, no. 10, p. e77916, 2013, doi: 10.1371/journal.pone.0077916.

[202] B. T. Grobelny, D. London, T. C. Hill, E. North, P. Dugan, and W. K. Doyle, “Betweenness centrality of intracranial electroencephalography networks and surgical epilepsy outcome,” *Clin. Neurophysiol. Off. J. Int. Fed. Clin. Neurophysiol.*, vol. 129, no. 9, pp. 1804–1812, Sept. 2018, doi: 10.1016/j.clinph.2018.02.135.

[203] W. J. E. M. Zweiphenning *et al.*, “Increased gamma and decreased fast ripple connections of epileptic tissue: A high-frequency directed network approach,” *Epilepsia*, vol. 60, no. 9, pp. 1908–1920, Sept. 2019, doi: 10.1111/epi.16296.

[204] C. Stergiadis, D. Kazis, and M. A. Klados, “Epileptic tissue localization using graph-based networks in the high frequency oscillation range of intracranial electroencephalography,” *Seizure - Eur. J. Epilepsy*, vol. 117, pp. 28–35, Apr. 2024, doi: 10.1016/j.seizure.2024.01.015.

[205] T. Fedele *et al.*, “High frequency oscillations detected in the intracranial EEG of epilepsy patients during interictal sleep, patients’ electrode location and outcome of epilepsy surgery.” CRCNS.org, p. 87 GB, compressed, 2017. doi: 10.6080/K06Q1VD5.

[206] T. Fedele *et al.*, “Resection of high frequency oscillations predicts seizure outcome in the individual patient,” *Sci. Rep.*, vol. 7, no. 1, Art. no. 1, Oct. 2017, doi: 10.1038/s41598-017-13064-1.

[207] H. G. Wieser *et al.*, “ILAE Commission Report. Proposal for a new classification of outcome with respect to epileptic seizures following epilepsy surgery,” *Epilepsia*, vol. 42, no. 2, pp. 282–286, Feb. 2001.

[208] F. Tadel, S. Baillet, J. C. Mosher, D. Pantazis, and R. M. Leahy, “Brainstorm: a user-friendly application for MEG/EEG analysis,” *Comput. Intell. Neurosci.*, vol. 2011, p. 879716, 2011, doi: 10.1155/2011/879716.

[209] B. Frauscher *et al.*, “Learn how to interpret and use intracranial EEG findings,” *Epileptic. Disord.*, vol. 26, no. 1, pp. 1–59, 2024, doi: 10.1002/epd2.20190.

[210] S. Ramaraju *et al.*, “Removal of Interictal MEG-Derived Network Hubs Is Associated With Postoperative Seizure Freedom,” *Front. Neurol.*, vol. 11, p. 563847, 2020, doi: 10.3389/fneur.2020.563847.

[211] D. J. Englot *et al.*, “Global and regional functional connectivity maps of neural oscillations in focal epilepsy,” *Brain J. Neurol.*, vol. 138, no. Pt 8, pp. 2249–2262, Aug. 2015, doi: 10.1093/brain/awv130.

[212] A. Zamm, S. Debener, A.-K. Bauer, M. Bleichner, A. Demos, and C. Palmer, “Amplitude envelope correlations measure synchronous cortical oscillations in performing musicians,” *Ann. N. Y. Acad. Sci.*, vol. 1423, May 2018, doi: 10.1111/nyas.13738.

[213] D. M. Halliday, “Nonparametric directionality measures for time series and point process data,” *J. Integr. Neurosci.*, vol. 14, no. 2, pp. 253–277, June 2015, doi: 10.1142/S0219635215300127.

[214] M. J. Kamiński and K. J. Blinowska, “A new method of the description of the information flow in the brain structures,” *Biol. Cybern.*, vol. 65, no. 3, pp. 203–210, 1991, doi: 10.1007/BF00198091.

[215] A. Bruns, R. Eckhorn, H. Jokeit, and A. Ebner, “Amplitude envelope correlation detects coupling among incoherent brain signals,” *Neuroreport*, vol. 11, no. 7, pp. 1509–1514, Dec. 2000.

[216] G. Iandolo *et al.*, “Changes in the Functional Brain Network of Children Undergoing Repeated Epilepsy Surgery: An EEG Source Connectivity Study,” *Diagn. Basel Switz.*, vol. 11, no. 7, p. 1234, July 2021, doi: 10.3390/diagnostics11071234.

[217] Ü. Aydin *et al.*, “Magnetoencephalography resting state connectivity patterns as indicatives of surgical outcome in epilepsy patients,” *J. Neural Eng.*, vol. 17, no. 3, p. 035007, June 2020, doi: 10.1088/1741-2552/ab8113.

[218] P. Garcés, M. C. Martín-Buro, and F. Maestú, “Quantifying the Test-Retest Reliability of Magnetoencephalography Resting-State Functional Connectivity,” *Brain Connect.*, vol. 6, no. 6, pp. 448–460, July 2016, doi: 10.1089/brain.2015.0416.

[219] D. A. Pierce, “R2 Measures for Time Series,” *J. Am. Stat. Assoc.*, vol. 74, no. 368, pp. 901–910, 1979, doi: 10.2307/2286421.

[220] M. B. (Maurice B. Priestley, *Spectral analysis and time series*. London ; New York : Academic Press, 1982. Accessed: May 10, 2025. [Online]. Available: http://archive.org/details/spectralanalysis0000prie

[221] K. J. Blinowska, “Review of the methods of determination of directed connectivity from multichannel data,” *Med. Biol. Eng. Comput.*, vol. 49, no. 5, pp. 521–529, Dec. 2011, doi: 10.1007/s11517-011-0739-x.

[222] M. F. Pagnotta and G. Plomp, “Time-varying MVAR algorithms for directed

connectivity analysis: Critical comparison in simulations and benchmark EEG data," *PloS One*, vol. 13, no. 6, p. e0198846, 2018, doi: 10.1371/journal.pone.0198846.

[223] M. Kamiński, M. Ding, W. A. Truccolo, and S. L. Bressler, "Evaluating causal relations in neural systems: Granger causality, directed transfer function and statistical assessment of significance," *Biol. Cybern.*, vol. 85, no. 2, pp. 145–157, Aug. 2001, doi: 10.1007/s004220000235.

[224] R. Oostenveld, P. Fries, E. Maris, and J.-M. Schoffelen, "FieldTrip: Open source software for advanced analysis of MEG, EEG, and invasive electrophysiological data," *Comput. Intell. Neurosci.*, vol. 2011, p. 156869, 2011, doi: 10.1155/2011/156869.

[225] A. Fornito, A. Zalesky, and E. Bullmore, *Fundamentals of Brain Network Analysis*. Academic Press, 2016.

[226] M. Rubinov and O. Sporns, "Complex network measures of brain connectivity: Uses and interpretations," *NeuroImage*, vol. 52, no. 3, pp. 1059–1069, Sept. 2010, doi: 10.1016/j.neuroimage.2009.10.003.

[227] J. F. Hipp, D. J. Hawellek, M. Corbetta, M. Siegel, and A. K. Engel, "Large-scale cortical correlation structure of spontaneous oscillatory activity," *Nat. Neurosci.*, vol. 15, no. 6, pp. 884–890, June 2012, doi: 10.1038/nn.3101.

[228] C. Li, H. Su, and Y. Liu, "Predicting Surgical Outcome in Patients With Drug-Resistant Epilepsy Using Autoregressive Connectivity and Virtual Resection," *IEEE J. Biomed. Health Inform.*, vol. 29, no. 3, pp. 2199–2209, Mar. 2025, doi: 10.1109/JBHI.2024.3510134.

[229] W. J. Youden, "Index for rating diagnostic tests," *Cancer*, vol. 3, no. 1, pp. 32–35, Jan. 1950, doi: 10.1002/1097-0142(1950)3:1%3C32::aid-cncr2820030106%3E3.0.co;2-3.

[230] E. van Diessen *et al.*, "Are high frequency oscillations associated with altered network topology in partial epilepsy?," *NeuroImage*, vol. 82, pp. 564–573, Nov. 2013, doi: 10.1016/j.neuroimage.2013.06.031.

[231] X. Tong *et al.*, "Real-time effects of interictal spikes on hippocampus and amygdala functional connectivity in unilateral temporal lobe epilepsy: An EEG-fMRI study," *Epilepsia*, vol. 60, no. 2, pp. 246–254, Feb. 2019, doi: 10.1111/epi.14646.

[232] J. Stiso, L. Caciagli, P. Hadar, K. A. Davis, T. H. Lucas, and D. S. Bassett, "Fluctuations in functional connectivity associated with interictal epileptiform discharges (IEDs) in intracranial EEG," Mar. 16, 2022, *bioRxiv*. doi: 10.1101/2021.05.14.444176.

[233] T. A. Guth *et al.*, "Interictal spikes with and without high-frequency oscillation have different single-neuron correlates," *Brain*, vol. 144, no. 10, pp. 3078–3088, Aug. 2021, doi: 10.1093/brain/awab288.

[234] S. Demont-Guignard, P. Benquet, U. Gerber, A. Biraben, B. Martin, and F. Wendling,

"Distinct hyperexcitability mechanisms underlie fast ripples and epileptic spikes," *Ann. Neurol.*, vol. 71, no. 3, pp. 342–352, Mar. 2012, doi: 10.1002/ana.22610.

[235] G. Varotto, L. Tassi, S. Franceschetti, R. Spreafico, and F. Panzica, "Epileptogenic networks of type II focal cortical dysplasia: a stereo-EEG study," *NeuroImage*, vol. 61, no. 3, pp. 591–598, July 2012, doi: 10.1016/j.neuroimage.2012.03.090.

[236] P. Shah *et al.*, "High interictal connectivity within the resection zone is associated with favorable post-surgical outcomes in focal epilepsy patients," *NeuroImage Clin.*, vol. 23, p. 101908, 2019, doi: 10.1016/j.nicl.2019.101908.

[237] G. W. Johnson *et al.*, "The Interictal Suppression Hypothesis in focal epilepsy: network-level supporting evidence," *Brain J. Neurol.*, vol. 146, no. 7, pp. 2828–2845, July 2023, doi: 10.1093/brain/awad016.

[238] A. Herlopian, "Networks through the lens of high-frequency oscillations," *Front. Netw. Physiol.*, vol. 4, Nov. 2024, doi: 10.3389/fnetp.2024.1462672.

[239] W. J. E. M. Zweiphenning *et al.*, "High frequency oscillations and high frequency functional network characteristics in the intraoperative electrocorticogram in epilepsy," *NeuroImage Clin.*, vol. 12, pp. 928–939, 2016, doi: 10.1016/j.nicl.2016.09.014.

[240] S. Lagarde and F. Bartolomei, "Sink into the epileptogenic zone: findings from directed SEEG functional connectivity decomposition," *Brain*, vol. 147, no. 9, pp. 2902–2905, Sept. 2024, doi: 10.1093/brain/awae256.

[241] Y. Höller *et al.*, "Reliability of EEG Measures of Interaction: A Paradigm Shift Is Needed to Fight the Reproducibility Crisis," *Front. Hum. Neurosci.*, vol. 11, p. 441, 2017, doi: 10.3389/fnhum.2017.00441.

[242] L.-R. Shao, C. W. Habela, and C. E. Stafstrom, "Pediatric Epilepsy Mechanisms: Expanding the Paradigm of Excitation/Inhibition Imbalance," *Child. Basel Switz.*, vol. 6, no. 2, p. 23, Feb. 2019, doi: 10.3390/children6020023.

[243] J. Engel, "Excitation and inhibition in epilepsy," *Can. J. Neurol. Sci. J. Can. Sci. Neurol.*, vol. 23, no. 3, pp. 167–174, Aug. 1996, doi: 10.1017/s0317167100038464.

[244] K. M. Gunnarsdottir, J. Gonzalez-Martinez, S. Wing, and S. V. Sarma, "Sources and Sinks in Interictal iEEG Networks: An iEEG Marker of the Epileptogenic Zone," *Annu. Int. Conf. IEEE Eng. Med. Biol. Soc. IEEE Eng. Med. Biol. Soc. Annu. Int. Conf.*, vol. 2021, pp. 6558–6561, Nov. 2021, doi: 10.1109/EMBC46164.2021.9630035.

[245] R. Malladi, G. Kalamangalam, N. Tandon, and B. Aazhang, "Identifying Seizure Onset Zone From the Causal Connectivity Inferred Using Directed Information," *IEEE J. Sel. Top. Signal Process.*, vol. 10, no. 7, pp. 1267–1283, July 2016, doi: 10.1109/JSTSP.2016.2601485.

[246] L. Bonilha *et al.*, "Presurgical connectome and postsurgical seizure control in temporal lobe epilepsy," *Neurology*, vol. 81, no. 19, pp. 1704–1710, Nov. 2013, doi:

10.1212/01.wnl.0000435306.95271.5f.

[247] L. Bonilha *et al.*, “The brain connectome as a personalized biomarker of seizure outcomes after temporal lobectomy,” *Neurology*, vol. 84, no. 18, pp. 1846–1853, May 2015, doi: 10.1212/WNL.0000000000001548.

[248] M. Cao *et al.*, “Virtual intracranial EEG signals reconstructed from MEG with potential for epilepsy surgery,” *Nat. Commun.*, vol. 13, no. 1, p. 994, Feb. 2022, doi: 10.1038/s41467-022-28640-x.

[249] I. A. Nissen *et al.*, “Identifying the epileptogenic zone in interictal resting-state MEG source-space networks,” *Epilepsia*, vol. 58, no. 1, pp. 137–148, Jan. 2017, doi: 10.1111/epi.13622.

[250] E. L. Juárez-Martinez *et al.*, “Virtual localization of the seizure onset zone: Using non-invasive MEG virtual electrodes at stereo-EEG electrode locations in refractory epilepsy patients,” *NeuroImage Clin.*, vol. 19, pp. 758–766, June 2018, doi: 10.1016/j.nicl.2018.06.001.

[251] Y. Wang *et al.*, “Interictal intracranial electroencephalography for predicting surgical success: The importance of space and time,” *Epilepsia*, vol. 61, no. 7, pp. 1417–1426, July 2020, doi: 10.1111/epi.16580.

[252] H. Akaike, “A new look at the statistical model identification,” *IEEE Trans. Autom. Control*, vol. 19, no. 6, pp. 716–723, Dec. 1974, doi: 10.1109/TAC.1974.1100705.

[253] L. L. Chen, R. Madhavan, B. I. Rapoport, and W. S. Anderson, “Real-time brain oscillation detection and phase-locked stimulation using autoregressive spectral estimation and time-series forward prediction,” *IEEE Trans. Biomed. Eng.*, vol. 60, no. 3, pp. 753–762, Mar. 2013, doi: 10.1109/TBME.2011.2109715.

[254] D. J. Krusienski, D. J. McFarland, and J. R. Wolpaw, “An evaluation of autoregressive spectral estimation model order for brain-computer interface applications,” *Conf. Proc. Annu. Int. Conf. IEEE Eng. Med. Biol. Soc. IEEE Eng. Med. Biol. Soc. Annu. Conf.*, vol. 2006, pp. 1323–1326, 2006, doi: 10.1109/IEMBS.2006.259822.

[255] D. J. McFarland and J. R. Wolpaw, “Sensorimotor rhythm-based brain-computer interface (BCI): model order selection for autoregressive spectral analysis,” *J. Neural Eng.*, vol. 5, no. 2, pp. 155–162, June 2008, doi: 10.1088/1741-2560/5/2/006.

[256] I. Rigoni, G. P. Padmasola, L. Sheybani, K. Schaller, C. Quairiaux, and S. Vulliemoz, “Reproducible network changes occur in a mouse model of temporal lobe epilepsy but do not correlate with disease severity,” *Neurobiol. Dis.*, vol. 190, p. 106382, Jan. 2024, doi: 10.1016/j.nbd.2023.106382.

[257] C. Geier and K. Lehnertz, “Long-term variability of importance of brain regions in evolving epileptic brain networks,” *Chaos Woodbury N*, vol. 27, no. 4, p. 043112, Apr. 2017, doi: 10.1063/1.4979796.

[258] Y. Höller *et al.*, “Reliability of EEG Measures of Interaction: A Paradigm Shift Is Needed to Fight the Reproducibility Crisis,” *Front. Hum. Neurosci.*, vol. 11, Aug. 2017, doi: 10.3389/fnhum.2017.00441.

[259] S. V. Gliske and W. C. Stacey, “The BEST Conceivable Way to Talk About Epilepsy Biomarkers,” *Epilepsy Curr.*, vol. 23, no. 3, pp. 175–178, 2023, doi: 10.1177/15357597231159714.

[260] FDA-NIH Biomarker Working Group, *BEST (Biomarkers, EndpointS, and other Tools) Resource*. Silver Spring (MD): Food and Drug Administration (US), 2016. Accessed: Oct. 01, 2025. [Online]. Available: http://www.ncbi.nlm.nih.gov/books/NBK326791/